Modelling of plastic yield surface of materials accounting for initial anisotropy and strength differential effect on the basis of experiments and numerical simulation

Teresa Fras

École Doctorale EMMA

THÈSE

Pour l'obtention du grade de

DOCTEUR de L'UNIVERSITE DE LORRAINE

Spécialité: Sciences des matériaux

Présentée par

TERESA FRĄŚ

Modélisation de la surface d'écoulement des matériaux incluant l'anisotropie initiale et l'effet différentiel des contraintes, approche expérimentale et numérique

---

A soutenir le 21.06. 2013 à Metz devant le jury composé de:

N. BAHLOULI	Professeur, ICube, Université de Strasbourg	Rapporteur
P. VERLEYSEN	Professeur, DMSE, Université de Gand	Rapporteur
P. LIPIŃSKI	Professeur, LaBPS, École Nationale d'Ingénieurs de Metz	Examinateur
M. MARTINY	Maître de conférences habilité, LEM3, Université de Lorraine	Examinateur
S. WOLNY	Professeur, École des Mines et de la Métallurgie de Cracovie	Examinateur
R.B. PĘCHERSKI	Professeur, École des Mines et de la Métallurgie de Cracovie	Directeur de thèse
A. RUSINEK	Professeur, LaBPS, École Nationale d'Ingénieurs de Metz	Directeur de thèse

Laboratoire de Mécanique Biomécanique Structures (LaBPS)
Ecole Nationale d'Ingénieurs de Metz (ENIM)
Université de Lorraine - Pôle M4: matière, matériaux, métallurgie, mécanique

Modelling of plastic yield surface of materials accounting for initial anisotropy and strength differential effect on the basis of experiments and numerical simulation

Teresa Frąś

Directors:
prof. Ryszard B. Pęcherski
prof. Alexis Rusinek

Université de Lorraine
Akademia Górniczo-Hutnicza im. Stanisława Staszica w Krakowie

Metz 2013

This work was supported by the French Government due to the scholarship *'Doctorat en cotutelle'* awarded by the French Embassy in Poland

Je tiens dans un premier temps à remercier Professeur Ryszard B. Pęcherski et Professeur Alexis Rusinek - mes directeurs de thèse, pour m'avoir confié ce travail de recherche, ainsi que pour leurs aides et leurs précieux conseils au cours de ces années.

Je tiens à remercier le Professeur Nadia Bahlouli et le Professeur Patricia Verleysen d'avoir accepté d'être les rapporteurs de ce travail.

Je remercie le DocteurMarion Martiny, le Professeur Paul Lipiński et le Professeur Stanisław Wolny d'avoir accepté de participer à ce jury.

Je remercie également le Docteur Raphael Pesci pour sa sympathie et sa disponibilité, les idées et ses conseils. Ce travail n'aurait pu aboutir sans l'aide de nombreuses personnes – Professeur Zdzisław Nowak, Monsieur Richard Bernier, Monsieur Marcin Nowak – merci.

Mes pensées iront vers ma famille, et surtout mes parents, qui m'ont soutenu tout au long de mes études. Ces remerciements ne seraient pas complets sans une pensée pour mes amis.

Resumeé

La thèse de doctorat propose le description physiquement cohérente de la limite d'élasticité du matériau sur la base des résultats des expériences associées à des simulations FEM. L'approche théorique est basée sur l'hypothèse de de la limite d'élasticité du matériaux de Burzynski. L'hypothèse de l'effort de matériau est dérivée de la définition de l'énergie de fin de course variable de changement de volume et de distorsion. En cas particuliers, les critères comprennent asymétrie de gamme élastique et, sous une forme élargie, il est applicable aux matériaux initialement anisotropes.

La thèse a démontré la nécessité de fournir une vue intégrée sur des expériences et des simulations numériques afin d'obtenir la description de l'apparition de la plasticité. Pour atteindre cet objectif, une méthodologie spécifique a été développé - la procédure qui combine des techniques expérimentales avec les simulations numériques pris en charge par la description précise du comportement du matériaux.

Comme une partie de l'approche de modélisation numérique, les analyses numériques été effectuées afin de corriger les inexactitudes des résultats expérimentaux présentés. En outre, la Burzyński condition isotrope été mis en œuvre dans la méthode des éléments finis via UMAT (user subroutine for ABAQUS).

La versatilité de la rendement description est illustrée par l'application de matériaux à structure amorphe et différents systèmes de cristaux cubiques: la structure FCC (face centered cubic) et BCC (body centered cubic). A titre d'exemples: - un matériau de type FCC structure - OFHC Cu, Oxygen Free High Conductivity Copper, un matériau de type BCC structure - E335, acier non allié de haute résistance et l'exemple des matériaux amorphes - polycarbonate (PC) et biopolymères (PLA/PBAT). Pour les matériaux les analyses précises ont été effectuées afin d'obtenir des propriétés microstructurales et mécaniques via large gamme de tests de résistance dans diverses conditions de chargement.

Le nombre de données exemplaires trouvés dans la littérature des matériaux sensibles à la pression et/ou initialement anisotrope ont été analysés. Il a été prouvé que les critères proposés donnent approximation précise de l'état du début de la plasticité par rapport à d'autres conditions d'usage courant. Les critères résultant semblent être une méthode universelle et largement applicable d'obtenir la description de l'apparition de la plasticité.

Contents

1 Framework of the Thesis **3**
1.1 Introduction . . . 3
1.2 Motivation . . . 3
1.3 Objectives . . . 4
1.4 Contents of the Thesis . . . 6
1.5 Original contributions . . . 7
1.6 Applications . . . 7

2 Materials **9**
2.1 Introduction . . . 9
2.1.1 Strength differential effect - SD effect . . . 10
2.1.2 Initial anisotropy . . . 11
2.2 Oxygen Free High Conductivity Copper - OHFC Cu . . . 13
2.3 E335 - high strength steel . . . 22
2.4 Mechanical properties of chosen polymers . . . 28
2.5 Concluding remarks . . . 32

3 Experimental techniques and their methodology **33**
3.1 Introduction . . . 33
3.1.1 Schematic representation of stress states . . . 35
3.1.2 Determining the yield strength . . . 36
3.2 Uniaxial tension and compression test . . . 38
3.2.1 FEM analysis of the tension and compression test . . . 42
3.3 Shear test . . . 46
3.3.1 The double shear test . . . 48
3.3.2 FEM analysis of the double shear test . . . 50
3.4 Biaxial compression test . . . 54
3.4.1 Preliminary results of biaxial compression test . . . 57
3.4.2 FEM analysis of biaxial compression test . . . 59
3.5 Complex stress state test . . . 69
3.6 Split-Hopkinson Pressure Bar test (SHPB) for dynamic compression . . . 73
3.7 Concluding remarks . . . 76

4 Burzyński material effort hypothesis **77**
4.1 Introduction . . . 77
4.2 General formulation of the yield condition . . . 78
4.3 Visualization of yield criteria . . . 80

4.4 Yield criteria in the literature . . . 83
4.4.1 Traditional yield criteria . . . 84
4.4.2 Criteria accounting for stress invariants J_2, I_1 and J_2, I_1, J_3 . . . 87
4.4.3 Phenomenological criteria . . . 94
4.5 Burzyński material effort hypothesis and the resulted criteria . . . 96
4.5.1 Elastic energy . . . 96
4.5.2 Hypothesis of variable limit energy of volume change and distortion . 97
4.5.3 Paraboloidal Burzyński criterion for isotropic materials . . . 100
4.5.4 Burzyński criterion for materials with initial anisotropy . . . 104
4.5.5 Smoothness of criterion for initially anisotropic materials . . . 107
4.5.6 Phenomenological formulation of the Burzyński criterion . . . 113
4.5.7 Concluding remarks . . . 117
4.6 User subroutine for the Burzyński isotropic criterion . . . 117
4.6.1 Analysis of the tensile test of notched specimens for E335 steel . . . 118
4.6.2 Experimental and numerical results . . . 120
4.6.3 Concluding remarks . . . 125

5 Experimental results and applications of the Burzyński criteria 127
5.1 Introduction . . . 127
5.2 Application for various materials . . . 129
5.2.1 Yield surface basing on the complex state test results . . . 129
5.2.2 Grey cast-iron . . . 132
5.2.3 Titanium alloy - Ti6Al4V . . . 134
5.2.4 Mg alloy . . . 137
5.2.5 Metallic glasses . . . 139
5.3 Application for FCC material - OFHC Copper . . . 141
5.3.1 Results of strength tests . . . 141
5.3.2 Yield surface for OFHC Cu . . . 146
5.4 Applications for BCC materials - E335 steel . . . 152
5.4.1 Results of strength tests for E335 . . . 153
5.4.2 Yield surface for E335 . . . 160
5.5 Applications for amorphous materials . . . 165
5.5.1 SD effect in the polymers and its influence on the yield state . . . 166
5.5.2 Results for polycarbonate . . . 174
5.5.3 Results for PLA/PBAT . . . 178

6 Conclusions 181

Appendixes 187
Appendix 1 - Constitutive models of strain rate sensitivity . . . 189
Appendix 2 - Algorithm of Burzyński paraboloidal criterion . . . 193
Appendix 3 - Project of biaxial compression set-up . . . 197

References 198

Chapter 1

Framework of the Thesis

This chapter outlines the motivation and the general objectives of presented Thesis. The scientific basis and methodology followed to achieve the aim of the Thesis are described. The contents of the Thesis are presented and shortly discussed. Finally, the original contributions are stated and possible applications of the results are given.

1.1 Introduction

Experimental investigations integrated with adequate description and modelling of mechanical behaviour of metallic materials and polymers is an important issue in modern technologies. Such approach is applied for instance in automotive and transportation industry as well as in the field of aeronautics or military. The comprehension of processes is possible as an outcome of theoretical and the experimental approach when experiment is justified by the results of numerical simulation. This is the view which is recently a leading tendency in the modern mechanics of materials. It can be said that the experiment suggests and adds credibility to the theory, while the theory suggests and interprets the experiment.

1.2 Motivation

Design engineering, in the field of the aerospace and automotive as well as military applications, in its increasing needs and interests causes the necessity of detailed and thorough analysis of the material's properties. In addition, many of the problems found in structural design are also relevant in machining processes and metal forming operations. For each process of industrial or structural design onset of the yielding is an important issue.

Rapid progress in the computational mechanics have allowed engineers to analyse complex structural components, assess structural reliability and optimize structural designs. The need for more accurate material models becomes increasingly evident, particularly when minimizing design margins becomes the approach for weight optimization or life-extension efforts. Yielding of a materials is an important issue in automotive or aerospace industry because the static design verification has to be performed on onset of (global) yielding on load level and

onset of plastic or ultimate stresses. Design verification demands for reliable safety coefficients in a structural analysis what is obtained by application of reasonably chosen yield condition. Such a condition is the mathematical formulation of a yield surface or curve.

Yield criteria are also an essential part of computer programs based on the finite element method. A numerical model can give predictions depending on the material model but the numerical results can be useless without a proper constitutive model which accurately describes the material behaviour. Similarly, if a virtual experiment performed in modern computing programs containing complex algorithms should mimic real results, its conditions must be determined by the correct description of material. Therefore, it is important to understand properly the material description and its constitutive model, as well as the yield criterion used in the calculations with the correctly identified parameters. Description of the material effort hypothesis is an actual and important topic for the proper determination of the safety of designed structures.

The formulation of proper yield theory was one of the earliest objectives considered in the past ages, e.g. by Leonardo da Vinci (1452-1519) or Galileo Galilei (1564-1642), also contemporary researchers were engaged in this topic, e.g. Huber (1872-1950), Hill (1921-2011), Theocaris (1921-2000). Currently, it is still an open subject for many researchers. Therefore, considerable efforts have been devoted to the formulation of strength theories and to their correlation with test data. However, it is difficult to claim that the fully adequate criterion exists, since hundreds of yield models have been proposed. Now, 'yield theories' are a part of most courses in Plasticity, Geomechanics, Soil Mechanics, Rock Mechanics, and Plasticity of Geomaterials, etc.

Above mentioned observations have laid the basis for preparation of this doctoral Thesis. In the Thesis there is proposed a complete approach to obtain the appropriate and physically consistent description of the beginning of plastic deformation, which is approximated by the yield condition. The methodology which combines advanced measuring techniques with numerical simulations supported by the accurate description of the material behaviour is presented. The combination of the microstructure analysis and experimental deformation for different loading conditions with numerical simulation of the processes allows to obtain description of the onset of the yielding.

1.3 Objectives

In the Thesis the theory of Burzyński is applied to describe the beginning of deformation of various materials. Włodzimierz Burzyński (1900-1970) was a Polish scientist in the field of mechanics of solids, the follower of M.T. Huber in the subject of the material effort hypotheses. In his Thesis from 1928 (the English translation published in 2009 [Burzyński 2009]) he proposed the general concept of material effort hypothesis based on the variable limit energy of volume change and distortion. In particular cases, the yield criterion includes asymmetry of elastic range. The extension of this approach is applicable to the initially anisotropic materials.

In the presented study the hypothesis of Burzyński is applied to the materials revealing the difference in strengths and/or initial anisotropy.

The phenomenon known as the strength-differential (SD) effect or asymmetry of elastic range means that flow stress of some materials is usually larger in uniaxial compression than in uniaxial tension. Whereas, initial anisotropy correlates to the processes of manufacturing which produce, due to the evolution of texture, the change of mechanical properties of material in such a way that they lose their isotropic character. The material in the 'as-received' state (without heat treatment after the processes of manufacturing) becomes usually anisotropic because of rolling, drawing or extrusion processes associated with the initial forming of metal sheets, bars or metal profiles stock. Proceeding with such materials must account not only for the inhomogeneous properties but should also anticipate undesirable features of anisotropic behaviour, such as premature fracture and undesirable shear banding.

The objectives of this doctoral Thesis are set as it is presented beneath.

> *The goal of the Thesis is physically consistent and experimentally justified description of material's yielding. Proper description of the material's yielding is based on the results of experiments coupled with FEM simulations. As a yield hypothesis the Burzyński material effort hypothesis has been applied. The resulting criteria concern: isotropic materials with SD effect, Eq. (4.33), and initially anisotropic materials, Eq. (4.45). To validate criterion the different examples of materials have been chosen: metals, theirs alloys and polymers.*

Thus, to obtain more accurate description of the yielding the following methodology is assumed.

- In order to demonstrate the versatility of the proposed yield description, there have been chosen materials presenting examples of amorphous structure and different cubic crystal systems: face-centered cubic crystal structure (FCC) and body-centered cubic crystal structure (BCC). As examples there are used the following materials: - a FCC-structure type material - OFHC Cu, Oxygen Free High Conductivity Copper, a BCC-structure type material - a non-alloy structural steel E335 (according to Standard EN 10025 - 2:2004 Technical delivery conditions for non-alloy structural steels) and example of the amorphous materials - polycarbonate (PC) and biopolymers (PLA/PBAT). For these material there is presented comprehensive discussion concerning their strength and mechanical properties. Application of the Burzyński criteria to a wide range of materials allows to show universality of proposed approach.
- The experiments in quasi-static and dynamic strain rates allow to obtain different, depending on the loading conditions, values of yield points. Apart from traditional quasi-static tension, compression there are described double shear test, complex stress state test and biaxial compression test. In dynamic ranges the compression test is performed with use of the Split Hopkinson Pressure Bar. The results allow to obtain data providing possibility of more accurate description of the yield surface.
- The numerical analysis is performed in order to correct the inaccuracies of presented experimental results. The practical correction methods are discussed.

- The isotropic Burzyński condition is implemented in finite element method via UMAT (user subroutine for ABAQUS). Implementation allows to develop a numerical methodology for analyzing the beginning of plastic deformation for a wide group of materials - metals, their alloys, polymers or metal matrix composites, which are characterized by the strength differential effect. An example of calculation with use of UMAT is presented in the Thesis.
- Different experimental data concerning metals and their alloys, polymers, metallic glasses found in the literature are applied to validate the discussed yield criteria.

1.4 Contents of the Thesis

The Thesis is divided into six chapters as reported beneath.

- The first chapter, which is an introduction, presents the general framework of the Thesis.
- In the second chapter, examples of materials described according the mechanical properties are presented. The study of literature concerning the discussed materials is also given. The chosen materials belong to various groups of crystalline structure - FCC, BCC and amorphous. The materials are affected by the strength differential effect or/and the initial anisotropy. There have been used as examples: OFHC Cu - Oxygen Free High Conductivity Copper, non alloy structural steel E335, polycarbonate (PC) and biopolymers (PLA/PBAT).
- In the third chapter the experimental techniques are reported. To present properties of the materials there have been chosen tests of: quasi-static and dynamic compression, quasi-static tension, double shear, complex stress state, biaxial compression. State of the art concerning discussed techniques is given, including their advantages and drawbacks. Also, the advantages of numerical simulations performed to analyse experimental results are discussed. The corrections obtained due to Finite Element Method (FEM) modelling are applied to the results of experiments.
- In the fourth chapter the background of yield criteria is given. The different yield concepts are shortly discussed. The energy based Burzyński hypothesis of material effort is formulated and described. The resulting criteria - for isotropic materials and for materials with initial anisotropy are described in detail. In addition, a specially written UMAT (user subroutine to define a material's mechanical behaviour in Abqus/Standard) with implemented isotropic Burzyński criterion has been validated for tensile test on notched specimen, [Vadillo et al. 2011].
- In the fifth chapter, there are shown examples of criteria's application to the literature-based experimental data. There are discussed yield states for various materials, visualized in the space of principal stresses and planes of stress. Then, the results of tests performed for exemplary materials are presented and discussed. After calculating the suitable yield strengths, the yield surfaces and limit curves are depicted. The wide range of experimental data obtained on purposes of the Thesis and found in the scientific literature is used to show the applicability of Burzyński yield criteria.

- Final conclusions are presented in the last, sixth chapter, which also provides recommendation for future research. Moreover, appendixes are attached with algorithm in which there are determined some aspects of the Thesis.

1.5 Original contributions

The original contributions carried out in this Thesis are outlined in the following points.

- Performing a wide experimental investigation in different loading conditions (compression, tension, shear, biaxial compression) in a wide range of strain rates allows to obtain the throughout mechanical characterization of the chosen materials (OFHC Cu, E335, PC and PLA/PBAT polymers).
- Designing, evaluation and validation of the methodology of the biaxial compression test.
- Elaborating the model describing influence of friction during the biaxial compression process.
- The extension of the Burzyński criterion for initially anisotropic materials accounting for strain, strain rate.
- Elaborating the algorithms with use of the Wolfram Mathematica allowing to obtain and visualize the yield surface in the space of principal stresses, yield curves in the plane state of stress, the meridional plane and octahedral plane for the isotropic materials with SD effect and materials initially anisotropic.
- Preparation of the examples of yield surface and curves for a wide group of materials.

1.6 Applications

Possible application of conclusions and observations included in the Thesis are as follow:

- The elaborated yield surface description with use of the Burzyński criteria for for different materials can be implemented in commercial FEM programs. This would broaden the range of application of the FEM programs allowing to obtain more accurate description of material yield.
- The new methodology of biaxial compression test can be incorporated in the experimental investigation. The test allows to verify the results of standard investigation concerning modelling of yielding state of a material.
- The algorithms visualizing yielding state, created for the purpose of the Thesis, can be applied commercially.

Chapter 2

Materials

To present a range of applicable possibilities of proposed in the Thesis criteria, the examples of materials with different microstructure are introduced. The discussed materials are: OFHC Cu - characterized by a face-centered cubic structure, steel E335 - the example of material of body-centered cubic structure and amorphous polymers - polycarbonate and biopolymers. An overview, based on the study of literature, of most important mechanical features of the examined materials is given in this Chapter.

2.1 Introduction

The concept of crystal defects was introduced in physics by Taylor, Polanyi and Orowan in the 1930s to describe crystal behaviour during deformation and explain plasticity in microscopic terms. Taylor, Polanyi and Orowan realized that plastic deformation could be explained in terms of the theory of dislocations. Dislocations can move if the atoms from one of the surrounding planes break their bonds and rebond with the atoms at the terminating edge. Dislocation motion leads to plastic deformation. Slip is the process by which a dislocation moves and causes a material to deform. Slip is easier in crystal planes of high planar atomic density crystal planes and along crystal directions of high linear atomic density. It occurs between planes containing the smallest Burgers vector (Burgers vector represents the magnitude and direction of the lattice distortion of dislocation in a crystal lattice, Callister and Rethwisch [2005]).

Later work on crystalline materials, especially metals, showed the strong dependence of mechanical properties on structure and the presence of such defects. To cover difference in material deformation according to mechanisms driving it, the different constitutive relation are assumed which describe separately cases of face-centered cubic (FCC), body-centered cubic (BCC) and amorphous materials, [Klepaczko and Chiem 1986; Nemat-Nasser et al. 1998a; Rusinek et al. 2007; Molinari and Ravichandran 2005].

In the face-centered cubic structure close-packed planes are the octahedral set of planes (111) and closed-packed directions are the cube face diagonals (110), [Smith 1956]. As the body-centered cubic structure does not have a close packed plane it requires higher stresses to initiate slip and withstands lower plastic deformation to failure than the FCC structure, [Kostryzhev 2009]. A slip system in BCC requires heat to activated. The deformation in a

material is depended on its microstructure, consequently the different constitutive models describe deformation and approximate flow of materials.

It is a matter of interest if proposed criteria describe well yielding of the groups of materials which structures are different. To demonstrate the capability of Burzyński criteria the materials of different microstructure have been examined more accurately. There are discussed as follows:

- face-centered cubic structure - OFHC Cu - Oxygen Free High Conductivity Copper,
- body-centered cubic structure - E335 - non-alloy structural high strength steel,
- amorphous structure - polycarbonate (PC) and biopolymers (PLA and PLAT/PBAT).

Advantage of applied yield criteria is their versatility and large applicable possibilities. To prove that criteria proposed in Thesis have this feature, a wide group of materials have been investigated. The detailed formulation of criteria can be used to describe yielding of different materials, concerning metallic materials and polymers. Materials may be characterized by the strength differential parameter or/and the initial anisotropy. The basic information about both effects is shortly presented in next Sections. A short study is reported concerning mechanical properties of selected materials basing on results from the literature. Their macroscopic and microscopic properties are also reported and discussed. Such short introduction is a physical background of obtained results of the strength tests - presented in Chapter 5. For collected experimental data the limit surfaces and curves are built to visualize the yield state of material.

2.1.1 Strength differential effect - SD effect

In order to get a comprehensive characterization of a material there should be performed not only the tension test (which is commonly used to determine normative properties of material) but also compression and shear. Extended experimental procedure allows to exhibit different behaviours for different loading types of examined material. Difference in characteristics obtained due to compression and tension have been reported by [Hirth and Cohen 1970] for martensitic steels which are stronger in uniaxial compression than in tension. This observation was confirmed in works of [Chait 1972; Spitzig et al. 1979; Spitzig and Richmond 1979] for other high strength steels. The examples of martensitic, quenched, tempered or maraging steels were studied. In [Drucker 1973] the phenomenon of asymmetry of elastic ranges was more generally formulated for metals and plastics. Experimental studies on the effect of superimposed hydrostatic pressure on the deformation behaviour of iron based materials [Spitzig et al. 1979], as well as of aluminum [Spitzig and Richmond 1984], have proved that strength differential phenomenon exists for many kinds of materials. The assumption that tensile and compressive yield strengths are equal diminishes when polymers are under consideration, what is proved in [Raghava et al. 1973]. The SD effect has been studied extensively also in recent years. Further examples which show the different response in tension and compression for different materials are presented in, e.g. [Casey and Sullivan 1985; Altenbach and Zolochevsky 1995; Wilson 2002; Altenbach and Zolochevsky 1996; Bai and Wierzbicki 2008]. Recently, the strength differential effect has attracted extensive interest due to the increasing adoption of hexagon-closed packed (HCP) metals and alloys to satisfy

the requirement for the high ratio of strength to density. For example, the tensile yield stress is much higher than the one in compression for magnesium alloys, [Lou et al. 2007; Cheng-wen et al. 2007; Yoshikawa et al. 2008; Rusinek 2011].

The phenomenon of inequality of the tensile and compressive yield strengths is known as the strength-differential (SD) effect. It can be also denoted as an asymmetric effect. The SD parameter is defined by the following relation:

$$\kappa = \frac{\sigma_Y^C}{\sigma_Y^T} \tag{2.1}$$

where σ_Y^C is the yield strength in compression and σ_Y^T is the yield strength in tension.

In the studies [Spitzig and Richmond 1984] the SD effect was interpreted as a direct consequence of the dependence of the flow stress on the hydrostatic stress (mean stress) in the specimen. The SD effect and a sensitivity of the flow stress to the hydrostatic pressure are related to volume expansion of the material as a consequence of plastic deformation, [Spitzig et al. 1979; Mahnken 2001].

According to [Fletcher and M. Cohen 1974; Casey and Jahedmotlagh 1984] for the SD effect is not related to frictional effect in compression testing, residual stresses from quenching and phase transformations, microscopic void formation or transfrormation-induced Bauschinger effect. Therefore, only a difference in the inherent response to tensile and compressive deformation can be responsible.

In [Hirth and Cohen 1970; Casey and Jahedmotlagh 1984; Mahnken 2001] there are presented following observation considreding SD effect: it remains constant over a considerable range of the plastic strain and it is not influenced by the strain rate if the tension and compression tests are performed with the same constant $\dot{\varepsilon}$, [Duckett et al. 1970].

In [Ghorbel 2008] based on the investigation for polymers for which difference in yield strengths is characteristic, it is reported that κ is independent on the temperature, what is established for different polymeric materials (for PET this observation was made by [Duckett et al. 1970], for PC information are collected in [Bauwens-Crowet et al. 1972]).

The further information about SD effect are presented in, e.g. [Chait 1972; Drucker 1973; Casey and Jahedmotlagh 1984; Mahnken 2001; Lou et al. 2013].

2.1.2 Initial anisotropy

Manufacturing processes of metals and alloys produce often, due to the evolution of texture, change of mechanical properties that they lose their isotropic character. Technological processes of production (ex. forging, stamping, rolling, extruding) results in the massive reorientation of structure during the large strain forming operation. The presence of anisotropy in structure may lead to premature failure or unexpected shear localization, [Arruda et al. 1993]. Two main sources of initial anisotropy result from the thermo-mechanical processes involved in metal production: crystallographic texture and intragranular dislocation structure. The material in the 'as-received' state becomes usually anisotropic because manufacturing processes associated with the initial forming of metal sheets, bars or metal profiles stock. Proceeding

with such materials must not only account for the inhomogeneous and direction-dependent properties but should also anticipate undesirable features of anisotropic behaviour, such as premature fracture and undesirable shear banding. The development of a strong texture will lead to orientation-dependent mechanical characteristics because the crystallographic structure of grains is intrinsically anisotropic. Concerning the intragranular structure, dislocation interactions depend on the Burgers vectors as well as on the slip direction. This leads to such effects like latent hardening or Bauschinger softening, [Rauch 1998]. It is difficult, however, to measure and describe in the direct way the initial anisotropy of elastic properties and yield behaviour. For initially anisotropic materials exact descriptions of its yielding behaviour becomes rather difficult.

Loading direction or stress state may result in a different response on the orientation of dominant slip-plane and the critical value of shearing stress. The yielding state of materials is often physically interpreted as observation that yielding of element in a material occurs when the shearing stress on a dominant slip-plane reaches its critical value, [Hu 2007]. If material is treated as isotropic, such physical interpretation can be described by Huber-Mises-Hencky criterion (Huber 1904: [Huber 2004], Mises 1913: [von Mises 1913]) for which the shear limit fulfils the relation given by Eq. (2.2):

$$\tau_Y^H = \frac{\sigma_Y}{\sqrt{3}} \tag{2.2}$$

where τ_Y^H is a yield strength in shear according to Huber-Mises approach and σ_Y is a yield strength in tension.

Isotropic yield of materials does not account for critical value of shearing stress on the dominant slip-plane, neither for the loading directions leading in the process of deformation. The needs of shear corrections is covered by Burzyński criterion, Eq. (4.26). Coefficient λ is proposed by Burzyński macroscopic relation incorporating yield strengths in compression, tension and shear -Eq. (2.3) which allows to capture the deviation of a value of experimental shear strength τ_Y from the HMH definition, Eq. (2.2):

$$\lambda = \frac{\sigma_Y^C \sigma_Y^T}{2\tau_Y^2} - 1 \tag{2.3}$$

where $\tau_Y, \sigma_Y^T, \sigma_Y^C$ are respectively experimental yield strengths in shear, tension and compression.

The detailed discussion about the shear correction factor Eq. 4.35 based on the work of Burzyński [Burzyński 2009] is presented in Section 4.5.4.

In further parts of this Chapter a discussion concerning mechanical and micro-structural properties of exemplary materials is given. The result of analysis of microstructure of each material is reported. The importance in industrial applications of studied copper, steel and polymers is stated basing on their functional properties. This is a preparatory part aimed to present shortly materials of different microstructure. For these materials there have been performed tests under different loading conditions discussed in Chapter 3, results presented in Chapter 5. Knowledge of rules governing structural deformation allows to understand processes recorded due to macroscopic observations.

2.2 Oxygen Free High Conductivity Copper - OHFC Cu

Copper has the highest conductivity of electricity and heat from all the 'base metals'. In addition, its other properties, such as relatively high strength, toughness, ease of processing and design, corrosion resistance, durability, non-toxicity make it an extremely valuable material in the electrical, electronics, energetic industries, as well as in construction and technical installations. Performance of copper recycling industry can reduce use of natural resources and reduce waste generation during disposal of used products - copper material are environmentally friendly, highly re-producting material, e.g.: [Publications 1998; Rosenberg et al. 2009]. The development of the electrical industry requires the use of increasingly refined copper characterized by increasingly better chemical, physical, technological and utility properties.

High Conductivity Oxygen Free Copper - OFHC Cu - is a material with specially shaped structure, small particle size, high purity - Class 5N. The amount of pollution does not exceed 25 ppm by weight. The reason of importance of purity of copper is that the most harmful impurities can significantly decrease electrical conductivity, increase the mechanical strength of the annealed wire, retard recrystallization, and will sometimes induce hot shortness during the hot rolling process in the production of rod, [www.copper.org].

Oxygen is intentionally alloyed with copper to act as a scavenger for dissolved hydrogen and sulfur to form the gases and melt. The presence of oxygen in the copper leads to reduce the service time of cables and conductors, it is the so-called 'hydrogen embrittlement'. Annealing of wires at high temperature leads to the reaction of hydrogen with oxygen and due to the resulting reaction, water vapor contributes to the cracking of the copper grain boundaries. In the case of oxygen free copper hydrogen embrittlement does not occur, neither other effects caused by the presence of oxygen.

Obtaining OFHC requires highly advanced production techniques, the process of melting high purity feedstock is performed under pressure, in the conditions that eliminate the access of oxygen and other pollution. A continuous casting and rolling process produces virtually all copper rod. Benefits of continuous casting include less microsegregation of impurities, reduction of copper oxide particles on the surface, fewer steel inclusions resulting from contact with mill rolls, almost total elimination of welds, and lower overall processing costs, [www.copper.org].

The thermal stability of the production determines the reproducibility of physical and chemical properties. Obtained chemical purity determines the high electrical conductivity. Copper exhibits high conductivity because its electrons show relatively little resistance to movement under an electric field. Copper in particular is an excellent conductor because outermost electrons have a large mean free path (about 100 atomic spacings) between collisions.

The electrical resistivity is inversely related to this mean free path. Signal running through the guide should face the least amount of obstacles, so that the sound is not distorted - this conditions is fulfilled in the production processes of OFHC Cu. Negligible presence of oxides and fewer grain boundaries in oxygen-free copper provide lossless transmission of sound and image signals. Small amounts of oxygen leads to improved performance properties, particularly ductility and corrosion resistance, the recrystallization temperature is also increased, [www.kghm.pl, www.copper.org, www.Philips.com].

Due to the specific properties OFHC Cu is used in modern, more demanding, computer and electronic technologies. For example, in hi-fi technology, cryogenics, semiconductor heat sinks, in diodes and hygristors for heavy current operations, to production of wires and cables, busbars, commutators, welding electrodes, contacts, contact springs, printed circuit boards, semiconductors, high vacuum and other electronic devices, tuyeres, heat exchangers, cables and busbars, www.kghm.pl, www.copper.org.

Microstructure analysis

Examined in the Thesis copper firstly has been analysed due to its microstructure. The pole figure and pictures with use of optical microscopy have been prepared. The samples has been cut from a bar of diameter 12mm. The surface which has been polished is perpendicular to the extrusion direction of the bar.

In Fig. 2.1 the pictures taken with use of an optical microscope at magnification of 5- and 10-x. The observed area is closed to the border of a sample. The material is homogenous without inclusions of other elements and phases. It is observed and that the average grain size is bigger close to the border (180 μm) of the extruded bar in comparison with the middle (30–70 μm). The tested material is of 99.999% (Class 5N) pure copper.

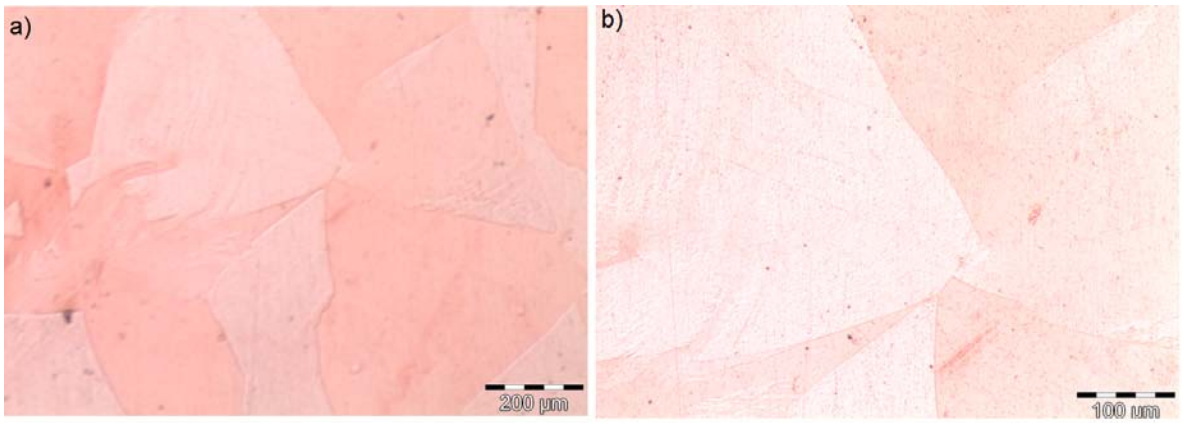

Figure 2.1: Obtained with use of the optical microscope picture of OFHC Cu made close to the border of a sample: (a) with 5x magnification and (b) 10x magnification.

The resulting figure is made in the direction (2 2 0), it is shown in Fig. 2.2. The OFHC Cu used in the Thesis is treated 'as-received', the material shows a texture effect due to the process of extrusion. Therefore, an initial anisotropy is induced. The values of isolines indicate that material can be treated as anisotropic.

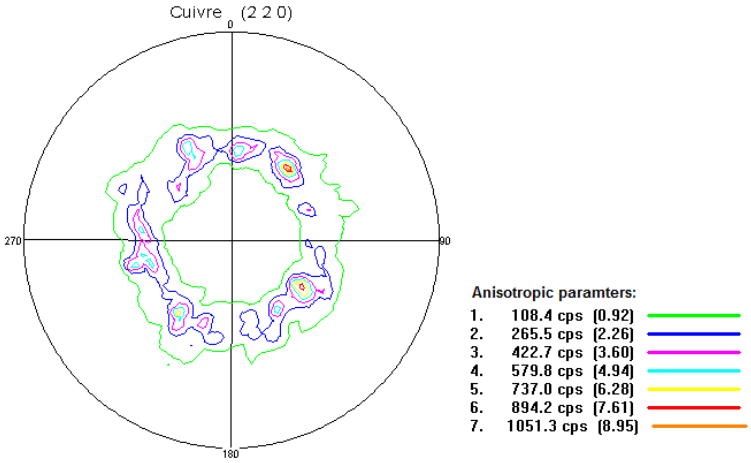

Figure 2.2: The pole figure for OFHC Cu.

Usually annealed OFHC Cu is considered as isotropic material, [Jankowiak et al. 2011]. However, the material used for the purposes of the Thesis is 'as-received', consequently it can be treated as initially anisotropic. Results of double shear test allow to asses if the shear strength differs from the Huber-Mises relation, Eq. (4.11). Concerning the difference in strengths - the tension and compression tests must be performed to obtain value of SD parameter κ. Usually, in the literature (e.g. [Jankowiak et al. 2011; Rittel et al. 2002b]) the SD parameter is close to 1.

Because of the important applications of Oxygen Free High Conductivity Copper in several industries, research on its behaviour and properties are rich and varied - this is echoed in the literature. Over the years, various studies concerning mechanical properties of OFHC Cu, its description and applications to advanced technologies on the basis of differently defined theoretical background. An understanding of the basis of microstructure, physical phenomenons driving deformation allows for accurately predicting material response for loading.

Recovery and recrystallization in OFHC

OFHC Cu demonstrates softening due to static and dynamic restoration processes, static thermal recovery and recrystallization, [Tanner 1998; Tanner and McDowell 1999; Doherty et al. 1997]. Recrystallization is an important issue in the thermomechanical processing of copper because it restores a worked metal to an unworked and formable state. It is possible to find in literature a OFHC copper called 'annealed'. In this case a heat treatment is done allowing process of recrystallization. The yield stress reduced and changing hardening.

The grains after manufacturing processes get elongated in the direction normal to the direction of applied force. The material gets strain hardened, i.e. its yield strength and hardness increase while ductility decreases. The strain hardening occurs because the dislocation density increases due to cold deformation. With increase in temperature the movement of dislocations gets easier and they readjust due to stresses locked in the lattice. Some dislocations having opposite sign may annihilate each other. This is a recovery process in which the residual stresses are reduced, however, the enhanced properties due to cold working are only little affected,

[Juneja 2010]. Due to the recovery in OFHC Cu, the density of local dislocations continuously increases, which creates instabilities in the substructure and recrystallization processes become possible, [McQueen and Jonas 1975].

Recrystallization is the process of new grains forming and growing through the material resulting in new regions of low dislocation density. Large numbers of dislocations are eliminated during recrystallization. Dynamic recrystallization occurs when the nucleation and growth occurs concurrent with straining under stress, [Kostryzhev 2009].

The average grain size decreased during the deformation conditions when the flow stress exhibited a single peak, which is consistent with grain refinement. During the deformation conditions when oscillations in the flow stress occurred, the average grain size increased, consistent with grain coarsening. These observations indicate that the softening observed at temperatures above 270°C, [Tanner 1998], are due to the changes in grain structure resulting from recrystallization. The effect of recrystallization is to change the grain structure which results in the reduction of the steady state flow stress. The initial peak strain, the strain corresponding to the peak in flow stress, decreases with increasing temperature at the same strain rate. The observed softening is consistent with the softening data shown in Fig. 2.3. A greater amount of softening occurs with increasing time.

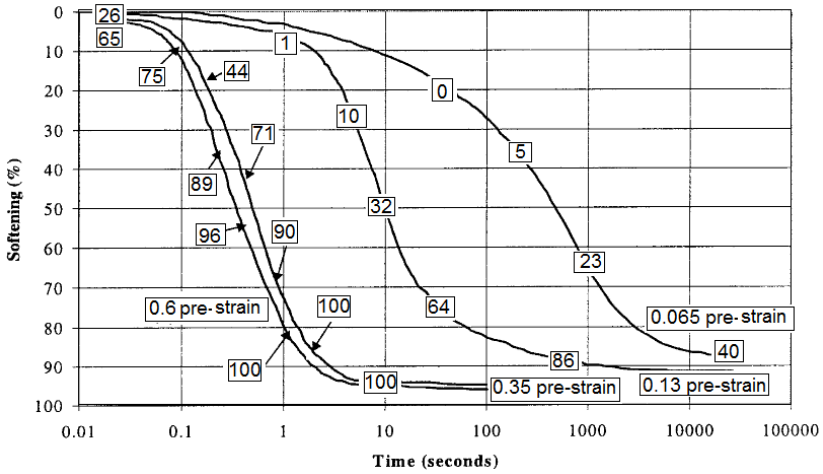

Figure 2.3: Relationship between softening and fractional amount of recrystallized grains in Cu [Kwon and DeArdo 1990]. Numbers in boxes represent the volume percentage of recrystallization.

In the case of adiabatic conditions of deformation the relation describing thermal softening is combined with the energy balance principle:

$$\Delta T(\varepsilon, \sigma) = \frac{\beta}{\rho C_p} \int_{\varepsilon_0}^{\varepsilon_{max}} \sigma d\varepsilon \tag{2.4}$$

where β is the Taylor-Quinney coefficient, ρ is the material density and C_p is the specific heat at constant pressure.

The macroscopic softening associated with recovery is attributed to the loss of dislocations which were generated and trapped by obstacles during deformation. The effect of pre-strain

in a material increases the kinetics of static recovery, [Kwon and DeArdo 1990]. Authors observed a significant increase in the amount of static recovery which occurs when the pre-strain is increased. The overall activation energy for recovery is often lower than for recrystallization.

After static recovery has occurred, another and often greater decrease in strength occurs through static recrystallization. Recrystallization results in the formation and growth of new grains which have lower dislocation densities than the worked grains they replace. Once nuclei are formed, the new grains grow into the deformed material by the migration of their boundaries. The driving force for the grain growth is provided by the difference in dislocation density between the interior of the new grain and the surrounding deformed material. As the new grains grow, the driving force decreases. In Fig. 2.4 the stages of static restaration are shown. On initial straining (A - B), static recovery can occur. At strains above B, which reflects the critical strain for recrystallization, both recovery and recrystallization occurs. C is the strain associated with the peak stress. Between C and D, both meta-dynamic and static recrystallization along with recovery occurs, [Tanner 1998].

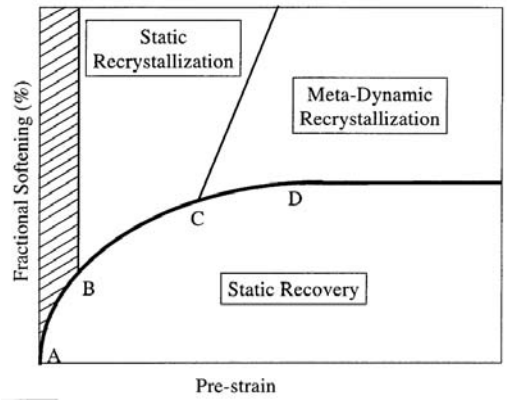

Figure 2.4: Categories of static restoration, [Tanner 1998].

When crystalline materials are deformed at elevated temperatures, the accumulated dislocations are continuously demaged by restoration processes. Recovery and recrystallization are the restoration processes that result in the release of the internal energy stored during deformation. These restoration processes returns the material, partially or completely, to its condition prior to deformation. When these changes occur concurrent with straining under stress, they are termed dynamic, and static in the absence of stress. The stacking fault energy of a material controls the ability of dislocations to cross-slip onto different slip planes. In materials of high stocking fault energy, dislocations cross-slip and recovery occurs readily, reducing the internal strain energy. During the deformation of low to medium stocking fault energy materials, dislocations are unable to cross-slip and recovery processes are partially inhibited. Due to the weak recovery in OFHC Cu, the density of local dislocations continuously increases, which creates instabilities in the substructure and recrystallization processes become possible, [McQueen and Jonas 1975].

The average grain sizes of OFHC Cu deformed in compression under various deformation conditions were determined in [Tanner 1998]. The investigation of the average grain sizes also indicates that recrystallization occurred. Single peak softening, flow stress reduction after

reaching apeak stress, is associated with grain refinement while multiple peak, oscillations in the flow stress, occurs during grain coarsening, [Tanner 1998]. The grain size decreases, from $59\mu m$ at 25°C to $27\mu m$ at 286°C and then starts to increase as the temperature rises further, Fig. 2.5. The grain size decreases with decreasing strain rate during deformation in compression at 269°C. The average grain size decreases from $51.8\mu m$ at $1.0s^{-1}$ to $31.3\mu m$ at $0.0004s^{-1}$. The nucleation of grains is driven by the stored energy of dislocations and requires an incubation time. Lower strain rates permit the nucleation of new grains and their subsequent growth.

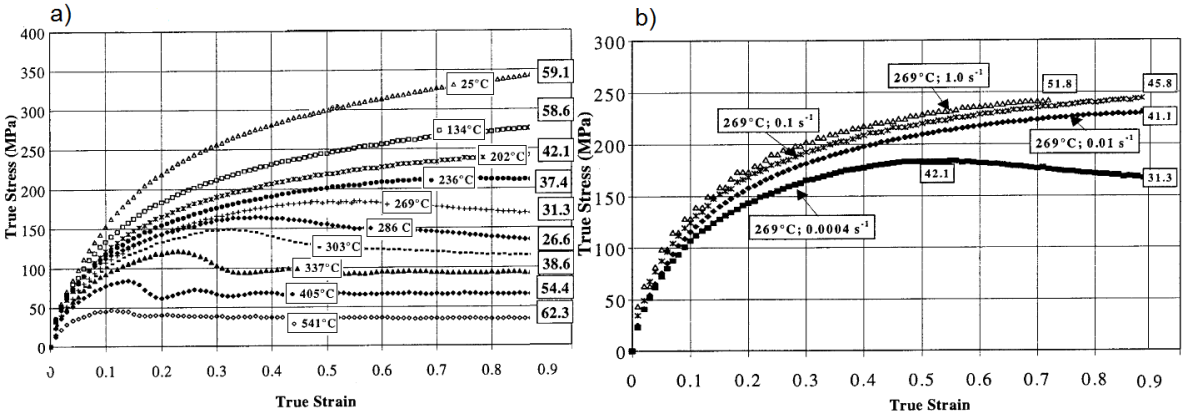

Figure 2.5: a) Average grain sizes for OFHC Cu from compression at constant strain rate 0.0004 s^{-1} at isothermal experiments, b) average grain sizes for OFHC Cu from compression at 269°C and various constant strain rates: 0.0004 s^{-1} and $1s^{-1}$. The sizes (μm) are shown at the corresponding strain and temperature, [Tanner 1998].

The mechanical properties depend upon the grain size, the relationship between grain size and flow stress is given e.g. by the Hall-Petch formula. Also Bonnavand, Bramley and Mynores model, [Bonnavand et al. 2001; Juneja 2010] incorporate effects of strain, strain rate, temperature, grain size and re-crystallization in yield strength description.

Constitutive models with an evolutionary relation which results in a balance between hardening and recovery of various forms, and the capability of compensatory softening at increasing temperature to account for the peak stress behavior and dynamic recrystallization effects has been a challenge for the researches. Consequently, there are few models which more or less properly approximate the behaviour of FCC metals, especially OFHC Cu.

Discussion of the constitutive models for OFHC Copper

An understanding of the microstructural processes of large strain deformation is necessary for proper macroscopic constitutive modeling. The OFHC Cu is a material of face-centered cubic structure. For such materials the dislocation gliding, is the most common mechanism. Dislocations move through the crystalline material and encounter obstacles to subsequent motion. Obstacles to dislocation motion, such as other defects, inhibit motion, requiring increased applied stress for continued motion. The relation between applied loading and plastic strain rate is largely determined by how these obstacles are overcome. Dislocation motion past obstacles is affected by the deformation conditions, including strain rate and temperature. Dislocation motion results from both applied stress and statistical fluctuations due to

thermal vibrations. Long range obstacles cannot be thermally assisted while short range obstacles can be overcome with thermal assistance. At equilibrium and 0K, the force required for a dislocation to proceed past a set of obstacles is called the mechanical threshold stress and is a measure of the resulting strength due to the particular obstacle configuration. Dislocations that overcome one set of obstacles will then move until another obstacle array is encountered. At temperatures above 0K, thermal activation assists the dislocation in proceeding past obstacles. As temperature increases above 0K, the stress required decreases. Dislocations are thermally assisted past short-range obstacles until the athermal stress level is reached. Athermal stress is the measure of the long range obstacle strength. Increasing the strain rate reduces the time available for thermal assistance resulting in increased stress levels. The investigation and understanding of microstructure are necessary to apply the the constitutive model. For FCC materials, co for OFHC Cu, there have been developed few viscoplasticity models describing the bahviour of material under large deformation in a wide range of strain rates.

FCC metals use to exhibit large strain hardening due to an increase in the amount of dislocation interactions with increasing strain, [Seeger 1957]. Strain hardening tends to be highly temperature and strain rate dependent, while the yield stress uses to have reduced dependence to such effects. FCC material represents high dependence of plastic strain on the volume thermally activated, strain hardening strongly varies with strain rate and temperature, [Nemat-Nasser et al. 1998a]. The behaviour of FCC metals can be precisely described by advanced constitutive relations. There could be citepd: the BCJ-SNL model, [Bammann et al. 1990], the Mechanical Threshold Stress model, [Klepaczko and Chiem 1986; Follansbee and Kocks 1988; Klepaczko 1988; Rusinek and Klepaczko 2001], and the McDowell model [Moosbrugger and McDowell 1990; McDowell 1992], the Molinari- Ravichandran model [Molinari and Ravichandran 2005] or Voyiadjis-Almasri model [Voyiadjis and Almasri 2008], are fit to isothermal, constant true strain rate data for compression and then compared to the experimental results for various deformation condition sequence experiments. Proposals for constitutive models characterizing FCC materials for the example of OFHC Cu, e.g.: [Khan and Cheng 1996; Liang and Khan 1999; Khan and Cheng 1998; Nemat-Nasser et al. 1998b; Frutschy and Clifton 1998; Molinari and Ravichandran 2005; Voyiadjis and Almasri 2008; Rusinek et al. 2010; Gao and Zhang 2010; Rodríguez-Martínez 2010; Rodríguez-Martínez et al. 2009]. The relation of the Modified Rusinek-Klepaczko model (MRK) and the Molinari-Ravichandran model (MR) which describe the behaviour of FCC metals are presented in the Appendix 1.

Experimental data for compression tests conducted with the strain rate of quasi-static and dynamic range have been presented in works, e.g.: [Rodríguez-Martínez 2010; Follansbee 1985; Nemat-Nasser et al. 1998b; Tanner and McDowell 1999; Liang and Khan 1999; Lennon and Ramesh 2004; Molinari and Ravichandran 2005; Voyiadjis and Almasri 2008; Rusinek et al. 2010; Zhang and Shim 2010; Jankowiak et al. 2011].

The wide spectrum of OFHC Cu data in different strain rates, temperatures under various loading conditions can be found in [Tanner 1998].

Beneath there are presented the short descriptions of constitutive relations which could be apply for FCC metals. In Fig. 2.7 there are examples of their applications in different strain rates at room temperature for OFHC Cu. Models were validated by [Tanner 1998] for obtained in his paper experimental results.

The Zerilli-Armstrong model [Zerilli and Armstrong 1987] is an empirical model which, like the Johnson-Cook model, has been successfully used, particularly for highs train rate applications. This model has a physical basis linked to thermally activated dislocation motion (Andrade, et al, 1994). This model was developed to be simple and easy to use for large scale predictive computations (Gray, et al, 1994). This model and its modificiation (Goldthorpe, 1991) include temperature dependence through the shear modulus, the Hall-Petch strengthening parameter and an athermal stress component are accounted. The strain rate sensitivity and the temperature-dependence influence on flow stress are included. The approach does not represent any thermal or strain rate history effects.

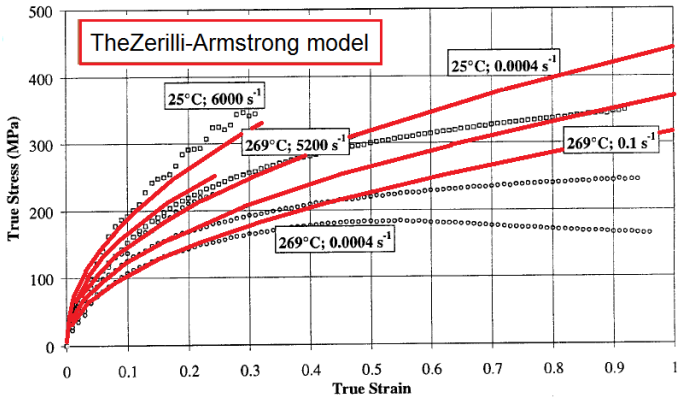

Figure 2.6: Correlation to OFHC Cu data using the Zerilli-Armstrong model. The model is shown using solid lines, while the experimental data are shown with open symbols, [Tanner 1998].

The McDowell model was formulated to have more flexibility to address strain rate and temperature history dependence [McDowell and Moosbrugger 1987; Moosbrugger and McDowell 1990; McDowell 1992, McDowell 2006, McDowell 2011]. It is a physically-based model developed to address slip in polycrystalline FCC metals. Constitutive relations are provided for the kinematics, kinetics, and substructure of FCC metals with micron-scale grains. The main innovative feature of this work is the treatment of the dislocation substructure in the weak shock loading regime. Here, the mobile and immobile dislocation densities are assigned as internal state variables and path-dependent differential equations are formulated for their evolution. This enables physical descriptions of slip resistance and the plastic low rate.

Klepaczko and Chiem (1986), Follansbee and Kocks (1988), and Klepaczko (1988) approach (called the Mechanical Threshold Stress Model - MTS) consists of a description of the material behavior at constant structure and a description of structure evolution during deformation. The observation that deformation in a polycrystal occurs by the accumulation and motion of dislocations with the rate-controlling mechanism being the interaction of dislocations with defects is accounted. The proposal is established as a direct relation between dislocation behaviour and macroscopic behaviour. Evolution of microstructure is considered to be a bal-

ance between dislocation accumulation and dynamic recovery processes. Dynamic recovery processes occur by dislocation cross slip which is both thermally activated and stress assisted. The modification and extension of Klepaczko concept have been proposed by [Rusinek et al. 2007] Rodriguez [Rodríguez-Martínez 2010]. The RK and MRK relations are presented in Appendix 1.

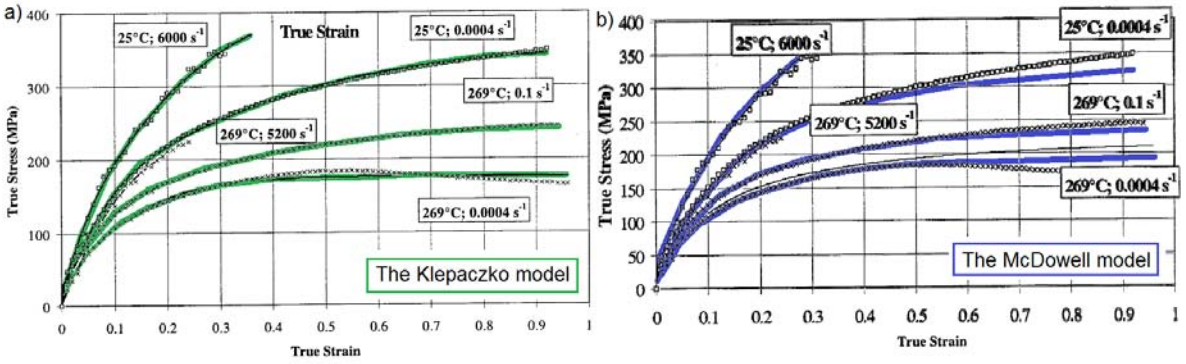

Figure 2.7: Correlation to OFHC Cu data using: a) the McDowell model and c) the Klepaczko model. The models are shown using solid lines, while the experimental data are shown with open symbols, [Tanner 1998].

Considering the results obtained by [Tanner 1998] who applied for obtained results various model, it can be concluded that the best fitting is provided by the Mechanical Threshold Stress Model. This observation is concerned only to strain rate sensitivity because in [Tanner 1998] and [Gaoa et al. 2012] there is remarked that the MTS model lacks capability to describe static thermal recovery and strain softening. However, in the presented Thesis the influence of temperature is not investigated. Consequently, the model proposed by Klepaczko and later, extended forms his approach are considered as suitable for modelling behaviour of OFHC Cu. To compare modelling with use of the modified Rusinek-Klepaczko relation (6.10) [Rusinek and Klepaczko 2001; Rodríguez-Martínez 2010], there has been chosen the Molinari-Ravinchandran relation (6.18), [Molinari and Ravichandran 2005; Durrenberger et al. 2008]. The proposal of Molinari-Ravinchandran is related to a characteristic length scale of microstructure which develop in metals during the deformation. For purposes of the Thesis there have been performed tests under different loading conditions in various strain rates at room temperature. The results of tests are presented in Chapter 5, Section 5.3. Basing on experimental results the yield curves due to Burzyński criteria (4.34), (4.45) is determined. Yielding of the OFHC Cu and its visualization represented by plastic surface was discussed , e.g.: [Hecker 1970; 1972a;b; Khan and Cheng 1998]. But, proposed by Hecker model is built on Malvern proposal (Section 4.4, Table 4.2) and it is non-convex.

In the next Section there is discussed the example of body-centered cubic material - it is a non-alloy structural steel E335, according to Standard EN 10025 - 2:2004 Technical delivery conditions for non-alloy structural steels

2.3 E335 - high strength steel

Structural steels with a ferrite-pearlite microstructure are widely used in civil, mechanical and chemical engineering. Increased working loads, reliability requirements, extreme temperature and chemically aggressive environments lead to an increased demand for high strength, combined with high toughness - what is assured by this kind of steels.

The use of welding as a joining method requires good weldability, for which the carbon content in a steel composition should be decreased. Together with the needs of good weldability, these have led to decreasing carbon content and increasing microalloying element level in the steel. A decrease in carbon content results in strength decrease, due to a decrease in the amount of the pearlite phase, [Kostryzhev 2009]. In steels the stress-strain curve depends on chemical composition. With an increase in carbon content the yield stress and the work-hardening exponent increase, Fig.2.8. The presence of spheroidal cementite particles in medium- and high-carbon steels prolongs Lüders strain and leads to work-hardening rate decrease, [Akiyama et al. 2002]. Alloying results in an upward shift of the stress-strain curve along the stress axis, which may happen due to phase balance change, grain refinement, solid solution and precipitation strengthening. The work-hardening exponent in carbon steels has been observed to be in the range 0.07 - 0.3 and decreases with an increase in strength, [Akiyama et al. 2002]. To overcome this strength drop, additions of different microalloying elements have been used to provide precipitation strengthening and grain size refinement. Thus, high strength structural steels are designed to provide better mechanical properties, weldability and greater resistance to atmospheric corrosion or pitting than conventional carbon steels.

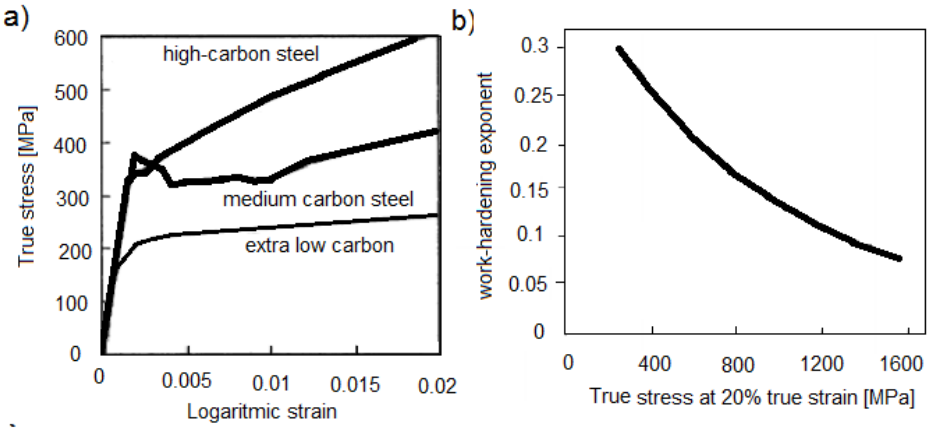

Figure 2.8: Stress-strain curve dependence on carbon content in ferritic steels, b) work-hardening exponent dependence on steel strength, [Kostryzhev 2009; Akiyama et al. 2002].

The steel industry can be considered as an indicator of economic progress, so it is a material of high importance for infrastructural and overall economic development, [Rusinek et al. 2009; Galán et al. 2012]. Applications of high strength steels include many industrial branches, e.g: oil and gas pipelines, heavy-duty highway and off-road vehicles, construction and farm machinery, industrial equipment, storage tanks, mine and railroad cars, barges and dredges, snowmobiles, lawn mowers, and passenger car components. Bridges, offshore structures, power transmission towers, light poles, and building beams and panels are additional

uses of these steels, [www.asminternational.org]. For many applications, the most important factor in the steel selection process is the favorable strength-to-weight ratio.

In next parts of the Section there are given information concerning mechanical properties of the studies steel which is E335 steel. According to Standard describing studied steel (EN 10025 - 2:2004 Technical delivery conditions for non-alloy structural steels) E335 steel is characterized by good formability and weldability according to its grade. It also offers improved weldability, formability, and toughness resulting from the specified alloying elements with limitations on carbon, sulfur, and residual element contents. The strength to weight ratios make them useful in structural applications, [Nemat-Nasser et al. 1998a; Galán et al. 2012]. Some physical properties of E335 sttel are reported in Table 2.1.

Magnitude	Symbol	Numerical value	Unit
Density	ρ	7,85	kg/dm3
Melting point	T_{mp}	≈1530	°C
Specific heat	c	0,50	kJ/kg°K
Thermal conductivity	λ	≈58	W/m°K
Thermal expansion coefficient	α	12 x 10-6	1/°K
Specific resistance	ρ	140...250	nΩm
Elastic modulus	E	210000	MPa
Shear modulus	G	78500	MPa
Poisson's ratio	v	0,3	–

Table 2.1: E335 steel. Physical properties of structural steel in temperature +20°C according to specification of producers, [www.ruukki.com].

Standard EN 10025-2 defines conventional structural steels in three yield strength classes 275/355/420 MPa. The tensile strength is bonded with the hardness. In the producent webside [www.ruukki.com] there is reported approximate conversion of hardness–to–tensile–strength values of steels. The hardness test performed on the studied steel turn out the value 210 in Vickers hardness HV10 scale. What according to table presented in the producent webside is suitable to the tensile strength equals to 675 MPa. Results of tension test are reported in Section 5.4 in Chapter 5. The obtained experimental value of tensile strength proves the approximation of this value obtained due to conversion table is proper.

Phase formation and their influence of properties of steel

It is possible to give a wide range of mechanical properties to steels by changing the size ad shape of the grains or changing its microconstituents. This property owes to several different ways that austenite can decompose according to increasing temperature and carbon content. The dependence between cooling temperature and carbon content is precedented in the phase equilibrium diagram. The Iron-Carbon phase diagram for steel is a complex graphs

showing conditions at which thermodynamically distinct phases can occur at equilibrium. The percentage of carbon present and the temperature define the phase of the iron carbon alloy and therefore its physical characteristics and mechanical properties. Consequently, properties of steel depends on composition and heat treatment.

Because the strength and toughness of steels can be enhanced by thermomechanical processing through grain refinement, dislocation hardening, strain induced precipitation of fine micro-alloying carbide particles the have been many studies concerning manufacturing processes or weldability. The better weldability of high strength steel allows a decrease of up to 50% in the total fabrication costs of components and structure, [Montemarano 1986]. The mechanical properties along with microstructures of steel are obtained due to forging and cooling, different cooling rates results in different properties of steel, what is studied in [Das et al. 2003].

A suitably performed process of steel manufacturing and heat treatment allows to obtain steel of higher strength. This is a reason, why conventional steel E335 for which the yield strength is supposed to rather low, has a yield strengths much higher - close to 550MPa.

Hardness and its relation with the yield strength

Generally, strength of a steel is proportional to its hardness, the higher the hardness, the stronger the steel. The standard method for measuring the hardness of metals, particularly those with extremely hard surfaces, is obtained due to application a standard pressure for a standard length of time by means of a pyramid-shaped diamond. The method is called the Vickers Hardness Test, hardness obtained in the test is signed as H_V. A correlation may be established between hardness and some other material property such as tensile strength, it covers also several other properties as resistance to deformation, resistance to friction and abrasion, [Cahoon et al. 1971; DeFries 1975]. In [Cahoon et al. 1971] it is shown that for offset strain equals to 0.2% the yield strength can be obtained from the expression:

$$\sigma_Y^T = \frac{H}{3} 0.1^{m-2} \approx 3.2 H_V \tag{2.5}$$

where H is the diamond pyramid hardness and m is Meyer's hardness coefficient which is bonded with strain hardening coefficient n, $n = m - 2$.

The relation was originally proposed in [Tabor 1951] for ultimate tensile strength. Authors of [Cahoon et al. 1971] derived the general expression correlates the yield strength with hardness, including the strain rate hardening coefficient. The Eq. (2.5) holds for brass, steel in either the cold rolled or tempered condition, and aluminum alloys in either the cold rolled or aged condition. To present the discussed material, the chemical composition obtained due to spectroscopic study is discussed, the microstructure is also analysed.

Chemical composition and microstructure analysis

The samples to microstructure, texture and chemical analysis were obtained from the middle of a rod from which specimens were cut. The analysed surfaces have been perpendicular to the direction of extrusion. The chemical composition obtained by the mean of the spectroscopic analysis is presented in Fig. 2.9 and Table 2.2.

Component	Mass [%]	Mass at. [%]
Si	0.3	0.6
Mn	0.75	0.76
Fe	98.95	98.24
Together	100	100

Table 2.2: E335 steel. Chemical composition obtained due to spectroscopic analysis.

The examined steel has a low carbon content (probably lower than 0.25 % of C) which spectrum is not recognized by the apparatus. The C content assures adequate formability and weldability. The amount of Mn is estimated as 0.75 wg., Si 0.3 wg. and Fe 98.85wt. The addition of Mn and Si allows for carbon compatibility. These additive elements generate carbides which increases strength of steels. Manganese reduces the brittleness of the steel, also helps to remove excess oxygen from molten steel. For C-Mn steels, increase in carbon content leads to an increase in pearlite content. At constant Mn content an increase in tensile strength is observed, which is due to a faster work hardening rate. An increase in Mn content lowers the eutectoid composition of carbon increasing the pearlite proportion, while Mn contributes to strength via solid solution strengthening and grain refinement, [Kostryzhev 2009].

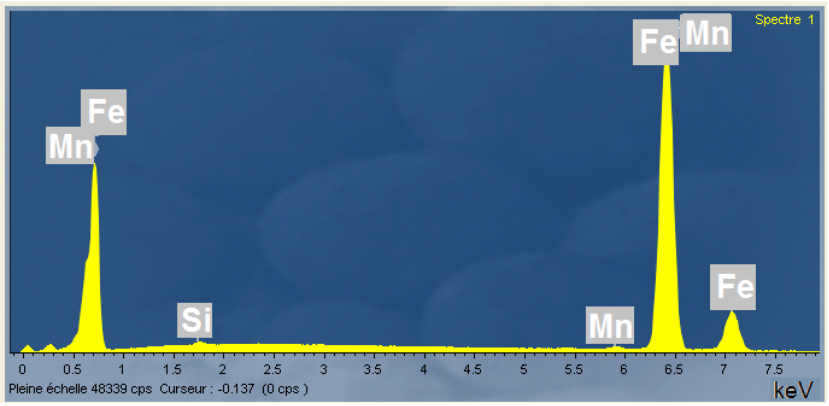

Figure 2.9: E335. Chemical composition.

The microstructure of the selected steel is analysed using SEM technique. Analysis of the images reveals that E335 steel is a ferritic-pearlitic steel where layers of pearlite lie between whole grains of ferrite. In Fig. 2.10 ferrite is represented by darker areas while pearlite is displayed in light grey. The analysis of microstructure image shows a banded arrangement of pearlite in the ferrite matrix. Average ferrite grain size is estimated about $15\mu m$ and perlite about $20\mu m$. The shape of the matrix grains is prismatic, the pearlite regions depending on the size and shape can be classified as elongated or prismatic ones. It can be summarized that no direction is extinguished, the structure can be treated as isotropic. It is known that ferrite have lower strength and hardness, but higher plasticity and toughness, whereas pearlite has reversed properties. The ferrite-pearlite steels, which contain respectively small amount of C (generally, less than 0.10%) must contain additions of strong carbide or forming from it elements for precipitation strengthening, grain refinement, and possibly transformation temperature control. Ferritic steels have a BCC kind of structure, [Tewari et al. 1966; Kostryzhev 2009].

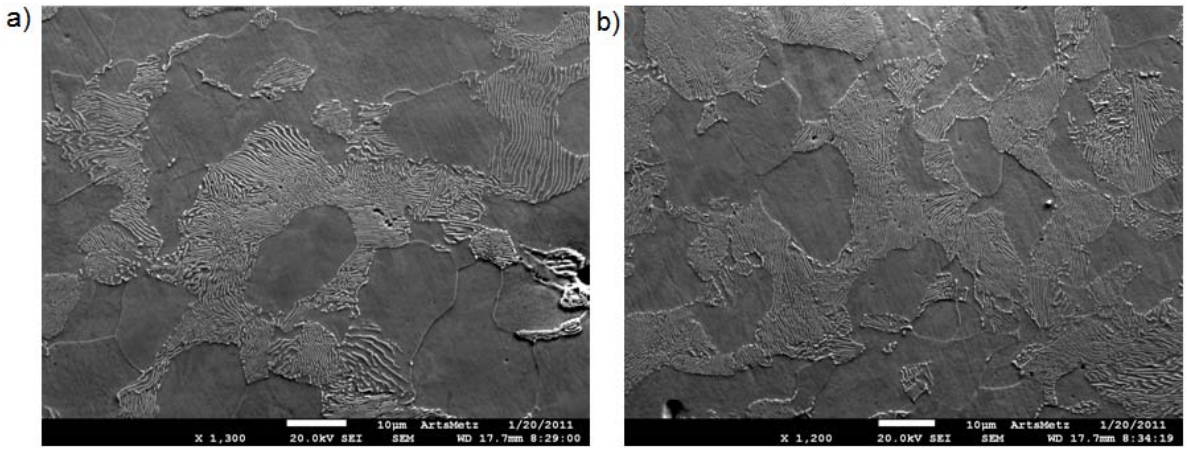

Figure 2.10: Metallographic section at a) 1300x and b) 1200x magnification.

Owing to the pole figures in the orientation {110} (Fig. 2.11) it can be noticed that E335 shows no anisotropic structure of the material - values suitable to isolines are smaller than 4. Therefore, the material can be considered as an isotropic material.

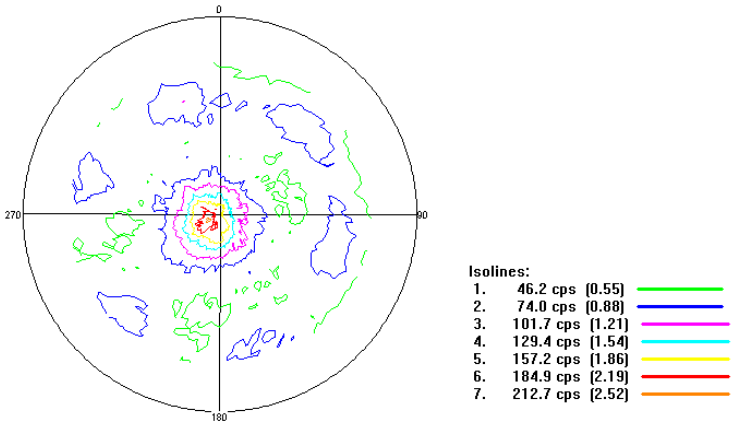

Figure 2.11: The pole figure for E335 in the orientation {110}.

As a traditional metal, steel has been the subject of extensive study in the past few decades, both experimentally and theoretically.

The constitutive models for BCC material

Compression tests under a wide range of strain rates and temperatures have been discussed in [Rusinek et al. 2009; Nemat-Nasser et al. 2001; Rodríguez-Martínez et al. 2009], [Gaoa et al. 2012]. To describe the thermo-visco-plastic behaviour of different high strength steels which are discussed in cited works, there should be used models taking into account strain hardening, strain rate and temperature sensitivity. Micro-mechanism of plastic deformation in the case of ferritic steels is dominated by dislocation gliding, what should be assumed in the constitutive relations desiring the material, [Rusinek et al. 2009]. In the absence of recrystallization, an increase in dislocation density results in an increase in yield stress, however toughness and ductility may decrease, [Kostryzhev 2009].

In [Rusinek et al. 2009; Rodríguez-Martínez et al. 2009] the Rusinek and Klepaczko (RK) model [Klepaczko and Chiem 1986; Rusinek et al. 2005; 2007] is applied for six different steels ferritic and austenitic, Eq. (6.9). In [Nemat-Nasser et al. 2001] a physicallybased model proposed by authors is used to high strength low alloy steel. The results in both cases are compared with modelling of the Johnson-Cook relation. In [Gaoa et al. 2012] there are discussed constitutive relations proposed by other authors describing dynamic thermo-mechanical response of BCC steel.

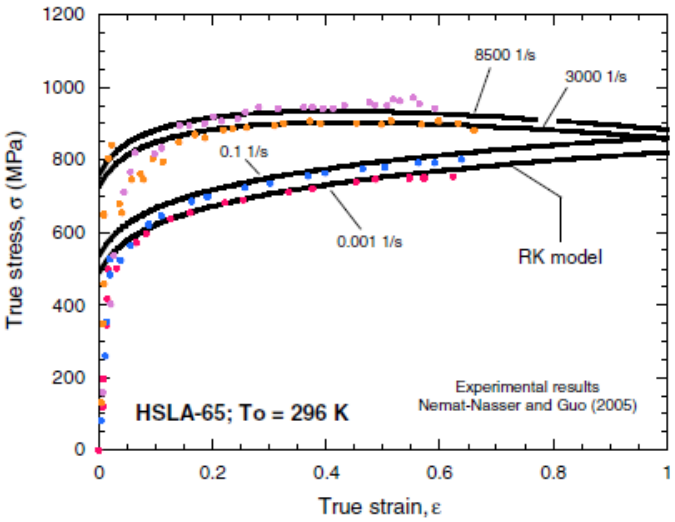

Figure 2.12: Strain rate sensitivity of HSLA-65 steel, comparison between RK model and experimental results, [Rusinek et al. 2009].

It can be stated that in the absence of dynamic strain aging, the RK and MR models predictions are in good agreement with the experimental results over a wide range of temperatures and strain rates. Models predict correctly the strain rate effect on plastic behaviour, also thermal softening due to adiabatic heating at high strain rates is properly modelled. Fig. 2.12 presents examples of application of the RK constitutive model for HSLA 65, the results are obtained in quasi-static and dynamic range of strain rate.

Consequently, it could be assumed for BCC that plastic deformation is dominated by dislocation gliding, which reduces the work hardening and the level of failure strain. Also, the plastic flow stress is strongly depended on the temperature and the strain rate. The microstructure of the material does not evolve in a manner to affect its flow stress, as the temperature and strain rate are changed. Strength of BCC steels is not temperature-sensitive at high temperatures, because when the temperature exceeds the room temperature, the flow stress of this material decreases at a rather low rate with increasing temperature. Thus, the material has good weldability.

It is difficult to find works which investigate into yield surfaces of high strength steel and yield dependence on strain and strain rate. In Paragraph 5.4, the experimental results under different loading conditions in different strain rates are presented and discussed. Then, basing on them the yield state of E335 is determined. There are also presented visualizations of yield surfaces and their cross-sections.

Another group of material for which the Burzyński criteria are applied are amorphous polymers. In next Section there are presented exemplary polymers - polycarbonate and biopolymers basing on corn. The stypy of literature is given concerning their mechanical properties.

2.4 Mechanical properties of chosen polymers

A polymer is a chemical compound or mixture of compounds consisting of repeating structural units created through a process of polymerization. Nowadays, the usage of polymer materials in structural applications is increasing due to combination of easy processability and mechanical properties. To ensure proper operation the polymers have to fulfils specific requirements regarding quality, safety, and mechanical performance (e.g. stiffness, strength and impact resistance). Consequently, the researches according the mechanical properties of polymers become more comprehensive and throughout. There are many groups of polymers classified due to broad classes of compounds, both natural and synthetic, with a wide variety of properties. In the Thesis, more insight analysis is devoted to the mechanical properties necessary to obtain yield surface of polycarbonate (PC), polylactic acid (PLA) and PLA/PBAT - a polymer with different proportion of PLA and Poly butylene adipate-co-terephthalate (PBAT).

For purposes of the Thesis, there have been performed strength experiments concerning PC: tension, compression and shear in the quasi-static strain rate. There have been also performed strength tests of PLA. Detailed characteristics of PLA/PBAT under tensile and compressive loading in different strain rates can be found in [Nihida et al. 2011; Nishida et al. 2012], data are also used to present comparison between yield surfaces of pure PLA and PLA/PBAT.

Basing on the results of the experimental tests and data found in the literature the yield surfaces of investigated polymers are obtained. The results of mechanical tests, discussion on them and resulting yield states together with their visualization are presented in Section 5.5.

Mechanical properties of Polycarbonate (PC)

Polycarbonate (PC) is an amorphous polymer with a glass transition temperature above room temperature. The PC glass transition temperature is of the order 148°C, and a beta relaxation temperature of the order -60°C. Amorphous glassy polymers are main components in many industrial and commercial products, such as automotive lighting, bus windows, http://www.poliweglan.com. PC is a light-transmissive material with a high resistance to heat and acids, widely used for its optical and mechanical properties. It has a good thermal resistance what makes it useful in the building industry, it is used for noise barriers, roofs, roof-windows, http://www.poliweglan.com. The material is also used in extreme temperature and loading condition such as impact-resistant aircraft windows. The increase in using polymers for several industrial applications leads to a strong need for the development of constitutive models dedicated to the simulation of the behavior during the manufacturing process or during the in-service phase.

Since the beginning of polymer science, numerous experimental studies have been carried out on polymers to characterize the mechanical behaviour as a function of temperature and strain rate. Among these studies, a great deal of attention has been given to the yield stress, e.g.: [Bauwens-Crowet et al. 1969; 1972; Shaban et al. 2007; Altenbach and Zolochevsky 1996; Altenbach and Tushtev 2001; Mulliken and Boyce 2006; Richeton et al. 2006; Ghorbel 2008].

Polymers are known to exhibit a strongly pronounced rate and temperature-dependent behavior and display non-linear responses during loading and unloading. Significant inelastic deformation, denoted as viscoplastic, may be observed even at very small deformation levels, [Shaban et al. 2007; Ghorbel 2008; Matadi Boumbimba et al. 2012]. The yield stress increases for the low temperatures as well as for the high strain rates. Strain rate and temperature are known to significantly influence the mechanical behavior of polymers. Concerning the stress–strain behavior the mechanical response at the low strain rates first is that an initial elastic response followed by yielding, strain softening and then a strain hardening. The yield stress increases with an increasing strain rate especially at high strain rates. The initial Young's modulus appears also to be strain rate dependent. Whereas, the yield stress and the initial Young's modulus are found to decrease with an increasing temperature; a similar effect is also observed for the strain hardening rate. This corroborates that the temperature rises at high strain rates controls the strain hardening rate, which depends itself on temperature. The closer the temperature is to the glass transition temperature, the lower the strain hardening rate.

For polycarbonate the yield stress in compression is greater than that in tension as observed e.g. in [Spitzig and Richmond 1979]. Many authors, e.g.: [Bauwens-Crowet et al. 1969; 1972; Shaban et al. 2007; Altenbach and Zolochevsky 1995; Mulliken and Boyce 2006; Richeton et al. 2006; Ghorbel 2008] have similar conclusions concerning also other polymers, like polymethil methacrylate (PMMA).

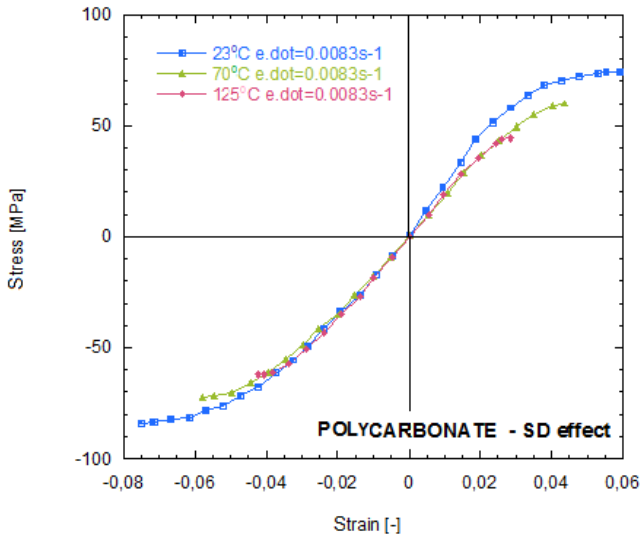

Figure 2.13: Experimental results of polycarbonate at different temperatures at quasi-static strain rate, [Shaban et al. 2007].

Fig. 2.13 presents the results of the uniaxial tensile and compression true stress–true strain curves of polycarbonate at strain rate equals to $8.3\text{x}10^{-3}s^{-1}$ and at three different temperatures (23°C, 70°C and 120°C). The pictures is a part of a study [Shaban et al. 2007]. Concerning the stress–strain behaviour, the mechanical response at the low strain rates is: an initial elastic response followed by yielding after which a plastic instability occurs. The results are shown for strains less than 8%. In [Richeton et al. 2006; Mulliken and Boyce 2006] there have been found the results of compression test in the wide range of strain rate and temperature. Data are shown in Fig. 2.14.

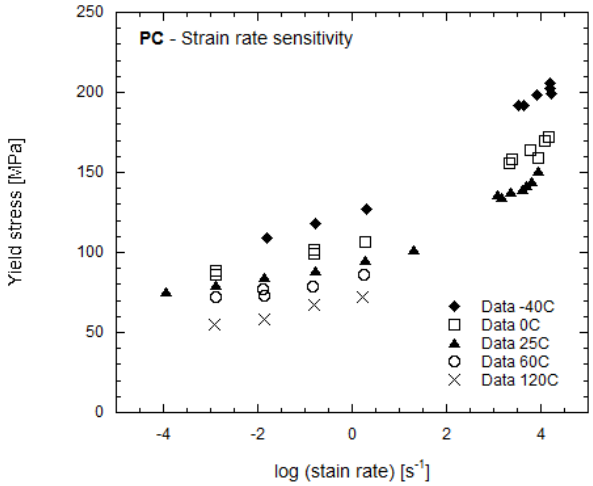

Figure 2.14: Polycarbonate. Strain rate and temperature sensitivity for different strain rates and different temperatures, [Richeton et al. 2006].

Looking at the Figs. 2.13 and 2.14 some observations can be noticed concerning the discussed material. The yield stress increases with increasing the strain rate, especially at high strain rates. A similar increase of the yield stress is observed at lower temperatures. Secondly, the yield stress in compression is higher than that in tension for the same strain rate and temperature. Increasing the strain rate, decreasing the temperature or applying a compression to the specimen gives the molecular chains less room to move, what reduces their mobility by making them stiffer. That means, the material needs extra energy to increase the yield stress, [Shaban et al. 2007].

The deformation of polymers are greatly effected by the hydrostatic pressure, as shows the difference observed between the stress-strain curves in uniaxial tension and uniaxial compression. This effect also leads to a pressure dependence of the yield stresses. The effect of hydrostatic pressure on the yield behavior of polymers was demonstrated experimentally in, e.g.: [Raghava et al. 1973; Theocaris 1995; Altenbach and Tushtev 2001; Ghorbel 2008; Khan and Farrokh 2010]. In contrast to metals, for polymers, the yield stress is often assumed to be equal to the maximum stress in the stress-strain curve. The general effect of hydrostatic pressure on the mechanical properties of polymers consists in increased yield stresses. Generally, SD parameter for different polymers varies from 1.1 to 1.3, [Raghava et al. 1973; Theocaris 1995].

Mechanical properties of biopolymers (PLA) (PLA/PBAT)

The increasing use of plastic products worldwide is causing considerable damage to the environment, differently than metals which are easily recoverable and recyclable, plastics wastes do not decompose easyly and fast. What is worse, plastics are more than 12 percent of the municipal solid waste stream, a dramatic increase from 1960, when plastics were less than one percent of the waste stream, [http://www.epa.gov/].

One way of solving problem with plastic wastes problem is introducing the concept of iso-functional recycling as recycled materials are increasingly used in design of structural components, [Bahlouli et al. 2012]. In works [Pessey et al. 2008; Bahlouli et al. 2012] the effect of recycling on the properties and durability of plastics. The recycling effects on two high impact polypropylenes (HiPP) are studied. The recycling process was simulated by performing several extrusion runs with the same material in order to get a better understanding of the multi recycling effects.

Another solution are biodegradable plastics - and such material are discussed in further parts of the Chapter. The biodegradable plastics (plastics that can decompose in the natural environment) and biomass plastics (plant-derived or recyclable-resource-based plastics) are recently extensively investigated, and new biodegradable and biomass plastics are continuously developed. The input materials for the production of these polymers may be either renewable (based on agricultural plant or animal products) or synthetic. Biopolymers are biodegradable, less expensive and more environmentally friendly in the process of production and distribution of wasted material. Biopolymers can be used in many industries: the textile industry, the production of plastic cutlery and bags, but also as interior part of cars, computers and cell-phones, in medical applications, packaging and confectionary, [Nihida et al. 2011; Nishida et al. 2012]. Biopolymers have been recognized as a promising alternative material for petroleum-based plastics.

Polylactic acid (PLA) is a typical biodegradable biomass polymer (plant-derived polymer), it is derived from the corn. PLA is a linear aliphatic thermoplastic polyester, produced from renewable resources and readily biodegradable, as an alternative to conventional polymers, such as polyethylene (PE), polypropylene (PP), polyethylene terephthalate (PET) and polystyrene (PS). Poly(lactic acid) is produced by ring-opening polymerization of lactide, and the lactic acid monomers are obtained from the fermentation of sugar feed stocks, [Carrasco et al. 2010]. Poly(lactic acid) has numerous interesting properties including good mechanical properties, thermal stability, processability and low environmental impact. PLA presents quite interesting properties if compared to commodity polymers as shown in Table 2.3, [Carrasco et al. 2010]. It can be highlighted that PLA presents the highest mechanical properties, but the lowest thermal resistance. However, when the applications allows, this polymer presents some advantages like good processability in conventional industrial transformation equipments and biocompatibility, Carrasco 2010: [Carrasco et al. 2010].

However, as a crystalline polymer, PLA is very brittle and its low toughness limits its application. Polymer blends/alloys or natural fiber reinforcing have been used to overcome the brittleness and low impact resistance of PLA. To improve resulted bio-material, PLA have

been blended with other flexible polymer: **Poly butylene adipate-co-terephthalate (PBAT)** as the blending polymer. PBAT is fully biodegradable and flexible, though its Young's modulus and tensile strength are inferior to PLA, breaking strain is much higher than PLA, [Yamura et al. 2009; Nihida et al. 2011; Nishida et al. 2012]. Polymer alloys of PLA and PBAT have great potential for the industry because of its better ductility and higher impact strength.

	PLA	PS	i-PP	PET
Relative density	1.24	1.04-1.06	0.91	1.37
Clarity	Transparent	Transparent	Translucent	Transparent
MECHANICAL PROPERTIES				
Tensile yield strength (MPa)	48-110	34-46	21-37	47
Tensile modulus (GPa)	3.5-3.8	2.9-3.5	1.1-1.5	3.1
Tensile elongation (%)	2.5-100	3-4	20-800	50-300
Notched Izod impact, 23°C (J/m)	13		72	79
THERMAL PROPERTIES				
Glass transition temperature (°C)	60	95	0	75
Melting temperature (°C)	153		163	250
Processing temperature (°C)	210	230	225	255

Table 2.3: Comparison of physical properties between PLA and commodity polymers, [Carrasco et al. 2010].

In the Thesis have been used data concerning mechanical tests of the polymer PLA/PBAT in the different relations (60:40, 70:30, 80:20) with different amount of addition of compatibilizing agent Dialkyl Peroxide - data were found in [Nihida et al. 2011; Nishida et al. 2012]. For the the PLA/PBAT have been found data concerning compression and tension test for a wide range of strain rates. The analysis of experimental results and discussion on the yield state is presented in Paragraph 5.5 of Chapter 5.

2.5 Concluding remarks

In this Chapter there are described materials which are examples of different microstructure: noble metal, high strength steel and polymer. Their general characteristics, industrial application, mechanical properties, basing on the study of literature and microstructure analysis are presented. Oxygen Free High Conductivity Cooper (FCC structured material) is treated as initially anisotropic - the material is in 'as-received' state, the pole figure indicated the non-isotropic behaviour of the material. The non-alloyed steel E355 - example of material with BCC structure, is an isotropic material. Polymers are generally characterized by SD effect and it is assumed according for polycarbonate and biopolymers. This information about studied materials along with strength tests results will be used in the further Chapters of the Thesis. The tests under different loading conditions have been performed on the exemplary materials - details concerned experimental techniques are given in next Chapter 3. Apart from tests and relations due to which it is possible to calculate material characteristics, the numerical analysis is proposed allowing to correct experimental results and understand better processes of deformation. Results and discussion on them are presented in Chapter 5.

Chapter 3

Experimental techniques and their methodology

A general summary of the experimental techniques for characterization of material in the quasi-static and dynamic range is reported. The study of literature concerning discussed tests is also included. The relations allowing to obtain characteristics of material under different loading conditions are given. Prior to the presentation of the test results, an analysis of performed experiments is made with use of Finite Element Method. The inaccuracies between numerical and experimental results are indicated. Finally, a pragmatic correction methods are proposed and applied.

3.1 Introduction

In this Chapter the experimental techniques used in the Thesis are described. The new experimental approach - biaxial compression test is also presented. The discussed experiments are applied to obtain the characterization of the studied in the Thesis materials. Study on the metals and polymers deformation in a wide range of strain rates needs using of different experimental techniques and describing them mathematical relations. Although the basic principles of the testing techniques are rather straightforward, interpretation of the experimental results is less obvious. Identification of the material behaviour from the test needs knowledge on the external conditions, friction influence, boundary conditions. The experimental results not only reflect the material behaviour but also depend largely on the test set-up and the specimen structural behaviour. To understand the complex interaction between external conditions and material behaviour, the finite element simulations and advanced measurement techniques are indispensable tools. New experimental techniques and approaches for interpretation of the experimental results are required to obtain better description of behaviour of material under the loading conditions. The strength tests are performed to determine the mechanical characteristic of the material.

In this Chapter there are described tests in a wide range of strain rates. The theoretical relations allowing recalculate measured values (usually force and displacement) to the stress-strain characteristics are also quoted.

For purposes of Thesis there have been performed tests in the quasi-static ($10^{-4}s^{-1} \leq \dot{\varepsilon} \leq 10^{-2}s^{-1}$) and dynamic strain range range ($10^{-2}s^{-1} \leq \dot{\varepsilon} \leq 10^{4}s^{-1}$). The test results characterizing the discussed materials are use to determine the yielding state for them. The performed tests are as follow:

- quasi-static and dynamic compression test;
- quasi-static tension test;
- double shear test;
- complex stress state test;
- biaxial compression test.

The discussion concerning the presentation of the stress state obtained due to the tests is given in Section 3.1.1.

The two first tests (uniaxial compression and tension) are conventional tests used to obtain basic characteristics of the material - details in Section 3.2. Under quasi-static compression and tension loading the testing procedure is normalized and well established for several materials. Compression needs consciousness of the friction influence on the material during the process, [Klepaczko and Malinowski 1977]. The discussion concerning the numerical modelling of friction is presented in Section 3.2.1. In terms of high-speed deformation there have been conducted tests of compression, carried out on the Split-Hopkinson Pressure Bar (SHPB), description of technique is given in Section 3.6.

Obtaining the shearing state of stress is possible due to different techniques, [Meyer and Halle 2011]. For discussed materials the double shear test is used - the technique is based on deformation of the specimen with two rectangular shearing zones permitting for large strains. The advantage of the double shearing is that there is no geometric instability caused by reduction of the cross-section of the specimen as in case of tensile test. Numerical analysis by finite elements has been performed in order to determine the calibration factor to correct the effects of the non uniformity of shear fields in the shear zones and of the concentration of stress at the bottom and at the top of the notch. The analysis of shear test is given in Section 3.3.2.

Complex stress states tests allows to obtain more points in the stress space, because due to the test the combined loadings are applied. Besides the complex stress test with use of a thin-walled tube (Section 3.5), an analysis of biaxial compression test is reported - Section3.4.

The device to biaxial compression test has been specially designed for the purposes of the Thesis. The experiment is based on the idea proposed in [Khan and Farrokh 2010] and the technique of channel die test [Vandresse et al. 2008]. Application of biaxial stress state results in obtaining additional experimental point in the negative range of the axis (σ_1, σ_3). The yield point in that range is especially important because the differences in yield curves are the more significant there.

Dealing with experimental data needs great care for experimental conditions, calibration of test machine and consciousness of friction influence on the test results, [Meyer 1975]. Also, influence of specimen geometry must be accounted, the geometry should be chosen as optimal

for the test, [Jankowiak et al. 2011]. Experimental results used for the theoretical discussion without awareness of errors can perturb the proposed and validated by an author approach.

To understand the complex interaction between the experimental conditions and structure of material the finite element simulations is an indispensable tool. Finite Element Method (FEM) is one of the most widely used tool for solving engineering, design or research problems. Inverse methods is characterized by versatility and simplicity of schematization areas with complicated geometry, it also allows to obtain material characteristics in heterogeneous or anisotropic range. Application of inverse methods allows to model a variety of physical problems. In the Thesis the aim of using FEM is analyzing and better understanding the processes in the material occurring during the deformation. Modelling with use of numerical simulation allows to perform preliminary experiments which after optimization are performed in reality. Due to results of numerical simulation, it is possible to assess strain distributions and stress states, what is helpful during the real test when loading condition are applied. It is also possible to optimize the geometry of a sample before process of manufacturing. FE modelling is also used to validate the model material obtained through experimentation. Due to numerical simulations there can be obtained results in the wider ranges of strain rate or loadings than in the really performed tests.

For numerical computations the commercial FEM software Abaqus has been used, in Standard module - to simulate processes in quasi-static strain rates and Explicit module - for the dynamic strain ranges, [Hibbitt et al. 2010].

3.1.1 Schematic representation of stress states

To validate the yield criterion the results of experimental tests are used, mainly presented as the yield points for defined offset strain. The discussion concerning the definition of offset strain and yield strength is presented in Section 3.1.2. The yield points are obtained due to various tests and they are used to describe the onset of plasticity approximated due to yield condition - discussion presented in Chapter 4.5.

There is assumed that relation (3.1) is valid:

$$\sigma_1 \geq \sigma_2 \geq \sigma_3 \tag{3.1}$$

The following states of stress are distinguished, what correspond to the suitable loading conditions, [Burzyński 2009]:

- three simple states of stress:

  - (I) - uniaxial tension: $\sigma_1 = \sigma_Y^T, \sigma_2 = 0, \sigma_3 = 0$,

  - (II) - uniaxial compression: $\sigma_1 = 0, \sigma_2 = 0, \sigma_3 = -\sigma_Y^C$,

  - (III) - pure shear: $\sigma_1 = \tau_S^Y, \sigma_2 = 0, \sigma_3 = -\tau_S^Y$,

- three complex states of stress:

  - (IV) - biaxial tension: $\sigma_1 = \sigma_Y^{TT}, \sigma_2 = \sigma_Y^{TT}, \sigma_3 = 0$,

  - (V) - biaxial compression: $\sigma_1 = 0, \sigma_2 = -\sigma_Y^{CC}, \sigma_3 = -\sigma_Y^{CC}$,

  - (VI) - triaxial tension: $\sigma_1 = \sigma_Y^{TTT}, \sigma_2 = \sigma_Y^{TTT}, \sigma_3 = \sigma_Y^{TTT}$,

  - (VII) - triaxial compression: $\sigma_1 = -\sigma_Y^{CCC}, \sigma_2 = -\sigma_Y^{CCC}, \sigma_3 = -\sigma_Y^{CCC}$.

Other states of stress are located between the above states.

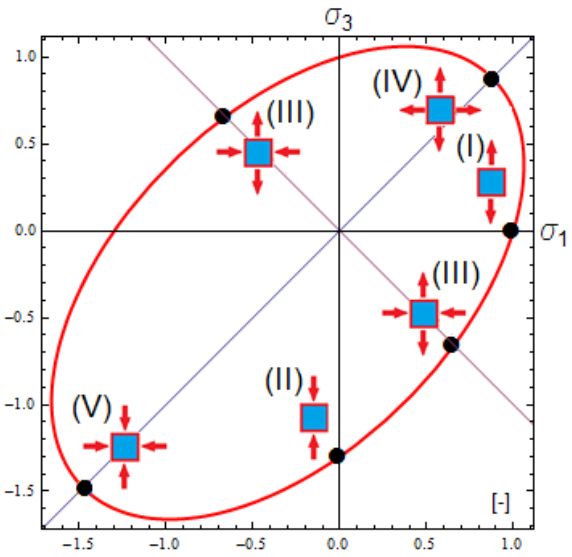

Figure 3.1: The yield curve with schematically indicated points obtained from different tests in the plane $\sigma_2 = 0$.

In Fig. 3.1 the experimental points are depicted on account for the relation (3.1), at the plane state of stresses $\sigma_2 = 0$. The loading directions during the strength tests are often the same as directions of the principal stresses, in that case the assumption (3.1) that $\sigma_1 \geq \sigma_2 \geq \sigma_3$ is not necessary.

3.1.2 Determining the yield strength

Technological processes of material production and the mechanical treatment, due to which the sample geometry is obtained can have negative influences on the material structure. In the material can appear irregularities, non-homogeneous structure, voids. Also residual stresses remain after the original cause of the stresses, external forces, heat gradient, result of deformations or structural changes in phase transformation. Their existence can be reduced due to the heat treatment in the thermal chamber, in the process of normalized annealing. The samples for strength test should be carefully chosen, without visible inaccuracies like voids or scratches on the outer surfaces. It is also essential to optimize the shape and dimensions

of the sample. Irregularities in the geometry of a sample lead to biased characteristics of the material behaviour. Material for specimen should be taken from the one rod, specimen should be cut and manufactured at the same time. The interfering factors should be avoided and the standardized procedures in order to obtain to determine desired characteristic should be followed. Such proceeding should allow to obtain searched information.

The material transition from the elastic state to the plastic is called yielding, [Sharper 2008]. For uniaxial stress state the moment of obtaining plasticity by the material is given by the yield strength. In cases of complex stress states expressing the moment when in the material occurs the plastic state is possible if the components of the stress tensor fulfil the function, called yield condition (examples of different yield functions are given in Chapter 4 of the Thesis). The yielding may be identified with the beginning of inelastic strain, as defined in Eq.3.2:

$$\varepsilon_{offset} = \varepsilon_{tot} - \frac{\sigma}{E} \tag{3.2}$$

where ε_{offset} is the offset strain, ε_{tot} is the total strain, σ is the stress and E is the Young's modulus.

Under the notion of the yield strength there is considered a value of stress due to which the irreversible plastic deformations begin in the material, it means the end of the elastic range. When using the terms 'yield', 'yield strength' or 'yield point', it should be certain that the specific type of yield required is clearly defined and specified as to limiting extension, offset value, or drop-of-the-pointer, etc. in order to avoid confusion and erroneous values.

There are two common methods of determining yield strength from a curve strain-stress:

- the Extension Under Load Method: This method involves drawing a vertical line from the point on the X-axis where the elongation equals the specified extension, e.g. Yield Strength = 0.5% extension;
- the Offset Method: The offset is the horizontal distance between the modulus line and any line running parallel to it - Fig. 3.2. In the Thesis this method is used.

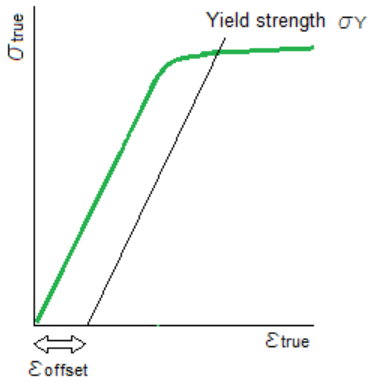

Figure 3.2: The definition of the yield strength depending on the assumed value of the offset strain.

In the Thesis the yield limit are determined for different values of the offset strain equal to:

- 0.0001 for the complex stress state test. The offset strain is equals to such a small value, because the subsequent steps of the test are interrupted immediately after elastic range ends;
- 0.002 for uniaxial stress of state, this value of the offset strain is commonly used;
- 0.01 for dynamic tests, in that range of strain the fluctuation of measured values should end and the curve should be stable;
- 0.0001, 0.001, 0.002, 0.005, 0.01, 0.012 - the yield points determined for few offset values allow to trace the evolution of a limit curve along with increasing deformation.

In next parts of this Chapter there are presented experimental techniques due to which the yield points are obtained. Then, it is possible to define the onset of plasticity using the criteria discussed in Chapter 4.5. As it was previously mentioned, in next Sections there are presented tests in quasi-static and dynamic range. There is also the new experimental method explained - the biaxial compression test. Further in the Chapter, the numerical analyses of the discussed strength tests are reported. Experiments were performed for the discussed in Chapter 2 materials, for which obtained results are summarized in Chapter 5.

3.2 Uniaxial tension and compression test

Many material properties such as the Young's elasticity modulus, tensile strength and uniform elongation can directly be deduced from a tensile test. Interpretation of the test results is straightforward because of the simple uniaxial stress state. Thus, the results of this widely accepted test method for material characterization can be compared with other materials data and results found in literature.

A compression test determines behavior of materials under compressive loads. The specimen is compressed and deformation at various loads is recorded. Compressive stress and strain are calculated and plotted as a stress-strain diagram which is used to determine elastic limit, proportional limit, yield point, yield strength and compressive strength.

Axial compression testing is a useful procedure for measuring the plastic flow behavior and ductile fracture limits of a material. Measuring the plastic flow behavior requires frictionless (homogenous compression) test conditions, while measuring ductile fracture limits takes advantage of the barrel formation and controlled stress and strain conditions at the equator of the barreled surface when compression is carried out with friction. Axial compression testing is also useful for measurement of elastic and compressive fracture properties of brittle materials or low-ductility materials. In any case, the use of specimens having large height/diameter ratios should be avoided to prevent buckling and shearing modes of deformation, [www.instron.pl].

Uniaxial compression tests are carried out using cylindrical samples, the cubic samples are used when the objective is checking the influence of anisotropy. Samples used in the

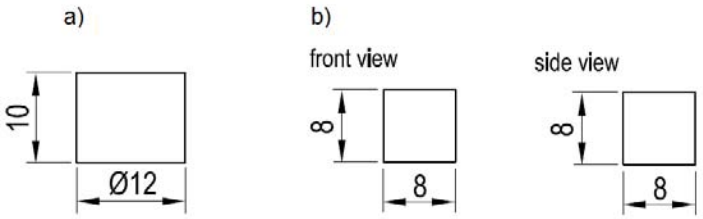

Figure 3.3: The geometry of the samples to the quasi-static compression test: a) cylindrical specimen and b) cubic specimen, [AST 2009].

experiments performed for the Thesis have been machined from a rod of a diameter 12mm, their geometry and dimension are presented in Fig. 3.3.

Tensile test is the primary method for determining the mechanical properties of a material. Uniaxial tensile testing is the most commonly used for obtaining the mechanical characteristics of isotropic materials. During the experiment the most important problem is that it is possible to measure the total external applied load and the displacement on a sample's surface. Therefore, the specimen's geometry, its shape and method of its loading are chosen with assumption that states of stress and strain are uniform, at least at gage length. The reason is that in each cross-section of the the sample, and each point of the cross-section (on the surface and inside of the sample) were the same stress and also strain. During tension test these conditions are fulfilled in thin rods of constant cross section or in the optimized geometries of dog-bone-shaped specimens, Fig. 3.4. A tensile specimen is a standardized sample cross-section. It has two shoulders and a gauge (section) in between. The shoulders are large so they can be readily gripped, whereas the gauge section has a smaller cross-section so that the deformation and failure can occur in this area.

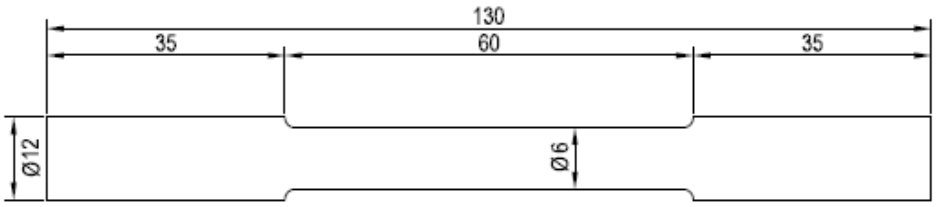

Figure 3.4: The geometry of the samples to the quasi-static tensile test, [AST 2011].

The tests on are performed with an electromechanical universal testing machine. The testing machine employs a variable speed electric motor, gear reduction system and one, two or four screws to move the crosshead up or down. A properly calibrated testing machine that can be operated at constant rates of crosshead motion is needed. During the test, the force $F(t)$ is recorded with use of a force gauge. The shortening (for compression) or elongation (for tension) $\delta(t)$ is measured due to the movement of the sensors fixed unit installed in the strength machine or extensometer. According to ASTM D790, [AST 2011], the error in force should not exceed +/- 1% of the maximum force expected. If crosshead motion is used to measure deflection, the total deformation of the testing machine should not exceed 1% of the total deflection of the test specimen. If testing machine deflection exceeds 1%, other means of measuring deflection should be used. For the purposes of measuring displacement, the testing machine must also be equipped with a displacement sensor. The maximum error of the force

measurement during the test has been equaled to 0.1%, the maximum error of the displacement measurement in the range specified for the displacement transducer has been equaled to 0.5%.

To eliminate the effect of sample geometry on the response of the material, the strain-stress relation is given in the engineering (nominal) coordinates, Eq. (3.3). Assuming an uniform deformation of the sample along the entire length and its unchanged cross-section, the sample's elongation (or shortening) is referred to inial length of the specimen l_0. A tensile (compressive) force is referred to the initial cross-sectional area A_0, [Nadai 1950; Chakrabarty 2000].

The stress value is determined by dividing the resultant external force F by the initial cross-sectional area of the sample A_0. Analyzing displacement, the hypothesis of flat sections is assumed: each flat section before deformation remains flat after deformation. This means that at each point of perpendicular to loading axis cross-section, there is the same value of displacement in direction of loading.

$$\begin{aligned} \sigma_{nom}(t) &= \frac{F(t)}{A_0} \\ \varepsilon_{nom}(t) &= \frac{l(t) - l_0}{l_0} \end{aligned} \tag{3.3}$$

As the measurements of the loading force and resulting displacement is obtained by the traverse of tensile machine, they can contain the influence of the calibration and backlash of machine jaw. These errors have an impact on the slope of the engineering stress-strain dependency. Because the tangent of a curve slope angle is equal to Young's modulus of an analysed material, the correction of the slope are necessary, according to Eq. (3.4), where E_{meas} is a modulus measured directly in the test and E_{theor} is the theoretical value of the Young's modulus from the literature.

$$\varepsilon_{cor} = \varepsilon_{nom} - \sigma_{nom} \frac{E_{theor} - E_{meas}}{E_{theor} E_{meas}} \tag{3.4}$$

The final modulus of elasticity should be the average of values calculated for several tests with comparable specimens. In Fig. 3.5 the principle of the strain correction is shown. The deviation of the elastic part of the curve from the theoretical value of the Young's modulus line is used to determine the stiffness of the specimen. The corrected stress-strain curve is obtained by subtracting the elongation from the original curve.

In order to plot the true curve of tensile behaviour of the material to the the moment of neck formation in the sample, the tensile force must be referred to the actual cross-sectional area of the sample. Since the measurement of the change of cross-sectional area during the deformation process is difficult, assuming that the volume element of the sample $A_0 dz$ before and after process of deformation remains unchanged, the length of the deformation element is equal to $d(1 + \varepsilon_{cor})$, Eq. (3.5), [Nadai 1950].

$$A_0 dz = A dz (1 + \varepsilon_{cor}) \tag{3.5}$$

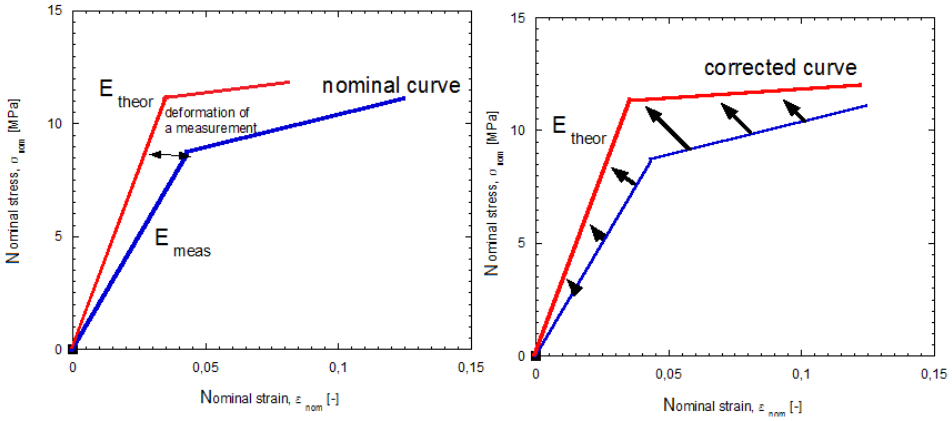

Figure 3.5: The principle of the correction of the Young's modulus $\sigma_{nom} - \varepsilon_{nom}$, [Peirs].

For preparing the true stress-strain relation of tensile behaviour of the material, the function is logarithmic:

$$\varepsilon_{true}(t) = \int_{l_0}^{l} \frac{dl}{l} = \ln \frac{l}{l_0} = \ln \frac{l_0 + \Delta l}{l_0} = \ln(1 + \varepsilon_{nom}) \tag{3.6}$$

True stres-strain relation for tension is expressed by Eq. (3.7), for compression: Eq. (3.8). collected charts for engineering and tensile relation are presented in Fig. 3.6.

$$\begin{aligned} \sigma_{true}(t) &= \sigma_{nom}(t)(1 + \varepsilon_{nom}(t)) \\ \varepsilon_{true}(t) &= \ln(1 + \varepsilon_{nom}(t)) \end{aligned} \tag{3.7}$$

$$\begin{aligned} \sigma_{true} &= \sigma_{nom}(1 - \varepsilon_{cor}) \\ \varepsilon_{true} &= -\ln(1 - \varepsilon_{cor}) \end{aligned} \tag{3.8}$$

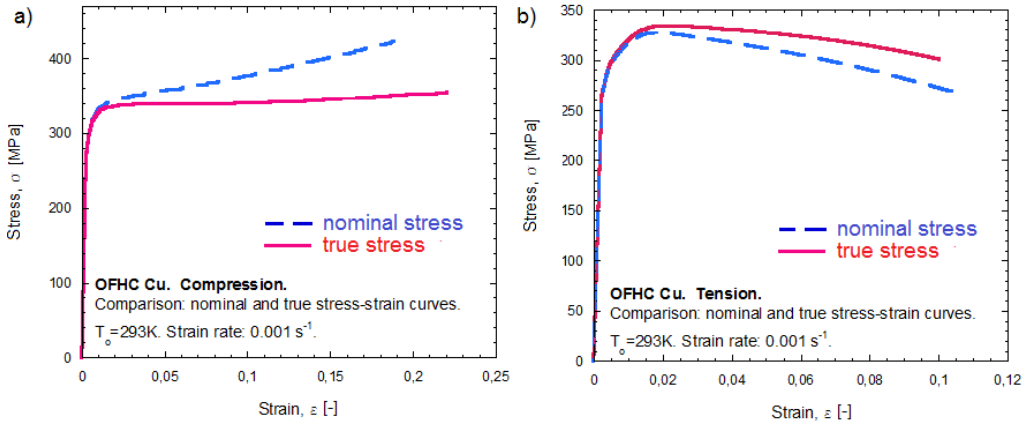

Figure 3.6: Comparison between engineering and true stress-strain curves for the test of a) compression and b) tension.

Experiments have been performed in series of 2-3 tests for each strain rate. Range of strain rate for performed tests has been from $10^{-4}s^{-1}$ to $10^{-1}s^{-1}$. The tests have been performed at room temperature $293K$ assuming isothermal conditions.

3.2.1 FEM analysis of the tension and compression test

Results of quasi-static compression or tension tests can be described by a function of stress dependence on strain. Stress-strain curve gives an overview on the behaviour of the material during the loading process - this relation is called constitutive. Functions which approximate the deformation of the material allow to record it in the programs for numerical computations. Such functions modelling the behaviour of material in numerical analysis can be constitutive models. In the Thesis, the constitutive relation which is used to model plastic behaviour of OFHC Cu is the Johnson-Cook relation [Johnson and Cook 1983], Eq. (6.1) in Appendix 1. The parameters which describe OFHC Cu are collected in Table 3.1. The model parameters have to be obtained by means of mechanical tests. Parameter A is a yield strength of the material defined for a quasi-static strain rate at room temperature. Parameters B, n are obtained due to approximation of true stress-trues strain curve of for example compression test. Parameter C describing strain rate dependency can be determined if yield points from tests of different strains are presented as dependence of $\ln(\dot{\varepsilon}_p)$. The flow stress is not temperature dependent $m = 0$. The test have been conducted at room temperature, consequently thermal-softening part is equals to 1. Details can be found in paper [Meyer and Kleponis 2001] and [Johnson and Cook 1983]. Parameters of the JC relation for OFHC copper can be also found in many works, e.g. [Tanner and McDowell 1999; Rodríguez-Martínez et al. 2009].

OFHC Cu	A [MPa]	B [MPa]	n [-]	C [-]	$\dot{\varepsilon}_0$ [s^{-1}]	T_0 [K]	T_m [K]	m [-]
	312	37.35	0.88	0.11	1.5	293	1340	0

Table 3.1: Parameters of the Johnson-Cook model for OFHC Cu, Eq. (6.1).

Summary picture compared curves obtained due to analytical relations (6.1) and experimental and numerical ones are presented in Fig. 3.7.

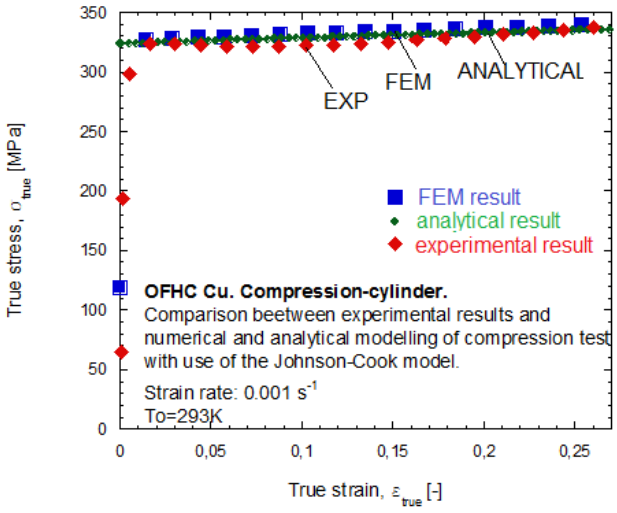

Figure 3.7: Comparison between experimental results and analytical and FEM modelling with use of the Johnson-Cook relation.

The experimental results for compression test performed at $\dot{\varepsilon} = 0.001s^{-1}$ are compared with analytical mododelling. There are also plotted results of numerical simulation when the

analytical model is used as a definition of material's behaviour in frictionless conditions, the numerical results are discussed in the next Paragraph.

In Table 3.2 there are presented the properties of OFHC Cu in elastic range. The Young's modulus and the Poisson's coefficient are defined with use of the calculations made on the basis of the complex stress state test.

OFHC Cu	E [GPa]	ν [-]
	127	0.3

Table 3.2: Elastic characteristics for OFHC Cu.

Validation of the numerical model of material

The quasi-static uniaxial compression test is one of the basic strength test used as testing procedure, yield limit obtained due to this test is often principal characteristic of a material. However, as it was highlighted in few works ([Jankowiak et al. 2011; Bell 1973; Kuhn and Medlin 2000]), the test is not free from influences of friction. There were introduced corrections which must be accounted if the experimental results are to be applied for validation of the yield surface. The yield limit in compression is corrected due to the friction, value of correction is depending on the specimen's geometry, [Jankowiak et al. 2011; Klepaczko and Malinowski 1977]. In this study, the compression test is used to describe material's bahaviour in the plastic range and also to analyse the strain rate sensitivity - basing on the Johnson-Cook and the Rusinek-Klepaczko models. Under quasi-static compression loading the model of material's behaviour is tested, normalized and established. To prove its correctness the FEM simulation is performed.

As the example of material the Oxygen Free High conductivity copper is chosen. Since, the OFHC copper is a well-known material, the behavior of this material during compression process has been frequently reported in the literature: [Nemat-Nasser et al. 1998b; J.Alexander and Beyerlein 2005; Bhattacharyya et al. 2005; Rittel et al. 2002a; Jankowiak et al. 2011]. However, as it is summarized in [Jankowiak et al. 2011] different authors using the same material estimated the different behaviour during the compressive test. These differences are mainly related to the geometry of the tested specimen and the friction influencing test. In [Jankowiak et al. 2011] the model of friction correction based on Malinowski-Klepaczko model [Klepaczko and Malinowski 1977] is validated for quasi-static and dynamic results.

The responsibility for the quality and further usefulness of the performed tests results requires the detailed knowledge on the experiments conditions, geometry and boundary conditions. Beneath, there is presented the discussion concerning the quasi-static compressive test.

Boundary conditions for the compression test are presented in points.

- Plates are modelled as rigid bodies with the reference points to which the loading conditions are applied. The bottom plate is fully fixed, to the upper plate the velocity is applied to obtain compression with the assumed strain rate, Fig. 3.8.

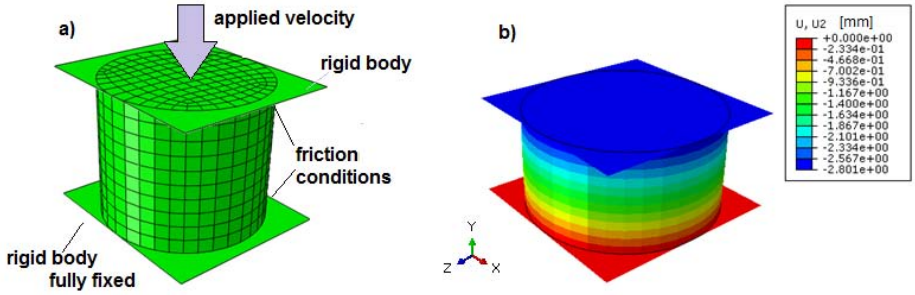

Figure 3.8: a) Boundary conditions of a quasi-static compression test, b) deformed mesh for the frictionless conditions.

- Specimen is modelled as a 3D deformable body meshed with elements C3D8R (an 8-node linear brick, reduced integration, hourglass control) of size 1mm, amount of elements in the specimen is 1460. There has been also performed the simulation with use of elements C3D8R of size 0.05mm, amount of elements on the specimen is 11360. The influence of an element type has been analysed, Fig. 3.9.c.

- Influence of the friction effect have been also examined. Different friction conditions have been assumed between upper and bottom plate and specimen, the summarizing graph is presented in Fig. 3.9.b.

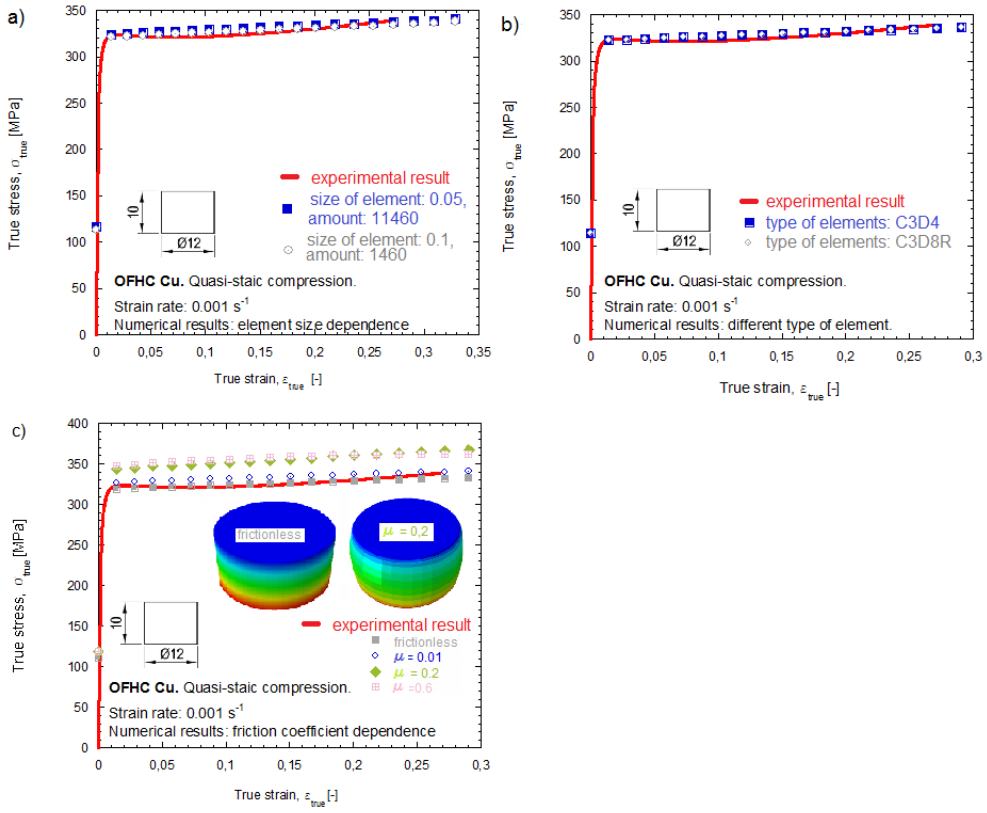

Figure 3.9: Results of numerical simulations and their a) dependence on elements size, b) dependence on element type, c) dependence on friction influence in comparison to experimental results.

Fig. 3.9 presents results of the numerical tests with different boundary conditions. Results are compared to show that size of elements has been chosen as optimal and also that type of the chosen element does not play role in the obtained results. Additionally, it has been proved that influence of friction on the results is considerable but the optimal results are obtained for frictionless numeric trial.

The numerical calculation can be summed up in few conclusions. Firstly, it can be stated that size of element equals 1x1mm is optimal. For elements of smaller size and consequently larger amount of them used to meshed the model - the time of calculation is too long and there is no difference in the obtained results, Fig. 3.9.a. Secondly, kind of element does not change the results of the calculation, Fig. 3.9.b. Friction affects the results of the simulation but judging on the obtained numerical results with different friction coefficients, Fig. 3.9.c - only simulation performed with frictionless conditions repeats the experimental result. It can be concluded that real experiment has been performed with large usage of lubricant - the samples did not barreled. The large amount of lubricant has been applied during the tests and the experimental results are not much affected by the friction.

To sum up, the constitutive model, elements, boundary conditions are considered as optimal and basing on such choice the numerical test allow to define experimental results. As a summary, the results of numerical simulations with use of the Johnson-Cook model performed for different strain rates are presented in comparison with experimental results - Fig. 3.10.

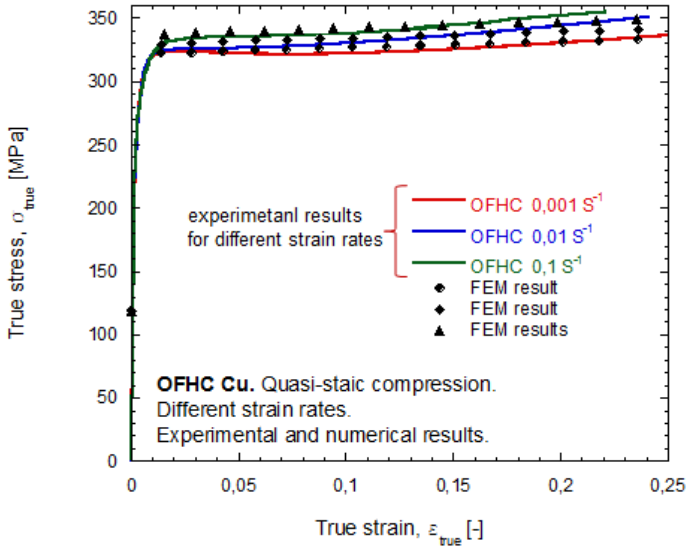

Figure 3.10: Results of numerical simulations with use of Johnson-Cook model performed for different strain rates - compared with experimental results.

Due to Fig. 3.10 it can be noticed that the OFHC Cu is strain rate sensitive. The true stress-true strain curves obtained due to numerical analysis have been calculated the same method as experimental results - procedure reported first Paragraph of the Section 3.2. Numerical results are compared with the experimental, the true stress-true strain curves have similar characteristics in different strain rates. This conclusion is also proved by the numerical simulation of the tension test, Fig. 3.11. The curves obtained in the experimental test and from numerical

simulation have similar characteristics. Dimensions of tensile test sample are shown in Fig. 3.4. Tensile tests for OFHC Cu have been carry out with only one strain rate equals to 0.001 s^{-1}. As it is reported in Fig. 3.6, the level of hardening is low, and the maximum stress is reached for a very small deformation - about $\varepsilon_{pl} = 0.02$.

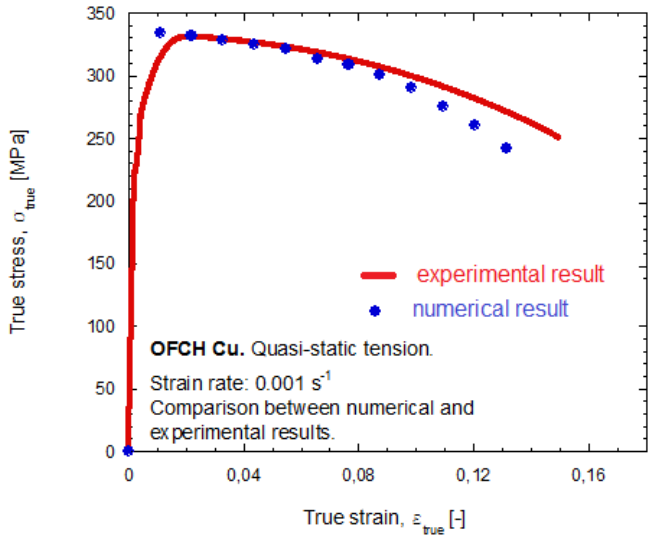

Figure 3.11: Summary of the experimental result (red line) with the result of numerical simulation (blue points) for the quasi-static tension.

In next Section there are discussed the shear tests, experiments due to which there is possible to obtain shear state of stresses in the material. All of possible shear techniques are affected by errors, mainly corresponding to inaccuracies of geometry and inhomogeneous of shear stresses, [Meyer and Halle 2011]. In the Thesis to obtain shear state of stresses the double shear test is used. However, in the Section there are shortly described other techniques, applicable for the bulk materials. The numerical analysis of double shear test is also reported.

3.3 Shear test

Deformations caused by shear are present in many industrial structures. Also there are manufacturing processes in which shear is specially induced. Some examples of these are: high speed cutting, deburring, blanking and impact shear cutting. Also, complex processes with shear dominated stress states are present in ballistic impact. Most methods of material processing or metal forming involving severe plastic deformation, e.g. equal channel angular pressing. In such processes the fundamental deformation or failure mechanism is shearing, [Meyer and Halle 2011; Bressan and Unfer 2006]. The importance of shear deformation modes and the theoretical background of the shear-driven phenomena can be found in e.g. [Pęcherski 1996; 1998; Nowak et al. 2002; Perzyna 2008]. Obtain reliable results for shear is a challenge accounting for the complexity of the shear process, especially when most of specimens geometry proposed in the literature are not optimal in order to produce data describing shear state of the material.

In [Meyer and Halle 2011] the six most commonly used shearing test techniques are reported. Different geometries for shear tests are analysed and modelled in FEM code to research their features and applicability. The examples of shear tests with use of the sheet material can be found in work of [Rusinek and Klepaczko 2001; Peirs et al. 2010; Guo and Li 2012; Peirs et al. 2013]. Beneath, some shear test applicable for bulk material are described.

The torsion test, [Nadai 1950; Duffy et al. 1971; Bressan and Unfer 2006] for which specimen presented in Fig. 3.12

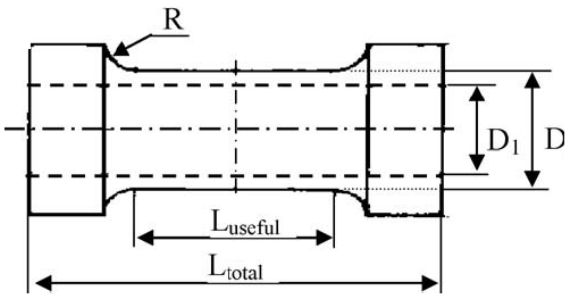

Figure 3.12: Specimen used in the experimental plastic torsion test, [Bressan and Unfer 2006].

This kind of test can be applied both in quasi-static and dynamic strain rates. The torsion tests are applied to materials with the aim to determine the mechanical properties such as the shear modulus, shear strength, rupture shear strain and the work hardening law. However, they can also be used in solid bodies (wheel shafts, rods, bars, beams, thin-walled cylinder etc.) to obtain the response in torsion loads. The test is frequently used in cylindrical shafts by applying a torque in its longitudinal axis. The shear stress versus shear strain curve can be determined from the simultaneous measurements of torque and the twist angle during the test for the previously selected specimen length.

The shear-compression test (SC), [Rittel et al. 2002a;b; Vural et al. 2010] for which specimen presented in Fig. 3.13.

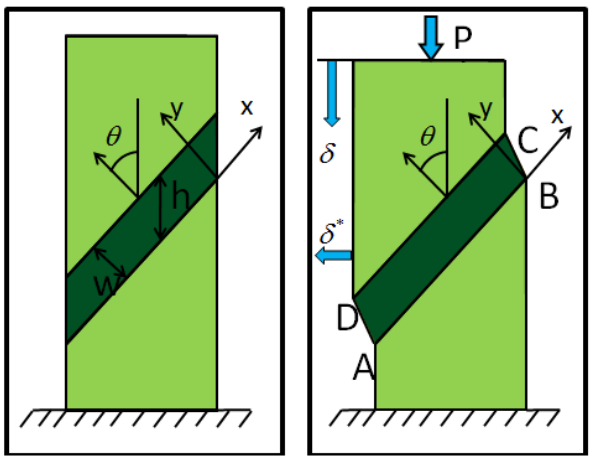

Figure 3.13: Principle of the deformation process in a shear-compression test.

The dominant deformation mode of the gage section of the shear-compression specimen (SCS) is shear, Fig. 3.13, [Rittel et al. 2002a;b; Vural et al. 2010]. In SC test by applying compressive force on the upper surface of the sample there is obtained in the slot zone (ABCD) the shear state, which is dominant deformation mode of the gauge section of the SC specimen. Numerical analysis of the SC test has shown that the state of strain and stress is quite complex and does not correspond to simple (or pure) shear, despite a dominant shear deformation, [Rittel et al. 2002b]. The stress and strain state in the gage section is necessarily three-dimensional, in contrast with commonly assumed situations of simple shear. Simplification is gained through the introduction of simple approximations for the Huber-Mises equivalent stress and plastic strain. Based on the numerical results, simple relationships were proposed to determine the equivalent plastic strain and stress. The detailed description of analytical approach is presented in [Rittel et al. 2002a;b; Vural et al. 2010].

In further parts of the Section there is discussed the methodology of the double shear test, the drawbacks and advantages are reported. The necessary numerical analysis of the test is also evaluated.

3.3.1 The double shear test

For discussed in the Thesis materials the double shear tests have been performed with quasi-static strain rates varying from 10^{-4} s^{-1} to 0,1 s^{-1}. A modified double shear (MDS) specimen is presented in Fig. 3.14. The double shear test is described in e.g. [Campbell and Ferguson 1970; Klepaczko 1994; Rusinek and Klepaczko 2001].

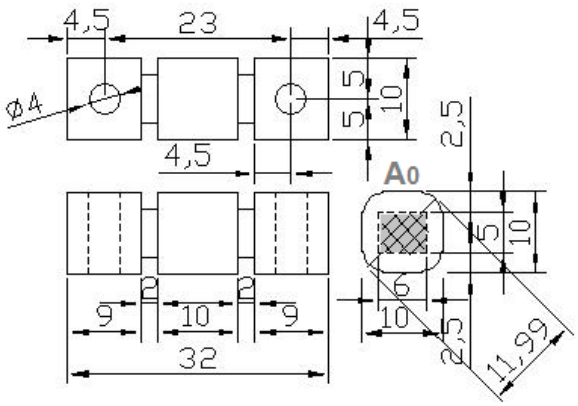

Figure 3.14: Geometry of sample for double shear test, the shear zone is indicated with gray colour.

In [Klepaczko 1994] it is shown that non-optimized design leads to intrinsic perturbation of the strain field in the shear zone and has an effect on the uniformity of stresses. After numerical calculation given in [Klepaczko 1994] the chosen geometry is optimal, [Rusinek and Klepaczko 2001; Glema et al. 2010]. Presented in Fig. 3.14 dimensions are chosen to minimise the error due to non-homogeneity of the shear stresses and strains at the shear zone of the specimen.

A characteristic features of the samples type MDS (modified double shear) are two rectangular shearing zones permit- ting for large strains within these zones. The shear stress in the zones is achieved by forcing the displacement of the center block. The idea of the test can be used both for bulk material, [Klepaczko 1994], and sheet material, [Gary and Nowacki 1994; Rusinek and Klepaczko 2001; Glema et al. 2010; Guo and Li 2012].

One of the major advantages of the double shearing is that there is no geometric instability caused by reduction of the cross-section of the specimen as in case of tensile test, [Rusinek and Klepaczko 2001]. The specimen may be used in a wide range of strain rates: quasi-static and dynamic. In cases of dynamic loading, the double shear specimen is loaded directly by a long projectile which can be accelerated to a desired impact velocity by the gas gun, [Klepaczko 1994].

Two main problems influences the results of shear tests with use of the double-notched specimen are: the strain nonuniformity at large deformation and the stress concentration at the corners of the shear section of the specimen. Due to stress concentrations in the gauge length, the shear failure is induced and driven by geometry and not by the material behavior itself. The accuracy of the experiment decreases because of the nonuniform distribution of shear deformation over the gauge section occurring when strain are large (this value is set as 20% of all possible strain in [Guo and Li 2012]). It happened when moment on the gauge section which originates from the disalignment of the loading direction with the specimen supporting. In order to overcome these problems, Klepaczko [Klepaczko 1994] redesigned the dimension of the specimen and increased the width of the shear section, what allows filleting at the corner of the shear section to reduce stress concentration. The deformation of the specimen should be simulated then it was possible to calibrate the shear stress/strain at the gauge section.

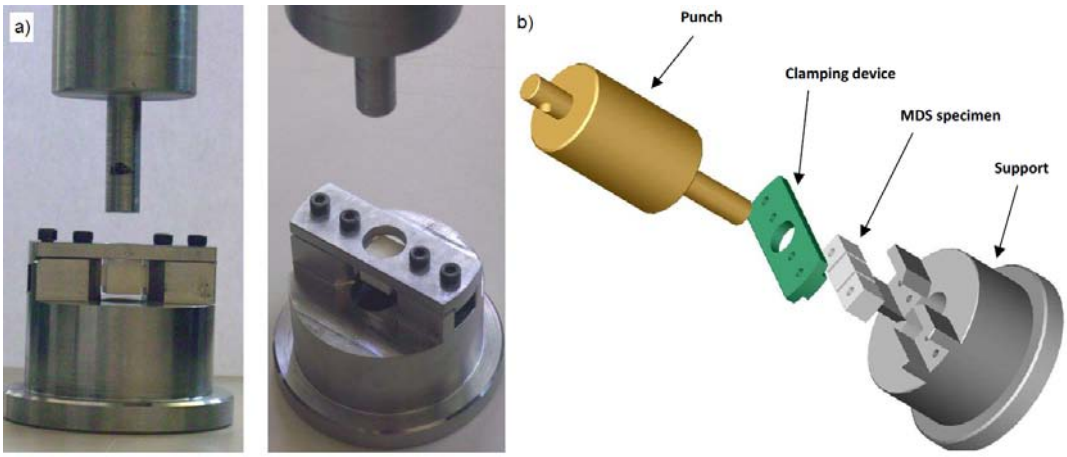

Figure 3.15: a) Picture of the overall testing device with a fixed specimen, b) view of the testing device.

The double shear tests have been performed using a hydraulic machine and specially designed jaws mounted in the grips of the testing machine INSTRON 5585H. The used samples, Fig. 3.14, were cut from a rod with diameter 12mm. The specimen is clamped using 2 screws allowing to reduce sliding and bending effect during shear loading. During the test a constant speed is imposed to the punch inducting a constants strain rate. In Fig. 3.15 there is presented

the set-up to double shear test. The device consists of the upper part in the form of a cylindrical punch attached to the upper head of the testing machine. The upper head of the machine is fixed to the machine load cell by means of which the force is measured. The lower part of the device consists of a tube support directly attached to the machine actuator. When the actuator moves up with a programmed velocity two shear zones of the specimen are deformed with the imposed shear strain rate. On the middle cube of the specimen, Fig. 3.16.b, a white point is painted allowing to use an optical extensometer due to which measurement of the displacement of the central part is possible.

During the test the axial force F(t) and axial displacement $\delta(t)$ of the central part of the specimen are measured as a function of time. The axial force $F(t)$ can be converted into the mean nominal shear stress. Dividing the measured displacement $\delta(t)$ by the width of the shear zone l_0, $l_0 = 2mm$ Fig. 3.14, the mean nominal shear strain is calculated. The mean shear stress τ and the mean shear strain γ are given by the relation, Eq. (3.9).

$$\begin{aligned} \tau_{nom}(t) &= \frac{F(t)}{2A_0} \\ \gamma_{nom}(t) &= \frac{\delta(t)}{l_0} \end{aligned} \tag{3.9}$$

where A_0 is the area the shearing zone, l_0 is the width of shear zone, Fig 3.14.

For the measured stress/strain curves, the error of stress comes from its nonuniform distribution across the shear section. The error of strain may be attributed to the additional deformation from other parts of the double-notch specimen, [Rusinek and Klepaczko 2001; Guo and Li 2012]. It should be noted that obtained stress/strain relationship is the overall response of the whole specimen. It may not be the same as the real stress/strain relationship of the shear section. In order to study errors quantitatively, to calibrate the recorded experimental data and to obtain more accurate mechanical properties of the material, the test should be simulated in the FE method. Numerical analysis by finite elements should be performed also in order to determine the calibration factor to correct the effects of the nonuniformity of shear fields in the shear zones. The numerical analysis of the double shear test is reported in the next Paragraph.

3.3.2 FEM analysis of the double shear test

As mentioned in [Rusinek and Klepaczko 2001; Guo and Li 2012] the the overall response of the whole specimen is recorded during the double shear test. However, it is assumed that this is the response of the shear section only. So, to obtain proper results of double shear test the numerical simulation which mimics the test conditions must be performed.

In case of Oxygen Free High Conductivity Copper to extract model of the material, the results of the compression test are used. The material model has been used to simulate processes of tension and compression and it is proved to mimic properly these tests. The mechanical and physical properties of OFHC Cu are reported in Tables 3.1 and 3.2. The process of shearing is simulated as quasi-static with strain rate 0.001 s^{-1}.

Due to symmetry of the specimen, a half of it has been modelled - Fig. 3.16.a. The boundary conditions are shown in Fig. 3.17.a. During the real process the side cubes are fully fixed and the movement of middle cube is imposed, what causes the shear state in the zones between the side cubes. These conditions are simulated in numerical process of shear. The side cube is fully fixed, to a half of the middle cube is applied velocity to induce its movement down. In Fig. 3.18 there is presented the deformation of the specimen along with the obtained final displacement of a middle cube of the MDS sample.

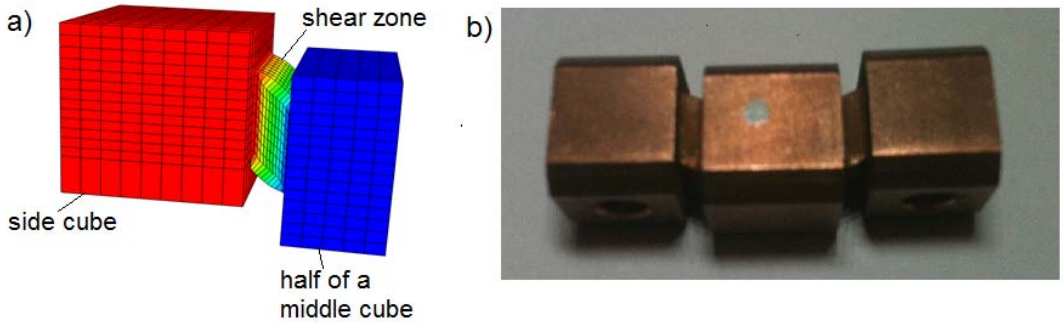

Figure 3.16: a) Half of a deformed specimen - numerical prediction, b) deformed specimen after experiment.

Numerical analysis has been performed in order to obtain the calibration factors to correct the effects of the nonuniformity of shear fields in the shear zones and the concentration of stress at the bottom and at the top of the notch. Possibility of finding correction factors permits to analyse more exactly the experimental results in order to identify more correctly the material behaviour in pure shear.

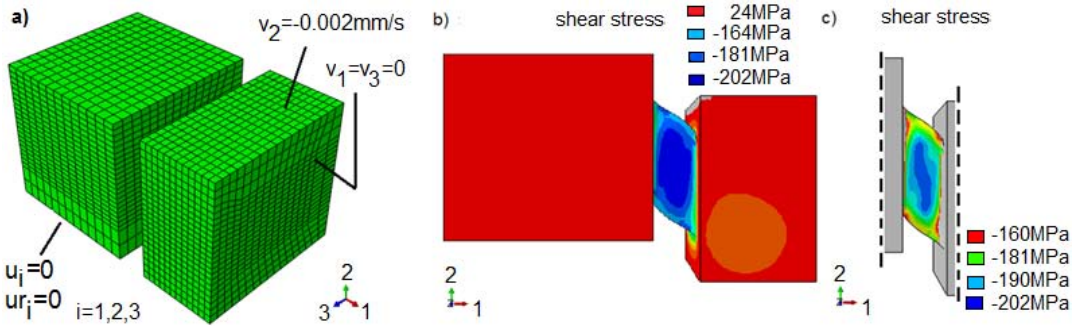

Figure 3.17: a) Boundary conditions, b) non-homogenous accounting for stresses shear zone, c) its magnification.

In Figs. 3.17.b-c and 3.18 distribution of shear stress is shown. It can be noticed that the stress and strain distributions is nonuniform near the notch bottoms, Fig. 3.17.b-c, what is the main reason of a stress concentration and a local plasticity. Heterogeneous distribution of shear stresses in the shear zone is also reported in [Meyer and Halle 2011]. Along with imposed deformation the flowing materials of shear zone is pressed into the cubic parts of a specimen what causes shear bands and consequently destruction of the specimen. As it can be see in Fig. 3.18.e the main deformation mode is shear.

The FE analysis show an uniformity of the strain field if the measurement is taken in the central part of the specimen. The shear stress is almost constant in the central part of the shear zone. This conclusion is confirmed also in [Rusinek and Klepaczko 2001; Guo and Li 2012]. Consequently, the analysis of the central part of the shear field has permitted to define a homogeneous shear zone in the specimen.

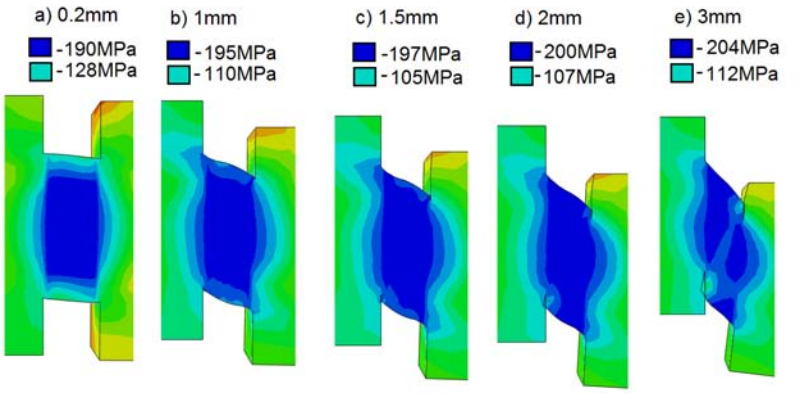

Figure 3.18: Deformation of the MDS specimen along with the obtained final displacement of the middle cube of the MDS sample: a) 0.2mm, b) 1mm, c) 1.5mm, d) 2mm, e) 3mm.

The nominal shear stress/shear strain in FE simulation are obtained using the same data processing method as in the experiment, Eq. (3.9). As a result of numerical simulations shear stress-shear strain diagram (Fig. 3.19 red points) have been obtained. Its level is higher than level of stresses obtained from the experiment (Fig. 3.19 green dashed line). There has been noticed that the sample's geometry causes underestimation of stress level with comparison to results obtained from the experiment - in numerical simulation obtained level of stresses is higher, Fig. 3.19. Consequently, there are proposed correction factors, Eq. (3.10).

These geometrical correction factors are dependent on the geometry of the sample - the material used to make the sample has no influence on them. Whatever the characteristics are used for the numerical simulations, the obtained coefficient for the one specific geometry is the same, [Rusinek and Klepaczko 2001]. Therefore, the coefficient of calibration is intrinsic due to the specimen geometry. In [Guo and Li 2012] it is also demonstrated that the calibration coefficients do not change significantly according to increasing time. In [Rusinek and Klepaczko 2001] it is shown that obtained level of final displacement does not change values of coefficienst, either. The coefficient remains constant in relation to the level of nominal shear strain which is applied to the specimen, [Rusinek and Klepaczko 2001; Guo and Li 2012]. Thus, using the geometry depicted in Fig. 3.14 the correction factors expressed by Eq. (3.10) should be used for each kind of material. Other geometry of MDS needs other values of calibration factors, [Rusinek and Klepaczko 2001]. The obtained intrinsic interference coefficients of the specimen due to the geometry effect are as follows:

$$\begin{aligned} \Psi_\tau &= 1.24 \\ \Psi_\gamma &= 0.9 \end{aligned} \tag{3.10}$$

Application of calibration coefficients leads to an increase of stress and a decrease of strain.

What, in consequence, allows to find proper formulation of shear stress-shear strain relations - Eq. (3.11) which is based on the relation Eq. (3.9).

$$\begin{aligned} \tau(t) &= \Psi_\tau \tau_{nom}(t) \\ \gamma(t) &= \Psi_\gamma \gamma_{nom}(t) \end{aligned} \tag{3.11}$$

Experimental graph of shear stress-shear strain (blue line) - Fig. 3.19 corrected due to obtained in numerical simulation factors - Eq. (3.10). Obtained level of experimental stresses is then comparable with level of results of numerical simulation. The results of double shear test for OFHC Cu are presented in Fig. 3.19.

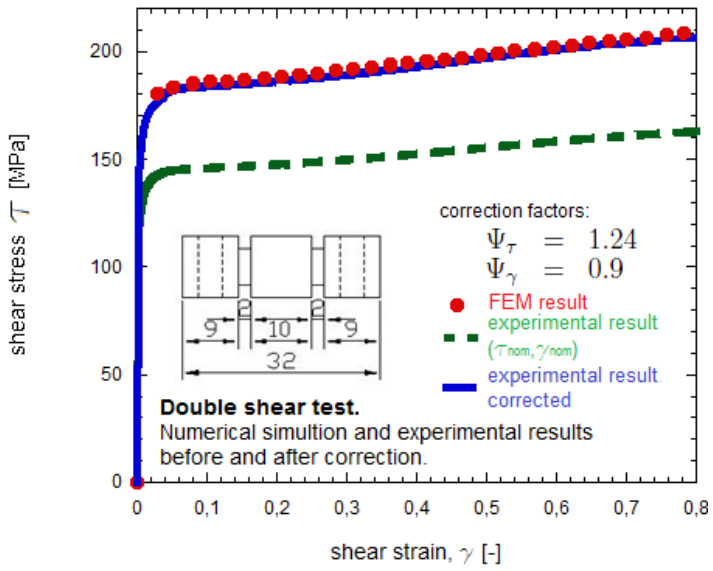

Figure 3.19: The values of correction factors used to correct results of double shear test.

The overall structural response of material during the double shear test is different from the mechanical property of the material itself, consequently the experiment must be calibrated according to stress-strain characteristic by use of the FE method. The obtained geometrical coefficients have values given by relation (3.10). The correction coefficients are dependent on the specimen geometry. For sheet specimens, there have been found other values of them. In [Guo and Li 2012] the correction coefficients are as follows $\Psi_\gamma = 0.5$ and $\Psi_\tau = 1.03$ when shear zone has dimensions 2.5mm x 1mm with 1.5mm of thickness. The correction coefficient determined in Rusinek and Klepaczko [2001] are $\Psi_\gamma = 0.65$ and $\Psi_\tau = 1.42$ for shear zone of dimensions 3mm x 10mm with thickness 0.8mm. In each case they are supposed to be obtained specially for chosen geometry. The optimal dimension of specimen must be also considered. The numerical calculation are in that case of great importance. Without it, the error of shear strain may be over 20%.

In next Section of this Chapter the designed on purposes of the Thesis device is discussed - it is a set-up allowing to obtain the biaxial compression stress of state in the material. The apparatus is shortly described, the analytical relations allowing to calculate stress-strain dependence are identified. The influence of friction is investigated and a model of friction correction

is proposed. Numerical analysis concerning the designed set-up is reported and discussed. This methodology is performed to obtain an additional point - which is of great importance because its coordinates have values from negative parts of axes σ_1, σ_3. The larger difference between yield conditions occurs in this region (and symmetrically in range of biaxial tension stress of state).

3.4 Biaxial compression test

To enable theoretical analysis and application of yield criterion, several strength tests should be performed to describe material behaviour. Beside rather standard uniaxial tension and compression and shear tests, the biaxial compression tests are proposed and validated with use of an inverse method due to which the friction influence is possible to estimate. Application of biaxial stress state results in obtaining additional experimental point allowing to define the yield surface more accurately. The conception of biaxial compression test is based on the channel die compression test. Due to the channel-die compression test it is possible to induce a plane strain in the most parts of the material volume. Obtained strength for biaxial compression is an important value when the criterion describing yielding state is chosen - it appears in the negative parts of axis (σ_1, σ_3), in the region when the differences between criteria are the most exact.

The conception of biaxial compression test is based on the channel die compression test [Havner 2007a;b; Havner and Sue 2007; Havner 2012; Vandresse et al. 2008]. It is reported that the idea of the test was developed in 1930's [Wever and Schmid 1930]. Then, the channel-die appliance was popularized in 1960's for the plane strain compression of materials, a superior channel die configuration was designed and adopted that gave remarkably uniform deformation, [Chin et al. 1966]. In general, it is used as a technological test to study of crystal deformation under biaxial stress and offers a potential for clarity of interpretation of constitutive behavior afforded only by an essentially uniform distortion and stress state a macroscopic scale, [Havner 2007a]. The brief outline of channel die appliance is given in papers of Hevner [Havner 2007a;b; Havner and Sue 2007; Havner 2012].

Recently, the channel die technique has been used to obtain the additional point to validate the yield surface [Khan et al. 2007; Khan and Farrokh 2010]. Due to the channel-die compression test is possible to impose plane strain in most of the sample. It consists of compressing a piece blocked by two walls. The strain rate tensor has thus two free components, against four in uniaxial compression. As friction occurs on four of the six faces of the sample, the friction analysis is a crucial issue in interpretation of test's results. The friction analysis is based on the conception proposed in [Klepaczko and Malinowski 1977] and then modified by [Jankowiak et al. 2011], Paragraph 3.4.2. The asset was to design the test into two parts - the initial state during which the uniaxial compression occurs and - final stage - when the biaxial compression is a leading state of deformation. Such a two-stage process of compression allows to estimate the friction coefficient.

The main idea of biaxial compression test is to apply compression loading $F(t)$ along the direction indicated as 3 in Fig. 3.20, the side walls of a sample are blocked (direction 2).

Together with deformation (Δu_3) of the specimen due to the compression loading there is a flow of material in direction 1 (Δu_1) - what is in agreement with biaxial state of stresses, Fig. 3.20.

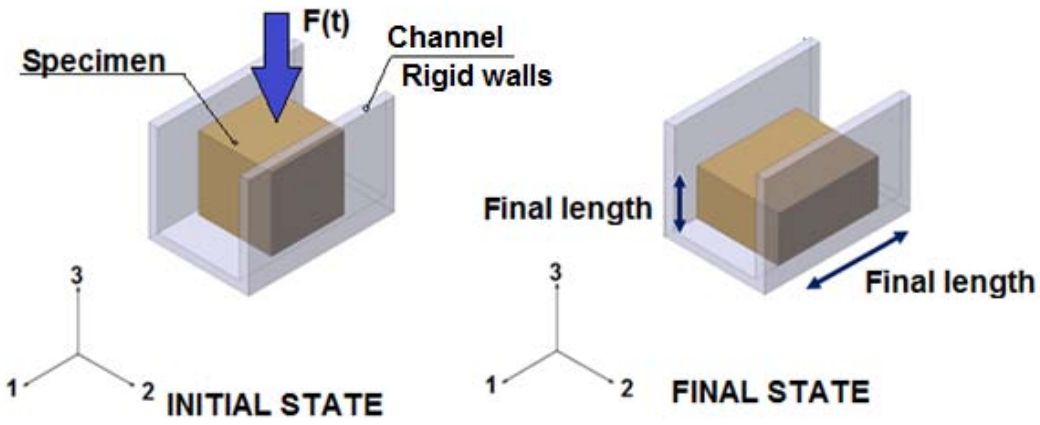

Figure 3.20: Schematic description of biaxial compression test.

The details of designed experimental set-up are presented in the appendix no 2, which contains detailed drawings of designed device. In Figs. 3.21, 3.22 there is presented the geometry of the designed set-up.

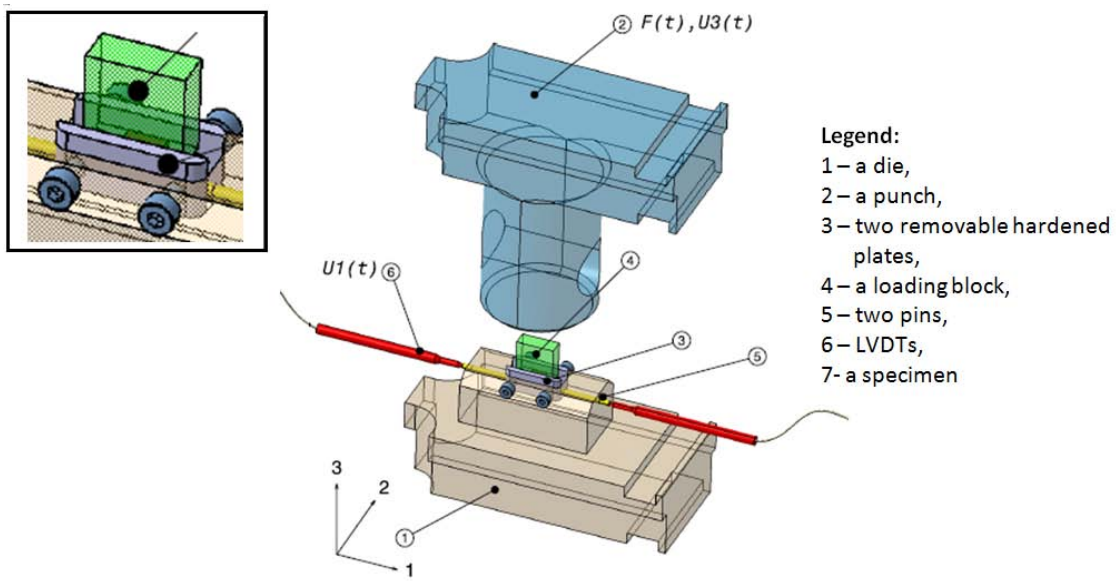

Figure 3.21: Set-up description to perform biaxial loading in quasi-static strain rate.

During the test, the force F(t) is measured by the force cell, the displacement Δu_3 is measured with use of the sensor displacement fixed on the mobile crosshead and the displacement Δu_1 is recorded using the Linear Variable Differential Transducers (LVDTs).

The above state of stress is possible due to the designed set-up presented in Figs. 3.21, 3.22. The specimen which is used for the biaxial compression test has a cubic shape with the

average dimensions of 8x8x8mm. The specimen is placed in the channel of the die. Compressive loading is applied through the punch which is in contact with the loading block inducting a compressive state of deformation to the specimen. Side walls of the channel are protected by the two removable hardened plates which are screwed to it. Two sides of the specimen are free, so due to the applied compressive loading along direction 3, they are deformed along direction 1, Fig. 3.20. This displacement is measured by the LVDTs.

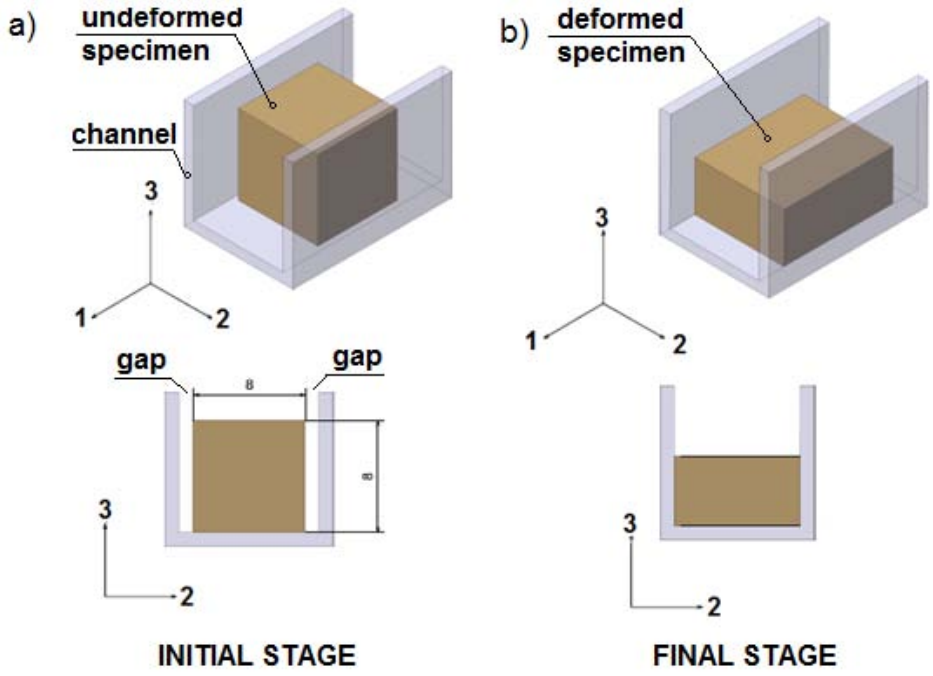

Figure 3.22: Deformation of a specimen during the biaxial loading: a) the initial state, uniaxial compression, b) final stage, biaxial compression.

In [Khan et al. 2007; Khan and Farrokh 2010; Vandresse et al. 2008] the large influence of the friction during the process of biaxial compression is emphasized. Two walls of the specimen and its bottom surface are in contact with the channel, the upper surface of the specimen is in contact with the punch, so the friction affects four out of the six walls of the sample. Even application of lubricant does not allow to avoid friction effect. During the experiment to minimise friction there has been used grease MoS2.

Friction effect is a phenomenon difficult to unambiguous estimation, especially in the process of the biaxial compression. However, its influence on process of uniaxial compression has been researched in e.g. [Klepaczko and Malinowski 1977]. Designing test of biaxial compression which is divided into two parts - the initial stage and the final state - allows to estimate the friction during the process, Fig. 3.22. As the initial state - the uniaxial compression is a process which occurs in the specimen to the moment when side walls touch the channel, Fig. 3.22.a. The biaxial compression, which starts afterwards, is considered as the final - proper stage of the experiment, Fig. 3.22.b.

Uniaxial compression is possible when specimen deforms freely to the moment when flowing material touches the side walls of the channel. Between the side walls of the sample and channel there are gaps - their size has been set averagely as 0.25mm. Due to uniaxial

compression test - there is possible to estimate friction coefficient value during the whole experimental process. Without the imposing uniaxial state of stress, it would not be possible to estimate the friction effect. The effect of friction on the process of uniaxial compression has been investigated and some models have been proposed, [Klepaczko and Malinowski 1977], [Jankowiak et al. 2011]. Knowing the friction influence in the initial stage of the experiment allows to estimate it during the final stage and consequently, it allows to obtain proper results for biaxial state of stress. The preliminary results obtained directly from the experiment, without analysis of friction and numerical simulation are presented in the next Paragraph.

3.4.1 Preliminary results of biaxial compression test

Starting from Hooke's law, basing on the experimental measurements and assuming the lack of friction, the following qualities can be defined, Eqs. (3.12), (3.13):

$$\begin{aligned} \sigma_1(t) &= 0 \\ \sigma_2(t) &= \nu\frac{F(t)}{A_0} \\ \sigma_3(t) &= \frac{F(t)}{A_0} \end{aligned} \tag{3.12}$$

and

$$\begin{aligned} \varepsilon_1(t) &= \frac{\Delta u_1(t)}{l_0} \\ \varepsilon_2(t) &= 0 \\ \varepsilon_3(t) &= \frac{\Delta u_3(t)}{l_0} \end{aligned} \tag{3.13}$$

where $\sigma_1, \sigma_2, \sigma_3$, $\varepsilon_1, \varepsilon_2, \varepsilon_3$ and $\Delta u_1, \Delta u_3$ are respectively the stresses, strains and differences of displacements according to the directions presented in Fig.3.20, $F(t)$ is the applied force, A_0, l_0 are respectively the initial cross-section and the initial length of a specimen, ν is the Poisson's modulus.

The lateral strain ε_1 is calculated with use of the displacement difference Δu_1, measured using LVDTs sensors. Compressive strain ε_3 is obtained due to the vertical deformation of the specimen - Δu_3. Thus, the axial stress intensity $\sigma_3(t)$ can be defined as a classical relation of force and the initial cross-section A_0, [Nadai 1950].

Results using Eqs. (3.12-3.13) are reported in Fig. 3.23. Basing on it, a large stress increase when the strain level close to $\varepsilon_3 \approx 0.1$ is observed. This effect is linked to the free gap between the specimen and the rigid wall of the set-up - Fig. 3.22. Therefore, until the specimen is not in contact with the rigid wall of the set-up, the specimen is under axial compression - Fig. 3.23. After it, a biaxial loading state causes a hardening increase.

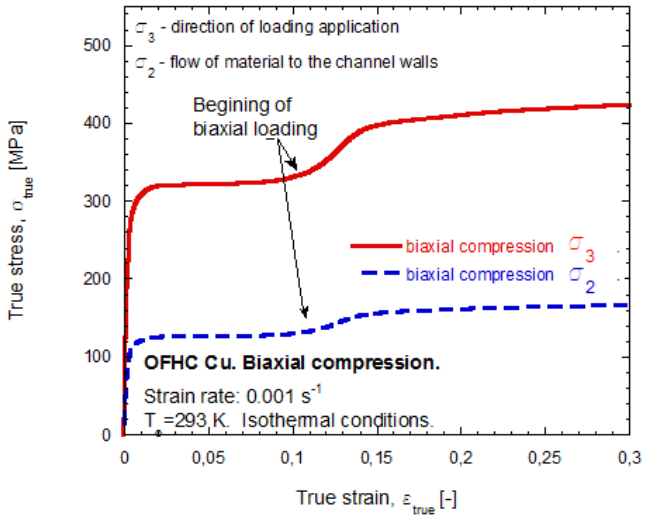

Figure 3.23: Experimental results under quasi-static biaxial compression.

The comparison between biaxial compression test and uniaxial compression tests is presented in Fig. 3.24. For the uniaxial compression tests two kinds of specimens were used: the cubic specimen of dimensions 8x8x8mm and the cylindrical specimen with diameter 12mm and height 10mm.

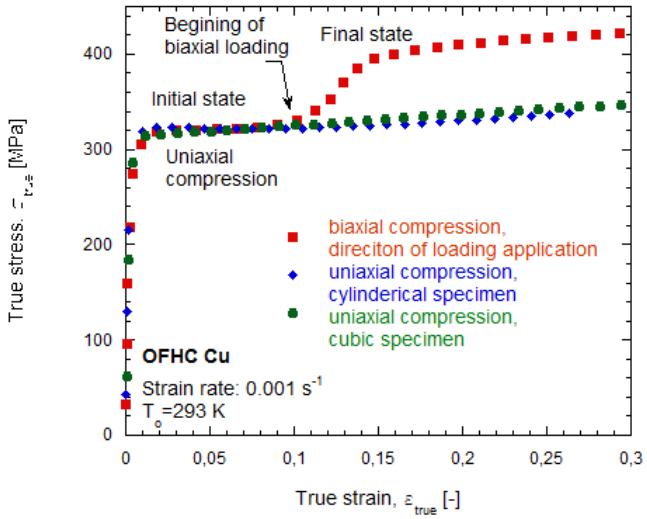

Figure 3.24: Comparison between biaxial loading and axial compression under quasi- static loading.

A good agreement is observed between uniaxial compression and the beginning of loading based on the new proposed set-up, Fig. 3.24. When the gaps are reduced due to material flow, the specimen is deformed due to the biaxial loading and the behaviour under this stress state can be defined. It has to be observed that the stress increase is relatively large using OFHC Copper. Consequently, the numerical model is built to investigate the material behaviour, the numerical analysis is presented in the next Paragraph.

3.4.2 FEM analysis of biaxial compression test

The experimental test of biaxial compression test has been simulated with the Finite Element commercial code ABAQUS [Hibbitt et al. 2010]. The numerical model consists of three parts: specimen, channel and punch. The dimensions of the specimen are set as 8x8x8mm, there is also assumed a gap between the specimen and the channel, 0.25mm free space from each side of the specimen. The channel and the punch are treated as the analytical rigid bodies, specimen is a deformable solid. It is meshed with 4096 8-node elements with reduced integration (C3D8R elements). There were studied mesh dependency - the number of elements has been chosen as optimal. The constitutive relation describing the material's model of material was validated on tensile and compressive tests.

The strength tests were performed using samples prepared from OFHC Cu. Mechanical and physical properties of OFHC Cu are given in Table 3.1 and 3.2. Tests were carried out in isothermal conditions at room temperature, in the strain rate equals to 0.001 s^{-1}.

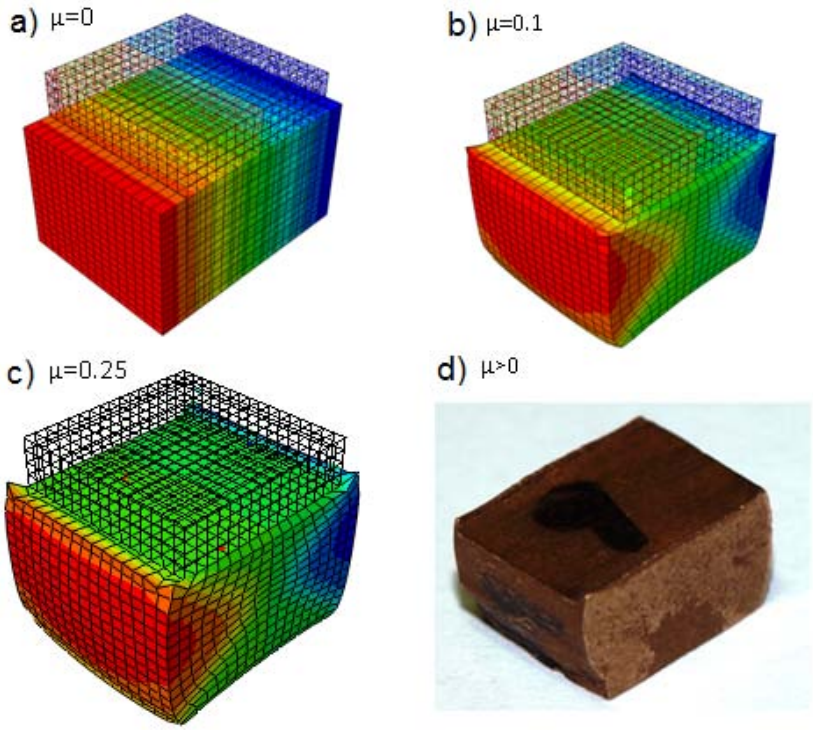

Figure 3.25: Influence of the friction on the final shape of the sample, results of numerical simulation performed for friction equals: a) $\mu = 0$, b) $\mu = 0.1$, c) $\mu = 0.25$, d) picture of a deformed specimen.

During the test, the friction influence is observed. It can be observed that the specimens were barreling, what is seen on example of the specimen deformed during the experiment - Fig. 3.25.d. This observation is proved by the numerical results - Fig. 3.25.c. The barreling of the specimen in the numerical test in friction conditions occurs, Fig. 3.25.b-c, whereas sample deformed in numerical simulation without friction influence has a shape of cuboid, Fig. 3.25.a.

In Fig. 3.24 the beginning of the biaxial compression process is indicated. It is assumed that the indicated by an arrow point the process of uniaxial compression occurs - Figs. 3.24, 3.26. The initial stage of biaxial compression is intentionally designed as uniaxial compression (because it is possible to estimate friction effect). The process of uniaxial compression occurs to the moment when gaps between the side walls of the channel and specimen disappears due to the flow of the material. To prove that observation the process of biaxial compression is simulated with use of two models. The first model - when there is no gaps between the specimen and walls of the channel (in Fig. 3.26 the results are marked with squares). The experimental result in direction 3 (direction of loading) are compared with numerical results. The obtained numerical result presents the same level of stresses during the whole process. Whereas, if the gaps between the channel and specimen are modelled, the stress-strain curve has two levels. The initial one - during the uniaxial compression test and final one - during the biaxial compression test, in Fig. 3.26 results are marked with dots. Gaps allow to obtain the uniaxial compression in the initial stage of the test, what is necessary to estimate the friction influence during biaxial compression process.

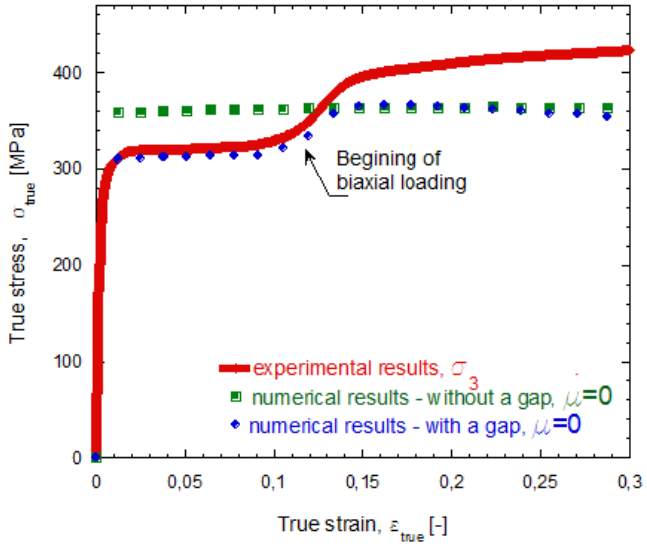

Figure 3.26: Numerical results obtained with use of a model without gaps between the specimen and the channel (indicated with squares) - then the uniaxial compression does not occur - and a model with them (indicated with dots).

In Fig. 3.27 there are presented results of numerical modelling with use of the model with gaps. With dots there is presented true stress-true strain relation in direction of loading (direction 3 according to Fig. 3.20) and with dashed line the dependence between displacement of the material in the direction of its flow (direction 1 according to Fig. 3.20) and true strain. It can be noticed that sudden increase of displacement and stress occurs for the same value of strain (close to $\varepsilon_{true} = 0.1$). This is caused by the onset of constrained plastic flow in the moment then deforming material touches the walls of the channel what is equivalent with the beginning of the process of biaxial compression.

Consequently, a parametric study has been performed based on configuration with a gap. The simulation with a gap but for different friction coefficients is reported in Fig. 3.28. Friction induces a stress increase - the higher value of friction coefficient, the higher level of

true stress-true strain curve. To research reason of the stress increase, an inverse method of modelling friction effect is proposed allowing better understanding of the test.

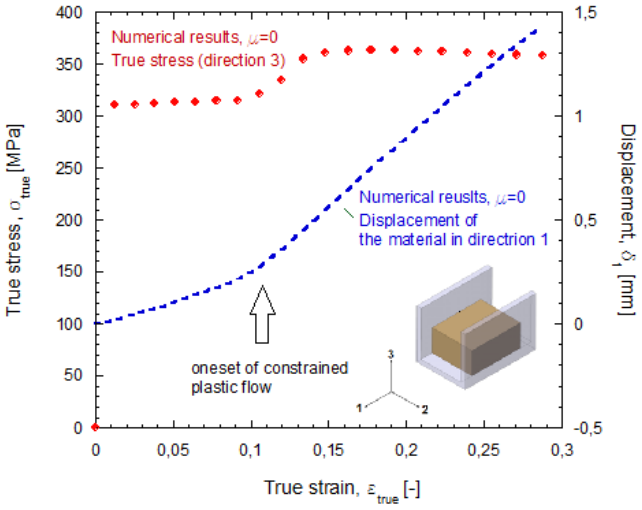

Figure 3.27: Onset of constrained plastic flow.

The numerical simulations performed with different friction coefficients have a feature which should be investigated. For $\mu = 0$ the level of true stress is decreasing starting from true strain equals to 0.15, then for curves obtained for higher values of friction coefficient the levels of curves saturate gradually. This can be contributed to weakening of the material due to the deformation process, it should be confirmed that this is not an effect of the channel walls influence.

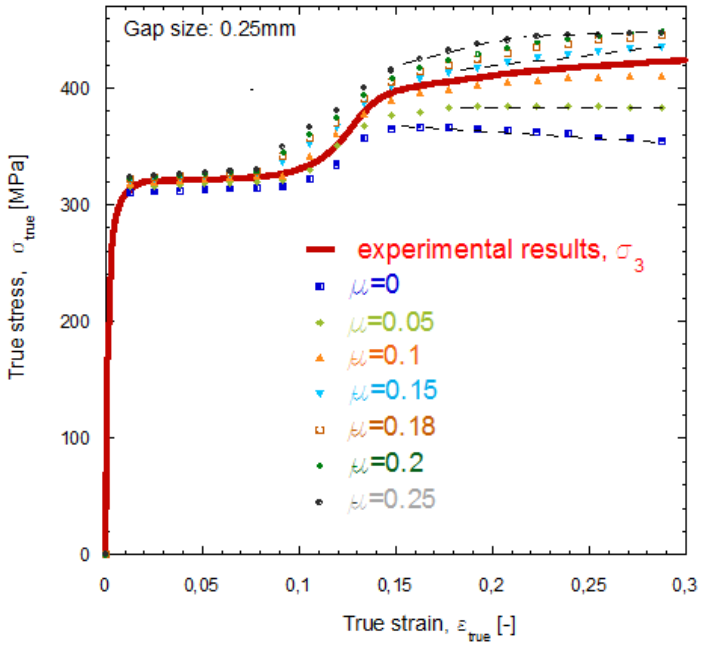

Figure 3.28: Comparison between experimental results of biaxial compression and results of numerical tests performed with different friction coefficients.

To prove this observation the different kind of numerical simulation is designed. The specimen is not set in the channel but instead, to its side walls the constant pressure of different magnitude is applied, the compressive load on the upper surface is applied as previous, Fig. 3.29. This simulation is to prove that decreasing of level of true stress-true strain is caused by the weakening of the material due to deformation, not influence of the set-up.

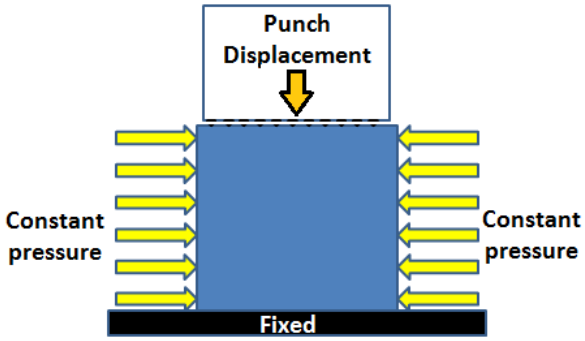

Figure 3.29: The model of numerical simulation with applied pressure for side walls of a specimen.

As a result, the material's response in true stress-true strain is presented and compared with numerical results obtained with use of a model with channel when assumed dimension of gaps is equals 0.25mm in frictionless conditions - Fig. 3.30. In the Fig. 3.30 there are presented results obtained due to application of pressure with different values. For pressure equals 80MPa the result (marked with squares) is too low, for pressure equals 300MPa - the applied pressure is too high and the obtained result is too low. The optimal value of pressure applied for walls seems the value close to 180MPa. Due to it the effect which side walls have on the specimen's deformation is repeated. What is more, the effect of weakling material due to deformation is also present. The slight decreasing of a curve can be reported.

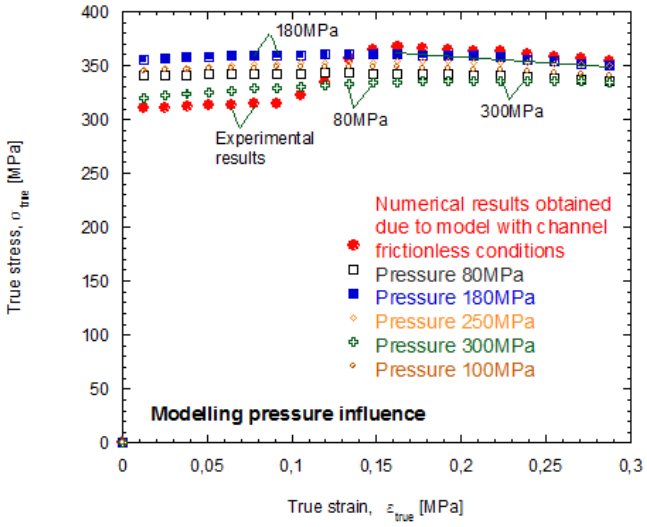

Figure 3.30: The true stress- true strain curves obtained due to numerical simulation with use of numerical model with applied pressure.

In Fig. 3.31, in x axis the values of applied pressure are given, in y axis the difference $\Delta Pressure$ between maximum value of pressure obtained on the side wall of a specimen and applied pressure which caused it. It can be noticed that starting from a value of pressure close to 185MPa, the pressure obtained in the material is smaller than applied. This observation proves that according to applied pressure material is not receptive to it because the dominant deformation is the flow of material caused by the punch.

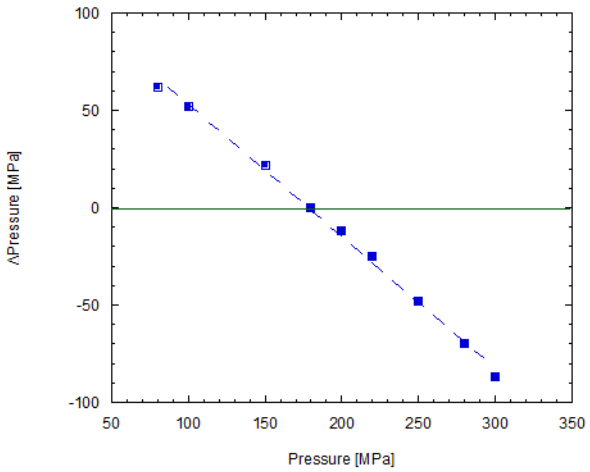

Figure 3.31: Difference between maximum value of pressure obtained on the side wall of a specimen and applied pressure which caused it.

The numerical process of losing strain and stress homogeneity increasing with growth of the friction influence is depicted in Fig. 3.32.

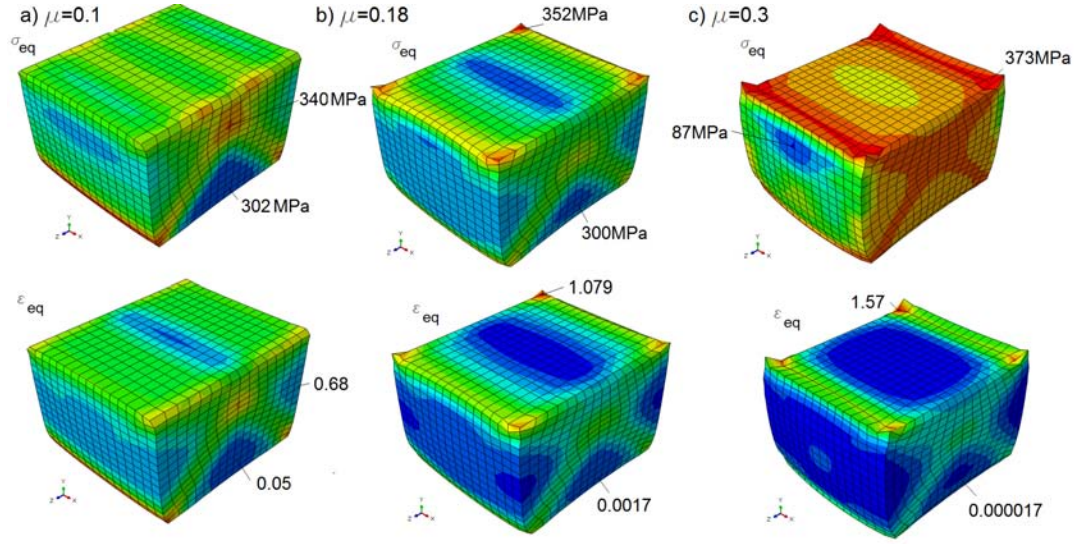

Figure 3.32: Comparison between numerical results presenting process of losing strain and stress homogeneity depending on the friction influence, in the first row equivalent strain: ε_{eq}, in the second row Mises equivalent stress, σ_{eq}.

In Fig. 3.32 there are pictures of deformed sample due to the process of biaxial compression performed with different friction coefficients: a) $\mu = 0.1$, b) $\mu = 0.18$, c) $\mu = 0.3$.

The upper pictures of deformed samples present maps of equivalent strain (ε_{eq}) and in the bottom pictures depict maps of Mises equivalent stresses (σ_{eq}). Increase of friction coefficient causes the larger and more inhomogeneous deformation of the specimen, what can be observed in the maps of stresses σ_{eq} and strains ε_{eq}.

The increasing of deformation with growth of the friction coefficient is also presented in Fig. 3.33.a, where results of numerical simulation performed with different friction coefficients μ are reported together with experimental points. Results of numerical simulations are presented as dependence between displacement in direction 1 (direction of flow material) and 3 (direction of applying load). Experimental displacements and displacement obtained due to numerical simulation are calculated from the moment of beginning of biaxial compression process - when the side surfaces of the specimen touch the channel, Fig. 3.33.b. Deformation leaded with a specific friction coefficient causes deformation of a specimen, its height shortens (Δu_3) and in direction 3, the material flows (Δu_1), the deformation in direction 2 is blocked due to the walls of the channel. With higher value of friction coefficient the larger deformation are obtained. The points bonding deformation in both direction are connected with the lines, which present dependence between difference in displacements influenced by friction coefficient. The experimental results are marked with dots. Experimental points lie in various lines obtained from numerical simulation. Consequently, it can be noticed that during the experiment the increasing deformation is characterized by different friction coefficient. The friction increases during the process of deformation.

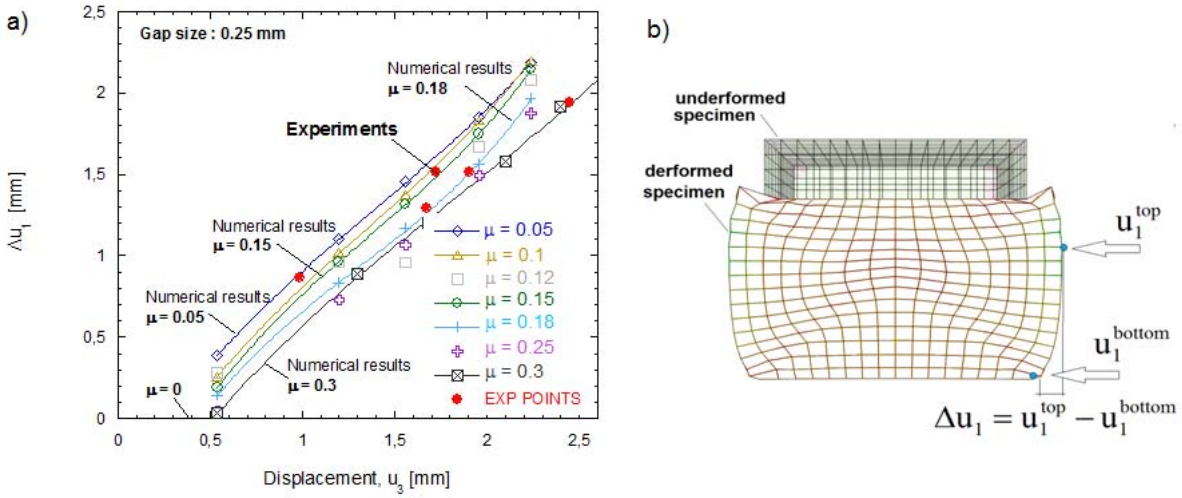

Figure 3.33: a) Friction coefficient analysis, results of numerical simulations recalculated accounting for beginning of the biaxial compression, b) Method of calculation the displacement difference: displacements were calculated from a moment when biaxial compression starts.

The influence of friction has a kinematic character - the larger deformation the highest value of friction coefficient. When strain level is lower than 15% then friction influence is not so high as when strain level is around 30%. For strains larger than 15%, friction coefficient is bigger than 0.2. This observation leads to proposition of a model which account for kinematic character of friction. The friction coefficient influences the stress level, it increases in comparison with the case when $\mu = 0$. Friction analysis based on the numerical simulation results and theoretical approach ([Klepaczko and Malinowski 1977; Jankowiak et al.

2011]), allows to estimate friction coefficient value and apply corrections to the results of the biaxial compression test. The proposed model of friction correction is discussed in the next Paragraph.

Model of friction correction

To define properly the material behavior under biaxial loading it is necessary to correct friction effect. To achieve this, a model has been developed taking into account the friction coefficient dependency on strain level, Fig. 3.34. The results are obtained coupling experiments and numerical results, Fig. 3.33. The suggested inverse method allow to better understanding of material behaviour influenced by the friction.

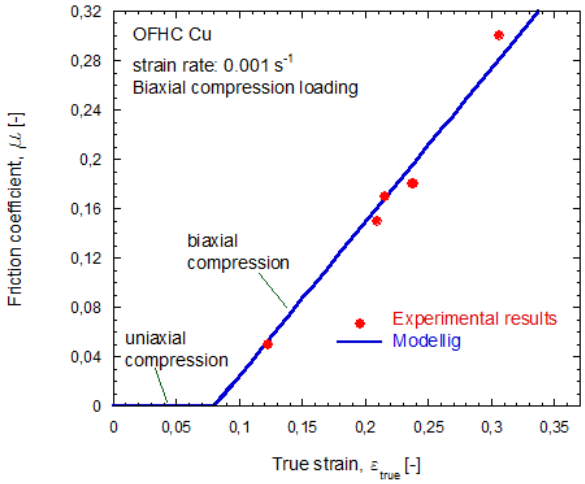

Figure 3.34: Friction coefficient value depending on strain level, comparison between experiments and analytical predictions, Eq. (3.14).

Based on presented above results, the following relation is proposed

$$\mu(\varepsilon) = \langle \mu_1 \cdot (\varepsilon - \varepsilon_{min}) \rangle \tag{3.14}$$

where ε_{min} is the strain where biaxial compression loading take place. The McCauley operator is defined as:

$$\begin{aligned} < \bullet > &= \bullet \Longleftrightarrow \bullet > 0 \\ < \bullet > &= 0 \Longleftrightarrow \bullet \leq 0 \end{aligned}$$

Moreover, it is observed that the friction coefficient μ induces a stress increase $\Delta\sigma_{friction}$ as reported previously in [Klepaczko and Malinowski 1977; Jankowiak et al. 2011]. Proposed by authors [Klepaczko and Malinowski 1977] correction of friction - Klepaczko-Malinowski model - Eq. (3.15), is based on a linear function accounting for constant friction coefficient value.

$$\begin{aligned} \sigma_{material} &= \sigma_{measured} - \Delta\sigma_{friction} \\ \sigma_{material} &= \sigma_{measured}(1 - \frac{\mu}{s_0}) \end{aligned} \tag{3.15}$$

where $\sigma_{material}$ is the material behaviour without friction effect and $\Delta\sigma_{friction}$ is the stress increase due to friction (coefficient μ) and the influences of specimens geometry s_0, when the specimen has a cylindrical shape.

The model Eq. 3.15 includes friction effect related to geometry s_0, however, this model is not suitable to the results of biaxial compression test, Fig. 3.35 due to application of different specimens. Presented in [Klepaczko and Malinowski 1977] model is a linear function of friction, whereas the function which describes dependency of results of biaxial compression test on friction coefficient has nonlinear character (as in work [Jankowiak et al. 2011]), Fig. 3.35.

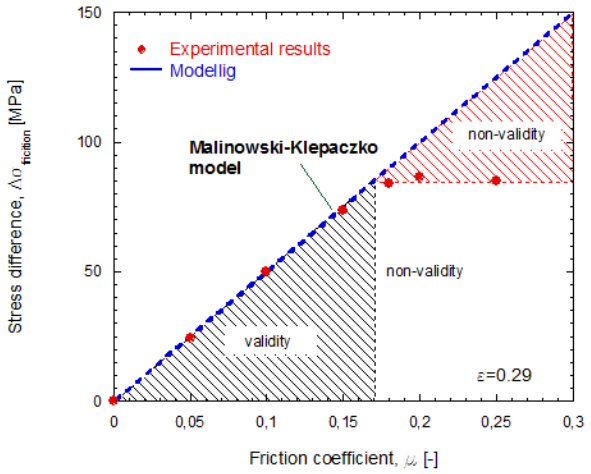

Figure 3.35: Friction effecting numerical simulation of biaxial compression, modelling with use of Eq. (3.14).

As it can be noticed in Fig. the model proposed by Malinowski-Klepaczko does not offer the suitable modelling of friction influence on material behaviour. Thus, basing on the Malinowski-Klepaczko [Klepaczko and Malinowski 1977] model, Eq. (3.15), and accounting for kinematic character of friction, the proposition of friction model is presented - Eq. (3.16). The values of model's parameters are collected in Table 3.3.

$$\begin{aligned} \sigma_{material}(\varepsilon) &= \sigma_{measured}(\varepsilon) - \Delta\sigma_{friction}[\mu(\varepsilon)] \\ \Delta\sigma_{friction} &= \gamma_1 \tanh \gamma_2[\mu(\varepsilon)]^{\gamma_3} \end{aligned} \tag{3.16}$$

where γ_i are the fitting constants.

μ_1	ε_{min}	γ_1	γ_2	γ_3
1.25	0.08	87	17.66	1.42

Table 3.3: Constants of Eq. (3.16) used to approximate experimental results.

For this reason and to be in agreement with numerical results, the stress change may be defined using Eq. (3.16). This relation allows to define the nonlinear dependence between friction and deformation. As it can be noticed in Fig. 3.33 durign the process of biaxial compression the friction was changed. Its value increasing along with increasing load.

It can be noticed that friction in process of biaxial compression has large effects on material behaviour - increasing friction coefficient causes also stress increase. The modelling of friction influence is presented in Fig. 3.36 - the nonlinear character of dependence between stress in material and friction coefficient can be noticed.

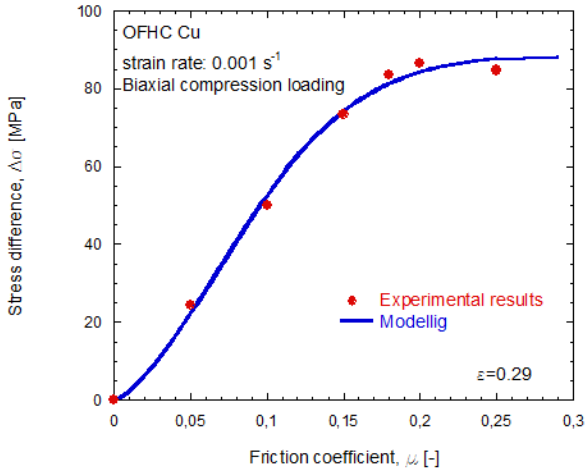

Figure 3.36: Stress increase due to friction, comparison between numerical results and analytical prediction, Eq. (3.16).

In Fig. 3.37 there is reported the parametric study of the Eq. (3.16). The determined parameters fit the most appropriately the experimental results presented in Fig. 3.36. In Fig. 3.37.a there are presented different values of parameter γ_1, then the figure 3.37.b presents dependence of relation (3.16) on parameter γ_2 and Fig. 3.37.c shows the fitting depending on γ_3. The function of Eq. (3.16) is sensitive for changing of parameters: the limit values of parameters are: in case of parameter γ_1 - 5%, parameter γ_2 and γ_3 20% respectively lower and higher It can be notice that differences in parameters' values cause large change of shape of the function.

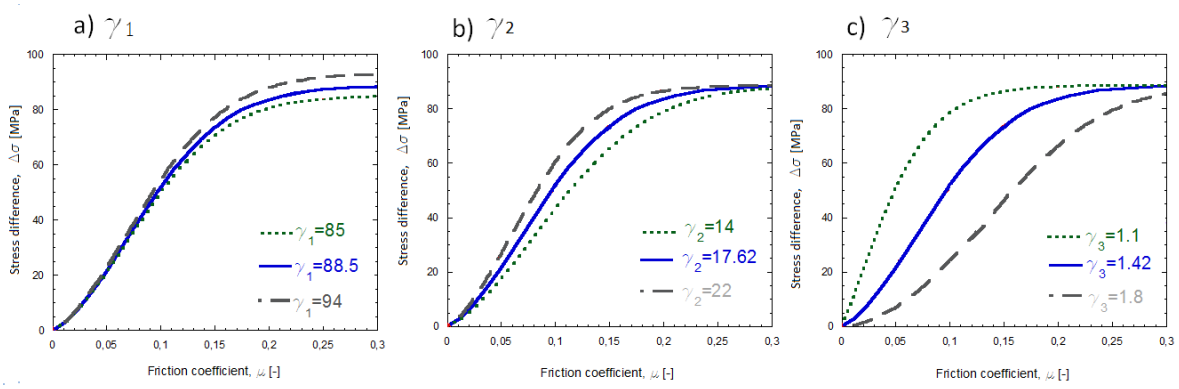

Figure 3.37: Study parameters for Eq. (3.16) for various values of parameter: a) γ_1, b) γ_2, c) γ_3.

In Fig. 3.38 there are presented results of uniaxial compression (marked with thin dashed line) and biaxial compression (marked with squares) - these are experimental results. The numerical results obtained in simulation in frictionless conditions using a model with gaps

between channel and specimen are plotted as dots. Analytical results obtained due to modelling with Eq.(3.16) are presented as lines. In analytical modelling with the friction coefficient assumed constant (in this case $\mu = 0.1$) the obtained results are plotted as line with dots. The analytical model with friction coefficient changing according to relation presented in Fig. 3.35 is signed with thick line. The function of $\tanh(\mu)$ is used to find the character the process of saturation. It can be applied for direct experimental measurements and then, if applying function of friction coefficient changes along with the increasing strain - to numerical results obtained in frictionless conditions. If friction is assumed as constant, the resulted stress-strain curve has a completely different and improper character. The analytical modelling with use of the friction coefficient changing along with increasing strain repeats the result obtained in numerical simulation which is considered as process of biaxial compression in frictionless conditions.

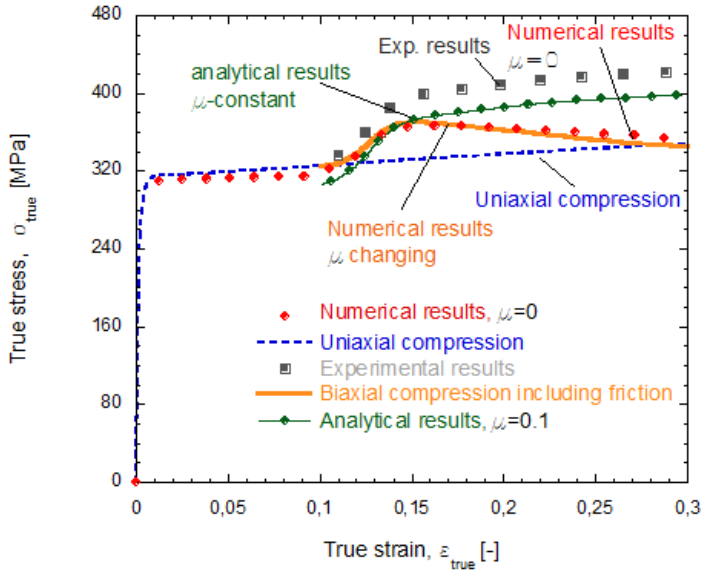

Figure 3.38: Comparison between compression and biaxial loading including direct measurement, results after correction Eqs. (3.14)-(3.16) and numerical results obtained under biaxial loading assuming no friction.

It can be concluded that the model proposed initially by [Klepaczko and Malinowski 1977] and extended by [Jankowiak et al. 2011] may be used to correct in an easy way the friction effect under biaxiac compression. Presented model allows to repeat behaviour of the material with use of analytical equations (3.14)-(3.16). As it is shown in Fig. 3.38 the models correlates well with experimental data of OFHC Cu. Corrected results of biaxial compression test can be used to validate the yield surface.

Discussion given in this Section aims to introduce the biaxial compression test. The designed set-up, which project is attached in the Appendix 3, is not difficult to manufacture and can be used as a additional verification technique in a laboratory of Mechanics of Materials. The methodology of biaxial compression must be undergo with a great care because of the large friction influence on the experimental results. The throughout numerical analysis presented in the Section should allow, however, to apply the proposed technique.

In next Section another test allowing to obtain complex state of stresses is shortly described, [Dietrich and Socha 2002; 2012]. Due to the test the several yield points being results of combination of compression/tension and torsion loadings are defined. The yield points are determined for the offset strain equals 0.0001 (Section 3.1.2) as subsequent steps (Fig. 3.41.b) of the test are stopped just after the elastic range of material characteristics ends. The method allows to plot the initial yield curve in the plane of measured values of axial stresses σ and shear stresses τ. Due to the simple recalculation, Eq. (3.18), the same points are defined in the plane of principal stresses. As a result the yield surface and its cross-section in the space of principal stresses is possible to determine.

3.5 Complex stress state test

Mechanical properties change due to the load history, it is an important issue for the industrial applications to analyse that evolution. The processes that causes initial plastic deformations are also the reason of the acquiring of undesired anisotropic properties in the material, which are difficult to remove by heat treatment. Therefore, it is important to study experimentally the influence of the load history on evolution of mechanical properties. In the Thesis to study the material's mechanical properties under the complex path of loading, there is used the test called *the complex stress state test* or *the tension-torsion-compression test*. The idea of the test is discussed by its inventor in papers [Dietrich and Socha 2002; 2012]. As a result of this test an initial yield surface can be obtained.

A single thin-walled tubular specimen subjected to sequent loads is used in the test. The aim of the test is obtaining the trace of loading in the two-dimensional stress space (σ, τ), where σ is an axial stress, and τ is a shear stress. The geometry of a thin-walled tubular specimen is presented in Fig. 3.39.

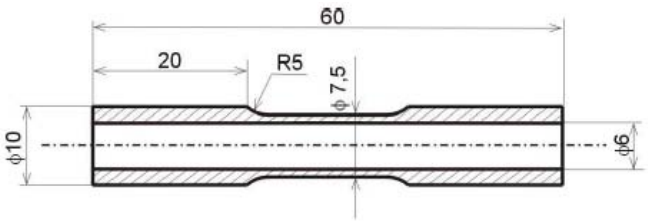

Figure 3.39: The dimensions of the thin-walled tubular specimen used in the complex stress state test.

Tests are performed using the MTS 858 load frame with nominal axial load of $\pm$25 kN and nominal torque of $\pm$200Nm. The TestStar II, a fully digital controller equipped with the MTS TestStar v.4.0D + TestWare-SXv.4.0D software is used for program and control a course of experiments.

Two sets of strain gauges are glued to the specimen, Fig.3.40.a.

- Three strain gauges positioned in a rosette-like layout: the rosette of the type 45° and rectangular one, Fig.3.40.b. This system allows for measurement of the axial strain (compressive or tensile) and the shear strain.

- Strain gauge to measure hoop strain, Fig.3.40.c.

In Fig. 3.40 the picture of specimen with strain gauges is shown.

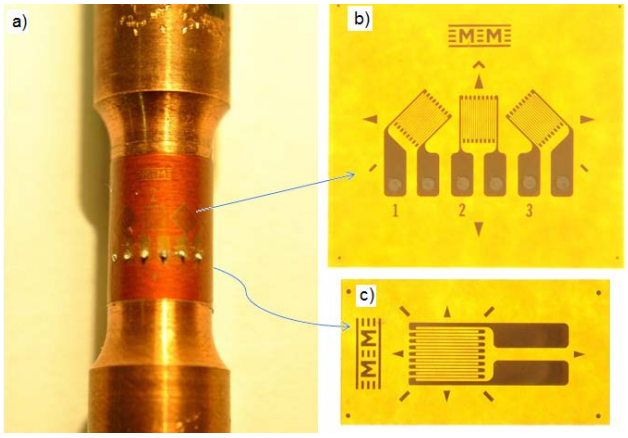

Figure 3.40: a) The thin-walled tube specimen with the strain gauges, b) the rosette-like strain gauge, c) the strain gauge to measure hoop strain.

The issue of the test are the sequential loading in different direction of the strain space as shown in Figs. 3.41-3.42. Loading starts at an axial tension (step no 1, the direction $0°$) and after unloading a next loading is performed in strain control mode for different combination of an axial force and torque. Then, there is a serie of steps with the progressive tension and torsion until the only torsion loading (step no 5, the direction $90°$). And then, through the progressive compression and reverse torsion loadings, the only compression loading is obtained (step no 9, the direction $180°$), then reverse torsion is indicated as a step no 13 or the direction $270°$. The initial yield surface determination program is ended for direction 17 which denotes repetition of the axial tension. For each step the load is applied until the sample reaches the first plastic deformation, then the specimen is unloaded and the next step of loading is started.

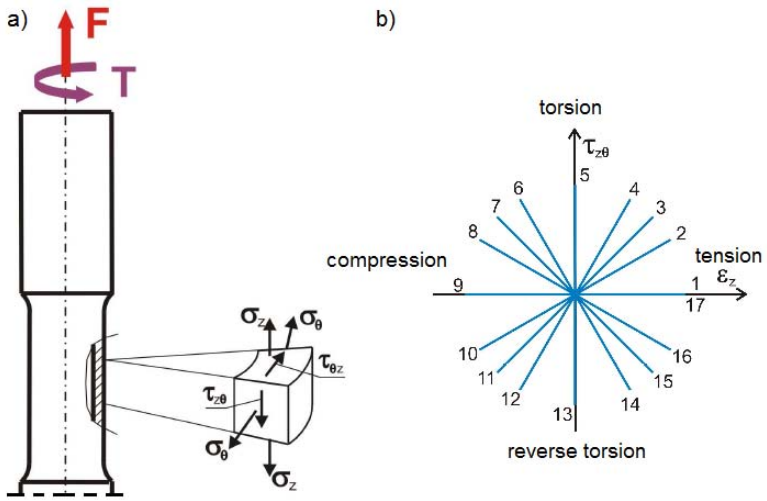

Figure 3.41: a) Diagram of the sample loading, b) assumed directions of loading for the procedure of determination an initial yield surface.

Fig. 3.42 presents schematically the directions of loading with use of arrows. In the horizontal axis there are given values of angle which are obtained in the subsequent steps of loading - which are adequate to steps from Fig. 3.41.b. In the vertical axis the values of yield points are signed. The example presents results of OFHC Cu for 2 specimens. From the this picture it is possible to observe how material's behaviour changes in the path of different loading. The yield strengths have been identified for offset strain equals 0.0001 - just after the end of the elastic range.

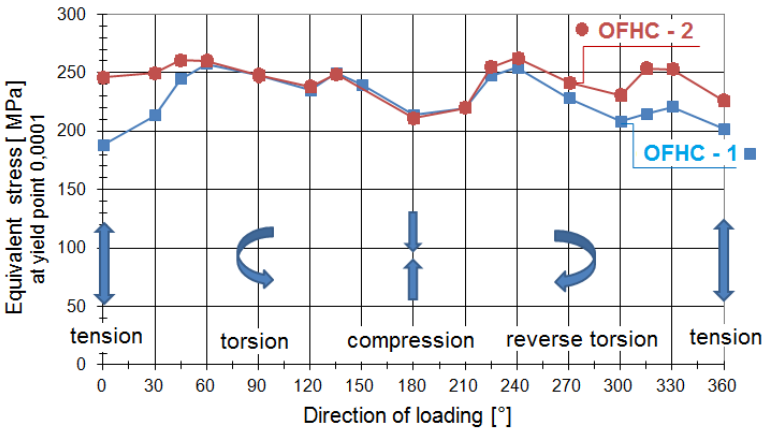

Figure 3.42: Relation between the yield points and the load directions.

The load sequences aim to determine the points of the initial limit curve in the plane state of stress: (σ, τ). As a result of the test the values of the Young's and shear moduli and also the Poisson's ratio are determined. The result of each loading combination is presented also as equivalent stress - equivalent strain relation, for each the Young's modulus is determined and finally, its value is calculated as average. The Poisson's coefficient is also an average value determined due to strain gauges reading, the shear modulus is a relation between them. Basing on them the algorithm has been developed which allows to plot the initial yield curve, which is approximated using a nonlinear regression of parametric ellipse - purely mathematical formula for an ellipse, Eq.(3.17).

$$\begin{aligned} x(t,k) &= S_x - A\sin(t)\sin(k) + B\cos(t)\cos(k) \\ y(t,k) &= S_y + A\sin(t)\cos(k) + B\cos(t)\sin(k) \end{aligned} \tag{3.17}$$

where S_x, S_y are coordinates of the center of symmetry, A, B are respectively the semi-major and semin-minor axes.

The plot presenting the yield curve in the plane (σ, τ) is given in Fig. 3.43.

Then, the yield strength values read in the (σ, τ) coordinates are recalculated to the principal stresses (σ_1, σ_3) with use of Eq. (3.18).

$$\sigma_{1,2} = \frac{\sigma}{2} \pm \frac{1}{2}\sqrt{(\sigma)^2 + 4(\tau^2)} \tag{3.18}$$

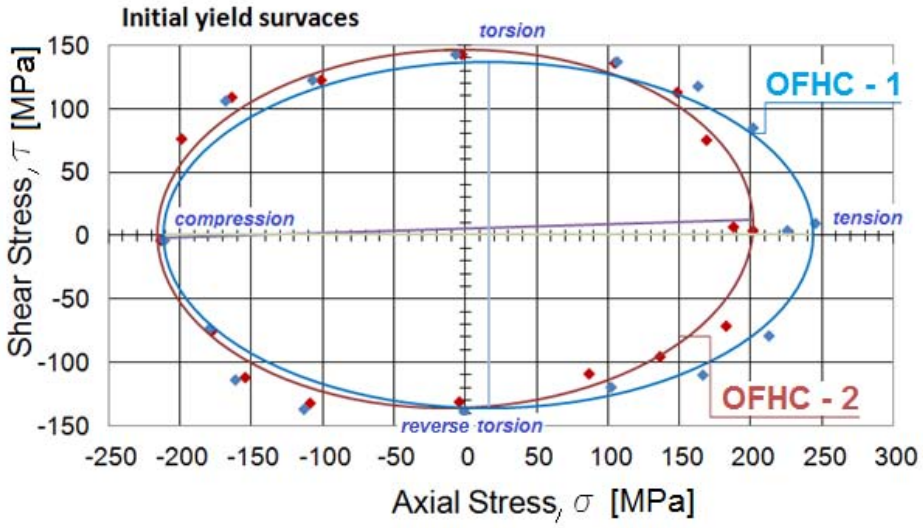

Figure 3.43: The yield surface obtained due to the approximation process with use of Eqs. (3.17).

Basing on these data deterimed due to Eq. (3.18) the yield surface in the space of principal stresses $(\sigma_1, \sigma_2, \sigma_3)$ is obtained, as well as its cross-section for $\sigma_2 = 0$. The example of set of yield points in coordinates of the plane (σ, τ) and the same yield points in coordinates of the plane (σ_1, σ_3) is presented in Fig. 3.44.

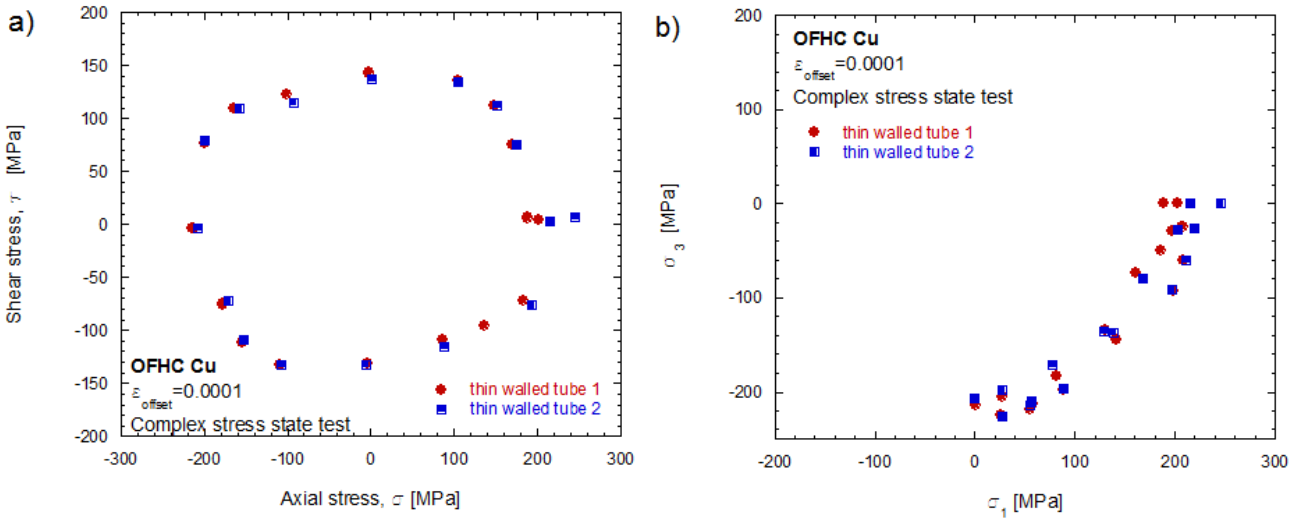

Figure 3.44: a) Yield points obtained due to the complex test in the plane (σ, τ), b) yield points after recalculating coordinates with use of relation (3.18) in the plane (σ_1, σ_3).

The result of the complex stress state test is a set of yield points defined for offset strain equals to 0.0001. Yield points are results of subsequent loadings being the combination of compression-torsion and tension-torsion. If they are plotted in the plane (σ, τ) the trace of the initial yield surface is obtained due to mathematical approximation. After recalculation coordinates of yield points to the coordinates of principal stresses they are placed in the forth quarter of the plane σ_1, σ_3 what allows to accurate approximation of an applied yield curve.

In Section 3.6 the dynamic compression test is described. The results of dynamic test are used to model yield of material in the dynamic range. Basing on information found about yield in quasi-static range, the data from dynamic compression can be used to obtain the yield state in higher strain rate ranges.

3.6 Split-Hopkinson Pressure Bar test (SHPB) for dynamic compression

The split-Hopkinson pressure bar is used to impose a dynamic loading on a specimen at the high strain rates ($10^2 s^{-1} \leq \dot{\varepsilon} \leq 10^4 s^{-1}$). Maximum possible strain rates is depended on the projectile impact velocity and the yield stress of the tested material. The technique originally proposed in 1949 by Hopkinson [Hopkinson 1914] was refined by Kolsky [Kolsky 1949; 1952] with use of two Hopkinson bars in series, known as split-Hopkinson bar. Using the technique of SHPB and the knowledge of elastic waves propagation the dynamic thermo-viscoplastic behaviour of material $\sigma(\varepsilon, \dot{\varepsilon}, T)$ can be derived, [Perzyna 1971; 2001]. Modified Hopkinson bars are also used to tests of tension and shear in dynamic ranges, [Rusinek and Klepaczko 2001; Peirs et al. 2011b; Verleysen et al. 2011]/

A conventional Split-Hopkinson Pressure Bar apparatus, which is schematically shown in Fig. 3.45, consists of a pneumatic gas gun (or a launching device), a striker, an input bar, an output bar, an energy absorption device, and a data acquisition system, Fig.3.45. The specimen is sandwiched between the input bar and the output bar - between them there is a layer of a molibden lubricant.

The diameter ϕ_b of the input and output bars, theirs density ρ_b, as well as the Young's modulus E_b are summerized in the Table 3.4. Also, in the Table there are characteristics of the specimen, its diameter ϕ_s and length L_s.

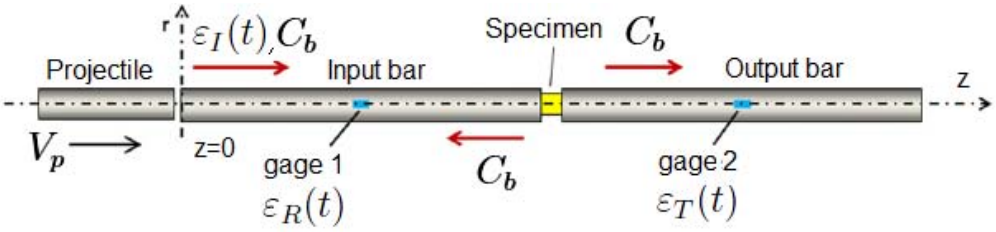

Figure 3.45: Details of geometry of SHPB techniques.

L_B [m]	ϕ_b [m]	ρ_b [kg/m^3]	E_b [GPa]	ϕ_s [m]	L_s [m]
0.018	7800	210	0.008	0.004	

Table 3.4: Characteristics of used in the experiment input and output bars.

When the projectile impacts the input bar, then the elastic, incident wave $(\sigma_I(t), \varepsilon_I(t))$ travels through the input bar to the specimen with an elastic wave speed C_b.

The elastic wave speed in a bar is defined as $C_b = \sqrt{\frac{E_b}{\rho_b}}$, where ρ_b is the density of the bar material and E_b is its Young's modulus. The incident wave intensity σ_I is proportional to the speed of the projectile V_p: $\sigma_I(t) = 0.5\rho_b C_b V_p(t)$. Wave amplitude ε_I is defined as a relation $\varepsilon_I(t) = \sigma_I / E_b$.

Due to the mismatch of mechanical impedances between the bar material and the specimen, part of the incident wave is reflected into the input bar as a reflected wave $(\sigma_R, \varepsilon_R)$. The rest of the incident wave transmits through the specimen, which is compressed at high rates, and goes into the output bar as a transmitted wave $(\sigma_T, \varepsilon_T)$. The incident and reflected signals are measured by the strain gages on the input bar whereas the transmitted signals are measured by the strain gages on the output bar. All three signals are recorded with a numerical oscilloscope. Fig. 3.46 presents the illustration of the discussed phenomena.

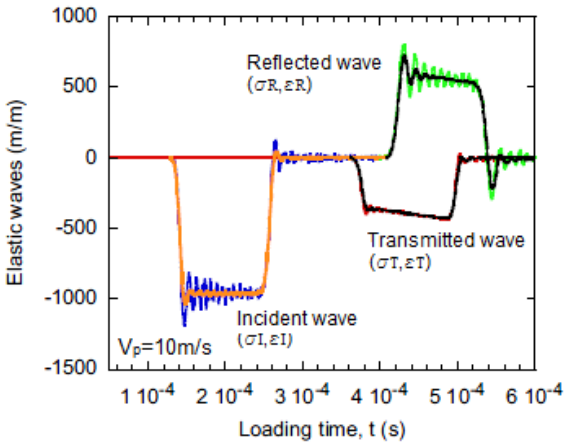

Figure 3.46: Description of elastic wave propagation along the Hopkinson bar.

One-dimensional stress-wave analysis on the bars is presented beneath, due to which it is possible to obtain force and displacement of the specimen which are subsequently calculated into the strain, strain rate and stress history in the specimen.

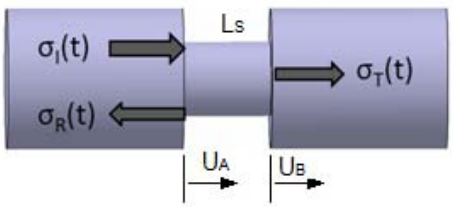

Figure 3.47: Faces of input and output bars with the specimen.

With use of the wave equation (3.19) which is determined by the method of characteristics, the displacements of rods, Fig. 3.47, are given as:

$$\frac{\partial^2 U}{\partial t^2} = C_b^2 \frac{\partial^2 U}{\partial x^2} \tag{3.19}$$

Then:

$$U_A(t) = C_b \int_0^t \Big[\varepsilon_I(t) - \varepsilon_R(t)\Big] dt \tag{3.20}$$

$$U_B(t) = C_b \int_0^t \varepsilon_T(t) dt \tag{3.21}$$

Relative displacements of the specimen faces $U_A(t), U_B(t)$, Fig. 3.47, allow to obtain the average value of the deformation ε_s and the average strain rate $\dot{\varepsilon}_s$ of the sample:

$$\varepsilon_s = \frac{U_A(t) - U_B(t)}{L_s} \tag{3.22}$$

$$\dot{\varepsilon}_s = \frac{1}{L_s}\Big[\frac{dU_A(t)}{dt} - \frac{dU_B(t)}{dt}\Big] \tag{3.23}$$

Knowing the characteristics of the incident, reflected and transmitted waves $\varepsilon_I(t), \varepsilon_R(t), \varepsilon_T(t)$ and using the Hooke's law, the equilibrium of forces between input and output bars should be stated:

$$F_A(t) = E_b A_b \Big[\varepsilon_I(t) + \varepsilon_R(t)\Big] \tag{3.24}$$

$$F_B(t) = E_b A_b \varepsilon_T(t) \tag{3.25}$$

where A_b is the bar cross-sectional area.

Consequently, the average stress level imposed to the specimen can be calculated as:

$$\sigma_s(t) = \frac{F_A(t) + F_B(t)}{2A_s} \tag{3.26}$$

where A_s is the current cross-sectional area of the sample.

After substitutions the average strain and stress in the sample are as follow:

$$\varepsilon_s(t) = \frac{C_b}{L}\Big[\varepsilon_I(t) - \varepsilon_R(t) - \varepsilon_T(t)\Big] \tag{3.27}$$

$$\sigma_s(t) = \frac{1}{2} E_b \frac{A_b}{A_s}\Big[\varepsilon_I(t) + \varepsilon_R(t) + \varepsilon_T(t)\Big] \tag{3.28}$$

Thus, starting from displacement of the face of the specimen, the recorded wave amplitudes $\varepsilon_I(t), \varepsilon_R(t), \varepsilon_T(t)$, and assuming the equilibrium of forces between input and output bars the average values of $\sigma_s(t), \varepsilon_s(t), \dot{\varepsilon}_s(t)$ are finally determined.

More information about SHPB technique can be found in e.g.: [Gilat 2000; Chen and Song 2010].

The software Waves Analysis and Study Program (WASP) has been used to analyse the elastic waves and estimate the material behaviour. Knowing characteristics of the three waves (incident, reflected and transmitted) allows to rebuilt the thermo-visco-plastic behaviour of the material tested under dynamic loading in terms of the stress–strain curve. It also allows to correct friction and adiabatic effects in order to obtain the intrinsic behaviour of the tested material, [Mandrea et al. 2010].

3.7 Concluding remarks

Presented in this Chapter experimental techniques have been used to obtain mechanical characterization of introduced in the previous Chapter 2 materials. There have been presented tests in the quasi-static (compression, tension, double shear, biaxial compression, complex test) and dynamic (compression) strain rates. Besides analytical approach allowing to calculate the suitable material's characteristics, there have been presented numerical analysis which simulating the test's conditions allow to correct experimental results. The obtained due to performed tests and corrected due to numerical simulation results are used in the subsequent Chapters. Constitutive relations have been presented in order to provide a macroscopic description of the plastic behaviour of materials within wide ranges of strain rate. Experimental results coupled with theoretical and numerical approach should be proceeded to analyse loading processes. Such approach is applied in the Thesis in order to understand the mechanisms responsible for deformation and in order to to obtain description of the onset of the plasticity.

The presented in this Chapter techniques allow to identify point in the space (or plane) of principal stresses due to which it is possible to determine the yield state (and its visualizations). In case of plane $\sigma_2 = 0$ (Section 3.1.1, Fig. 3.1) points are located on the axes of system of coordinates σ_Y^T, σ_Y^C or in the fourth quarter of system of reference τ_Y, results of the complex stress state. The yield point resulted from biaxial compression test is located in the third quarter what makes it an important result - because in this range there is a largest difference between yield conditions. Consequently, it would be a challenge to obtain results in the second quarter of the system of reference. The test which allows to obtain results in this range is, for example, the biaxial tension. The techniques of biaxial tension is discussed in e.g. [Belhabib et al. 2008; Teaca et al. 2010], but the discussion presented in theses papers concerns sheet materials. The experiments in biaxial tension for bulk materials would be an interesting possibility of experimental investigation for verification of yield conditions.

In next Chapter the discussion on yield conditions in reported. Firstly, there is given a historical background concerning the most important yield conceptions. Then, there is presented study of the art concerning the other yield criteria which were proposed by different authors. Next, the Burzyński material effort hypothesis is introduced. The resulting from it criteria are described. The examples of the their application based on the results for discussed in Chapter 2 materials and various data found in the literature are given in Chapter 5.

Chapter 4

Burzyński material effort hypothesis

The yielding and failure of materials is a topic of great current interest. The main subject of this Thesis is the description of criteria for materials accounting for SD effect and/or initially anisotropy. Before introducing used in the Thesis criteria, the state of the art concerning the yield criteria is presented. Different approaches for describing yielding are shortly discussed. General outline is given for techniques of presenting the plastic surface and limit curve. Finally, the energy based material effort hypothesis, originally proposed by W. Burzyński in 1928 (translated in English in 2009) [Burzyński 2009], is presented and described. The special cases of the hypothesis according to different groups of materials are discussed. More deep insight is expressed to paraboloid yield criterion, the criterion is applied for isotropic materials with strength differential effect. Then, the extension of criterion is proposed for materials which are characterized by initial anisotropy. Also, the phenomenological formulation of the criterion is given incorporating into the yield function strain, strain rate and temperature.

4.1 Introduction

Metals or polymers are used in many man-made structures, like ships, planes, cars, buildings. They should be designed for a set of failure modes that govern their structural reliability, because their failure under accidental loading can lead to catastrophic collapse of individual components or whole structures resulting in gross losses of life or property. Modelling of the behaviour of such materials, should involves three aspects, the first of them is defining the initial yield surface - specifying the states of stress for which plastic flow first begins, then determination of the associated flow law - connecting the plastic strain increment with the stress and stress increment, and finally,a hardening rule, specifying the behavior of the yield or flow surface as workhardening progresses. To effect such a description, the theory of plasticity has evolved, which is predictive in the sense of the consequences of stability, i.e. normality of the plastics train increment vector and convexity of the initial and all subsequent yield surfaces. Consequence of performed in such a way process of analysis leads to a comprehensive look on the material behaviour. Such approach is needed in the industrial applications, in which processes of designing demand for reliable structural and strength analysis what leads to obtain the safety factors of the designed structure.

It is a very important issue to choose a strength theory: yield criterion (or failure criterion) and material model in research and design. The load carrying capacity of structures, forming limit of FEM simulations, size of plastic zones, orientation of shear band and plastic flow localization will be much affected by the choice of strength theory. Strength theory deals with the yield and failure of materials under a complex stress state. It includes yield criteria and failure criteria, as well as multiaxial fatigue criteria, multiaxial creep conditions, and material models in computational mechanics and computer codes. It makes an important foundation for research on strength of materials and structures. The concept of yielding is of great significance in theoretical research and engineering application, and is also very important for the effective utilization of materials. Particularly, for design purposes, a reliable strength prediction for various combinations of multiaxial loading is important.

In this Chapter author focuses on the yielding description. To obtain this aim, firstly, the general function describing yield state is presented, Section 4.2. Then, in Section 4.3 the methods of depicting yield state of material are presented. Visualization of yield state allows to understand better which phenomena are responsible for the process of plastic deformation in material. Pictures visualizing yield curve and yield surface are useful for the illustration and better understanding of material's properties.

Various approaches to approximate onset of the plasticity have been proposed during the ages. In Section 4.4 there is presented a short study of the art concerning the development of yield theories during the decades, mainly in the XXth century.

Finally, in the Section 4.5 the Burzyński material effort hypothesis is discussed. The general theory of Burzyński is discussed, it is applied for materials for which the yield strength in uniaxial tension differs from that in uniaxial compression - Section 4.5.3. The extended formulation of Burzyński criterion - Section 4.5.4 - covers needs of materials initially anisotropic because of manufacturing processes. The Huber-Mises-Hencky criterion (HMH criterion) is a special case of the presented theory.

4.2 General formulation of the yield condition

The yield criterion is a function (its domain may be differently defined), which describes the limit surface of the elastic state in the material. Thus, the yield criterion defines the end of elastic state of material and also the beginning of the irreversible plastic deformations. The yield surface can be described as a set of points located in the stress space, which correspond to the same value of the strain, [Nadai 1950]. If the material's response on the loading, written in the suitable coordinates, lies inside of the yield surface - then the state of material can be treated as elastic. If such a point is on the surface - then the state of material can be considered as plastic.

For uniaxial states of stress, the beginning of the plastic state is determined by the value of yield strength limit. In case of complex stress states, the plastic state of the material is possible only when the components of the stress tensor fulfill a function - called the yield condition.

The yield condition of the material is described by a stress function $f(\sigma_{ij})$, which describes a hypersurface dependent on the stress tensor components σ_{ij} satisfying the conditions, [Nadai 1950]:

- $f(\sigma_{ij}) < 0$ - points within the surface determine the elastic state of the material,
- $f(\sigma_{ij}) = 0$ - points lying on the surface determine the plastic state of the material.

where σ_{ij} is a second-order tensor, called the Cauchy stress tensor.

The stress tensor has three eigenvalues which are called the principal stresses: $\sigma_1, \sigma_2, \sigma_3$. The stress tensor σ_{ij} can be also expressed as the sum of two other stress tensors: the mean normal stress tensor - σ_m and the stress deviator tensor - S_{ij}. The σ_m is the mean stress value or value of the hydrostatic pressure, with use of the principal stresses it may be calculated as Eq. (4.1).

$$\sigma_m = \frac{1}{3}(\sigma_x + \sigma_y + \sigma_z) = \frac{1}{3}(\sigma_1 + \sigma_2 + \sigma_3) \tag{4.1}$$

The general form of the plastic criterion is a function of stress state, which should not depend upon the chosen coordinate system or an element on which the stress tensor operates. Thus, the criterion is presented as a function of stress invariants. The function of criterion written with use of the invariants of stress tensor and its deviator has a form:

$$f(I_1, J_2, J_3) = 0 \tag{4.2}$$

where I_1 is the first invariant of the stress tensor, J_2, J_3 are respectively the second and third deviatoric stress invariants.

The invariants may be written with use of principal stresses:

$$\begin{gathered} I_1 = \sigma_{ii} = \sigma_1 + \sigma_2 + \sigma_3 \\ J_2 = \frac{1}{2}S_{ij}S_{ij} = \frac{1}{6}[(\sigma_1 - \sigma_2)^2 + (\sigma_2 - \sigma_3)^2 + (\sigma_1 - \sigma_3)^2] \\ J_3 = S_1 S_2 S_3 = (\sigma_1 - \sigma_m)(\sigma_2 - \sigma_m)(\sigma_3 - \sigma_m) \end{gathered} \tag{4.3}$$

Yield criterion can be a function of tensor components but then it would be dependent on the choice of the reference system. In addition, the yield surface would be depicted in the six-dimensional space of stresses σ_{ij}. Therefore, the function of the yield criterion is usually written with use of the principal stresses $\sigma_1, \sigma_2, \sigma_3$.

Since approximation of the onset of the plasticity is often conected with its visualization in next Section the most common methods of depicting the yield surfaces and curves are presented.

4.3 Visualization of yield criteria

In this Section there are presented methods of depicting yield criteria. Usually, the surface is presented in the principal stress space - the Haigh-Westergaard space. Haigh in [Haigh 1920] and Westergaard in [Westergaard 1882] introduced the limit surface in a 3D principal stress space, Fig. 4.1.

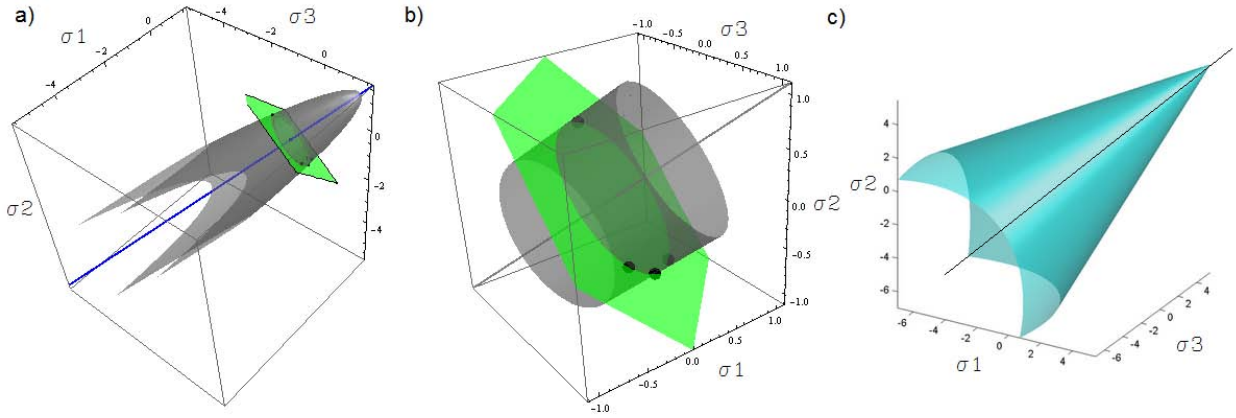

Figure 4.1: The yield surfaces in the space of principal stresses $(\sigma_1, \sigma_2, \sigma_3)$: a) a paraboloid of revolution - the Burzyński criterion, b) a cylinder of revolution - the Huber-Mises-Hencky criterion, c) a cone - the Drucker-Prager criterion. All three cases are detailed formulation of the Burzyński hypothesis.

A single point in the Haigh–Westergaard space is representative of the stress tensors having the same principal values. Due to the arbitrariness in the ordering of the eigenvalues of a tensor, six different points correspond in the Haigh–Westergaard representation to a given stress tensor. As a result, the yield surface results symmetric about the projections of the principal axes on the deviatoric plane, [Bigoni and Piccolroaz 2004]. The advantage of plotting yield surface in such space lies in simplicity of visual presentation.

The cross-section of the plastic surface is given in the plane state of stress, e.g. $\sigma_2 = 0$. The plane of principal stress, e.g. $\sigma_2 = 0$ is often used to present results of experiments and obtained due to the limit curves, Fig. 3.1. It is mainly due to the simplicity of presentation. The description of yield points presented in Fig. 3.1 is given in Section 3.1.1.

For isotropic materials the analysis of yielding can be referred to the Haigh–Westergaard representation. Since the invariants proposed by Haigh–Westergaard (p, q and θ) have clear physical meaning, they have been employed to express the strength criterion or constitutive model by many researchers (e.g.: [Bigoni and Piccolroaz 2004; Bai and Wierzbicki 2008]). In the Haigh–Westergaard representation, the hydrostatic and deviatoric stress components are defined by the invariants:

$$p = \frac{I_1}{3} \tag{4.4}$$

$$q = \sqrt{2} J_2 \tag{4.5}$$

The position of the stress point in the deviatoric plane is described by the angle θ) defined as, [Lode 1926]:

$$\theta = \frac{1}{3} \arccos\left(\frac{3\sqrt{3}}{2} \frac{J_3}{J_2^{\frac{3}{2}}}\right) \tag{4.6}$$

The invariant p is a distance of the deviatoric plane to the origin of principal stress space, p represents the hydrostatic component of current stress point. The invariant q is a distance of the current stress point to the hydrostatic axis, and therefore represents the magnitude of deviatoric stress. The invariant θ - the Lode angle reflects the relative position of current stress point in the deviatoric plane, and θ is an indication of the magnitude of σ_2 in relation to σ_3 and σ_1. When $\sigma_1 = \sigma_2 > \sigma_3$ then θ becomes $\frac{\pi}{6}$ and the material is in triaxial compression. When $\sigma_1 > \sigma_2 = \sigma_3$ then θ becomes $-\frac{\pi}{6}$ and the material is in triaxial extension, $-\frac{\pi}{6} < \theta < \frac{\pi}{6}$.

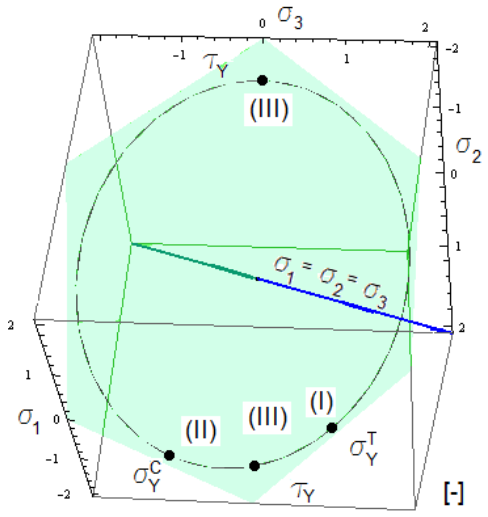

Figure 4.2: The HMH criterion in the octahedral plane with experimental points.

The results of the strength tests and the limit curve built on the basis of them are often presented as functions of polar coordinates. Therefore, the yield criterion becomes dependent on the radius and the Lode angle θ. Visualization of the criterion is then presented in the octahedral plane - the plane which is equally inclined to the axis of the hydrostatic compression, Fig. 4.2. The angle θ is clockwise and its rotation due to radius makes the trace in the octahedral plane. Then, θ for uniaxial tension or compression is equals: $\theta = \pm\pi/6$ and for pure shear: $\theta = 0$. In Fig. 4.2, in the octahedral plane there is depicted the Huber-Mises-Hencky criterion (HMH criterion) - the picture is schematic.

The results of the strength test and the yield criterion can be also plotted in the meridional plane (σ_e, σ_m), where σ_e is the equivalent Mises stress, Eq. (4.7), and σ_m is the mean stress, Eq. (4.1).

$$\sigma_e = \sqrt{\frac{1}{2}[(\sigma_x - \sigma_y)^2 + (\sigma_y - \sigma_z)^2 + (\sigma_x - \sigma_z)^2] + 3(\tau_{xy}^2 + \tau_{xz}^2 + \tau_{yz}^2)} =$$

$$= \sqrt{\frac{1}{2}[(\sigma_1 - \sigma_2)^2 + (\sigma_2 - \sigma_3)^2 + (\sigma_1 - \sigma_3)^2]} \tag{4.7}$$

This way of presenting yield curves was firstly proposed by Burzyński in the work [Burzyński 2009]. In Fig. 4.3, quoted after the paper [Życzkowski 2001], there are presented different yield criteria as functions of $f(\sigma_e, \sigma_m) = 0$, Eq. (4.8).

$$\frac{\sigma_Y^C \sigma_Y^T}{3\tau_Y}\sigma_e^2 + \left(9 - \frac{3\sigma_Y^C \sigma_Y^T}{\tau_Y}\right)\sigma_m^2 + 3(\sigma_Y^C - \sigma_Y^T)\sigma_m - \sigma_Y^C \sigma_Y^T = 0 \tag{4.8}$$

In fact, the curves obtained in the the meridional plane are the traces of the yield surfaces from the space of principal stresses. A curve plotted in the meridional plane is one of the cross-sections of the surface of revolution plotted in the Haigh-Westergaard space. Yield curves in the plane (σ_e, σ_m) depicted in the Fig. 4.3 are plotted according to the relation (4.8). All presented beneath cases are a special formulation of Burzyński criterion, [Burzyński 2009]. By roman numerals are indicated states of the stresses, according to designation presented in Section 3.1.1.

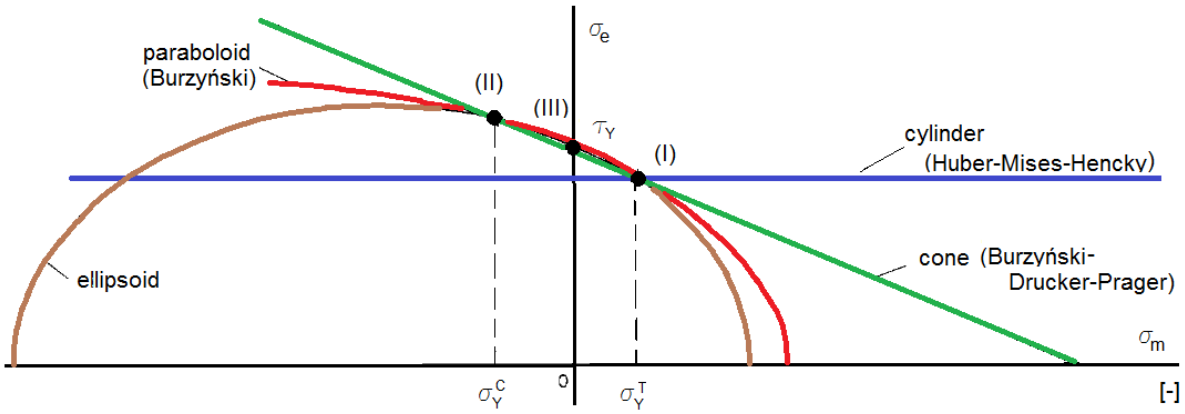

Figure 4.3: Representation of the limit curves in the plane (σ_e, σ_m) according to various yield criteria, [Życzkowski 2001].

The following cases can be considered basing on the relation (4.8):

- $3\tau_Y^2 > \sigma_Y^C \sigma_Y^T$ - the criterion is depicted by a half-ellipse. Additionally, if $\sigma_Y^C = \sigma_Y^T = \sigma^Y$, then in the meridional plane a half-circle is obtained. In the space of principal stresses is plotted the ellipsoid with axis of symmetry given by the hydrostatic pressure. The case is discussed in the work of Burzyński [Burzyński 2009];

- $3\tau_Y^2 = \sigma_Y^C \sigma_Y^T$ - the graphical representation of the criterion is an arm of a parabol. The parabol is visualization of the Burzyński criterion which in the principal stress space is depicted by the paraboloid of revolution, [Burzyński 2009];

- $\sqrt{3}\tau_Y^2 = \frac{2\sigma_Y^C\sigma_Y^T}{\sigma_Y^C\sigma_Y^T}$ - in the space of principal stresses the cone is obtained, the trace of the criterion in the meridional space is an arm of cone. This surface is characteristic for the criterion proposed by Drucker and Prager [Drucker and Prager 1952; Prager 1953];

- $\sigma_Y^C = \sigma_Y^T = \sigma_Y$ and $3\tau_Y^2 = \sigma_Y$ - the line suits to the HMH criterion, depicted in the space of principals stresses by the cylinder of revolution. This is a proposal suggested by Huber-Mises-Hencky: [Huber 1904; 2004; von Mises 1913; Hencky 1923; 1924].

In next Section there is reported the short overview concerning the proposed during the ages yield criteria. Presentation of such conceptions is rather difficult to present, because many various models have been proposed. The phenomenon of yielding has been studied from the view points of mechanics, physics and metallurgy, and many mathematicians contributed to refine the mechanics of plasticity. The research results are applied to geophysics and strength of materials.

4.4 Yield criteria in the literature

Starting from the beginning of yield conceptions, in the 15th-16th centuries Leonardo da Vinci 1452-1519 and Galileo Galilei 1564-1642, may be the earliest researchers of the strength of materials and structures, [Timoshenko 1953]. Later in the time more and more approaches of yielding were given. A comprehensive bibliography and discussion on strength theories before the 1930s can be found in the works of e.g.: [Burzyński 2009; Fromm 1931; Ros and Eichinger 1949]. Some surveys were contributed by e.g.: [Mohr 1914; Schleicher 1926; Marin 1935]. A lot of strength theories and yield conditions were presented in 20th century, ranging from the one-parameter model criterion (e.g. the Huber-Mises-Hencky criterion) to the multi-parameter models (e.g. the Cazacu-Barlat conception [Barlat et al. 2002]). A history of strength treatments has been given by, e.g.: [Timoshenko 1953; Paul 1968].

Some of criteria have been reviewed, analysed, and compared in monographs e.g.: [Michno and Findley 1976; Życzkowski 1967; Lubliner 2008; Skrzypek and Hetnarski 1993; Maohong 2002]. Authors of [Chaboche 1997; 2008; Osakada 2010] provided an extensive review of the yield ideas for metals.

W. Burzyński in his doctoral dissertation [Burzyński 2009], systematized criteria chronologically but divided them due to the measure of the material effort. He suggested three aspects, measurements of stress (e.g. the Tresca criterion) or strain (e.g. the Becker criterion [Becker 1916]) or energy (e.g. the HMH criterion). In [Theocaris 1995] criteria are presented according to the shape of yield surface obtained in the space of principal stresses (starting from the cylinder of Huber, through the cone of Drucker, finishing on the paraboloid of revolution of Theocaris). However, in the papers [Khan and Farrokh 2010; Ghorbel 2008; Maniatty et al. 1999]) authors starting from the classical criteria, present the criteria that conceptually precede their own proposals. According to other categorization there can be distinguished criteria describing yielding of metals, polymers, ceramic, soils, rocks, concrete, composites with particles or fiber, laminates or others.

In the Thesis the yield concepts developed for isotropic materials are summarized, the main characteristics and similarities with the criteria proposed in the further Section 4.5 are highlighted. For general applications involving different criteria describing the beginning of the inelastic states, it would be useful to have an unified formulation, in which a single set of equations is written with the same parameters. It will be the functions of invariants of the stress tensor and its deviatoric form - I_1, J_2 and J_3 or Lode angle θ. The yield concepts are divided into categories:

- the traditional criteria for isotropic materials, referred as the canon of the theory of plasticity, which often are the base for further conceptions;

- the criteria for isotropic materials, taking into account the influence of the invariants of the stress tensor and its deviator, $f(I_1, J_2) = 0$ or $f(I_1, J_2, \theta) = 0$;

- the phenomenological criteria taking into account the strain, strain rate, temperature, texture or other empirical observations.

4.4.1 Traditional yield criteria

Since the concept of plasticity was first applied to metals, in which the influence of mean stress on yielding is generally negligible [Bridgman 1923;], the oldest and most commonly used yield criteria are those that are independent of the mean stress. Later, when a yield criterion was to apply plasticity theory to soils, rocks, and concrete, depending on the mean stress becomes necessary. Fundamental postulates concerning the yield surfaces for isotropic material in the first half of the 20th century were introduced by: [Mohr 1900; 1914; Huber 2004; von Mises 1913; Hencky 1924; Drucker and Prager 1952; Bishop and Hill 1951b] with the convexity of yield surface determined. After that the convexity of yield surface was generalized to the strain space by Ilyushin in 1961, [Mao-hong 2002]. Since then the study of strength theory has been developing on a more reliable theoretical and empirical basis.

Identification & References		**Parameters**	**Shape in** $(\sigma_1, \sigma_2, \sigma_3)$
[Coulomb 1773; Mohr 1914]	$f(I_1) = \frac{\mu_Y}{3} I_1 - \tau_Y$	μ_Y - material constant	conical prism
[Tresca 1864]	$f(J_2, J_3) = 4J_2^3 - 27J_3^2 - -36\tau_Y^2 J_2^2 + 96\tau_Y^4 J_2 - 64\tau_Y^6$		prism
[Huber 2004; von Mises 1913] [Hencky 1924]	$f(J_2) = J_2 - (\sigma_Y)^2$		cylinder
[Drucker and Prager 1952]	$f(I_1, J_2) = \alpha I_1 + \sqrt{J_2} - \tau_Y$	α - sensitivity to pressure	cone

Table 4.1: The traditional criteria used for the isotropic materials.

In Table 4.1 there are presented the equations of the criteria for isotropic materials which are reckoned as the classical cannon of the yield theory, [Chakrabarty 2000; Nadai 1950; Sharper 2008]. In Table there are presented references, equation describing the yield concept written with use of the stress tensor invariants and a shape of the yield surface which is plotted in the space of the principal stresses. In Fig. 4.4 the comparison between the discussed yield conception is given, the limit curves are in the plane $\sigma_2 = 0$ and in the octahedral plane.

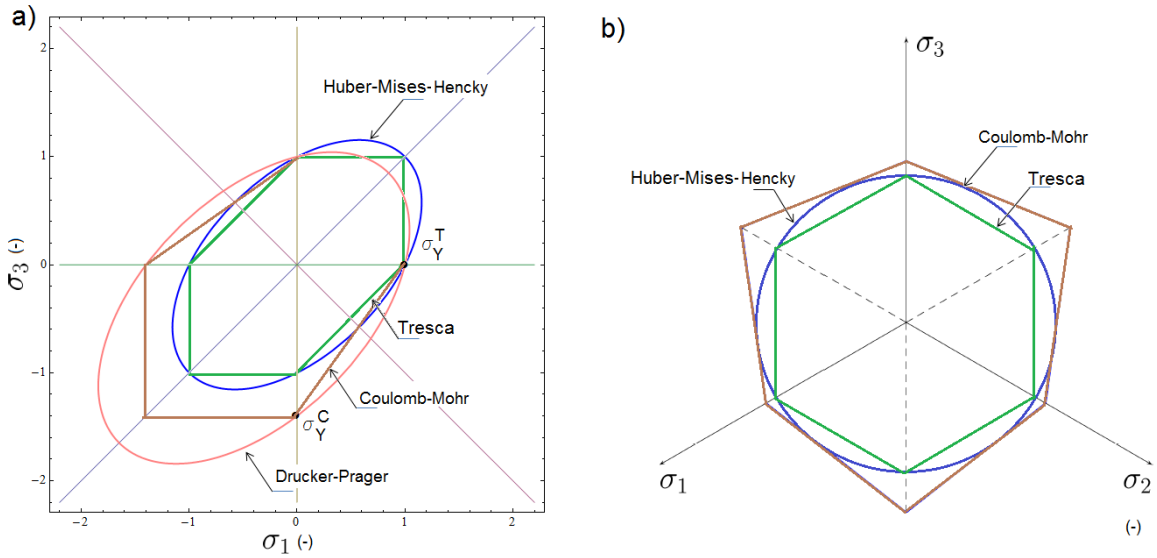

Figure 4.4: Comparison between traditional criteria in: a) the plane $\sigma_2 = 0$ and b) the octahedral plane.

Coulomb 1736-1806 may be the first researcher in the maximum shear stress strength theory, [Timoshenko 1953]. The work [Coulomb 1773] is began with a discussion of experiments which were made for the purpose of establishing the strength of some kind of sandstone. Coulomb assumed that fracture occurs due to sliding along a certain planes, when the component of force along one plane becomes larger than the cohesive resistance in shear. He proposed that cohesive resistance along the shear plane with friction caused by the normal force acting on the same plane should be considered. This should bring the theory into better agreement with experimental results. This is the first and traditionally used in soil mechanics criterion, e.g.: [Chen 1968; Ghorbel 2008; Ibraim et al. 2012]. The shear and normal stresses are assumed to be functionally related at a point on a potential failure surface according to the Mohr hypothesis. It also assumed independence of the intermediate principal stress.

In 1864, Tresca presented two notes dealing with the flow of metals under compression, [Tresca 1864]. His proposal embodies the assumption that plastic deformation occurs when the maximum shear stress over all planes attains a critical value, A maximum shear stress criterion was also proposed by Guest, [Guest 1900]. This theory gives better agreement with experiment for some ductile materials and is simple to apply. The Tresca criterion of maximum shear stress is a modification of the Coulomb-Mohr criterion. The criterion is applied in the geomechanics, it is also proved to be proper in the plasticity of aluminium alloys, [Taiebat and Carter 2008]. The Tresca yield expression in terms of the principal stress-deviator invariants is quoted after [Lubliner 2008].

Mohr (1835-1918) used the stress circle method [Mohr 1900] in developing his theory of strength in 1900. The concept according to which failure (rupture) occurs on a plane in a body if the shear stress and normal stress on that plane achieve a critical combination. The Mohr criterion - [Mohr 1914] may be considered as a generalized version of the Tresca criterion [Tresca 1864]. Both criteria were based on the assumption that the maximum shear stress is the only decisive measure of impending failure. However, while the Tresca criterion assumed

that the critical value of the shear stress is a constant, the Mohr criterion considered the limiting shear stress as a function of the normal stress in the same section at an element point.

The yield criterion combining Coulomb friction with the Huber-Mises yield criterion, was proposed in [Drucker and Prager 1952; Prager 1953]. It was formulated for granular materials: sand, soils and it has been applied also to the brittle materials, e.g. concrete [Ivorra et al. 2010; Jiang et al. 2011; Shen et al. 2012]. Designed as an extension of the Coulomb-Mohr, the Drucker-Prager proposal takes into account the hydrostatic pressure. It is a linear function of the first and second invariants of stress tensor and its deviator. The Drucker–Prager yield criterion is often used to model the pressure sensitive yielding. However, it is known that the criterion represented by a conical failure surface in the space of principal stresses can only roughly approximate real behaviour of a material in the limited range of hydrostatic stress and fails to describe properly the states near to the apex of the failure cone.

The Huber-Mises-Hencky (HMH) yield criterion is an one-parameter criterion, widely used for metallic materials with the same yield stress both in tension and in compression.

The criterion is applied to the bodies assumed as isotropic and insensitive to hydrostatic pressure. The criterion formulated independently by three authors, originally proposed by Maxwell in 1865, proposed independently by Huber 1904: [Huber 2004]. It suggests that the yielding of materials begins when the second deviatoric stress invariant reaches a critical value. For this reason, it is called the criterion of the second invariant of the stress deviator J_2. The criterion is also known as the maximum-octahedral-shear-stress criterion or the maximum-distortional-energy criterion (because for the criterion the complementary energy of an isotropic, linearly elastic material is uncoupled into volumetric and distortional parts). Due to its simplicity, it is one of the most commonly used criterion in the science and industry.

In the arbitrary system of reference the criterion is expressed as follows:

$$(\sigma_x - \sigma_y)^2 + (\sigma_y - \sigma_z)^2 + (\sigma_z - \sigma_x)^2 + 6(\tau_{xy}^2 + \tau_{yz}^2 + \tau_{zx}^2) = 2(\sigma_Y)^2 \tag{4.9}$$

in the principal stress axes:

$$(\sigma_1 - \sigma_2)^2 + (\sigma_2 - \sigma_3)^2 + (\sigma_3 - \sigma_1)^2 = 2(\sigma_Y)^2 \tag{4.10}$$

The yield limit in shear according to the tensile fulfils the relation:

$$\tau_Y^H = \frac{\sigma_Y}{\sqrt{3}} \tag{4.11}$$

4.4.2 Criteria accounting for stress invariants J_2, I_1 and J_2, I_1, J_3

The postulates of the classical theory of metals plasticity [Bridgman 1923] assumes that the hydrostatic pressure has no or negligible effect on the material strain hardening, and that the flow stress is independent of the third deviatoric stress invariant (or Lode angle parameter). The existence of materials which behaviour deviates from the classical metal plasticity was a challenge for the scientist since experiments revealed such observation, [Spitzig and Richmond 1979; Bai and Wierzbicki 2008]. In [Spitzig and Richmond 1979; 1984] the authors demonstrate that the effect of hydrostatic pressure on yielding of aluminum alloys.

Inspired by the extensive experimental results reported by Spitzig, the more recent authors repeated his observations applying them to the yield conceptions. Later tests show that many materials such as certain metals, polymers, ceramics, metallic glasses and metallic alloys exhibit pressure sensitive yielding and plastic dilatancy, e.g.: [Taylor and Quinney 1931; Grassi and Cornet 1949; Coffin 1950; Raghava et al. 1973; 1974; Spitzig and Richmond 1979; 1984; Wilson 2002; Lu and Ravichandran 2003]. In [Wilson 2002] authors studied notched 2024-T351 aluminum bars in tension. The experiment with notched specimens have been repeated by [Bai and Wierzbicki 2008; Gao et al. 2012] and simulated numerically by [Vadillo et al. 2011]. In above mentioned papers the same conclusion has been drawn - plasticity of metals is dependent on hydrostatic pressure.

Experiments also show that many other materials such as certain polymers, ceramics, metallic glasses and metallic alloys exhibit not only pressure sensitive yielding but also plastic dilatancy (Pampillo and Davis 1971; Spitzig and Richmond 1979, 1984; Chen and Reyes-Morel 1986; Lu and Ravichandran 2003) [Bai and Wierzbicki 2008; Gao et al. 2012]. Also, the geomechanics community has long recognized the necessity to incorporate the hydrostatic stress and the Lode angle into the yield functions of geomaterials (Drucker and Prager 1952; Bardet 1990; Menetrey and Willam 1995; Bigoni and Piccolroza 2003; Yang and Elgamal 2008). Influence of the third invariant in a function of the yield criterion can be explained by the remarks that yielding of material is mainly caused by shearing processes, [Ghorbel 2008]. For materials pressure insensitive (e.g. materials with HCP type of crystallographic structure), the beginning of the plasticity in the material mainly corresponds to the evolution of shear bands, [Ghorbel 2008; Raniecki and Mróz 2008]. The introduction of the third invariant of the deviatoric stress tensor in the proposed criterion did not affect the yield stress in uniaxial tension, uniaxial compression, or in purely hydrostatic pressure. However, differences in the calculated yield strength were observed under pure shearing, [Khan and Farrokh 2010].

Due to convincing experimental results, there have been searched for new concepts of a yield function extension that it could properly describe beginning of the plasticity. Considerable efforts were provided to understand the physical origins and to propose a concise mathematical model of the yield surface. Therefore, the attempts of better accounting for the physical phenomena responsible for the plasticity in the material were made. The models which can predict plastic flow in isotropic materials with or without a flow stress asymmetry. The effect of the Lode angle parameter on plastic yielding has been studied by Cazacu and Barlat (2004), Cazacu et al. 2006, Racherla and Bassani 2007. Their models incorporate the difference in strength under compression and tension. They showed that the forming limit

diagram of sheets was sensitive in that difference. However, their models did not have enough flexibility to predict plane strain yielding. The effect of the Lode angle parameter on plastic yielding has been studied by [Cazacu and Barlat 2003; Bai and Wierzbicki 2008] discussed a pressure and Lode dependent metal plasticity model and its application in failure analysis. In paper [Brunig et al. 1999] there is described a I_1–J_2–J_3 flow theory in numerical simulation of the deformation and localization behaviour of hydrostatic-stress sensitive metals.

In general, the hydrostatic pressure is controlling the size of the yield surface while the Lode angle parameter is responsible for its shape, [Bai and Wierzbicki 2008]. A general form of asymmetric metal plasticity, considering both the pressure sensitivity and the Lode dependence, is nowadays one of a leading tendency in the yield criteria for isotropic materials.

It can be concluded, however, that in spite of the great number of studies dealing with the yielding of metalic and polymeric materials, there is no consensus concerning the choice of the most appropriate criterion. Several ways of accounting for the effect of hydrostatic pressure and Lode angle in plasticity were proposed. Below in Table are summarized some of them.

Identification & References		**Parameters**
[Hu and Pae 1963]	$J_2 = \tau_Y^2 + \alpha I_1 + \beta I_1^2$	α, β - material constants
[Raghava et al. 1973; Theocaris 1995]	$J_2 + 3(\sigma_Y^C - \sigma_Y^T)I_1 - \sigma_Y^C \sigma_Y^T$	
[Needleman and Tvergaard 1984] [Gurson 1977]	$\frac{J_2^2}{\bar{\sigma}^2} + +2q_1 f \cosh\left(\frac{3q_2 I_1}{2\bar{\sigma}}\right) - 1 - (q_3 f)^2 = 0$	q_1, q_2, q_3 - parameters of void shape, f - voids volume density, $\bar{\sigma}$-flow stress hardening
[Spitzig et al. 1979; Brunig 1999]	$\sqrt{J_2} - c(1 - \alpha I_1) = 0$	α - hydrostatic stress coefficient, c - strength coefficient
[Altenbach and Tushtev 2001]	$\sqrt{J_2} + (\sqrt{J_2} + k)exp\left(\frac{I_1}{\xi_0} - 1\right) - k = 0$	k, ξ_0 - material constants
[Christensen 2006a]	$a_1 I_1 + a_2 I_1^2 + a_3 J_2 + a_4 I_1^3 + a_5 I_1 J_2 + a_6 J_3 + ... = 0$	α - non-dimensional parameter $I_1 < \frac{2-\alpha}{1+\alpha}$ - for ductile, $I_1 > \frac{2-\alpha}{1+\alpha}$ - for brittle
[Ghorbel 2008]	$\left(\frac{\sqrt{3J_2}}{\sigma_Y^T}\right)^n + \frac{\kappa^n - n}{\kappa+1}\left(\frac{I_1}{\sigma_Y^T}\right) - \frac{\kappa(\kappa^{n-1}+1)}{\kappa+1} = 0$	
[Ghorbel 2008]	$\frac{3J_2}{\sigma_Y^T}\Psi(J_2, J_3) + \frac{7(\kappa-1)}{8} I_1 - \frac{7\kappa}{8}\sigma_Y^T = 0$	$\Psi(J_2, J_3) = 1 - \frac{27}{32}\frac{J_3^2}{J_2^3}$
[Malvern 1969]	$J_2\left[1 - \frac{cJ_3^2}{J_2^3}\right] - \tau_Y^2 = 0$	c - non-dimensional matching parameter
[Bigoni and Piccolroaz 2004]	$F(\sigma) = f(I_1) + \frac{J_2}{g(\theta)}$ $f(I_1) = -M\sigma_Y^C\sqrt{(\Phi - \Phi^m)[2(1-\alpha)\Phi + \alpha}$ $g(\theta) = \frac{1}{\cos[\beta\frac{\pi}{6} - \frac{1}{3}\cos^{-1}(\gamma 3\cos\theta)]}$	if $\Phi \in [0,1]$ and $\Phi = \frac{I_1 + \sigma_Y^T}{\sigma_Y^C + \sigma_Y^T}$, M controls the pressure sensitivity, α, m define the distortion of the meridian section, β, γ model the shape of the deviatoric section
[Cazacu and Barlat 2004]	$J_2^{1.5} - cJ_3 - \tau_Y^6 = 0$	$c = \frac{3\sqrt{3}((\sigma_Y^T)^3 - (\sigma_Y^C)^3)}{2((\sigma_Y^T)^3) + (\sigma_Y^C)^3)}$
[Hu and Wang 2005]	$AI_1 + \sqrt{J_2} + B\frac{J_3}{\sqrt{J_2^3}} - C = 0$	A, B, C - experimental parameters of materia
[Raniecki and Mróz 2008]	$(J_2)^{3n_1/2} - c(J_3)^{n_1} - \tau_c^{3n_1} = 0$	n_1, c, τ_c are material parameters
[Bai and Wierzbicki 2008]	$\sigma_{yld} = \bar{\sigma}(\bar{\varepsilon_p})[1 - c_\eta(\eta - \eta_0)]\left[c_\theta^s + (c_\theta^{ax} - c_\theta^s)\left(\gamma - \frac{\gamma^{m+1}}{m+1}\right)\right]$	$\bar{\sigma}(\bar{\varepsilon_p})$ - flow function, $c_\eta, c_\theta^t, c_\theta^s, c_\theta^c, m$ - material constants η - triaxiality parameter, η_0 - reference triaxiality parameter

Table 4.2: The criteria used for isotropic materials accounting for (I_1, J_2) and (I_1, J_2, J_3).

The accounting for the invariants of the stress tensor and its deviator have been approach of many authors. Two invariants J_2 and J_3 are independent of mean normal stress, which then comes into criterion through I_1. The invariants are taken to specify yield functions for isotropic materials. The conceptions how to incorporate them in a criterion also were different.

The extension of the Huber-Mises-Hencky criterion by accounting for the SD effect was independent proposal of few authors. Apart from more widely discussed conception of Burzyński [Burzyński 2009], the same proposal made [Raghava et al. 1973; Theocaris 1995]. In [Lubliner 2008] there is also mentioned that [Schleicher 1926] worked on the similar problem.

In [Raghava et al. 1973] the criterion is applied to calculate yielding for polymers. P.S. Theocaris is the author of the EPFS criterion: the elliptic paraboloid failure surface, which subsequent narrowed forms allow to capture yielding of three symmetries of material properties. The theory is based on the suggestion that more reasonable yield surface then a cylinder proposed by Huber-Mises (Eq. 4.9) is a closed form - a paraboloid. Geometrical analysis of formulated in such a way that has allowed the author to define the yield surface, [Theocaris and Philippidis 1987]. The Theocaris criterion takes into account the asymmetry, and in the space of principal stresses the criterion can be depicted as an elliptic paraboloid (or paraboloid of revolution for the isotropic materials) with symmetry axis parallel to the axis of the hydrostatic pressure (for the anisotropic materials) or given by it (for isotropic materials).
The general form of the criterion:

$$H_{ij}\sigma_i\sigma_j + h_i\sigma_i - 1 = 0 \tag{4.12}$$

(i, j = 1, ..., 3) where: H and h means the 4th and 2 nd rank order failure tensors.

$$H_{ij} = \frac{1}{\sigma_{Ti}^Y \sigma_{Ci}^Y} \tag{4.13}$$

$$h_i = \frac{1}{\sigma_{Ti}^Y} - \frac{1}{\sigma_{Ci}^Y} \tag{4.14}$$

For isotropic material $i = j = const$, the criterion is the same as the criterion proposed by Burzyński (1928) and Raghava (1973).

The polynomial expansion of the stress tensor invariants. Authors of [Hu and Pae 1963] expanded the HMH criterion by proposition of own criterion of the second order, which accounts for the asymmetry of elastic range, what means considering the effect of hydrostatic pressure. Constants are determined experimentally. In the space of principal stresses the conception is represented by the paraboloid of revolution with an axis of symmetry given by the axis of hydrostatic pressure. Its cross section for $\sigma_2 = 0$ is expressed by an ellipse. In later works, the criterion has been applied for polymers - [Silano et al. 2007; Pae 1977]. In [Khan and Farrokh 2010] the criterion has been expanded and included the influence of strain and strain rate.

In [Rees 1982] the proposed criterion is a linear relation between the elements of the stress tensor. The author quotes the data material Ti-Al alloy and alloy Zr to validate the limit curve.

In [Brunig 1999] author deals with the numerical simulation of the large elastic-plastic deformation and localization behaviour of metals which are plastically dilatant and sensitive to hydrostatic stresses. The model is based on a generalized macroscopic theory taking into account macroscopic as well as microscopic experimental data obtained from tests with iron based metals. It shows that hydrostatic components may have a very pronounced effect on the onset of localization and the associated deformation modes, and that they generally lead to a notable decrease in ductility, [Brunig 1999]. His equation represents an extended version [Drucker and Prager 1952] and it is repeated after [Spitzig et al. 1979; Spitzig and Richmond 1979; 1984]. This yield condition is often used to describe inelastic material behavior of soils but in this case both coefficient a, c were chosen to be constant and no work-hardening effects are taken into account.

Proposed in [Christensen 2006a;b] conception is a material yield-failure theory for isotropic materials that attempts to span the range from ductile to brittle materials. At the first-degree level of the formulation - is one parameter to be evaluated, at the second-degree level there are three parameters and at the third degree level there are six parameters. The first-degree level cannot give the operative physical effects. The second degree level is considered but if it does not successfully capture the requisite physical effects, then the third degree level is used. The references from which various aspects at the Christensen theory of yield and failure are collected in works from 1997 to 2006: [Christensen 1997a;b; 2004; 2005; 2006a;b].

Isotropic yield criterion with threefold rotational symmetry about the origin is proposed in [Cazacu and Barlat 2004]. This criterion is an odd function in the principal values of the stress deviator and contains a single material parameter c. This only one parameter is expressible in terms of the yield strengths in compression and tension. If the yield function was convex, this constant is limited to a specified numerical range. Authors formulated a macroscopic isotropic yield criterion capturing the asymmetry in yielding for pressure-insensitive metals.

Authors of [Hu and Wang 2005] proposed a stress state dependent yield criterion for isotropic ductile materials. Authors idea states that the yielding (or irreversible deformation) takes place when a shearing stress on a slip plan reaches critical value. The yield criterion assures the convexity in wide range of material properties so that it can be used as the plastic potential in the implementation of predicting the subsequent yield surface, [Hu and Wang 2005; Hu 2007]. The yield criterion reveals a clearly transforming procedure with respect to its simplified form when applied to different materials from a general compressive isotropic material to an ideal incompressive isotropic material. An yield state can be formulated as:

$$\tau =\geq \tau_0(1 + \varphi(\mu_\sigma)) + \mu\sigma_N \tag{4.15}$$

where τ is a shear stress on the defined slip-plane caused by an external load, τ_0 is a critical value of a shear stress under the plane-strain state, $\varphi(\mu_\sigma)$ is a function of the stress state variable μ_σ, μ is the frictional coefficient between the slipped grains, and σ_N is the normal compressive stress on the defined slip-plane.

The generalized criterion which in one form could cover other proposition and could be applied for many groups of materials has been the aim of many authors. The first such proposal could be denoted to [Nadai 1937]. The beginning of a plasticity in the material given by the relation between the octahedral shear stress τ_{oct} and the octahedral normal stress σ_{oct}. The criterion of the space of principal stresses is depicted with use of the surfaces of revolution:
- a cone, if: $9\tau_{oct} = 2(3c_0\sigma_{oct} - c_1)$, c_1, c_2 - material constants are dependent on the yield limits.
- a paraboloid, if: $\sigma_{oct} = a_1 + a_2\tau_{oct}^2$, a_1, a_2 - material constants.

In paper of [Ghorbel 2008] there is shown that traditional criteria are not capable of predicting the viscoplastic responses of all thermoplastic polymers when they are subjected to any general biaxial stress state. To improve the prediction of isotropic polymers yield behavior under any ranges of biaxial stress state, and to establish a generalized yield criterion which accounts for shear banding, along with hydrostatic pressure dependency, author proposed to include the first and third invariant of the deviatoric stress in the expression of the yield equation. Due to the experimental values obtained at the plastic flow and combining criteria derived from the modified the HMH model and the Raghava model [Raghava et al. 1973], the expression in the normalized meridional plane is given. The generalized criterion concerns different types of polymers.

The nonlinear dependence between invariants . In [Altenbach and Tushtev 2001] there is proposed a static failure criterion based on an exponential dependence between the mean stress and the equivalent stress. The two material parameters can be determined by two simple tests — the uniaxial tension and compression. The locus of the criterion is nearly conical for low hydrostatic pressures and tends to a cylindrical form if an increased hydrostatic pressure is applied. The validity of the criterion is demonstrated for polymers.

The criterion proposed in [Malvern 1969] is nonlinear dependence between invariants of deviatoric tensor. The drawback of the proposition is the fact that it is not convex. Because J_3 vanishes for pure shear, it is attractive to insert the tabular data from the shear tests and then determine the parameter c to provide correspondence to the compression test data for uniaxial stress calculations. The $c = 2.64$ violates the requirement that the surface is convex. Criterion was used in the report [Huffington 1992] in application for OFHC Cu.

A class of nonsingular yield conditions depending on three parameters analysed for isotropic materials exhibiting strength differential effect and pressure insensitivity has been proposed in [Raniecki and Mróz 2008]. The condition can be applied in the analysis of high strength alloys or of shape memory alloys in order to specify the onset of yield, or of martensitic or austenitic transformation. The conditions can easily be generalized to account for mixed hardening and back stress anisotropy. It has a form given by the Eq. (17), Table 4.2. The identification of material parameters can then be carried out for specific cases of tested materials. For $n_1 = 1$ the criterion has the same form as the criterion of [Cazacu et al. 1997], for $n_1 = 0$ the formula transforms into Drucker-Prager criterion. The criterion is specified and visualized for a shape memory alloy TiNi.

The many-parameters criteria have been also in favour of researchers. They are more difficult to unequivocal determining but account for more physical observations.

In the study of [Bai and Wierzbicki 2008] an analysis of the influence of the hydrostatic pressure and the third invariant of the stress tensor on the process of yielding of material is presented. The authors repeated the experiment performed by [Wilson 2002] for aluminum 2024-T351. It was the quasi-static tensile test of notched specimens with circular cross section. The experiment confirmed the observed effects of the influence of the mean stress on the deformation of the material. The authors also performed tensile test on the notched samples but with the rectangular cross-sections. It turned out that the criterion taking into account only the effect of the mean stress does not provide a satisfactory improvement in that case. But the outcome obtained due to simulation which taken into account also the effect of the third invariant of the stress tensor deviator significantly improved results. The magnitudes of correction due to the deviatoric state parameter (Lode angle parameter) is large and in some cases reaches 20%. The yield surface is asymmetric in the space of principal stresses losing three planes of symmetry as compared to the Tresca yield condition with six plane of symmetry, so it is asymmetric in any of the Tresca's six symmetry planes. The locus is determined experimentally from two types of test procedures. One is based on classical round specimens or flat specimens in uniaxial tests, and the other one uses a series of tests on a double curvature butterfly specimen subjected to biaxial loading under different combination of tension/shear and compression/shear. The test points are then fitted to a smooth surface which describes the dependence of the equivalent strain to fracture on the average stress triaxiality and the normalized third invariant of the deviatoric stress tensor. It is shown that the best fit of test data is provided by a surface which is asymmetric with respect to the Lode angle parameter.

The concept of a shrinking yield surface with hydrostatic pressure was put forward in [Gurson 1977] and later extended by modifications in [Needleman and Tvergaard 1984; Koplik and Needleman 1988] in their studies of ductile fracture by the nucleation, growth and coalescence of voids. Deformation in metals causes increases in the porosity, its saturation, and eventually creation of micro-cracks. This observation was the basis of the criterion. The model considers the influence of the first invariant of the stress tensor and a function accounting the voids influence on the deformation precess. This is the first criterion, which takes into account the observations of the degradation of a material. The use of the model requires knowledge of the 9 parameters: three material constants q_i, cavities density function f, the three parameters of saturation (void nucleation parameters) and two parameters of degradation, [Peirs; Vadillo and Fernandes-Saez 2009].

The proposal of [Bigoni and Piccolroaz 2004] is an example of single surface yield function - a model based on an interpolation formula made of two known simple convex yield functions. Such yielding conceptions are used for quasibrittle and frictional materials for which yielding is complicated by many effects - consequently, into the function of criterion there are included functions of first and third invariant of tensor and its deviator. The yield function allows the possibility of describing a transition between the shape of a yield surface typical of a class of materials to that typical of another class of materials. An it is in agreement with a variety of experimental data relative to soil, concrete, rock, granular media, metallic and composite powders, certain types of ceramic, metallic foams, porous metals, and polymers.

The yield function represents a single, convex and smooth surface in stress space approaching as limit situations well-known criteria and the extreme limits of convexity in the deviatoric plane. The yield criterion of such manner concerning geometerials have been proposed by, e.g.: Shima and Oyane 1977; Kuhn and Downey 1971; Green 1972; Doraivelu *et al.* 1984; Desai 1989; de Boer and Dresenkamp 1989; Khoei and Azami 2005; Ehlers 1995; Bigoni and Piccolroaz 2004; Aubertin and Li 2004. The detailed description of single surface yield function can be found in [Bigoni and Piccolroaz 2004; Bier and Hartmann 2006]. The function of a yield criterion proposed [Bigoni and Piccolroaz 2004] is a sum of components describing the pressure-sensitivity and the deviatoric function describing the Lode-dependence of yielding. The seven, non-negative material parameters define the shape of the associated single, smooth yield surface. According to different values of parameters the yield function reduces to classical criteria of yielding.

4.4.3 Phenomenological criteria

The research in the yield criteria developed in two directions: one was to build the criteria on the basis of micromechanics, structure, physical base - considerations, while another was to find direct interpolations to experimental data. Examples of yield functions generated within the former approach are numerous, e.g.: [Huber 1904] or [Gurson 1977] and others presented in previous Paragraphs. The latter approach was also broadly followed providing some yield conditions. A purely phenomenological point of view is assumed in this Paragraph - allowing to present yield criteria based on the phenomenological observation and conclusion tailoring under the assumption of isotropy to interpolate experimental results with a mathematical function.

Identification & References		**Parameters**
[Kuroda 2004]	$\frac{\sqrt{J_2}}{1-\beta_M I_1} - g(\varepsilon_e)\left(\frac{\dot{\phi}}{\dot{\phi}_0}\right)^m = 0$	$\dot{\phi}$ nonnegative overstress function, β_M - material constant, m - rate sensitivity parameter $\dot{\phi}_0$ - reference value of the $\dot{\phi}$, $g(\varepsilon_e)$ - strain hardening function
[Khan and Farrokh 2010]	$\sqrt{J_2} - \alpha_0^*\left(\frac{\dot{\varepsilon}}{\dot{\varepsilon}^*}\right)^{\beta_0^*} - \sum_{i=1}^{N} \alpha_i I_1^i = 0$	$\alpha_i, \alpha_0^*, \beta_0^*$ - material constants, $\dot{\varepsilon}^*$ - the reference strain rate

Table 4.3: The phenomenological criteria used for isotropic materials.

In literature concerning the phenomenological plasticity, it has long been recognized that the notion of rate-independence of plastic response is only a convenient approximation at low homologous temperatures. But plastic flow due to dislocation motion may be inherently rate-dependent even at low temperatures. For example, studies on micromechanical behavior of polycrystalline metals have shown that macroscopic inelastic deformations are a consequence of motion of dislocations and similar microscopic defects. Even at small strain levels and moderate homologous temperatures, dislocations migrate thus giving rise to small inelastic strains. Therefore, rate-dependent plasticity theories dealing with the finite deformation behavior of metals become more and more important even in moderate temperature applications.

In work of [Kuroda 2004] there is presented a phenomenological plasticity model accounting for hydrostatic stress sensitivity and vertex- type of effect. The hydrostatic stress-sensitivity effect is incorporated into the phenomenological model with vertex-type of effect, [Kuroda and Tvergaard 2001]. The model adopts a dependence of the plastic strain rate on the total strain rate, which was motivated by the original idea of [Simo 1987]. In the model, the vertex-type of effect is represented as a non-normality of plastic flow on an apparent smooth yield surface, it accurately reproduces strain localization phenomena. The same type of dependence of the plastic strain rate on the total strain rate has been also assumed in a proposed constitutive model for frictional granular geomaterials, [Nemat-Nasser 2000].

The criterion presented in the work of [Khan and Farrokh 2010] is based on the criterion of [Silano et al. 2007], which is a linear dependence of first and second invariants of stress tensor. The criterion was extended for strain rate influence. In paper [Khan and Farrokh 2010] the criterion is applied for polymer Nylon 101. A precise definition of yield was established for the polymer by deforming several specimens to certain levels of strain and measuring the residual strains after unloading and strain recovery. The material was subjected to different loading conditions (uniaxial to multiaxial) at four different quasi-static and intermediate strain rates to determine several points on the material's yield loci. An empirical hydrostatic pressure dependent yield equation (with four material constants) was developed to simulate material's behaviors as a function of strain rate. The capability of the developed criterion was examined by simulating high strain rate yield behavior of the material in tension and in compression.

In this section there have been presented different concepts concerning yield criteria. The criteria have been divided into 3 categories: traditional ones, yield functions including invariants of stress tensor and its deviator and phenomenological ones, which describe yield depending on strain rate or other empirical observations. Criteria have been shortly discussed, their references have been quoted, also equations describing their functions have been collected in the Tables 4.1, 4.2, 4.3.

In next Section the Burzyński material effort hypothesis is introduced basing on this doctoral thesis from 1928 (work was later translated in English [Burzyński 2009]. The resulting from the hypothesis criteria can be applied for isotropic materials characterised by asymmetry of elastic ranges (Section 2.1.1) as well as the initial anisotropy induced by manufacturing processes (Section 2.1.2). The detailed discussion is presented in the next Section.

4.5 Burzyński material effort hypothesis and the resulted criteria

From the fundamental point of view, a superior yield criterion should have a physically based interpretation which can make the predicted result more reasonable. Energy as a multi-level scalar quantity can be assumed as an appropriate universal measure of the change of the strength of chemical bonds – material effort.

First such a conception belongs to J.C. Maxwell in 1856. Maxwell suggested that the total strain energy per unit volume can be resolved into two parts: the strain energy of volume change and the strain energy of distortion. Maxwell made the statement in his letter to William Thomson: *'I have strong reasons for believing that when the strain energy of distortion reaches a certain limit then the element will begin to give way'*, [Timoshenko 1953]. Maxwell already formulated the theory of yielding which now is called the maximum distortion energy theory. But he never came back again to this question, and his ideas became known only after publication of Maxwell's letter in the 1930s. It took researchers considerable time before they finally developed the theory identical with that of Maxwell. E. Beltrami (1885) stated that as a material effort measure there was proposed the density of total elastic energy. A different conclusion was drawn by M.T. Huber who took the density of elastic energy of distortion as a measure of the material effort, [Huber 2004].

The Burzyński approach to the material effort is called *the hypothesis of variable limit energy of volume change and distortion*. It was proposed originally by Burzyński in his doctoral Thesis in 1928 and later translated in English in 2009, [Burzyński 2009; 2008]. The proposed concept is based on the hypothesis that certain portions of elastic energy density accumulated in the deformed body can be applied to define the measure of material effort. It may be understood as the physical state of a body, comprehended in the sense of elasticity or plasticity or material strength, and generated by a system of stresses, and related with them strains, [Burzyński 2009].

To understand better the proposed criterion, the phenomenon of strain energy in the body should be briefly described.

4.5.1 Elastic energy

The relation describing the density of elastic energy Φ at the representative volume element in the linear-elastic body is given by Eq. (4.16). It is a linear relation between stress, strain and strain energy Φ. A homogeneous quadratic function is independent on the choice of system of reference.

$$\Phi = \frac{1}{2}\sigma \cdot \varepsilon \tag{4.16}$$

Because stresses appear and disappear with the strain - in a natural state of material the value of elastic energy is zero.

Definition of elastic energy, explanation of its decomposition for case of isotropic solids was derived by [Stokes 1867] and Helmholtz 1907 ([Landau and Lifshitz 1986]). Decomposition of the density of elastic energy for isotropic solids may be described as a sum of the density of distortional energy Φ_f and the density of energy of volume change Φ_v, Eq. (4.17):

$$\Phi = \Phi_f + \Phi_v \tag{4.17}$$

For an isotropic body densities of elastic energy is expressed by the relations, [Burzyński 2009]:

$$\Phi_f = \frac{1}{12G}\Big[(\sigma_x - \sigma_y)^2 + (\sigma_x - \sigma_z)^2 + (\sigma_y - \sigma_z)^2\Big] + \frac{1}{2G}\Big(\tau_{xy}^2 + \tau_{yz}^2 + \tau_{xz}^2\Big) =$$

$$= \frac{1}{12G}\Big[(\sigma_1 - \sigma_2)^2 + (\sigma_1 - \sigma_3)^2 + (\sigma_2 - \sigma_3)^2\Big] \tag{4.18}$$

$$\Phi_v = \frac{1-2\nu}{6E}\Big(\sigma_x + \sigma_y + \sigma_z\Big)^2 = \tag{4.19}$$

$$= \frac{1-2\nu}{6E}\Big(\sigma_1 + \sigma_2 + \sigma_3\Big)^2 = \frac{1-2\nu}{12G(1+\nu)}\Big(\sigma_1 + \sigma_2 + \sigma_3\Big)^2$$

The presented above definition of elastic energy is a base for the Burzyński material effort hypothesis - discussed in further Paragraphs.

4.5.2 Hypothesis of variable limit energy of volume change and distortion

The formulation of the Burzyński energy-based hypothesis can be stated as follows: *the measure of material effort defining the limit of elastic range is a sum of the density of elastic energy of distortion and a part of density of elastic energy of volume change being a function of the state of stress and particular material properties*, [Burzyński 2009]. It can be written in a mathematical form, Eq. (4.20):

$$\Phi_f + \eta\Phi_v = K \tag{4.20}$$

where Φ_f is the density of elastic energy of distortion, Eq. (4.18), Φ_v is the density of elastic energy of volume change, Eq. (4.19), K is the value of the density of elastic energy in the limit state and η is the function depended on the mean stress, Eq. (4.21):

$$\eta = \omega + \frac{\delta}{3\sigma_m} \tag{4.21}$$

The following relations were assumed - Eqs. (4.22) - to replace the set of the material constants (ω, δ, K) by the set of the yield strength values measured in the simple strength tests: tension, compression and sher, respectively: $\sigma_Y^T, \sigma_Y^C, \tau_Y$, [Burzyński 2009].

$$\begin{aligned} \frac{1-2\nu}{1+\nu}\omega &= \frac{1-2\chi}{1+\chi} \\ \frac{1-2\nu}{1+\nu}\delta &= \frac{3(\sigma_Y^C-\sigma_Y^T)}{1+\chi} \\ 12GK &= \frac{3\sigma_Y^C\sigma_Y^T}{1+\chi} \\ 12G\Phi_f &= 2\sigma_e^2 \end{aligned} \tag{4.22}$$

The Poisson's ratio is expressed by ν and the *plastic parameter* by χ, Eq. (4.23). The plastic parameter χ is defined by Burzyński the intuitive, and in a certain sense, artificial factor to determine and distinguish the plastic state of the body.

$$\chi = \frac{\sigma_Y^C\sigma_Y^T}{2\tau_Y} - 1 \tag{4.23}$$

Further transformations of Equation (4.21) to Equation (4.20) allows to obtain the formula for the material effort in the meridional plane (σ_e, σ_m), Eq. (4.24).

$$\frac{2(1+\chi)}{3}\sigma_e^2 + 3(1-2\chi)\sigma_m^2 + 3(\sigma_Y^C-\sigma_Y^T)\sigma_m - \sigma_Y^C\sigma_Y^T = 0 \tag{4.24}$$

Knowing that the mean stress is given by the relation Eq. (4.1) and the equivalent stress is given by Eq. (4.7) the criterion can be written in the coordinates (x, y, z):

$$\begin{aligned} \sigma_x^2+\sigma_y^2+\sigma_z^2-2\chi(\sigma_x\sigma_y+\sigma_y\sigma_z+\sigma_z\sigma_x) &+ \\ +2(1+\chi)(\tau_x^2+\tau_y^2+\tau_z^2)+(\sigma_Y^C-\sigma_Y^T)(\sigma_x+\sigma_y+\sigma_z) &= \sigma_Y^C\sigma_Y^T \end{aligned} \tag{4.25}$$

and in the system of the principal stresses:

$$\begin{aligned} \sigma_1^2+\sigma_2^2+\sigma_3^2-2\chi(\sigma_1\sigma_2+\sigma_2\sigma_3+\sigma_3\sigma_1) &+ \\ +(\sigma_Y^C-\sigma_Y^T)(\sigma_1+\sigma_2+\sigma_3) &= \sigma_Y^C\sigma_Y^T \end{aligned} \tag{4.26}$$

The cross-section in the plane $\sigma_2 = 0$ is given by the formula:

$$\sigma_1^2+\sigma_3^2-2\chi\sigma_3\sigma_1+(\sigma_Y^C-\sigma_Y^T)(\sigma_1+\sigma_3) = \sigma_Y^C\sigma_Y^T \tag{4.27}$$

The yield point for shear is given by the relation:

$$\tau_Y = \sqrt{\frac{\sigma_Y^C\sigma_Y^T}{3}} \tag{4.28}$$

Depending on the type of the material, what can be expressed by the different values of χ, the Burzyński isotropic criterion, Eq. (4.27), is written with use of various relations. Also, its visualizations in the space of principal stresses and in the meridional plane have different shapes.

- If $3\tau_Y^2 > \sigma_Y^C\sigma_Y^T$ what suits $\chi < \frac{1}{2}$, then in the space of principal stresses the criterion can be represented as an elipsoid, in the plane (σ_e, σ_m) (Fig. 4.3) criterion is depicted by a half-ellipse.

- If $3\tau_Y^2 = \sigma_Y^C \sigma_Y^T$ then $\chi = \dfrac{1}{2}$, consequently in the space of principal stresses the criterion has a form of paraboloid of revolution for materials with asymmetry of elastic range. In case of equality of yield stresses of compression and tension, the shape of yield surface is a cylinder of revolution. In the plane (σ_e, σ_m) the graphical representation of the criterion is an arm of a parabol (Fig. 4.3). For $\sigma_Y^C = \sigma_Y^T = \sigma^Y$ it is a straight line parallel to the axis σ_m. Generally, this form of criterion is called the paraboloid yield criterion and it can be applied for the majority of materials which can yield plastically.

- If $\chi > \dfrac{1}{2}$ then in the principal space of stresses there is presented as a hyperboloid for which only one sheet has a physical sense. Then $\dfrac{2}{\sqrt{3}} \dfrac{\sigma_Y^C \sigma_Y^T}{\sigma_Y^C + \sigma_Y^T} < \tau_S^Y < \sqrt{\dfrac{\sigma_Y^C \sigma_Y^T}{3}}$, in the plane (σ_e, σ_m) the graphical representation of the surface is an arm of a hyperboloid.

In each of these cases, the axis of symmetry of a figure is given by the hydrostatic pressure axis $\sigma_1 = \sigma_2 = \sigma_3$, and its cross-section in a plane $\sigma_2 = 0$ is an ellipse with center point on the plane (σ_1, σ_3) given by:

$$\left[\frac{1}{2(\chi - 1)}(\sigma_Y^C - \sigma_Y^T), \frac{1}{2(\chi - 1)}(\sigma_Y^C - \sigma_Y^T)\right] \tag{4.29}$$

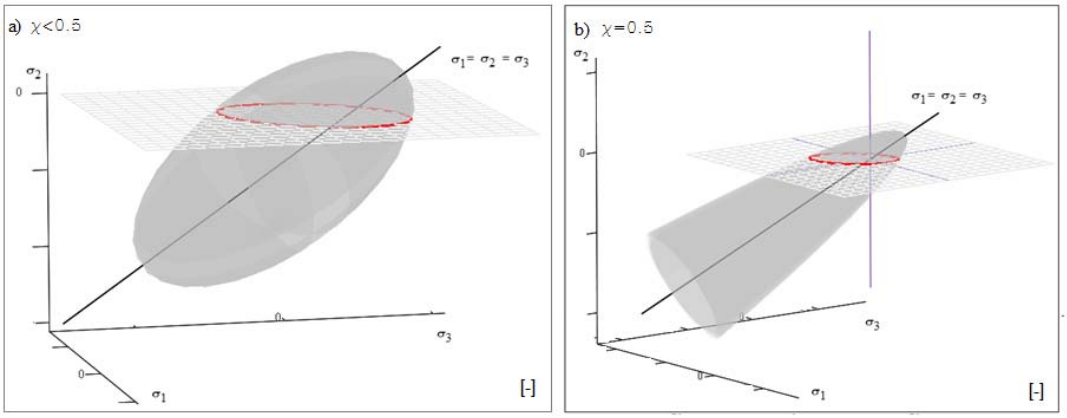

Figure 4.5: Cases of the Burzyński hypothesis, Eq. (4.26), depending on χ: a) $\chi < \frac{1}{2}$, an ellipsoid of revolution, b) $\chi = \frac{1}{2}$, a paraboloid of revolution.

The Burzyński proposal is applicable for group of the material characterized by the strength differential effect (SD effect), $\kappa \neq 1$, Eq. (2.1), [Drucker 1973]. SD effect results from a wide variety of causes and can be strongly dependent on the offset chosen to define yield stress, [Drucker 1973]. It is observed that many materials are characterized by this parameter: geological materials [Drucker and Prager 1952], high strength steels and hard deformable alloys [Taylor and Quinney 1931], martensitic steels and other alloys [Drucker 1973], ultrafine grained and nano-metals, [Schuh and Lund 2003; Lund and Schuh 2003], gray cast-iron

[Grassi and Cornet 1949], plastics and polymers [Drucker 1973; Theocaris 1995]. Consequently, the Burzyński hypothesis accounting in its formulation for SD parameter is applicable to many classes of materials: metals and their alloys, polymers, composites.

The Burzyński hypothesis is a physically based, coherent theory - that fact may be treated as its main advantage. Bonding material effort measurement with the variable limit energy of volume change and distortion makes the hypothesis universal and independent of the system of reference. Another quality of the hypothesis is simplicity of unequivocal obtained yield surface, just three results of classical strength tests are required: a yield stress in compression σ_Y^C, in tension σ_Y^T and a yield stress in shear τ_Y. In addition, the particular cases of general theory can be compared with other more specific yield criteria.

4.5.3 Paraboloidal Burzyński criterion for isotropic materials

In the further part of the Thesis, the paraboloidal Burzyński criterion, the formula (4.26) with the assumption that $\chi = \frac{1}{2}$ (Eq. 4.23) will be mainly used. Consequently, if $\chi = \frac{1}{2}$ then dependence between yield stresses is given as:

$$\tau_Y = \sqrt{\frac{\sigma_Y^C \sigma_Y^T}{3}} \tag{4.30}$$

The Burzyński criterion has the same form as the criterion proposed by [Raghava et al. 1973]. The same proposal for isotropic materials in the 1980th was also given by [Theocaris 1995]. However, the hypothesis is much older than the proposition of Raghava and Theocaris - the Burzyński concept of the yield criterion was published in 1928. The Burzyński hypothesis and its particular cases should be treated as first original proposal of the yield criterion which couples material effort with density of energy of volume change and density of distortional energy.

Since, the criterion takes into account the asymmetry of elastic range, σ_Y^C may be different from σ_Y^T, so it can be defined as a function of invariants of stress tensor and its deviator $f(J_2, I_1) = 0$. The hydrostatic pressure given by first invariant of stress tensor is accounted.

$$f(J_2, I_1) = J_2 + 3(\sigma_Y^C - \sigma_Y^T) I_1 - \sigma_Y^C \sigma_Y^T \tag{4.31}$$

or

$$\frac{1}{2}\sigma_e^2 + 3(\sigma_Y^C - \sigma_Y^T)\sigma_m - \sigma_Y^C \sigma_Y^T = 0 \tag{4.32}$$

In the space of principal stresses the rewritten formula (4.31) with use of (4.1) and (4.7) can be presented as:

$$\begin{aligned} \sigma_1^2 + \sigma_2^2 + \sigma_3^2 - (\sigma_1\sigma_2 + \sigma_2\sigma_3 + \sigma_3\sigma_1) \quad &+ \\ +(\sigma_Y^C - \sigma_Y^T)(\sigma_1 + \sigma_2 + \sigma_3) \quad &= \quad \sigma_Y^C \sigma_Y^T \end{aligned} \tag{4.33}$$

and for the plane state of stresses, $\sigma_2 = 0$:

$$\sigma_1^2 + \sigma_3^2 - \sigma_1\sigma_3 + (\sigma_Y^C - \sigma_Y^T)(\sigma_1 + \sigma_3) = \sigma_Y^C \sigma_Y^T \tag{4.34}$$

The graphical representation of the criterion (4.33) in the space of principal stresses is a paraboloid of revolution with an axis of symmetry: $\sigma_1 = \sigma_2 = \sigma_3$. Its cross-section in the plane $\sigma_2 = 0$ is an ellipse with axes of symmetry $\sigma_1 = \sigma_3$ and $\sigma_1 = -\sigma_3 - 2(\sigma_Y^C + \sigma_Y^T)$, the center is determined by a point with coefficients $[-(\sigma_Y^C - \sigma_Y^T), -(\sigma_Y^C - \sigma_Y^T)]$.

If $\sigma_Y^C = \sigma_Y^T = \sigma^Y$ then value of yield strength for shear is the same as for the HMH criterion, Eq. (4.10), and shear stress value is then given by a relation (4.11) - as there is no strength difference the limit surface becomes then a cylinder of revolution.

The stress states described in the Paragraph 4.3 with assumption of ordered principal stresses $\sigma_1 \geq \sigma_2 \geq \sigma_3$ for the Burzyński isotropic criterion (4.33) - a particular case of Eq. (4.8) an arm of parabola, is shown in the meridional plane (σ_m, σ_e), Fig. 4.6.

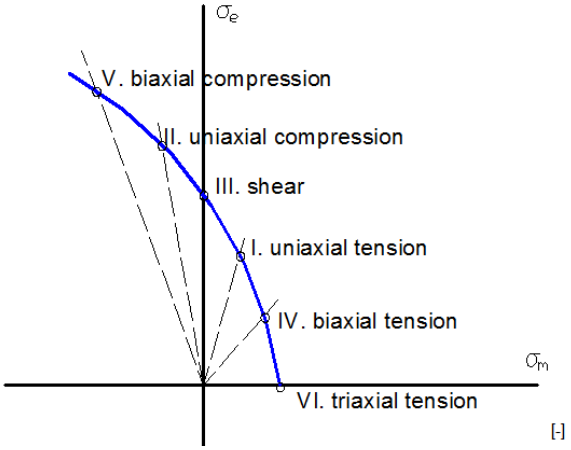

Figure 4.6: Representation of the stress states in the meridional plane (σ_m, σ_e) for the Burzyński paraboloidal criterion, Eq. (4.32), [Burzyński 2009].

In Fig. 4.7 there is presented the paraboloid Burzyński criterion for the isotropic materials, the schematic representation of the criterion for an exemplary data when SD parameter κ is equaled to 1.3. It means that yield strength in compression is 30% larger than yield limit in tension, SD parametr is calculated with use of relation (2.1). The surface and all limit states have been plotted due to the algorithm implemented in the code of the Wolfram Mathematica - the explanation to the algorithm is attached in the Appendix nr 2.

In Fig. 4.7.b the yield surface is depicted in the space of the principal stresses, Eq. (4.33). It is a paraboloid of revolution with axis of symmetry $\sigma_1 = \sigma_2 = \sigma_3$, in Fig. 4.7.a its cross-section in the plane $\sigma_2 = 0$ is given. It is an ellipse, which is the limit curve obtained due to relation (4.34), presented in the plane $\sigma_2 = 0$. In Fig. 4.7.c there are curves of the Burzyński criterion (red line) and the Huber-Mises-Hencky (HMH) criterion (blue dashed line) in the meridional plane (σ_m, σ_e). The Burzyński criterion is given as an arm of a parabol, whereas HMH criterion, Eq. (4.10) is represented by a straight line - which is suitable to a cylinder of revolution in the space of principal stresses. With dots the exemplary experimental test data are indicated: σ_Y^C, σ_Y^T, τ_Y as it is schematically presented in Fig. 4.6. In Fig. 4.7.d the comparison between the Burzyński criterion and the HMH criterion in the plane $\sigma_2 = 0$ is given. It is noticed that larger difference SD parameter κ from 1, the bigger discrepancy between the

Burzyński yield curve and the HMH curve, Fig. 4.8. The σ_Y^C changes its value from 1.0 to 1.5 and σ_Y^T is equals 1. The yield strength in shear is calculated with use of relation (4.30).

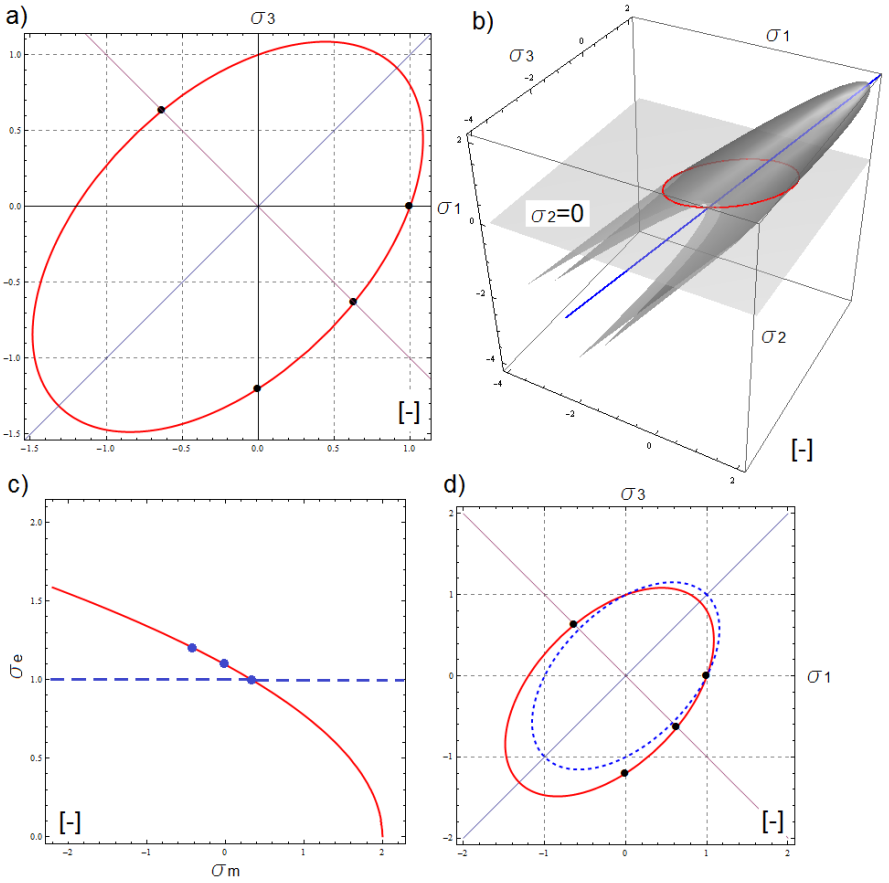

Figure 4.7: The paraboloid Burzyński criterion for isotropic materials, the schematic representation of the criterion for an exemplary data when SD parameter equals 1.3. The explanation of component pictures in the text above Figure.

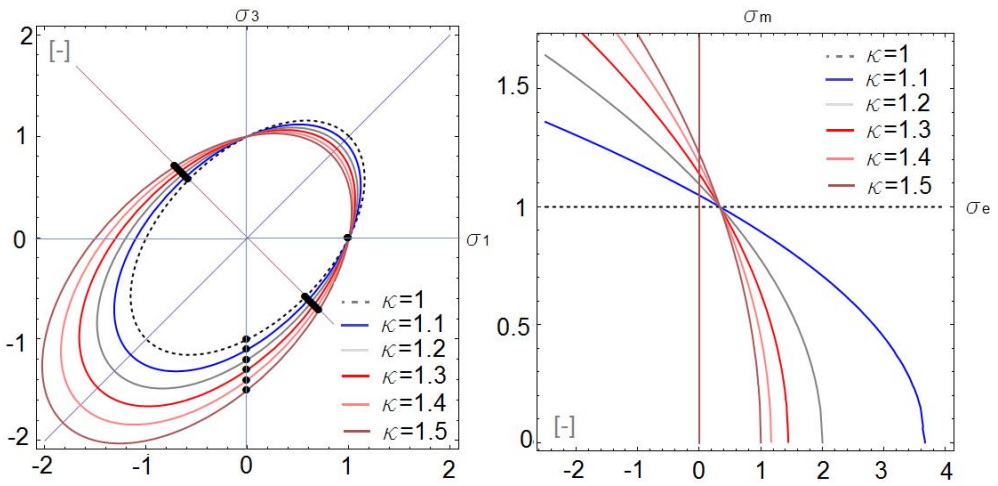

Figure 4.8: The evolution of the Burzyński limit curve according to the changed SD parameter

In Fig. 4.9 there are presented the yield surfaces - according to the changing SD parameter κ. As H the length from the peak of a paraboloid to the octahedral plane is signed and as R the radius of a cross-section which the paraboloid marks in the octahedral plane is signed. When κ equals 1 then the limit surface is a HMH cylinder of revolution. In Fig. 4.9 there are presented limit surfaces with the cross-section in the octahedral plane. In such perspective it also possible to notice, how the surface changes according to the SD parameter. The smaller SD parameter value, then the surface becomes narrower and its peak is more remoted from the octahedral plane.

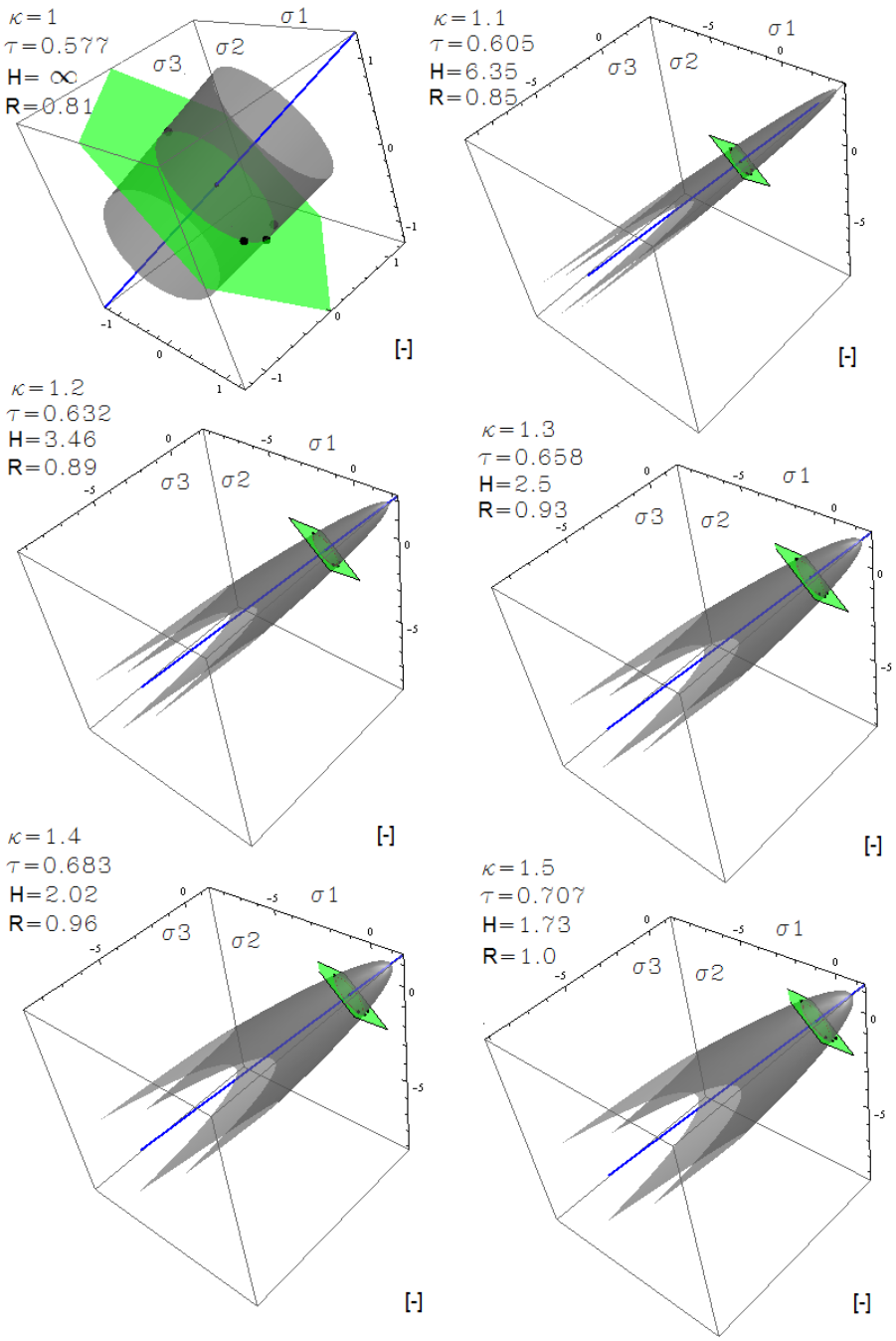

Figure 4.9: The evolution of the Burzyński limit surface according to the changed SD parameter, the cross-section in the octahedral plane.

4.5.4 Burzyński criterion for materials with initial anisotropy

Initial anisotropy occurs in the material primarily due to thermo-mechanical pre-processing and plastic deformation during the manufacturing processes - Paragraph 2.1.2. It appears that often plastic deformation induced anisotropy is small compared to initial anisotropy which is the result of a large deformation during initial processing operations such as rolling or extrusion. The material in the 'as-received' state becomes usually anisotropic. Due to the complexity involved in accounting the initial anisotropy, proceeding with data must not only account for the inhomogeneous and direction-dependent properties but should also anticipate undesirable features of anisotropic behaviour, such as premature fracture and undesirable shear banding.

Usually, to cover anisotropic character of the material in the yield criteria the multi-parameters functions are designed, e.g.: [Barlat et al. 2002; Tsai and Wu 1971]. However, a comparably simpler yield models are definitely in a favor with researchers and engineers. The objective is to propose certain simplified account for the aforementioned initial anisotropy with use of the model of isotropic material as regards elastic and plastic yield properties with certain correction of the yield shear strength. This correction embodies the overall effects of initial anisotropy and inhomogeneous properties of metallic solid in the state as received. In materials with a slight initial anisotropy which is produced for instance by texture induced in manufacturing process, the main effect which is observed is deviation of shear strength with respect to the predicted one from the HMH yield condition, Eq. (4.11). According to the proposition in [Burzyński 2009] such an effect can be described in a relatively simple way within the framework of the model for isotropic material with use of certain shear strength correction factor - λ.

The multi-surface Burzyński criterion is determined in the space of the principal stresses, Eq. (4.37). Burzyński expands the criterion for isotropic materials, Eq. (4.33) by accounting for the initial anisotropy, by the shear strength correction factor - λ. Burzyński derives the factor λ ([Burzyński 2009], pp. 194-195) as a constant resulting from certain relations between the elastic moduli for anisotropic solid. However, to reduce the number of constants in the yield criterion Burzyński replaces the description of considered anisotropic material with a model of isotropic solid. The whole effect of anisotropy is contained in the additional correction factor λ, which may be also explicitly calculated using the results of strength tests, Eq. (4.35). Because general formulation (4.24) is already narrowed to its paraboloidal (4.32) form then to fulfil condition of paraboloidal surface, a shear correction coefficient is calculated as, [Burzyński 2009]:

$$\lambda = \frac{\sigma_Y^C \sigma_Y^T}{2\tau_Y^2} - 1 \tag{4.35}$$

The λ parameter takes values in the range $0 < \lambda < 1$. In particular case if $\lambda = 0.5$ then there is obtained the paraboloid Burzyński criterion for isotropic materials, Eq. (4.26) and the limit of the shear is expressed in Eq. (4.28). And if also $\sigma_Y^C = \sigma_Y^T = \sigma_Y$ then the Burzyński criterion changes to the HMH criterion (4.10) (its visualization is a circular cylinder).

If criterion (4.37) is presented in the meridional plane (σ_m, σ_e) according to the relation (4.25)

accounting for the λ coefficient determined under the assumption that $\chi = 0.5$, then the limit curve does not change - it is shown schematically in Fig. 4.6. However, the equivalent stresses is expressed by a different relation:

$$\sigma_e^2 = 2(1-\lambda)(\sigma_2-\sigma_3)^2 + 2\lambda(\sigma_3-\sigma_1)^2 + 2(1-\lambda)(\sigma_1-\sigma_2)^2 \tag{4.36}$$

Substituting expressions (4.36) to equation (4.32) there is obtained a relation determined in the space of the principal stresses:

$$\begin{aligned}(1-\lambda)(\sigma_2-\sigma_3)^2 + \lambda(\sigma_3-\sigma_1)^2 + (1-\lambda)(\sigma_1-\sigma_2)^2 \quad + \\ +(\sigma_Y^C - \sigma_Y^T)(\sigma_1+\sigma_2+\sigma_3) = \sigma_Y^C\sigma_Y^T\end{aligned} \tag{4.37}$$

and in the plane $\sigma_2 = 0$

$$\sigma_3^2 + \sigma_1^2 - 2\lambda\sigma_3\sigma_1 + (\sigma_Y^C - \sigma_Y^T)(\sigma_1+\sigma_3) = \sigma_Y^C\sigma_Y^T \tag{4.38}$$

Formulation (4.37) is also based on the assumption of stress order Eq. (3.1). Consideration of all the possible combinations of the principal stresses leads to obtaining multi-surface condition, Table 4.4.

case:	σ_1	σ_2	σ_3
1	σ_1	σ_2	σ_3
2	σ_1	σ_3	σ_2
3	σ_2	σ_1	σ_3
4	σ_2	σ_3	σ_1
5	σ_3	σ_1	σ_2
6	σ_3	σ_2	σ_1

Table 4.4: Cases of order of the principal stresses.

Substituting all above cases to the equation (4.37), ordering its components, the Burzyński multi-surface criterion in six detailed equations is obtained. It is noticed that some of above substitutions give the same resulted function, thus cases $f_1 = f_6$ (blue colour in Fig. 4.10), $f_2 = f_4$ (green colour in Fig. 4.10) and $f_3 = f_5$ (grey colour in Fig. 4.10). Finally, three surfaces are obtained:

$$f_1 = \sigma_1^2 - (2\lambda-2)\sigma_2^2 + \sigma_3^2 + (\sigma_1\sigma_2+\sigma_2\sigma_3)(2\lambda-2) - 2\lambda\sigma_1\sigma_3 + (\sigma_Y^C-\sigma_Y^T)(\sigma_1+\sigma_2+\sigma_3) - \sigma_Y^C\sigma_Y^T$$

$$f_2 = \sigma_1^2 + \sigma_2^2 - (2\lambda-2)\sigma_3^2 + (\sigma_1\sigma_3+\sigma_2\sigma_3)(2\lambda-2) - 2\lambda\sigma_1\sigma_2 + (\sigma_Y^C-\sigma_Y^T)(\sigma_1+\sigma_2+\sigma_3) - \sigma_Y^C\sigma_Y^T$$

$$f_3 = \sigma_2^2 + \sigma_3^3 - (2\lambda-2)\sigma_1^2 + (\sigma_1\sigma_2+\sigma_1\sigma_3)(2\lambda-2) - 2\lambda\sigma_2\sigma_3 + (\sigma_Y^C-\sigma_Y^T)(\sigma_1+\sigma_2+\sigma_3) - \sigma_Y^C\sigma_Y^T$$

Each of the above equations is valid for a specific area, their inter-section gives the final, the resulted Burzyński criterion. The inner contour of the three curves determines the yield condition in the plane, Fig. 4.10, and in the space of principal stresses, Fig. 4.11.

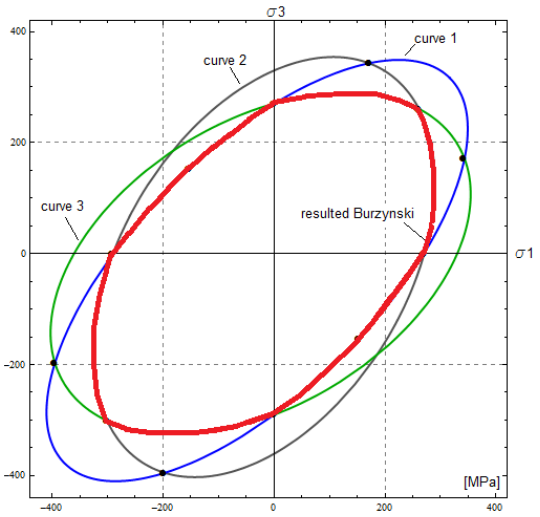

Figure 4.10: The inter-section of the Burzyński multi-surface criterion in the plane $\sigma_2 = 0$, with red line the resulted limit curve is expressed.

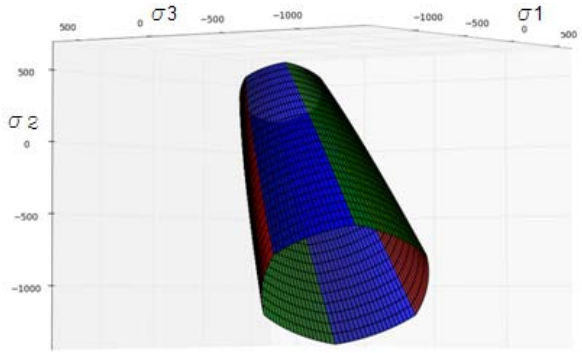

Figure 4.11: The inter-section of the Burzyński multi-surface criterion in the space of principal stresses.

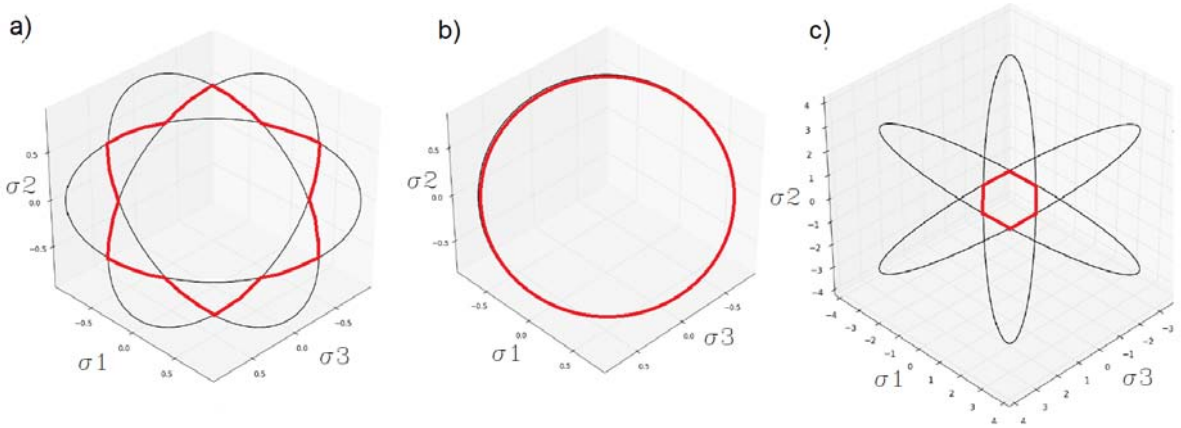

Figure 4.12: The cross-section of the resulted Burzyński multi-surface in the octahedral plane for: a) $\lambda = 0$, b) $\lambda = 0.5$, c) $\lambda = 1$, [Nowak 2012].

In Fig. 4.12 there are presented cross-sections of the resulted Burzyński multi-surface according to different values of shear correction parameter λ. It can be see that for $\lambda = \frac{1}{2}$ the criterion has a cylindrical cross-section - the same as for the isotropic Burzyński condition (4.34). For $\lambda < \frac{1}{2}$ the obtained surface is not convex. If $\lambda = 1$ the criterion changes into the Tresca criterion, because most parts of analysed relations are reduced to zero. Thus, the equations have forms $(\sigma_i - \sigma_j)^2 = \sigma_Y^C \sigma_y^T$ and $i, j = 1..3$ which are valid in suitable parts of system of reference.

4.5.5 Smoothness of criterion for initially anisotropic materials

Convexity of a yield function and its relations to convexity of the corresponding yield surface is essential when new criterion is proposed, [Bigoni and Piccolroaz 2004]. Convexity of the yield surface is one of the assets of classical elastoplastic flow theory, [Zattarin et al. 2004] (the other two are: a potential function enabling the determination of the plastic strain rate via the flow rule and the possibility to describe the influence of microstructure evolution of the material on the yield function through internal variables and hardening rules). Convexity supported by experiments is a useful mathematical property, which limits analysis and becomes of fundamental importance in setting variational inequalities for plasticity. As for the multi-surface Burzyński criterion, the function of yielding can be non-convex, as it is presented in Fig. 4.12.a. It is non-convex when shear correction coefficient $\lambda < \frac{1}{2}$.

Another feature of yield surface which should be avoided are corners. In case of resulted multisurface Burzyński criterion the resulted surface is smooth only if $\lambda = \frac{1}{2}$. This is a case when discussed criterion is the same as isotropic case (4.34). There are hypothesis with cornered surfaces which are of fundamental importance in plasticity theory, like Tresca or Coulomb–Mohr yield criteria. Theoretical speculations suggest that corners should be expected to form in the yield surface for single crystals and polycrystals (Hill, 1967) and smoothness of the yield surface might be considered a mere simplification in the constitutive modelling of metals. However, evidence supporting corner formation is weak and smoothness of the yield surface is a broadly employed concept. Corners are often included in the constitutive description of a material for the mere fact that an appropriate, smooth yield function is simply not available (this is usually the case of the apex of the Drucker–Prager yield surface and of the corner which may exist at the intersection of a smooth, open yield surface with a cap), [Bigoni and Piccolroaz 2004]. Moreover, if the criterion is to be implemented in FEM code, the corners should be avoided. Occurrence of corners in the yield surface is difficult to explain on the basis of material behaviour in the plastic range. This is the reason for 'smoothing' the resulted criterion with the only one curve. The new limit curve is a results of approximation with use of fitting parameters A_i, B_i, C_i - Eqs. (4.39), which should fulfil conditions covered by Eqs. (4.40 - 4.44), [Nowak 2012].

$$\begin{aligned}
\Phi_1(\sigma_1, \sigma_3) &= \sigma_1^2 - A_1\sigma_1\sigma_3 + A_2\sigma_3^2 + A_3(\sigma_Y^C - \sigma_Y^T)\sigma_1 + A_4(\sigma_Y^C - \sigma_Y^T)\sigma_3 - \sigma_Y^C\sigma_Y^T \\
\Phi_1(\sigma_1, \sigma_3) &= \sigma_1^2 + \sigma_3^2 - B_1\sigma_1\sigma_3 + B_2(\sigma_Y^C - \sigma_Y^T)\sigma_1 + B_3(\sigma_Y^C - \sigma_Y^T)\sigma_3 - \sigma_Y^C\sigma_Y^T \\
\Phi_1(\sigma_1, \sigma_3) &= C_1\sigma_1^2 - C_1\sigma_1\sigma_3 + \sigma_3^2 + C_3(\sigma_Y^C - \sigma_Y^T)\sigma_1 + C_4(\sigma_Y^C - \sigma_Y^T)\sigma_3 - \sigma_Y^C\sigma_Y^T
\end{aligned} \tag{4.39}$$

To obtain parameters A_i, B_i, C_i the following relations must be solved, Eqs. (4.40-4.44). The conditions for smoothness of a function of the Burzyński criterion are presented as follows:

for uniaxial tension:

$$\sigma_1 = \sigma_Y^T, \sigma_3 = 0 \tag{4.40}$$
$$\Phi_1(\sigma_1, \sigma_3) = 0, \Phi_2(\sigma_1, \sigma_3) = 0$$

for uniaxial compression:

$$\sigma_1 = -\sigma_Y^C, \sigma_3 = 0 \tag{4.41}$$
$$\Phi_1(\sigma_1, \sigma_3) = 0, \Phi_2(\sigma_1, \sigma_3) = 0$$
$$\sigma_1 = 0, \sigma_3 = -\sigma_Y^C \tag{4.42}$$
$$\Phi_2(\sigma_1, \sigma_3) = 0, \Phi_3(\sigma_1, \sigma_3) = 0$$

for biaxial compression:

$$\sigma_1 = -\sigma_Y^{CC}, \sigma_3 = -\sigma_Y^{CC} \tag{4.43}$$
$$\Phi_1(\sigma_1, \sigma_3) = 0, \Phi_3(\sigma_1, \sigma_3) = 0$$

In Fig. 4.13 there are indicated points in the cross-section $\sigma_2 = 0$ in which the subsequent surfaces of the multi-surface Burzyński criterion are valid. The equality of first derivatives is necessary in the points (A), (B), (C) plotted in Fig. 4.13:

points (A):
$$\frac{\partial \Phi_1(\sigma_1, \sigma_3)}{\partial \sigma_1} = \frac{\partial \Phi_2(\sigma_1, \sigma_3)}{\partial \sigma_1}, \frac{\partial \Phi_1(\sigma_1, \sigma_3)}{\partial \sigma_2} = \frac{\partial \Phi_2(\sigma_1, \sigma_3)}{\partial \sigma_2}$$
points (B):
$$\frac{\partial \Phi_1(\sigma_1, \sigma_3)}{\partial \sigma_1} = \frac{\partial \Phi_3(\sigma_1, \sigma_3)}{\partial \sigma_1}, \frac{\partial \Phi_1(\sigma_1, \sigma_3)}{\partial \sigma_2} = \frac{\partial \Phi_3(\sigma_1, \sigma_3)}{\partial \sigma_2} \tag{4.44}$$
points (C):
$$\frac{\partial \Phi_3(\sigma_1, \sigma_3)}{\partial \sigma_1} = \frac{\partial \Phi_2(\sigma_1, \sigma_3)}{\partial \sigma_1}, \frac{\partial \Phi_3(\sigma_1, \sigma_3)}{\partial \sigma_2} = \frac{\partial \Phi_2(\sigma_1, \sigma_3)}{\partial \sigma_2}$$

Consequently, after solving above equation the final formulation of the Burzyński criterion is given by Eq. (4.45).

$$\sigma_1^2 - R_B \sigma_1 \sigma_3 + \sigma_3^2 + (\sigma_Y^C - \sigma_Y^T)(\sigma_1 + \sigma_3) - \sigma_Y^C \sigma_Y^T = 0 \tag{4.45}$$

where:

$$R_B = 2 - \frac{\sigma_Y^C \sigma_Y^T + 2(\sigma_Y^C - \sigma_T^C)\sigma_Y^{CC}}{(\sigma_Y^{CC})^2} \tag{4.46}$$

and σ_Y^{CC} is a yield stress in biaxial compression, defined as it is schematically presented in the Section 4.3 in Fig. 3.1.

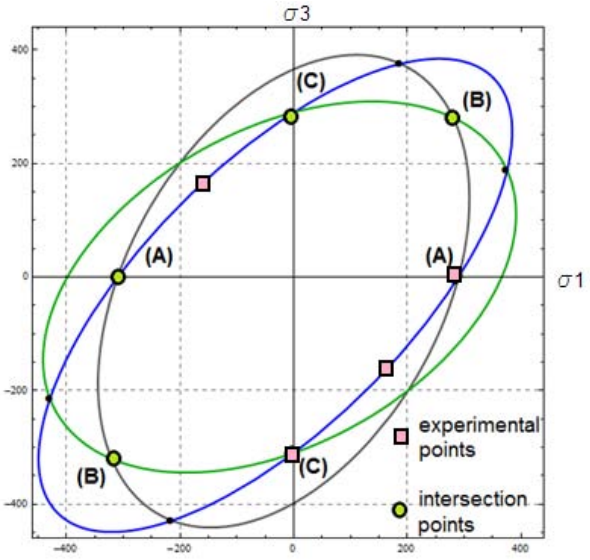

Figure 4.13: Experimental points and points of intersection which are used to find the final formulation of the Burzyński criterion, Eq. (4.39).

The comparison between the component curves the multisurface criterion and the final Burzyński criterion for initially anisotropic materials, Eq. (4.45), is presented in Fig. 4.14. The final yield surface obtained with use of smooth-out criterion with coefficient R_B is an elliptic paraboloid.

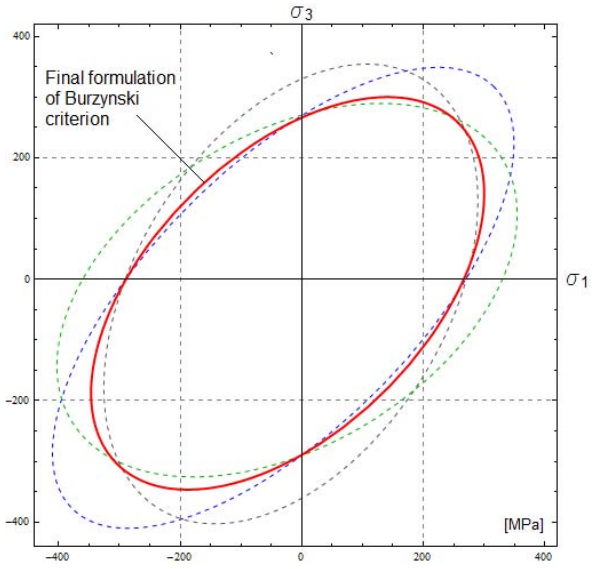

Figure 4.14: Approximation of the inter-section of the Burzyński multi-surface criterion with a final formulation, Eq. (4.45).

The R_B coefficient is a relation between results of strength tests - yield limit in tension, compression, shear and biaxial compression. However, as it was shown in the Section 3.4 the biaxial compression test is a test demanding a knowledge of many external conditions (friction, pressure, geometrical inaccuracies) and it is not easy to perform. Whereas, the yield strength in shear is more often obtained as a parameter characterized the behaviour of the

material. Consequently, assuming that yield stress in shear also belongs to the limit curve Eq. 4.45, the yield stress in biaxial compression σ_Y^{CC} can be given as a relation of yield stresses in tension, compression and shear. The purely mathematical relation allows to calculated yield strength in biaxial compression:

$$\sigma_Y^{CC} = \frac{2(\sigma_Y^C - \sigma_Y^T)\tau_Y^2 + \sqrt{4(\sigma_Y^C - \sigma_Y^T)^2\tau_Y^4 + 4\sigma_Y^C\sigma_Y^T\tau_Y^2(-\sigma_Y^C\sigma_Y^T + 4\tau_Y^2)}}{2(-\sigma_Y^C\sigma_Y^T + 4\tau_Y^2)} \tag{4.47}$$

The coefficient R_B takes values from 0 to 2, if R_B equals to 1, then the criterion takes form of the isotropic Burzyński criterion, Eq. 4.34. Beneath there is presented the parametric study concerning limit curves possible to obtain with use of Eq. 4.45.

Assuming that $\sigma_Y^C = \sigma_Y^T = 1$ and:
a) $R_B = 0$ - curve signed with blue line,
b) $R_B = 1$ - curve given in red line,
c) $R_B = 2$ - grey-lined curve. The values of R_B from 0 to 2 - and suitable to them limit curves in the plane $\sigma_2 = 0$:

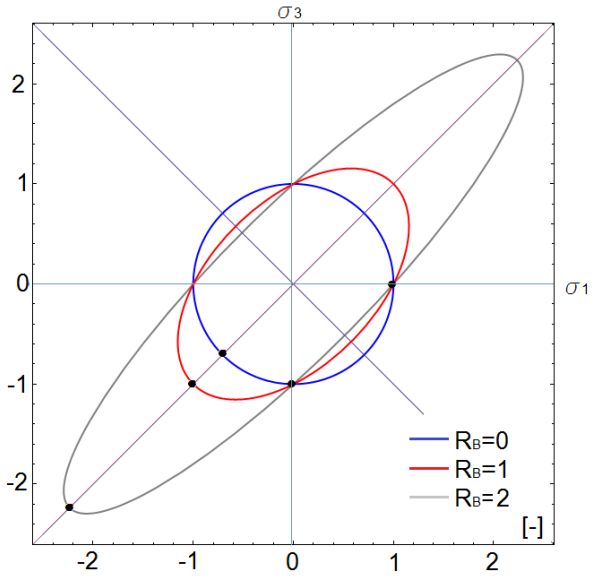

Figure 4.15: Limit curves depending on the different values of R_B coefficient.

In the table 4.5 there are collected different values of yield strengths $\sigma_Y^C, \sigma_Y^T, \tau_Y$ - basing on them the SD parameter κ and R_B coefficient are calculated. Resulted curves are collected in the Figs. 4.16 and 4.17. Different dependence between stresses allow to present range of applicability of the criterion (4.45).

The Fig. 4.16 presents the following cases plotted in the meridional plane (σ_m, σ_e):
a) $R_B = 1$, $\sigma_Y^T = 1$, different SD parameters> 1,
b) $R_B = 1$, $\sigma_Y^C = 1$, different SD parameters< 1,
c) $\sigma_Y^T = \sigma_Y^{CC} = 1$, different SD parameters> 1 - resulted various R_B,
d) $\sigma_Y^C = \sigma_Y^{CC} = 1$, different SD parameters< 1 - resulted various R_B.

Figure	σ_Y^C [-]	σ_Y^T [-]	κ [-]	τ_Y [-]	σ_Y^{CC} [-]	R_B [-]
4.16.a) 4.17.a)	1	1	1	0.577	1	1
4.16.a) 4.17.a)	1.1	1	1.1	0.605	1.15	1
4.16.a) 4.17.a)	1.2	1	1.2	0.632	1.31	1
4.16.a) 4.17.a)	1.3	1	1.3	0.658	1.47	1
4.16.b) 4.17.b)	1	0.9	1.11	0.547	1.05	1
4.16.b) 4.17.b)	1	0.8	1.25	0.516	1.11	1
4.16.b) 4.17.b)	1	0.7	1.42	0.483	1.18	1
4.17.c)	1	1	1	0.63	0.81	0.47
4.17.c)	1	1	1	0.51	1.84	1.7
4.17.d)	1	1	1	0.577	1.1	1.17
4.17.d)	1	1	1	0.577	1.2	1.3
4.17.d)	1	1	1	0.577	1.3	1.4
4.16.c) 4.17.e)	1.1	1	1.1	0.605	1	0.7
4.16.c) 4.17.e)	1.2	1	1.2	0.632	1	0.4
4.16.c) 4.17.e)	1.3	1	1.3	0.658	1	0.1
4.16.d) 4.17.f)	1	0.9	1.11	0.547	1	0.9
4.16.d) 4.17.f)	1	0.8	1.25	0.516	1	0.8
4.16.d) 4.17.f)	1	0.7	1.43	0.483	1	0.7

Table 4.5: Different values of yield strengths and R_B coefficient which are corresponding to limit curves presented in the Figs. 4.16 and 4.17.

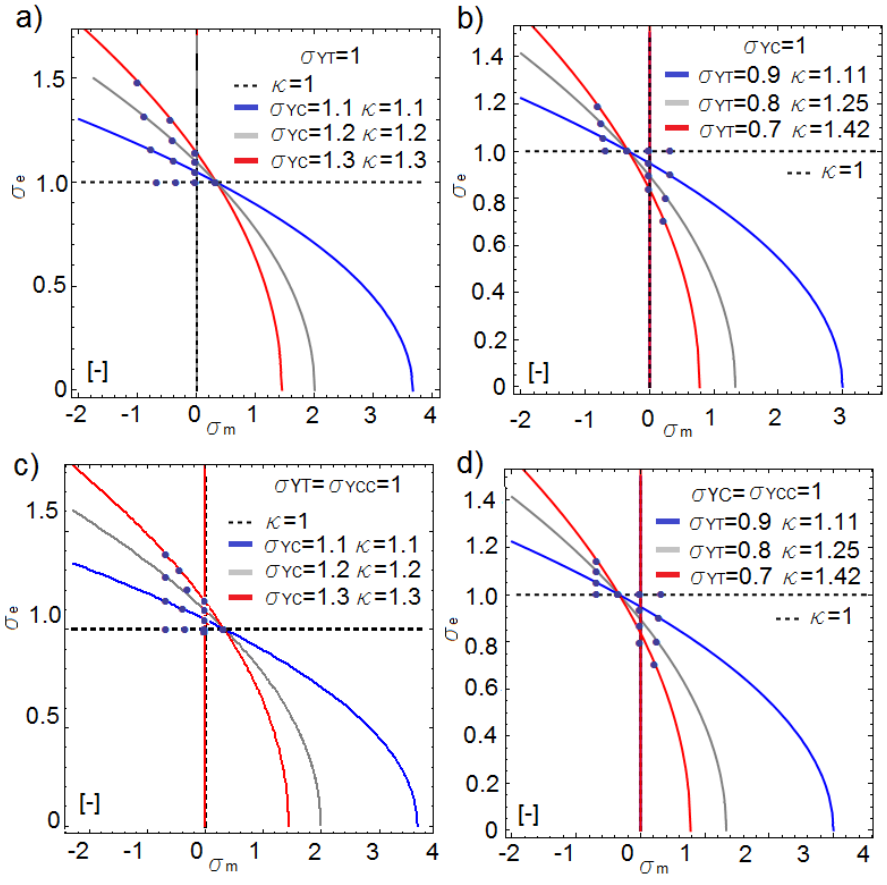

Figure 4.16: Limit curves in the meridional plane obtained due to the criterion (4.45).

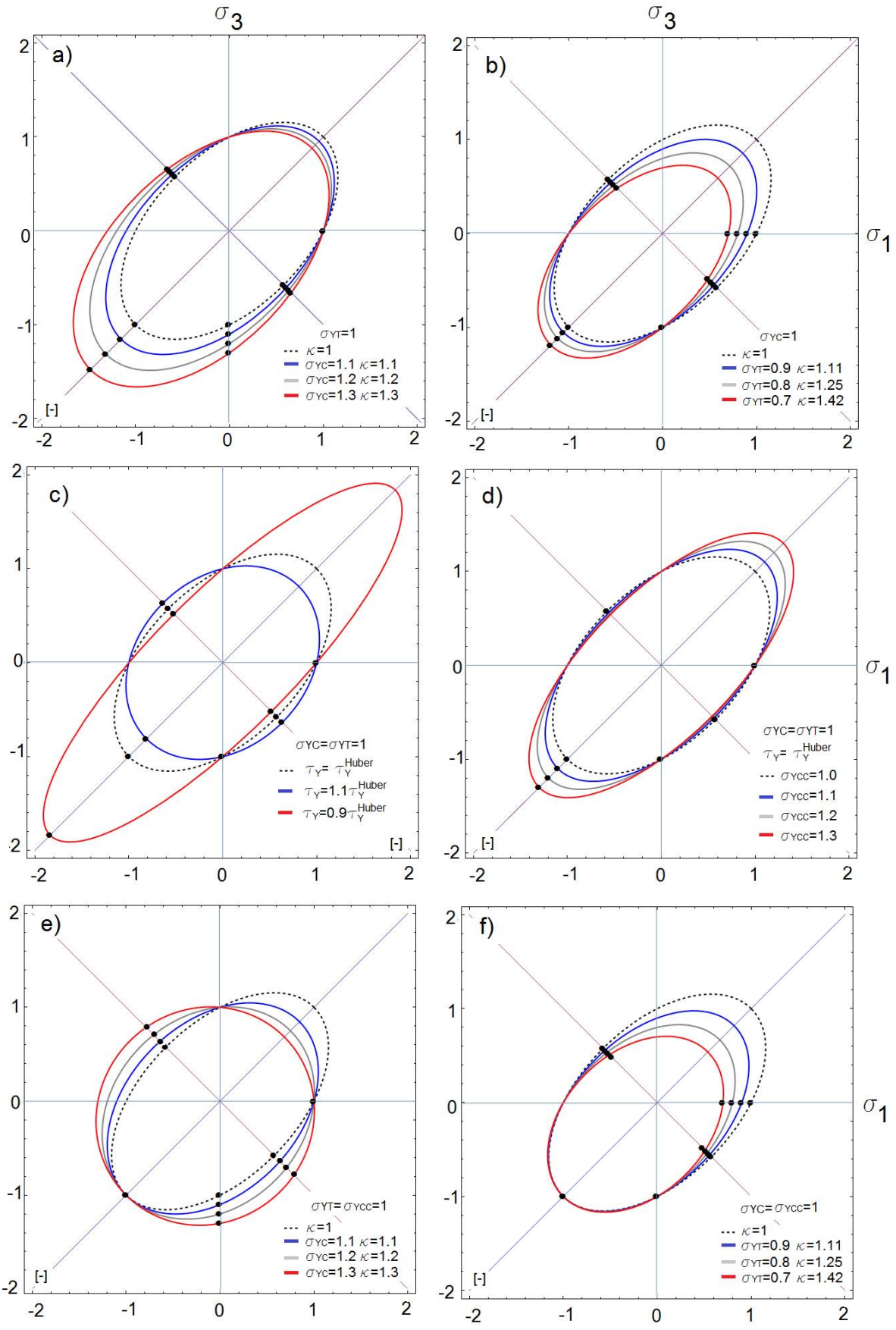

Figure 4.17: Limit curves in the plane $\sigma_2 = 0$ obtained due to the criterion (4.45).

The Fig. 4.17 presents the following cases plotted in the plane $\sigma_2 = 0$:
a) $R_B = 1$, $\sigma_Y^T = 1$, different SD parameters> 1,
b) $R_B = 1$, $\sigma_Y^C = 1$, different SD parameters< 1,
c) $\sigma_Y^T = \sigma_Y^C = 1$, SD parameter=1, τ_Y multiple of τ_Y^{thoer} calculated according to Eq. (4.11) - resulted various R_B,
d) $\sigma_Y^T = \sigma_Y^C = 1$, SD parameter=1,$\tau_Y = \tau_Y^{thoer}$, different values of σ_Y^{CC} - resulted various R_B,
e) $\sigma_Y^T = \sigma_Y^{CC} = 1$, SD parameter$> 1$ - resulted various R_B,
e) $\sigma_Y^C = \sigma_Y^{CC} = 1$, SD parameter$> 1$ - resulted various R_B.

4.5.6 Phenomenological formulation of the Burzyński criterion

The yield points in tension, compression and shear (respectively $\sigma_Y^T, \sigma_Y^C, \tau$) for the materials OFHC Cu and E335 steel are collected in Tables 5.11 and 5.19. In Sections 5.3 and 5.4 the discussion concerning experimental results of theses materials is given. Basing on the data collected in Tables the values of R_B coefficients are calculated due to Eq. (4.46). When R_B coefficients are plotted as a function of strain and strain rate - as it is shown in Fig. 4.18 - it turns out that the coefficient has the same tendency for both materials. The points of R_B coefficients are marked with different points for each strain rate. The graphs shows that the character of R_B along with increasing strain has an increasing, exponential shape, with increasing strain rate the level of R_B parameters is also increasing. Some constitutive models are also function of strain and strain rate and temperature - e.g. the Johnson-Cook model [Johnson and Cook 1983] or the Rusinek-Klepaczko model [Klepaczko 1987]. Basing on such ideas and noticing that function of R_B has a similar characteristic for 2 different materials, it is possible to built a function of strain, strain rate in the similar manier as authors of the JC models made it.

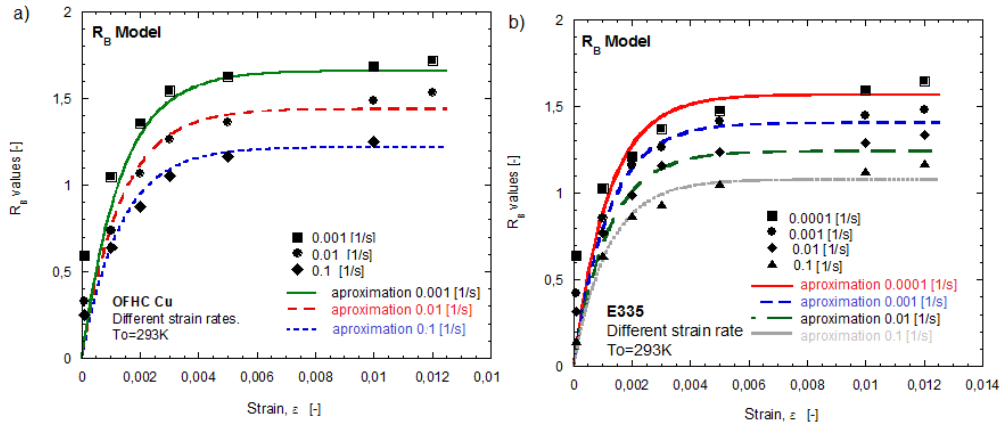

Figure 4.18: R_B correction coefficients marked with different points according to increasing strain rate and offset strain. Approximation of R_B with a function Eq. (4.48) indicated with lines for: a) OFHC Cu and b) E335 steel.

Consequently, the R_B coefficient can be described by a function $f(\varepsilon, \dot{\varepsilon})$ - Eq. (4.48):

$$R_B(\varepsilon, \dot{\varepsilon}) = A[1 - \exp(-B\varepsilon)](1 - C \ln \frac{\dot{\varepsilon}}{\dot{\varepsilon}_0}) \tag{4.48}$$

where A, B, C are the material constants, $\dot{\varepsilon}_0$ is the reference strain rate.

Parameters A and B are obtained due to linear approximation dependence of R_B on strain rate (as example - Fig. 4.20.b). The C parameters is obtained as a slope of logarithmic strain versus stress, $\dot{\varepsilon_0}$ is the reference strain rate assumed as lower than the lowest strain rate in test. Basing on the relation (4.48) it is possible to approximate the R_B function - as it is show in the Fig. 4.18, in which there are presented characteristics of R_B coefficient for OFHC Cu and E335 steel. The material parameters are collected in the Tables 5.12 and 5.19 in the Sections 5.3 and 5.4.

It may be noticed that: higher strain rates, lower R_B level and increasing offset strains then exponentially increasing R_B values. In case of OFHC Cu and quasi-static range of strain rates for which the R_B function is studied - $0.001s^{-1}$ is the lowest value of strain rate, R_B coefficients have for this strain rate the highest level. It seems to be a proper behaviour of modelling function because values of R_B tends to the upper limit of its possible range - namely 2, Figs. 4.18.a and 4.19 It is not possible otherwise - that for even smaller strain rates R_B coefficients have more possibilities of obtaining lower levels which tend to 0. For higher strain rates $0.01, 0.1s^{-1}$ function of R_B tends to zero - the levels become gradually smaller what makes possible to determine or preview level of function (4.48) for dynamic rates.

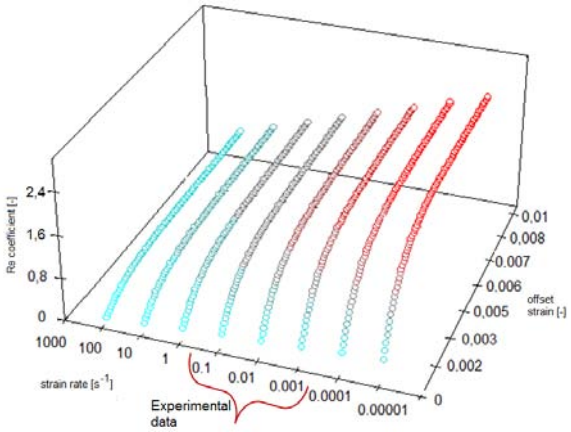

Figure 4.19: R_B dependence on strain rate and offset strain - prediction and experimental result. The solid lines represent the model prediction, while symbols represent R_B coefficients.

The function of R_B is purely empirical, built to bond the behaviour of material depending on the strain and strain rate with a mathematical function describing this dependence. It is possible to add the temperature depended part similar to the JC relation because temperature according to strain rate has a constant character. At this moment, however, the author does not have sufficient data to verify correctness of this assumption. Basing on the function (4.48) it is possible to predict behaviour of the material for different strain rates. Moreover, this kind of formulation is possible to implement in the FEM code - what make the calculation with use of the Burzyński condition for initially anisotropic materials more accurate. The example of application the Burzyński yield criterion in its phenomenological form using the function of R_B correction coefficient is presented in next Paragraph. The example is prepared for the literature data of Nylon 101, [Khan and Farrokh 2010].

Example of application of phenomenological formulation of the Burzyński criterion

The material presented in [Khan and Farrokh 2010] is a polymer - Nylon 101. The material has been subjected to different loading conditions: uniaxial tension, uniaxial compression (in two different directions), pure torsion, pure reverse torsion, combined tension-torsion and biaxial compression (in two different directions), at four different strain rates: 0.0001, 0.001, 0.001, 0.1 s^{-1} at room temperature. Data are collected in Table 4.6. In [Khan and Farrokh 2010] data are used to validate proposed by authors criterion. The capability of the developed criterion was examined by simulating high strain rate (430 and 1370 s^{-1}) yield behaviour of the material. In Table 4.6 these two data are added.

Experiment	Strain rate (s^{-1})											
	0.00001		0.0001		0.01		1		430		1370	
	σ_1[a]	σ_2	σ_1	σ_2	σ_1	σ_2	σ_1	σ_2	σ_1	σ_2	σ_1	σ_2
Tension (Ext. Dir.)	68.8	0	78.4	0	92	0	102.3	0	122	0	0	-150
Compression (Ext. Dir.)	−73.9	0	−83.3	0	−94.3	0	−107.1	0				
Compression (90° to Ext. Dir.)	0	−72.9	0	−84.8	0	−94.9	0	−105.3				
Torsion	37.6	−37.6	42.5	−42.5	52.4	−52.4	61.71	−61.7				
Reverse Torsion	−40.3	40.3	−46.7	46.7	−54.3	54.3	−63.7	63.7				
Tension-Torsion	54.3	−19.3	61.1	−23.3	74.3	−30.1	N/A	N/A				
Biaxial (Ext. Dir.)	−87	−33	−95	−32.2	−110.1	−41.3	−127	−48.9				
Biaxial (90° to Ext. Dir.)	−37	−86	−41.1	−99	−42.4	−112.6	−55.15	−131.3				

All stresses are in MPa.

Table 4.6: Nylon 101. The yield stress at 0.5% offset definition, [Khan and Farrokh 2010].

In Fig. 4.20.a there is depicted the strain rate sensitivity for Nylon 101. As for the most of the polymers, nylon has a positive strain rate sensitivity. Dependence of R_B coefficient on the strain rate is depicted in Fig. 4.20.b. R_B correction has been calculated using relation (4.46). For materials with positive strain rate sensitivity - the coefficient has a decreasing tendency along with the increasing strain rate.

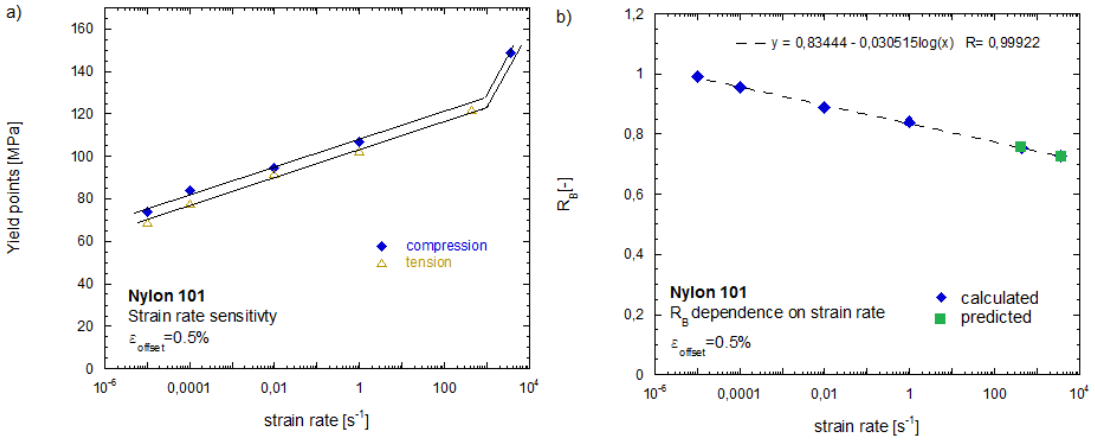

Figure 4.20: Nylon 101, [Khan and Farrokh 2010]. a) Strain rate sensitivity, b) dependance of R_B coefficient on the strain rate.

As it is shown in [Khan and Farrokh 2010] the yield points of Nylon are defined for one value of the offset strain equals 0.5%, consequently only one part of the relation (4.48) is possible to determine, its dependence on the strain rate. Because a wide experimental schedule has been obtained for quasi-static strain rates - for four values of strain rate

$(0.0001, 0.001, 0.001, 0.1\ s^{-1})$ it is possible to calculate the exact R_B values - Table 4.7. However, the values of R_B at high strain rates are possible to predict due to the linear dependence between R_B coefficient and strain rate (parameters printed in the Fig. 4.20.b).

[MPa] / [s^{-1}]	σ_Y^C	σ_Y^T	κ	τ_Y	τ_{Yteor}	$\frac{\tau_Y}{\tau_{teor}}$ [%]	σ_Y^{CC}	R_B [-]
0,00001	72,00	68,00	1,06	40,40	40,40	0,00	74,07	1,00
0,0001	83,30	78,40	1,06	47,00	46,66	0,73	83,94	0,96
0,01	96,00	91,00	1,05	55,00	53,96	1,92	93,24	0,89
1	107,00	102,00	1,05	62,00	60,32	2,79	101,37	0,84
430	128,10	122,00	1,05		72,18			0,75
3670	145,00	138,10	1,05		81,70			0,73

Table 4.7: Nylon 101, [Khan and Farrokh 2010]. Summary of yield points values used to plot yield curves presented in Fig. 4.21.

Such an approximation of R_B values is necessary when only one yield point for a specific strain rate is known and also, there is a difference between yield point in shear obtained from the experiment and known due to the theoretical relation (4.30). For Nylon, in case of $\dot{\varepsilon} = 430s^{-1}$ the yield point in tension is determined, whereas for $\dot{\varepsilon} = 1370s^{-1}$ only yield point in compression. Additionally, the difference between theoretical values of yield point in shear varies from 0 to 3%, Table 4.7. Unknown material data make difficult to predict properly the state of yielding if the traditional criterion cant be used, material is assumed to have asymmetry of elastic range, the theoretical value of yield point in shear does not fulfils the Huber-Mises relations (4.30). But if there is a relation between yield points depending on the strain rate (and/or the offset strain), it allows to predict missing values and define more accurately limit curves.

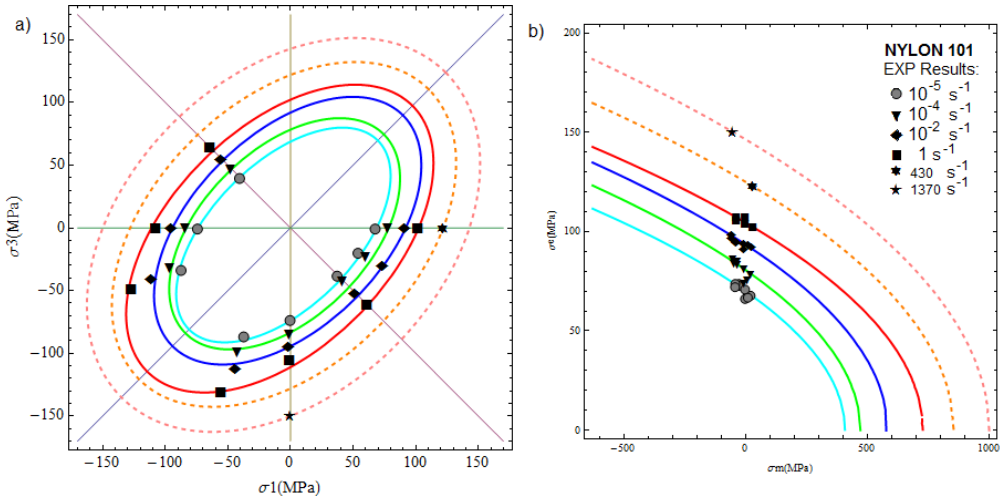

Figure 4.21: Nylon 101, [Khan and Farrokh 2010]. The yield curves at different strain rates in the planes: a) $\sigma_2 = 0$ and b) meridional.

Fig. 4.21 illustrates the yield curves of Nylon 101 as a function of strain rate along with the experimental data. Due to positive strain rate sensitivity of this polymer, the material's yield loci expand uniformly as the strain rates increase. With solid lines are depicted yield curves obtained due to relation (4.45). With dashed lines there are indicated yield curves obtained due to prediction of R_B value with assumption that SD parameter is close to 1.05, Table 4.7.

4.5.7 Concluding remarks

The analysis of the Burzyński energy-based material effort hypothesis [Burzyński 2009] has been the main aim of this Chapter. The specific cases of the hypothesis can be applied to describe yielding of isotropic materials - Eq. (4.33). The original Burzyński proposal to describe yielding of the initially anisotropic materials is expressed by the multi-surface formulation, so to avoid corners the method of obtaining a smooth surface has been presented, Eq. (4.45). The issue of the convexity of the criteria has been also discussed. The extended formulation of the criterion (4.45) allowing to include phenomenological behaviour of materials in the function depending on the strain, strain rate is proposed, Eq. (4.48).

Additionally, the isotropic case of paraboloidal Burzyński criterion for isotropic materials has been implemented in the FEM code, [Vadillo et al. 2011]. The results of the numerical calculation of tensile test of notched specimens are presented and discussed in next Section 4.6.

The Burzyński criteria can be applied for a wide range of materials in a wide range of strain rates and temperatures. In the Chapter 5 there are given examples of criteria applications for different materials.

4.6 User subroutine for the Burzyński isotropic criterion

In commercial finite element code (realized by commercial software e.g. Abaqus or Ansys) there are implemented classical yield criteria, e.g. the Huber–Mises-Hencky criterion, Eq. (4.10) or the Drucker–Prager criterion and also others having mostly an empirical character. Their advantage is that they are generally applicable to most of the materials, widely known and easy to use.

In author's opinion, the implementation in FEM of the Burzyński criterion would be an efficient step in accurate description of the onset of plasticity for a wide group of materials - metals, their alloys, polymers, metal matrix composites for which the asymmetry of elastic ranges is noticed. The implementation could find wide applications in practical analysis of complex states of stress in plasticity as well as viscoplasticity.

The original proposal of implementation of the Burzyński isotropic criterion (4.33) in the finite element code with use of Abaqus user subroutine UMAT is presented in the paper of [Vadillo et al. 2011]. In IPPT PAN the similar UMAT with the Burzyński isotropic criterion has been developed independently, [Nowak and Nowak 2012].

Within the finite element method the integration process is local in space and occurs at quadrature points of the finite elements. The incremental integration of the constitutive model is a strain-driven process in which the total strain tensor increment at each quadrature point is given at a certain time and both the stress and the state variables should be updated, [Vadillo et al. 2011].

The Burzyński isotropic criterion Eq. (4.26) rewritten into Eq. (4.49) is implemented in the FE code:

$$\Phi(\sigma_m, \sigma_e, \sigma_Y^T) = \frac{1}{2\kappa}\left\{3(\kappa-1)\sigma_m + \sqrt{9(\kappa-1)^2\sigma_m^2 + 4\kappa\sigma_e^2}\right\} - \sigma_Y^T \tag{4.49}$$

Required steps to write algorithm with use of user subroutine UMAT are presented e.g. in [Fernandez-Saez and Vadillo 2009; Vadillo et al. 2011; Wang et al. 1997] and e.g. www.imechanica.org/files/writingumat.

In order to analyse the behaviour of the proposed model and the integration algorithm, the tensile test of notched specimens have been performed. The test is based on the concept of [Wilson 2002], later repeated by other authors [Bai and Wierzbicki 2008; Vadillo et al. 2011; Gao et al. 2012]. The results of calculation with use of UMAT with implemented the Burzyński isotropic condition are compared with results of calculation with the traditional Huber-Mises plasticity model covered by commercial FE code of Abaqus/Standard.

4.6.1 Analysis of the tensile test of notched specimens for E335 steel

Experimental observation of Bridgman led to the conclusions that the yielded material is incompressible, either yielding does not depend on hydrostatic stress and the flow stress is independent of the third deviatoric stress invariant (or Lode angle parameter), [Bridgman 1947]. The above conclusions became tenets in the classical metal plasticity. However, in his later work Bridgman withdrew the second statement refereing to possible errors, [Bridgman 1952].

By the time the last series of measurements was being made under the arsenal contract, however, skill in making the measurements had so increased, and probably also the homogeneity of the material of the specimens had also increased because of care in preparation, that it was possible to establish a definite effect of pressure on the strain hardening curve. Citation after [Wilson 2002].

Also later, assumption about lack of pressure influence on deformation process were questioned and there were reported experimental observations which proved its incorrectness, [Richmond and Spitzig 1980; Spitzig and Richmond 1984]. Also, the effect of the third deviatoric stress invariant should be included in the constitutive description of the metal materials.

This issue was refreshed by [Wilson 2002]. Wilson studied effect of the mean stress pressure on the metal deformation. His experiments and nonlinear finite element analysis of 2024-T351 aluminum smooth and notched round bars revealed the effect of hydrostatic stress on yielding.

Nonlinear finite element analysis using the von Mises (yielding is independent of hydrostatic stress, Eq. (4.10)) and the Drucker-Prager (yielding is linearly dependent on hydrostatic stress, Eq. (4)) yield functions was performed. The von Mises results overestimated experimental load displacement curves by 10–65%. The Drucker-Prager results matched the experimental results, Fig. 4.22.

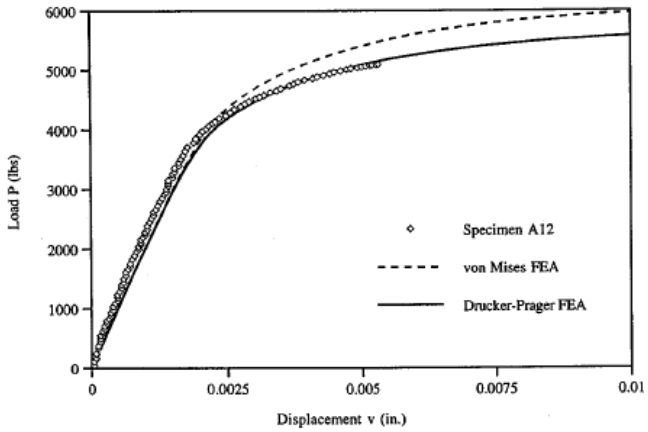

Figure 4.22: Experimental and numerical load-displacement results for notched round specimen, [Wilson 2002].

Since Drucker-Prager criterion covers the requirements of materials with asymmetry of elastic range, it gives better fitting to results of tensile tests for notched specimen. However, it is known that the criterion represented by a conical failure surface in the space of principal stresses can only roughly approximate real behaviour of a material in the limited range of hydrostatic stress and fails to describe properly the states near to the apex of the failure cone, [Theocaris 1995].

Consequently, the conception of experiment proposed by Wilson encourages other authors to apply their own propositions - which account for hydrostatic pressure influence [Vadillo et al. 2011] (or Lode angle [Bai and Wierzbicki 2008; Gao et al. 2009; 2011; 2012]). Authors used the same material as Wilson - 2024-T351 aluminum.

To prove the influence of hydrostatic stress on the plasticity of metal - the round bar specimens are used. The tensile test which confirms influence of third invariant of deviatoric stress tensor has been performed on flat grooved specimens, 4.23.b.

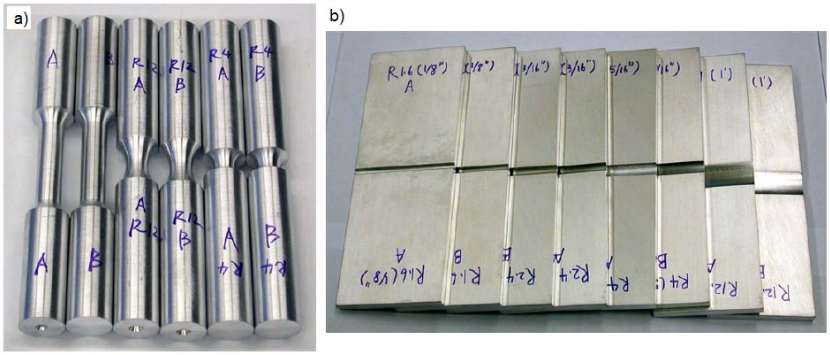

Figure 4.23: a) A group of smooth and notched round bar specimens, b) a group of flat grooved specimens, [Bai and Wierzbicki 2008].

The feature of grooved specimens allows to see in a direct way the effect of the Lode angle parameter on metal plasticity, Fig. 4.24.b. In Fig. 4.23.a there are presented round notched bars, for which results of tensile test, Fig. 4.24.a proved Wilson's observations about metals pressure sensitivity.

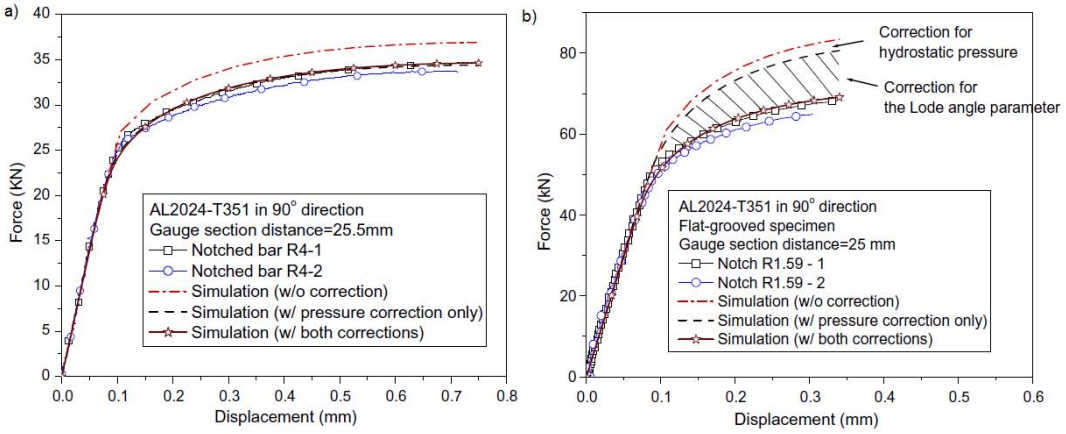

Figure 4.24: A comparison of force-displacement curves between experimental results and numerical results for: a) notched round bars, b) flat grooved specimens, [Bai and Wierzbicki 2008].

4.6.2 Experimental and numerical results

Basing on papers of [Wilson 2002; Vadillo et al. 2011; Gao et al. 2009; Bai and Wierzbicki 2008] there has been performed numerical simulation with use of round bar specimens with different notched zone. The geometry and dimension details of the notched round bar specimens are given in Fig. 4.25, their picture: Fig. 4.26. The material which has been used for the experiments is steel E335 (Chapters 2, 2.3).

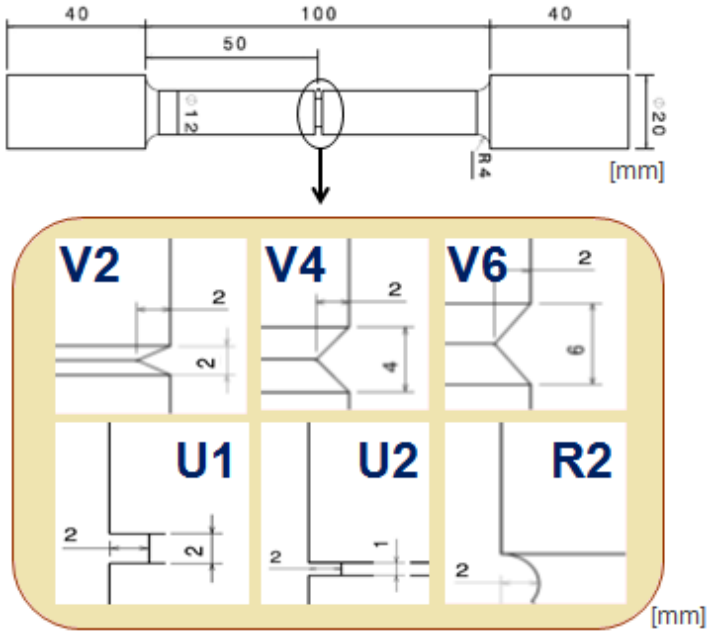

Figure 4.25: Notched specimen with different notch shapes.

The quasi-static tension test for each specimen has been performed in the isothermal conditions at room temperature, the process has the constant strain rate equals to 0.001 s^{-1}. During the test, the force has been measured by the force cell, the vertical displacement with use

of the optical extensometers. The recording of temperature has revealed that the increase of temperature during the test has not been high, consequently it can be concluded that temperature change has not affected the process of deformation.

Figure 4.26: The picture of manufactured specimens, the notched zones are blackened for observation with use of the thermographic camera.

From experiment of tensile test performed with use of a smooth specimen there are obtained material's characteristics. The experimental true stress–true strain material characteristics $\sigma_{true} - \varepsilon_{true}$ for a smooth specimen has been calculated due to relation (3.7). In the elastic range, Table 4.8: the Young's modulus, and the Poisson's coefficient. In the plastic range: the experimental true stress–true strain material characteristic $\sigma_{true} - \varepsilon_{true}$ obtained from uniaxial tensile tests performed for a smooth specimen with strain rate equals 0.001 s^{-1} is approximated with use of the power-law hardening relationship: $\sigma(\varepsilon) = A + B\varepsilon^n$, Table 4.9.

E335 steel	E [GPa]	ν [-]
	225	0.3

Table 4.8: Elastic characteristics for the E335 steel.

E335	A [MPa]	B [MPa]	n [-]
	546	537.32	0.29

Table 4.9: E335. Parameters of constitutive relation due to which the plastic behaviour is modelled.

Due to the symmetry of a model, only a quarter of the specimen needs to be taken into account. The numerical analysis consists of the model of a sample which is meshed with use of axisymetric hexagonal elements CAX8R (8-node axisymmetric elements with reduced integration). Their amount is about 3000 for each kind of the notched specimen and with a refined mesh near the notched region. The finite element mesh and the detail of the mesh in the notched region for each case is presented in Fig. 4.27.

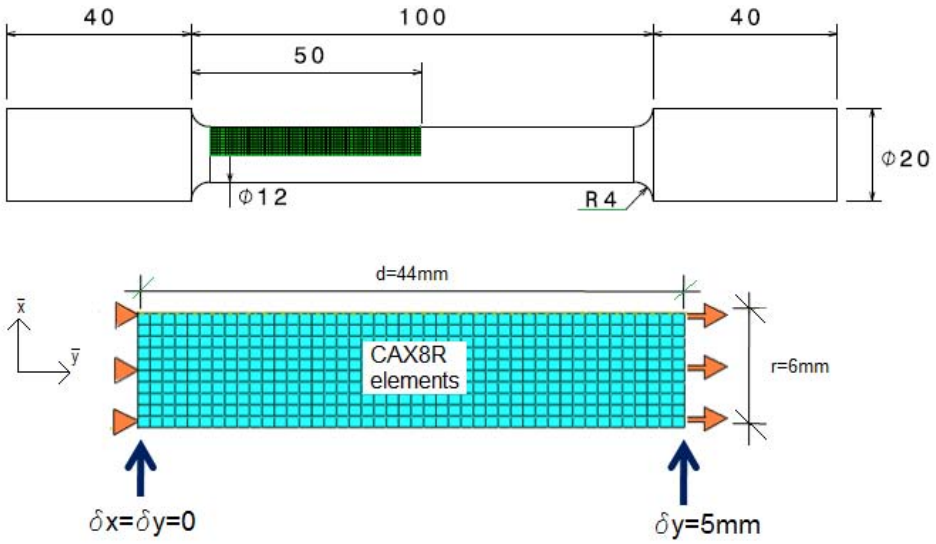

Figure 4.27: Configuration of a notched specimen with its numerical axisymmetric model.

During the test there are assumed boundary conditions which mimics the experimental conditions: the specimen is fully fixed from one its end, whereas displacement is controlled on its second end. The final elongation is equals 5mm. Mesh for each kind of notch is presented in Fig. 4.28.

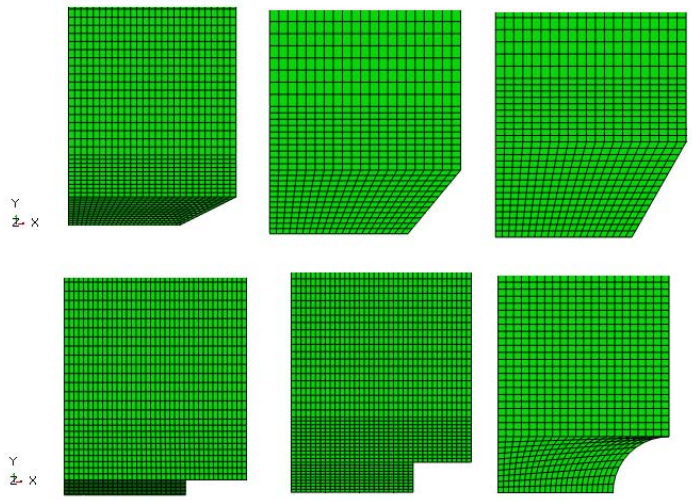

Figure 4.28: The finite element mesh and the details of mesh near to the notch regions.

As a result, for each kind of the notched specimen there is obtained the force-displacement relation which is compared with experimental result. The calculation are performed with use of Abaqus/Standard finite element code and user subroutine UMAT with implement the Burzyński criterion for isotropic materials. Different values of strength differential parameter κ have been accounted.

In Fig. 4.29 there is presented the diagram of numerical algorithm for modelling behaviour of notched and smooth specimen during the tensile test.

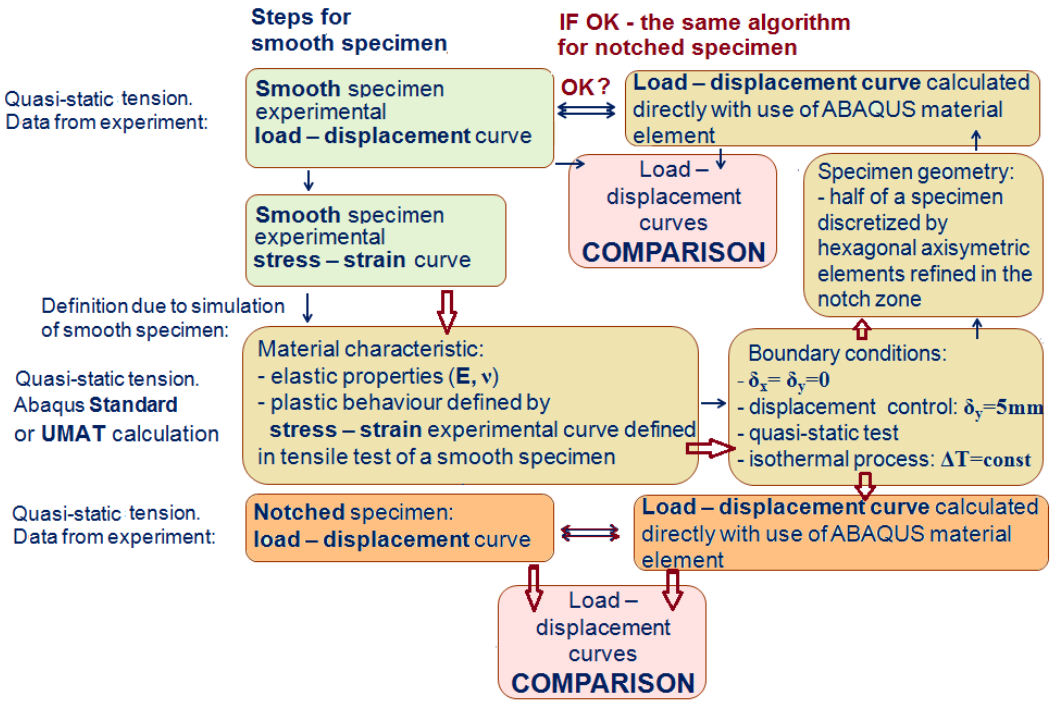

Figure 4.29: Diagram of numerical algorithm of modelling behaviour of the notched specimen in the deformation proces.

In Fig. 4.30 there are presented the load–displacement curves obtained in the numerical situation using the Burzyński paraboloid model for different values of the strength differential factor $\kappa = 1.0$, $\kappa = 1.1$, $\kappa = 1.2$, $\kappa = 1.3$. These results are compared with the experimentally observed behaviour of the specimen. If the behaviour of the material at compression is the same as at tension, $\kappa = 1.0$, then yielding of the material can be modelled with use of the HMH yield criterion. In case of E335 steel the modelling with use of the HMH yield criterion overshoots the real response of the material.

In Table 4.10 for each kind of notch there are presented differences between maximum values of force F obtained in the experiments and suitable to them, values of force calculated in the numerical tests.

Force [kN]	V2	V4	V6	U1	U2	R2
Experiment:	65.18	61.16	57.96	70.4	55.08	50.95
Simulation:	67.47	62.44	59.67	72.37	56.65	53.5
Difference:	2.29	1.28	1.71	1.97	1.57	2.55
Percentage:	3.4%	2.1%	2.9%	2.7%	2.8%	4.8%

Table 4.10: Difference between maximum value of force F obtained in the experiment and suitable to it, value of force calculated in the numerical test.

Comparison between experimental and numerical curves $F-\delta$ for different notched specimens made with steel E335 is given in Fig. 4.30.

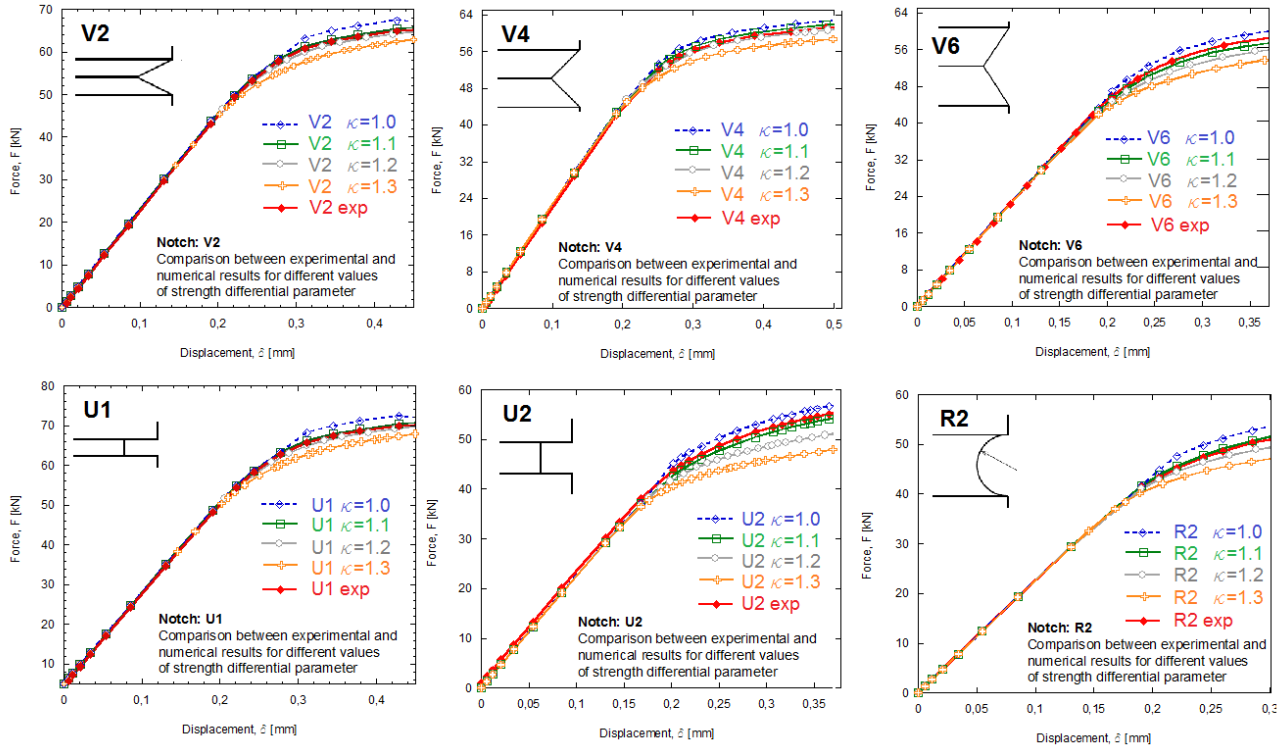

Figure 4.30: Load–displacement results for each kind of notched specimen.

There can be noticed that the influence of hydrostatic pressure in the notched area causes the discrepancy between experimental response of the material on the tensile loading and its numerical simulation with use of the yield criterion without accounting for the first invariant of the stress tensor I_1. The comparison between experimental values of forces and numerical ones are given in Table 4.10. The differences vary from 2% to 5%. It is not a big difference in the levels of the forces - but it is noticeable. The largest difference between numerical calculation and experiment is noticed for a R2 shaped notch.

Basing on this observation and literature examples it may be assumed that this notched zone is the most susceptible to hypostatic influence. The Burzyński isotropic conditions which in its function accounts for the mean stress - consequently includes hydrostatic pressure. This allows to obtain curve force-displacement similar to the experimental one. Changing SD parameter κ allows to find the suitable level of forces. In all of the analysed notched specimens, the strength differential parameter κ which allows to repeat the experimental result is different then $\kappa = 1.0$ - Fig. 4.30. It turns out that it takes value around $\kappa = 1.1$.

4.6.3 Concluding remarks

To sum up, with use of the implemented in UMAT Burzyński yield condition there have been simulated tensile test of notched specimens made with steel E335. The comparison between numerical and experimental results reveals that the application of the plasticity theory with the paraboloid case of the Burzyński yield condition correlates better with experimental data than the results obtained with use of the classical plasticity theory - the Huber–Mises-Hencky yield condition. Consequently, it is concluded that plasticity model with the paraboloid yield condition makes it possible to describe adequately yielding of the material characterized by the strength differential effect.

In next Chapter there are presented results of strength tests discussed in Chapter 2. The results for OFHC Cu, steel E335, polycarbonate and biopolymers are discussed in details. Experimental results of different groups of materials quoted after different literature sources are also given. For theses results the presented in this Chapter criteria - for materials characterised by SD parameters and/or initial anisotropy are applied. The wide range of applicable possibilities allows to claim that proposed by Burzyński criteria assure a proper description of the onset of the plasticity.

Chapter 5

Experimental results and applications of the Burzyński criteria

In this Chapter there are presented results of tests which methodology is discussed in the Chapter 3. Tests have been performed for metallic materials of BCC and FCC structure and polymers described in Chapter 2. Due to presented results it is possible to define the yield strengths for different loading conditions, what allows to describe the onset of yielding state for exemplary materials. The Burzyński criteria accounting for pressure influence and initial anisotropy are applied. There are also quoted data found in the scientific literature of materials characterized by above effects. Proposed criteria are validated for material data and yield surfaces and yield curves are visualized. In this Chapter it is proved that proposed in the Thesis criteria give more accurate approximation of yielding state in comparison to other commonly used conditions.

5.1 Introduction

As it is shown in Section 4.4, there are many different types of criteria due to which it is possible to obtain the yield surface. However, in this study the attention is focused on energy-based criteria proposed by Burzyński. In this Chapter there are presented the examples of application of Burzyński criteria: for isotropic materials with SD effect, Eq. (4.33), and for initially anisotropic materials, Eq. (4.45). The criteria are validated for data found in the literature and also for experimental results obtained in the LaBPS. The yield surfaces are depicted in the space of principal stresses $(\sigma_1, \sigma_2, \sigma_3)$. The limit curves, depicted in the plane state of stress $\sigma_2 = 0$, are compared with limit curves obtained with use of the Huber-Mises-Hencky (HMH) criterion, Eq. (4.10).

The advantage of Burzyński approach is the small number of parameters necessary to obtain the description of yielding state. Namely, there are three material data - yield strength in compression σ_Y^C, tension σ_Y^T and in shear τ_Y - which must be extracted. Knowing these three values allows to plot limit figures, other yield points - like yield strength in biaxial compression - allow to verify chosen criterion. Occurrence of strength difference is expressed by the SD parameter κ calculated with use of relation (2.1).

In case of initially anisotropic materials the extended Burzyński criterion is used in which the description of initially anisotropic material is approximated by means of isotropic model with the strength correction factor, Eq. (4.45), then the value of R_B is indicated, Eq. (4.46). For isotropic materials $R_B = 1$. As it is discussed in Section 2.1.2 the initial anisotropy is induced in the material by manufacturing processes. Qualitatively, it may be expressed as difference between measured yield strength in shear and value of shear strength calculated with use of theoretical relation proposed by Huber (4.11) or Burzyński (4.30).

In this Chapter there are presented and discussed yield surfaces and curves for various materials. Data needed to plot a yield surface and its cross-sections in different planes are collected in a table which accompanies the pictures with visualization of the yield state. The example of table with data and description of used values is presented as Table 5.1.

In the Tables there are collected information about material mechanical properties.

- First row: name of a material, strain rate in which experimental results were obtained and value of the offset strain for which data yield points were defined.
- Second row: yield strength in compression σ_Y^C and value of SD parameter κ.
- Third row: yield strength in tension σ_Y^T and value of R_B parameter.
- Fourth row: yield strength in shear τ_Y and unit in which data are given (usually it is [MPa], when yield strengths are normalized - it means divided by yield strength in compression σ_Y^C - values are unitless.
- To compare surfaces obtained due to Burzyński criterion the Huber-Mises-Hencky (HMH) theory is used, Eq. (4.10), for which (with assumption that $\sigma_Y^C = \sigma_Y^T$) there is needed only one parameter - yield strength σ_Y. To show difference between experimental shear yield stress τ_Y, its theoretical value, τ_Y^H, is calculated with use of the relation (4.11). These data are collected in the fifth row.
- In sixth row as H the length from the peak of a paraboloid to the octahedral plane is signed and as R the radius of a cross-section which the paraboloid marks in the octahedral plane is indicated. H and R allow to notice how the paraboloid (if the yield surface is given by a paraboloid) looks in the space of the principal stresses.

Discussed examples are accompanied by such tables in which there are collected all information necessary to obtain approximation of a yield state due to Burzyński conditions.

Knowing above mentioned values of material characteristics, it is possible to present yield state of the material. In each picture the similar schema is used. In the upper left picture (a) there is presented the yield surface in the space of principal stresses $(\sigma_1, \sigma_2, \sigma_3)$. In the upper right picture (b) there is given its cross-section in the plane $\sigma_2 = 0$. In the bottom left picture (c) there is presented trace of the Burzyński surface (red line) in the meridional plane (σ_m, σ_e) compared with the trace of the HMH cylinder (blue dashed line). Next, in Fig. (d) the comparison between the cross-sections of Burzyński and HMH surfaces in the plane $\sigma_2 = 0$ is given. With red line the Burzyński limit curves are indicated, whereas with blue dashed line the HMH limit curves are plotted.

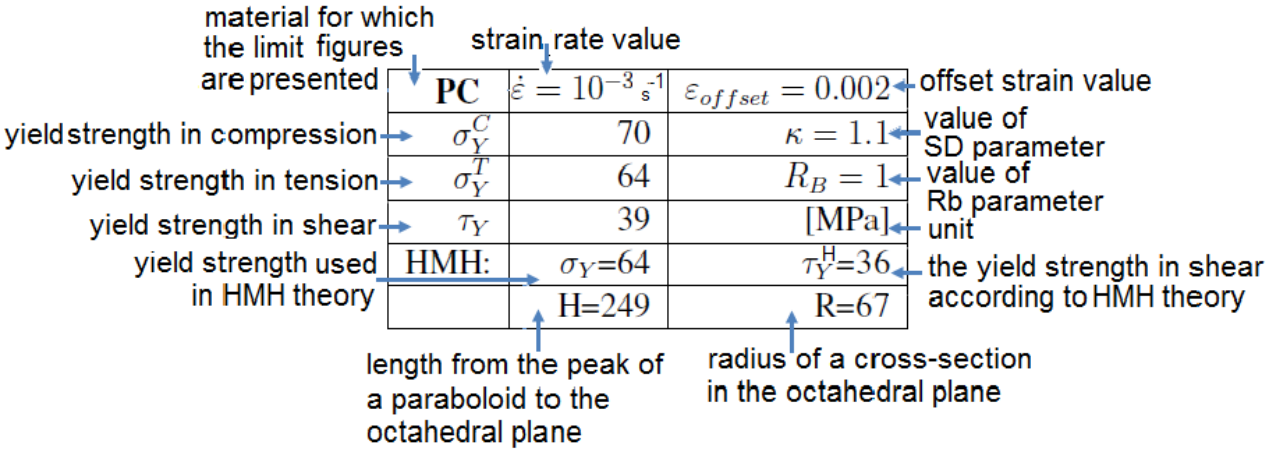

Table 5.1: Explanation to tables in which there are collected data used to plot the limit figures.

5.2 Application for various materials

In this Section there are given examples of application of Burzyński criteria for various groups of materials. There are shortly discussed yield states for grey cast iron, t metalic alloys, magnesium alloy, titanium alloy - Ti6Al4V, metallic glass. Chosen materials exhibit asymmetry of elastic range or initial anisotropy. Examples are based on the literature data.

5.2.1 Yield surface basing on the complex state test results

When metal is subjected to complex loading paths or has a complex deformation history the elastoplastic deformations modify the microstructure of the metal so that its mechanical state can no longer be considered isotropic, [Zattarin et al. 2004]. In that case the classical Huber-Mises or Tresca conceptions do not give a proper modelling. Such phenomenon cab be noticed in Figs. 5.3 and 5.1 because metallic alloys have undergone complex load paths due to which the initial yield surfaces have been determined.

A detailed description of the complex state of stress test was presented in Chapter 3.5. Due to the different loading conditions as indicated in Fig. 3.41 - the 17 yield points have been obtained. Points are defined for offset strain $\varepsilon_{off} = 0.0001$. Yield points in tension, compression and torsion, as well as results of different torsion-compression and torsion-tension loadings allow to obtain the trace of initial yield curve in the plane (σ, τ). Points are recalculated with use of relation (3.18) from the plane (σ, τ) to the plane of principal stress $\sigma_2 = 0$, Fig. 3.44.

In [Bishop and Hill 1951a; C. et al. 1987; Lipinski and Berveiller 1989; Zattarin et al. 2004] authors try to explain the obtained initial yield curves and subsequent yield surfaces on the basis of the micromechanical modelling. Because due to their considerations it seems to be impossible to reproduce initial yield surface without taking into account the evolution of the material microstructure, [Zattarin et al. 2004]. The micromechanical modelling seems to

be particularly well suited to describe the material evolution during deformation processes. In above mentioned works the proposed approach devoted to complex path loads proposes the separation of the influence of second-order internal stresses and the crystallographic texture on the evolution of yield surfaces (anisotropic hardening).

In beneath presented examples the evolution of yield state is not considered. The more complex the strain history is, the more complex the evolution of yield surface and the more difficult the analytical description of this evolution becomes. Here, only the visualization of initial yield surface is presented with use of Burzyński criterion for initially anisotropic materials (4.45).

In case of so small offset strain definition, after calculation the value of R_B coefficient, it turn out that it is close to 0. Then, the shape of a limit curve in the plane $\sigma_2 = 0$ is close to a circle.

In Fig. 5.1 there are presented initial yield curves for mild chrome molybdenum steel with addition of manganese and nickel - **A336 GR5** - Fig. 5.1.a and for **AlSi7MgCu0.5** - Fig. 5.1.b.

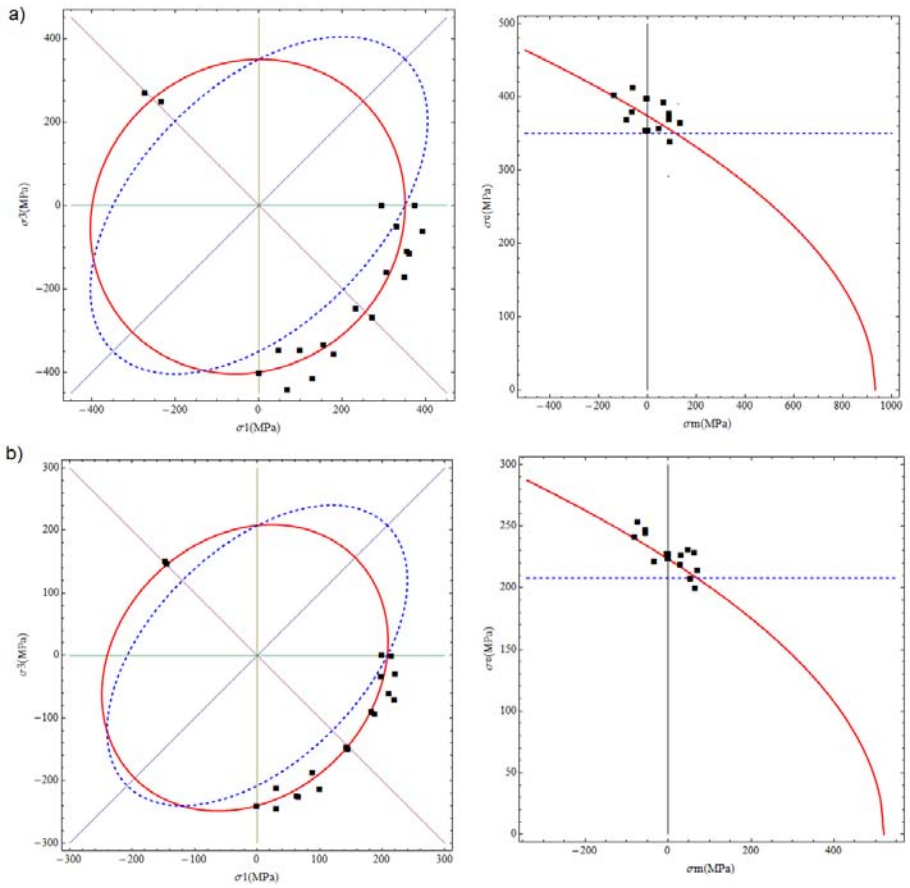

Figure 5.1: The limit curves describing the experimental data for: a) alloy AlSi7MgCu0.5, b) A336 GR5. Blue dashed line - the HMH criterion, Eq. 4.10, red line - the Burzyński criterion, Eq. 4.38.

Alloy AlSi8Cu3 - [Dietrich et al. 2010]

The yield points have been determined from the report [Dietrich et al. 2010] - Fig. 5.2. Basing on above diagrams it is possible to plot suitable yield surface and yield curves:

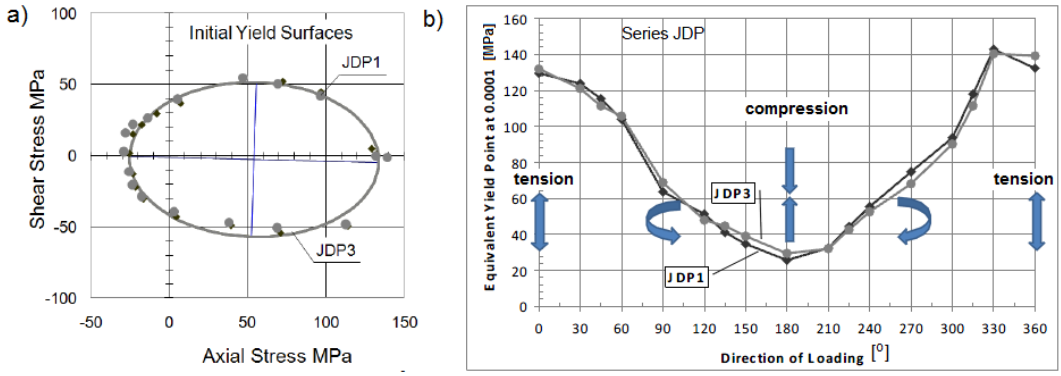

Figure 5.2: The points in the complex stress state test for an alloy AlSi8Cu3: a) in the plane (σ, τ), b) in the schemat of direction loading, [Dietrich et al. 2010].

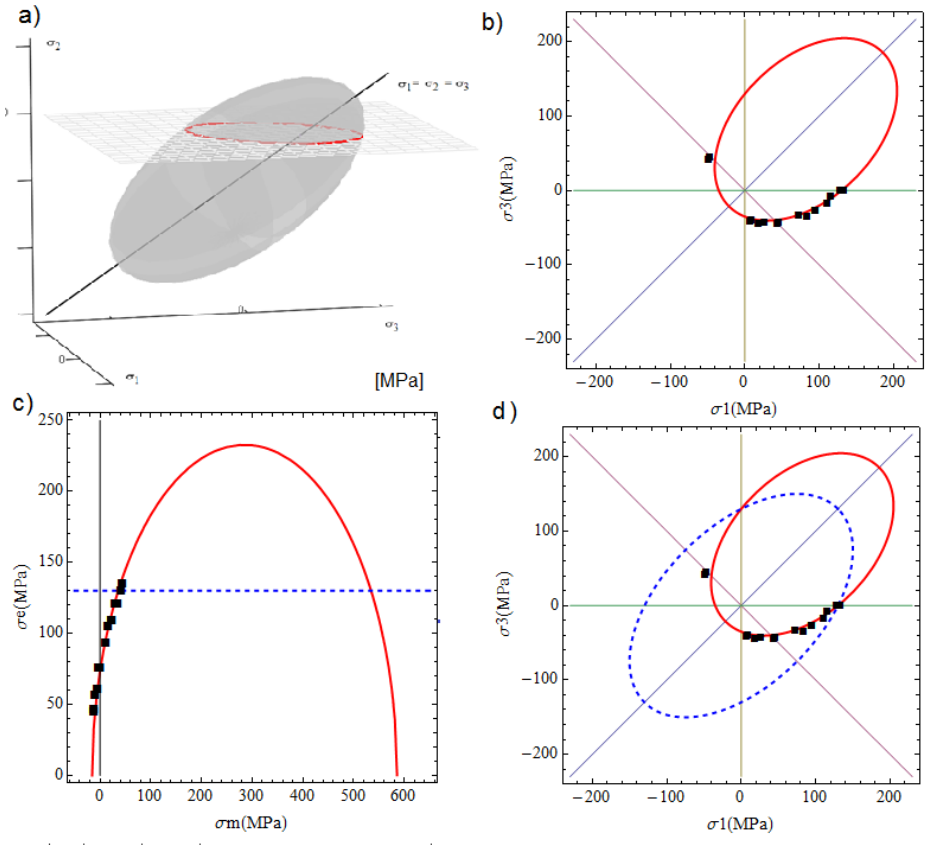

Figure 5.3: AlSi8Cu3 alloy. Presentation of the Burzyński condition in a) the space of principal stresses, b) the plane $\sigma_2 = 0$. Comparison with the HMH criterion presented in c) the meridional plane, d) the plane $\sigma_2 = 0$.

In Fig. 5.1 there are presented yield initial curves for two kind of metallic alloys Alloys AlSi7MgCu0.5 and A336 GR5. Beneath, in the tables there are colleceted data used to obtain curves:
- for mild chrome molybdenum steel with addition of manganese and nickel - **A336 GR5** - Table 5.2.a, and for **AlSi7MgCu0.5** - Table 5.2.b.

a)	quasi-static	$\varepsilon_{offset} = 0.0001$
σ_Y^C	400	$\kappa = 1.17$
σ_Y^T	340	$R_B = 0.09$
τ_Y	260	[-]
HMH:	σ^Y= 340	τ_Y^H=212
	H=1308	R=301

b)	quasi-static	$\varepsilon_{offset} = 0.0001$
σ_Y^C	240	$\kappa = 1.15$
σ_Y^T	208	$R_B = 0.37$
τ_Y	145	[-]
HMH:	σ^Y= 208	τ_Y^H=128
	H=900	R=182

Table 5.2: a) alloy AlSi7MgCu0.5, b) A336 GR5 - material data, [Dietrich et al. 2010].

5.2.2 Grey cast-iron

Behaviour of the grey cast-iron has been studied by the many authors due to its complicated microstructure, mechanical properties and importance in the industry, e.g.: [Grassi and Cornet 1949; Coffin 1950; Hjelm 1994; Altenbach et al. 2001; Alvarez et al. 2004]. As a material it is used for housings where tensile strength is non-critical, such as internal combustion engine cylinder blocks, pump housings, valve bodies, electrical boxes, and decorative castings.

It is a type of cast iron that has a microstructure of distributed graphite lamellae in a pearlite matrix. The graphite has the shape of a three dimensional flake. In two dimensions, as a polished surface will appear under a microscope, the graphite flakes appear as fine lines. The graphite has no appreciable strength, so it can be treated as voids. The tips of the flakes act as preexisting notches, therefore, it is brittle. For materials which contain voids, pores etc. different stress-strain curves can be obtained in tension and compression test. In addition, such materials often show inelastic volumetric deformations. Grey cast-iron is a typical example of this kind of material. In tension, grey cast iron exhibits brittle behaviour, in compression, the macroscopic yield response of grey cast iron is dominated by the steel matrix with a yield limit three or more times higher than that in tension. Strain hardening under compression is much stronger than that under tension. Consequently, grey cast-iron is a highly asymmetric material in case of elastic ranges.

The examples of application paraboloidal Burzyński criterion Eq. (4.33) for data found in [Grassi and Cornet 1949; Coffin 1950] concerning grey cast-iron are presented in Fig. 5.4.

Grey cast-iron - [Grassi and Cornet 1949; Coffin 1950; Theocaris 1995]

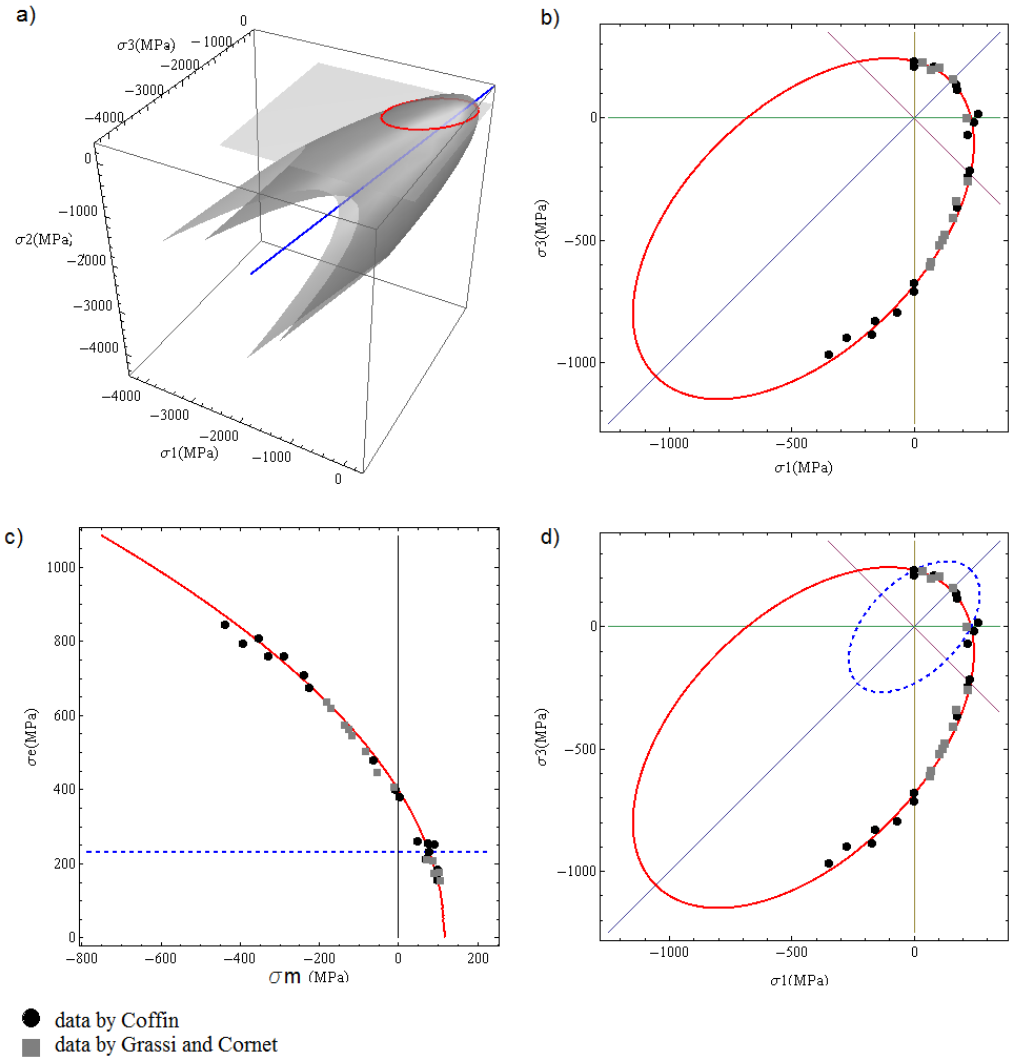

Figure 5.4: Grey cast-iron, [Grassi and Cornet 1949; Coffin 1950]. Presentation of the paraboloidal Burzyński condition in a) the space of principal stresses, b) the plane $\sigma_2 = 0$. Comparison with the HMH criterion presented in c) the meridional plane, d) the plane $\sigma_2 = 0$.

Grey cast-iron	quasi-static	$\varepsilon_{offset} = 0.002$
σ_Y^C	685	$\kappa = 2.95$
σ_Y^T	232	$R_B = 1$
τ_Y	230	[MPa]
HMH:	σ^Y = 232	τ_Y^H=133
	H=202	R=325

Table 5.3: Grey cast-iron - material data, [Grassi and Cornet 1949; Coffin 1950].

5.2.3 Titanium alloy - Ti6Al4V

The experimental data from strength test of titanium alloy Ti6Al4V were presented and analysed in the doctoral Thesis of [Peirs] and other works of Peirs, Verleysen and coworkers [Peirs et al. 2010; 2011a; 2013]. Titanium alloy has been extensively studied in the strength test of quasi-static and dynamic strain rate, results are presented and discussed in above mentioned papers.

The discussed Ti alloy offers an excellent combination of high strength, light weight, formability and corrosion resistance. Some of the many applications where this alloy is used for include aircraft turbine engine components, aircraft structural components, aerospace fasteners, high-performance automotive parts, marine applications, medical devices, parts for chemical installations, sports equipment, [Peirs].

Ti6Al4V is considered as a metals with low strain hardening, which causes unstable plastic flow and strain localisation in experiments. The material is characterized by high values of the yield limits and respectively low strain hardening, relatively high test forces are required to deform the material. The material is sensitive to strain rate.

Tests listed in the below table allowed to obtained results in different loading conditions for sheet material and bulk material.

	Sheet material	Bulk material
Tests in quasi-static and dynamic ranges	- Tension in 2 directions - Plain strain - Shear	- Tension in 2 directions - Compression - Torsion - Torsion-compression

From results presented in works of Peirs there have been extracted yield points for different tests in quasi-static strain rate and dynamic strain rate. Data are collected in Tables 5.4 and 5.5. The experimental investigation was throughout and provided the detailed description of material behaviour under different loading conditions. Consequently, each yield curve is based on at least 4 points differently located in the plane of stresses $\sigma_2 = 0$. Yield curves obtained for collected data are prepared basing on the Burzyński isotropic condition (red line) and to compare - the Huber-Mises-Hecky criterion. Resulted yield curves in the plane $\sigma_2 = 0$ are presented in Figs. 5.8 5.8, 5.5, 5.8. In fact, for obtained results the HMH criterion seems to be a sufficient and suitable approximation of yield state. Both for sheet and bulk materials in dynamic and quasi-static ranges of strain rate the Burzyński criterion offers similar curves as the HMH conditions. The lack of data in the second and third quarter of the plane results in similarity between both conditions. In this case, the result of complex or biaxial test would allow to unequivocal approximation of the yield state for Ti alloy.

Ti6Al4V	Sheet	Eq. (4.45)	Ti6Al4V	Sheet	Eq. (4.45)
	$\dot{\varepsilon} = 0.005\text{s}^{-1}$	$\varepsilon_{offset} = 0.002$		$\dot{\varepsilon} = 755\text{s}^{-1}$	$\varepsilon_{offset} = 0.002$
σ_Y^C	980	$\kappa = 1$	σ_Y^C	1190	$\kappa = 1$
σ_Y^T	980	$R_B = 0.76$	σ_Y^T	1190	$R_B = 1.06$
τ_Y	590	[MPa]	τ_Y	680	[MPa]
HMH:	σ^Y= 980	τ_Y^H=565	HMH:	σ^Y= 1190	τ_Y^H=687

Table 5.4: Ti6Al4V - material data for sheet material, [Peirs].

Quasi-static and dynamic strain rate, data for sheet material:

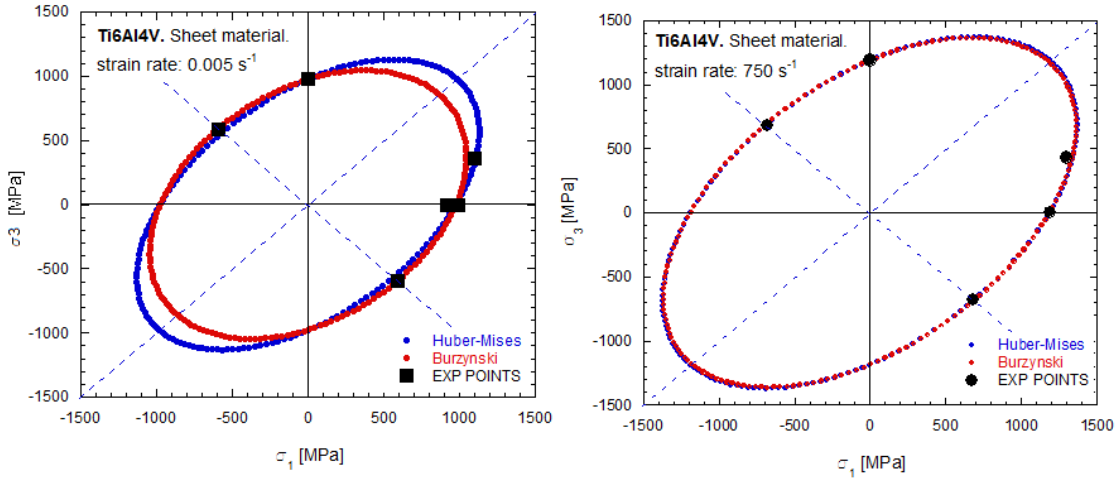

Figure 5.5: Ti6Al4V, yield curve for sheet material, quasi static strain rate.

Comparison between the HMH curves and the Burzyński curves for dynamic and quasi-static strain rate, data for the sheet material:

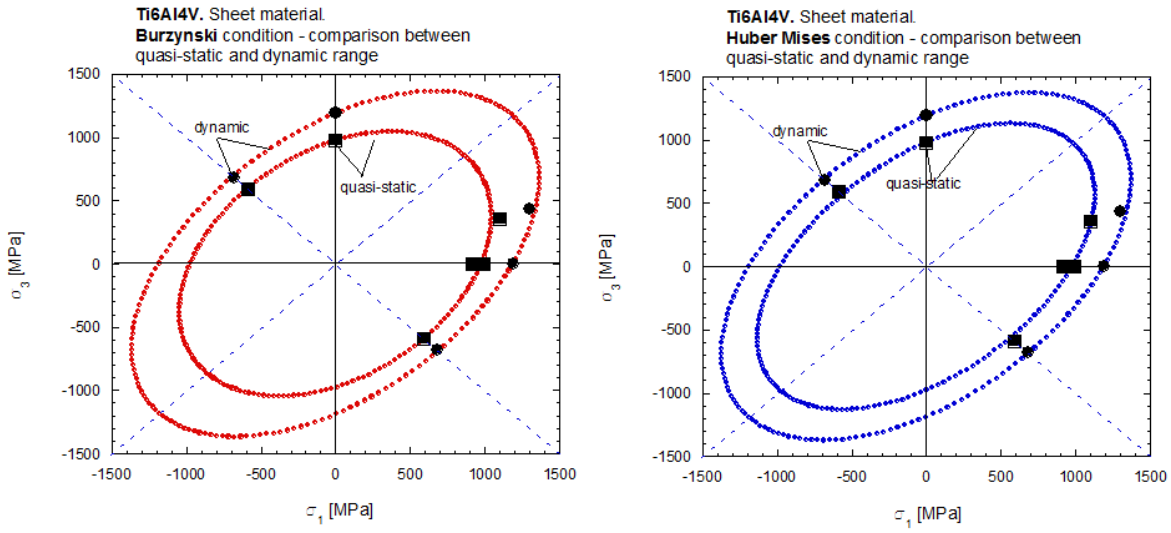

Figure 5.6: Ti6Al4V, sheet material. Comparison between quasi-static and dynamic range.

Ti6Al4V	Bulk	Eq. (4.45)	Ti6Al4V	Bulk	Eq. (4.45)
	$\dot{\varepsilon} = 0.005\text{s}^{-1}$	$\varepsilon_{offset} = 0.002$		$\dot{\varepsilon} = 1050\text{s}^{-1}$	$\varepsilon_{offset} = 0.002$
σ_Y^C	920	$\kappa = 1.23$	σ_Y^C	1070	$\kappa = 1$
σ_Y^T	1140	$R_B = 1.06$	σ_Y^T	1070	$R_B = 0.4$
τ_Y	540	[MPa]	τ_Y	690	[MPa]
HMH:	σ^Y= 920	τ_Y^H=590	HMH:	σ^Y= 980	τ_Y^H=617

Table 5.5: Ti6Al4V - material data for bulk material, [Peirs].

Quasi-static and dynamic strain rate, data for bulk material:

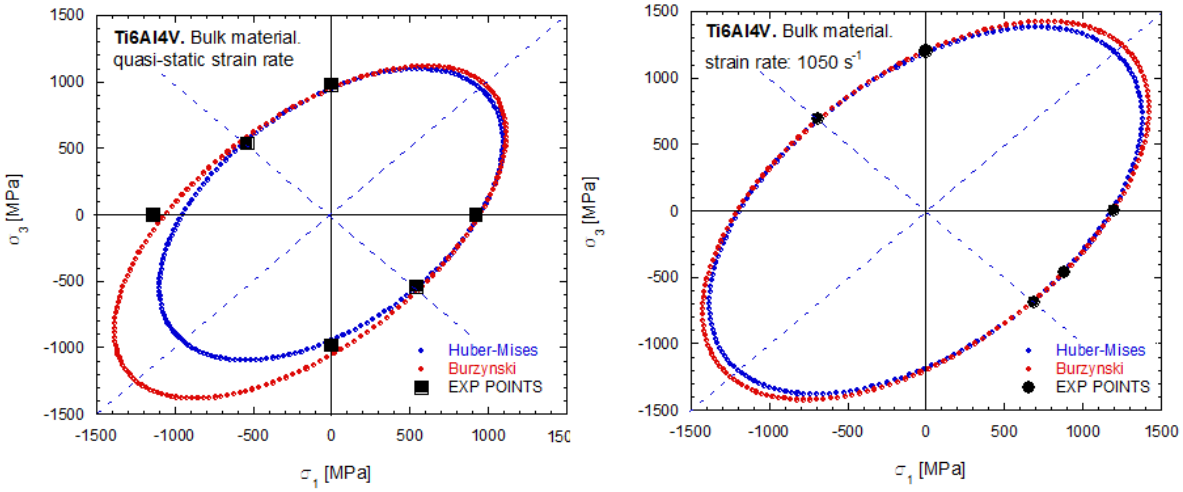

Figure 5.7: Ti6Al4V, bulk material. Limit curves.

Comparison between the HMH curves and the Burzyński curves for dynamic and quasi-static strain rate, data for the bulk material:

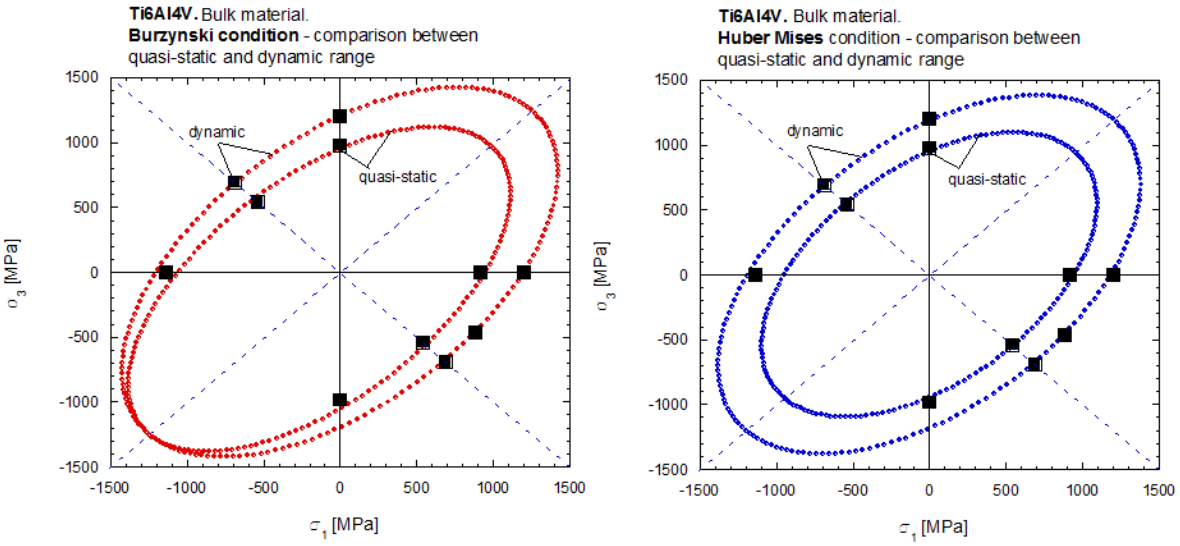

Figure 5.8: Ti6Al4V, bulk material. Comparison between quasi-static and dynamic range.

5.2.4 Mg alloy

If the strength differential parameter is smaller than 1 ($\kappa < 1$), it means that the yield limit value in tension is greater than that one in compression. This phenomenon occurs when in the process of compression the material changes its state to plastic due to the twinning mechanism, [Ball and Prangnell 1994]. Such characteristic could be also obtained for pressure-insensitive metals and basal or near-basal textures common for cold-rolled hexagonal close packed (HCP) materials, [Cazacu and Barlat 2004].

Generally, the yield strength for tension is asymmetric to that for compression in the case that both slip and twinning take place or only twinning happens. Due to the strong basal pole alignment in the thickness direction, twinning is easily activated by compression perpendicular to this direction, but is not active in tension. Because of the directionality of twinning, at low strain levels a very pronounced strength differential effect is observed: generally, the compressive strengths are much lower than the tensile strengths, [Graf and Hosford 1993]. In magnesium, for example, twinning occurs depending on grain size and it occurs more readily in compression than in tension. At high strain levels, when twinning has practically ceased, the SD effect is markedly diminished. On the other hand, the strong crystallographic texture, exhibited by such materials, leads to a pronounced anisotropy: higher strength in the transverse direction than in the rolling direction. Hence, the yield loci of rolled hexagonal close-packed (HCP) metals are highly asymmetrical in shape. The asymmetry of elastic ranges $\kappa < 1$ is ascribed to increased twinning in compression.

An example of such a material is magnesium and its alloys, e.g.: [Cheng-wen et al. 2007; Wu et al. 2008]. Magnesium has a high specific strength with a density that is only 2/3 that of aluminum and 1/4 that of iron. It also has high thermal conductivity, high dimensional stability, good electromagnetic shielding characteristics, high damping characteristics, good machinability and is easily recycled.

In the LaBPS there has been investigated AZ31 Mg alloy - (Mg-3%Al-1%Zn, mass fraction). It is known that the addition of Zn reduces the critical resolved shear stress for prismatic slip with a consequent decrease in the tension/compression asymmetry, [Mann et al. 2004]. For Mg alloy the tension and compression test have been performed, [Rusinek 2011]. Tensile specimens with a gauge dimension of 5mm (diameter) and 14mm were machined from the plate, the tensile direction of the samples is parallel to the rolling direction of the plate. Compressive specimens with a dimension of 8mm diameter and 12mm height were machined from the same plate. The axis direction of the samples is along rolling direction. The test have been performed at strain rate equals to $0.001s^{-1}$.

The yield surface is built due to Eq.(4.26) but according to relation (4.23) the calculated plastic parameter χ is less than $\frac{1}{2}$, the criterion predicts elliptical yield loci.

The material data of the magnesium alloy AZ31 used to plot the surface coincide with the data found in [Yoshikawa et al. 2008] are collected in Table 5.6. Due to them it is possible to visualize the yield state for the Mg alloy.

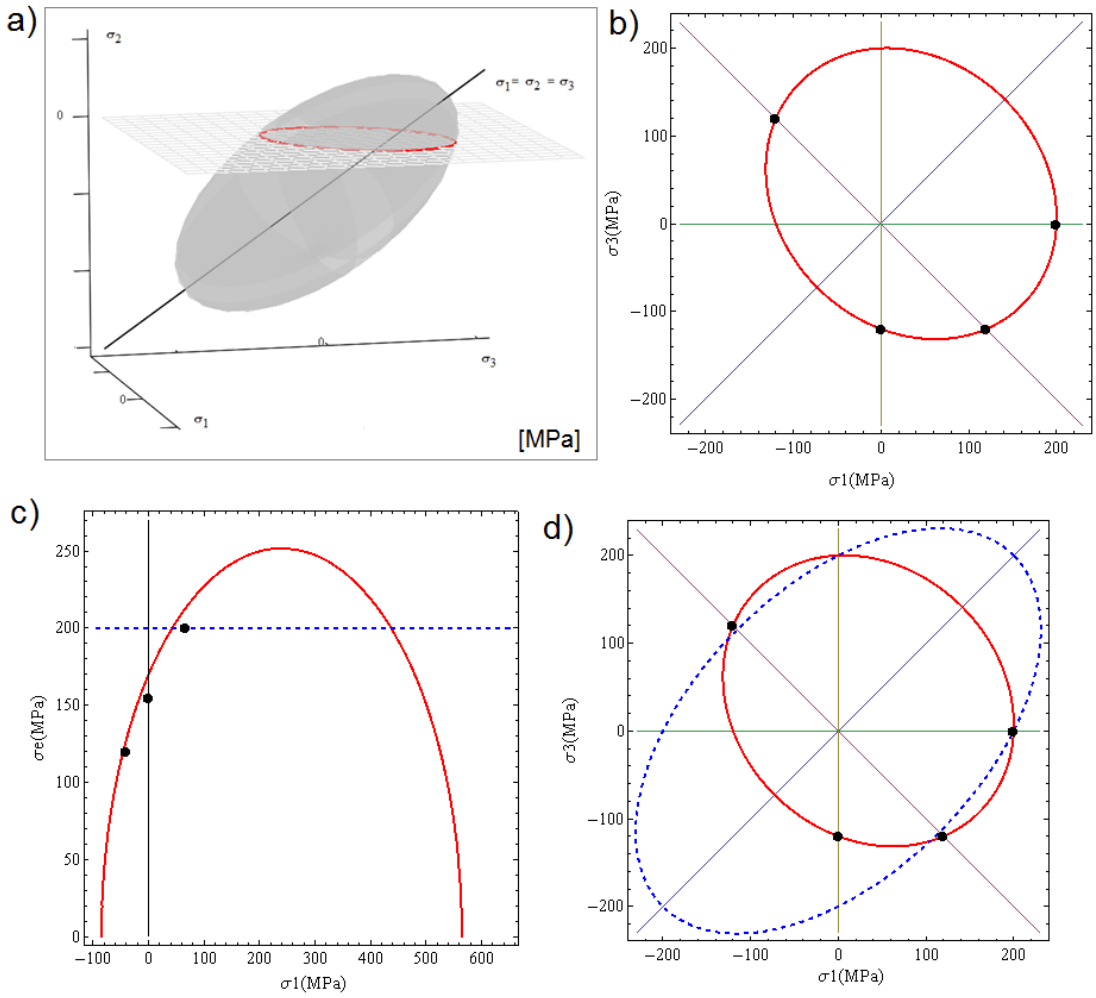

Figure 5.9: Magnesium alloy AZ31, [Yoshikawa et al. 2008]. Presentation of the Burzyński condition in a) the space of principal stresses, b) the plane $\sigma_2 = 0$. Comparison with the HMH criterion presented in c) the meridional plane, d) the plane $\sigma_2 = 0$.

AZ31	$\dot{\varepsilon} = 10^{-3}$c	$\varepsilon_{offset} = 0.002$
σ_Y^C	120	$\kappa = 0.6$
σ_Y^T	200	$\chi = 0.4$
τ_Y	120	[MPa]
HMH:	$\sigma^Y = 200$	τ_Y^H=115

Table 5.6: Magnesium alloy AZ31 - material data, [Yoshikawa et al. 2008].

5.2.5 Metallic glasses

Authors of [Lund and Schuh 2003] performed molecular simulations of multiaxial deformation in a model metallic glass using a energy minimization technique. The finding pronounced asymmetry between the magnitudes of the yield stresses in tension and compression, with the uniaxial compressive strength approximately 24% higher. At ambient temperature, metallic glasses deform by a process of shear banding, where plastic strain is highly localized into strips of nanometer-thickness and (often) macroscopic length. The operation of shear bands on the nanometer-scale gives rise to unique mechanical properties at macroscopic scales. For example, the very low values of tensile elongation recorded for amorphous metals are attributed to rapid failure along a single shear band. In constrained modes of loading like compression, plastic yielding is observed, but it does not occur smoothly, the strain is carried by a single shear band. These properties have been investigated in a variety of glassy alloys with very different compositions, and appear general to this class of materials. One important consequence of shear localization in amorphous metals is that the macroscopic yield criterion may exhibit a dependence not only upon the maximum shear stress, but also upon the hydrostatic pressure or the normal stress acting on the shear plane.

In the tables beneath there have been collected data read from the Figures found in [Lund and Schuh 2003]. The yield curves in the paper [Lund and Schuh 2003] are plotted due to Coulomb-Mohr criterion. In Figs. 5.10 and 5.11 there are collected two data sets, one obtained by authors of [Lund and Schuh 2003] using the standard 0.2% offset and the other obtained using a larger 0.5% offset. Solid points and open points represent the data from the 2609 and 2781 atom systems, respectively. The two resulting yield curves obtained due to the Burzyński isotropic criterion 4.34 are quite similar. The qualitative difference between curves is that the greater relative scatter in the data obtained using the 0.2% offset, which results from a greater sensitivity to noise near the yield point in the stress–strain curve. The primary quantitative difference between these figures is the consistently lower magnitudes of the stress components obtained using the 0.2% offset. As indicated by the uniaxial tension and compression tests the yield curves are distinctly asymmetric, with the elastic envelope defined by the data in quadrant III being considerably larger than that in quadrant I. This asymmetry is in direct proportion to the strength differential observed in uniaxial loading.

Metallic glass	quasi-static	$\varepsilon_{offset} = 0.002$		quasi-static	$\varepsilon_{offset} = 0.005$
σ_Y^C	0.031	$\kappa = 1.16$	σ_Y^C	0.039	κ =1.23
σ_Y^T	0.0265	$R_B = 1$	σ_Y^T	0.0315	R_B =1
τ_Y	0.016	[-]	τ_Y	0.02	[-]
HMH:	σ^Y= 0.0265	τ_Y^H=0.016	HMH:	σ^Y= 0.0315	τ_Y^H=0.02
	H=0.1	R=0.03		H=0.094	R=0.028

Table 5.7: Metallic glasses - material data, [Lund and Schuh 2003].

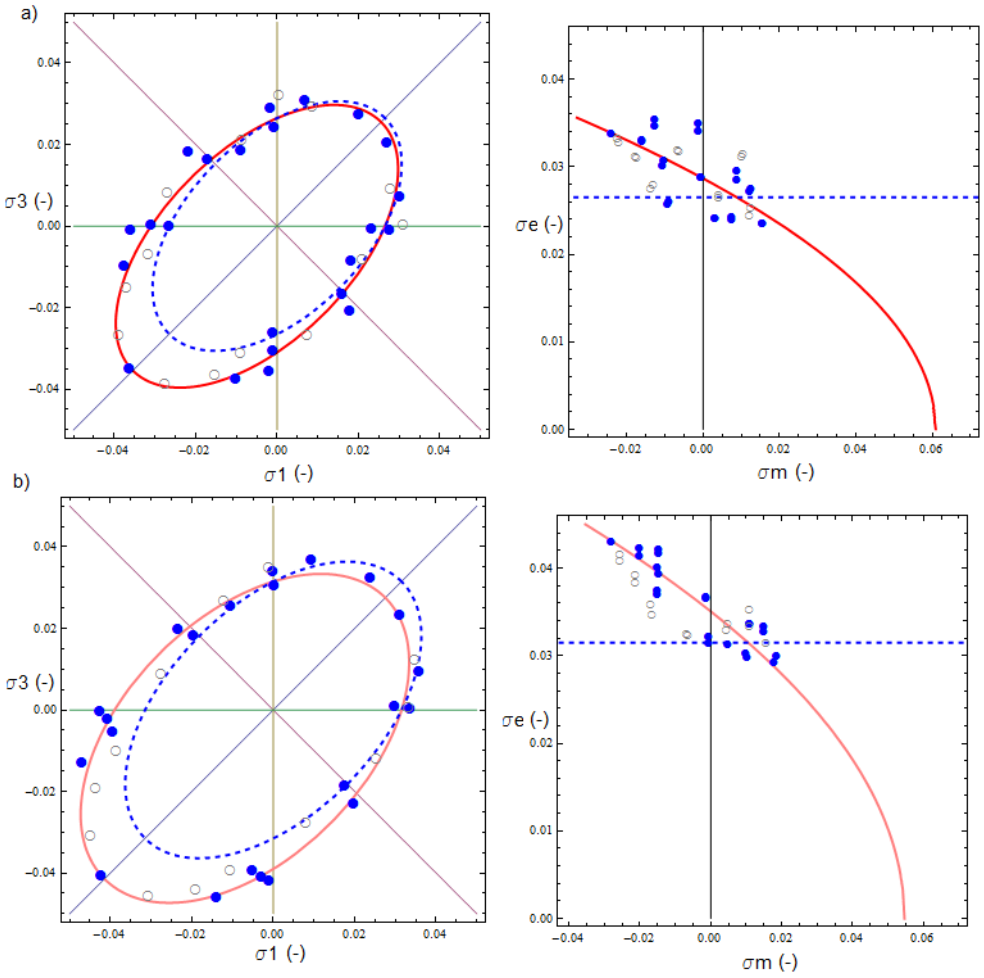

Figure 5.10: Metallic glass - experimental data collected by [Lund and Schuh 2003]. Presentation of the paraboloidal Burzyński condition in comparison with the HMH criterion presented in the plane $\sigma_2 = 0$ and in the meridional plane for data collected for offset strain equals a) 0.002 and b) 0.005.

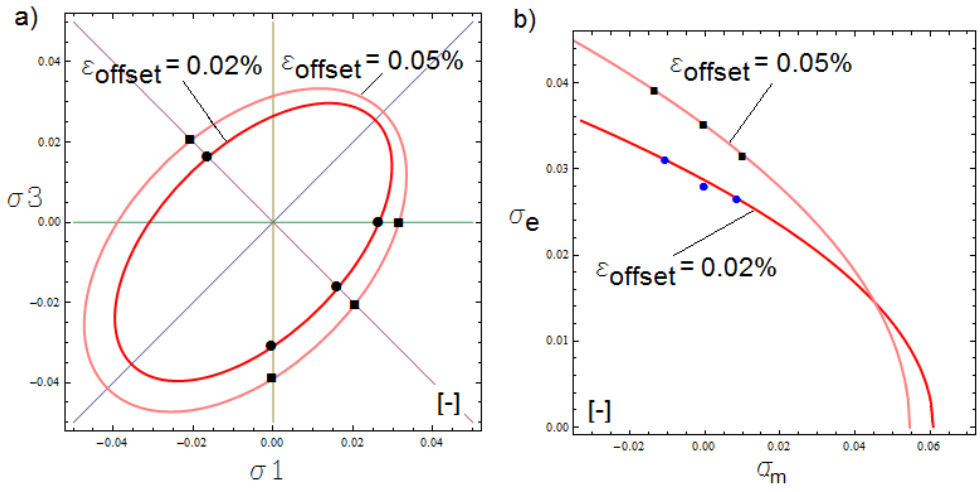

Figure 5.11: Comparison between yield curves for data of metallic glass collected for the offset strain equals to 0.002 and 0.005 presented in a) the plane $\sigma_2 = 0$ and b) in the meridional plane.

5.3 Application for FCC material - OFHC Copper

In this Thesis, the OFHC Cu as received is studied. The characteristic of OFHC Cu basing on the study of literature is presented in Chapter 2. The microstructure analysis is also discussed in Chapter 2. In this Chapter are given results of mechanical tests. The constitutive relations - the Johnson-Cook model, the modified Rusinek-Klepaczko model and the Molinari-Ravichandran model are applied to apraximate flow of the material and strain rate sensitivity. Finally, the limit surface describing the yield state are presented and discussed.

5.3.1 Results of strength tests

In this part there are presented results of quasi-static tests. For the OFHC copper there have been performed the following tests at room temperature under isothermal conditions:

- quasi-static tensile test for strain rate equalled to 0.001 s^{-1},
- quasi-static compressive test for strain rates equalled to 0.001, 0.01, 0.1 s^{-1} performed with use of cylindrical and cubic specimens,
- double shear test for strain rates equalled to 0.001, 0.01, 0.1 s^{-1},
- complex state of stress test,

and in dynamic range of strain rate:

- compression test with use of the Split-Hopkinson Pressure Bar.

Detailed description of the experimental techniques and data analysis is presented in Chapter 3. In this section the final results are presented in the form of true stress-true strain curves or - as in case of the complex stress state test - as a set of points.

Result of the complex stress state test

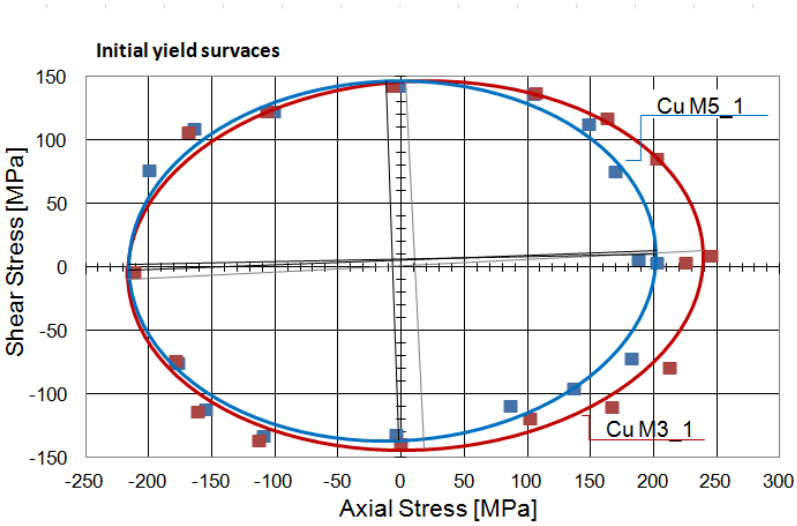

Figure 5.12: Results of the complex state of stress test.

The test of complex state of stress is discussed in Section 3.5. The results of this test are plotted in the plane of physical stresses: axial stress - shear stress (σ_{ax}, τ), Fig. 5.12.

The yield strengths have been identified for offset strain equals to 0.0001. The results of OFHC Cu are also presented in Fig. 3.42 where schematically directions of loading are indicated with use of arrows. The set of yield points in coordinates of the plane (σ, τ) and the same yield points in coordinates of the plane (σ_1, σ_3) is presented in Fig. 3.44.

Test in quasi-static strain range

With use of the cubic samples, the quasi-static compression test has been performed at strain rate equals to $0.001s^{-1}$. Loading has been applied along different orientation of the cube. The direction of rod extrusion, from which the specimens have been machined, has been indicated on each specimen. Therefore, the compressive loading has been applied in direction being in accordance with extrusion of the rod (*the longitudinal direction*) and in two perpendicular to it: (*the perpendicular direction*), (*the transversal direction*). Results of the test are presented in Fig. 5.13.a. It could be noticed that the difference in values of yield points defined for offset strain 0.002 is close to 5%.

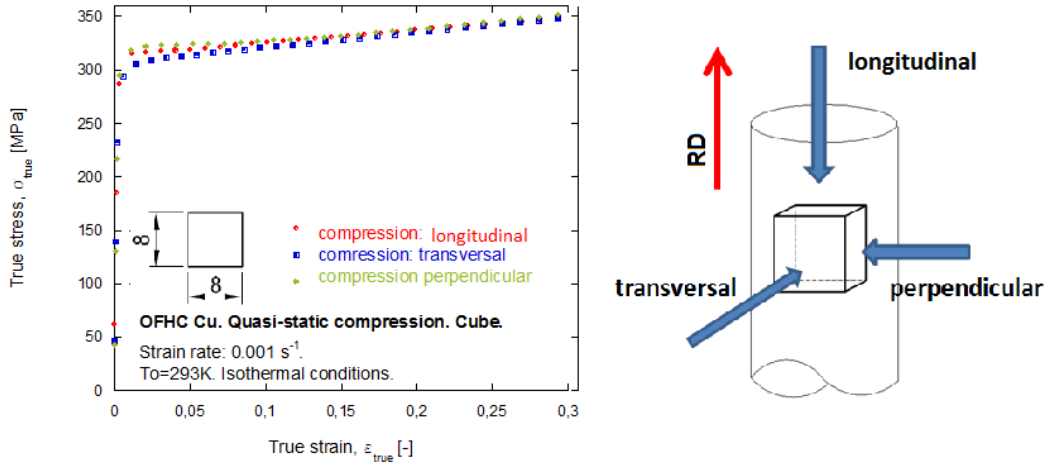

Figure 5.13: OFHC Cooper. Results of quasi-static compression test with use of cubic specimens loaded along different directions.

compression cube						
strain rate:	orientation of loading:		[MPa]	relation between yield limits		
0,001 [1/s]	longitual	transversal	perpendicular	long/trans	long/perp	trans/perp
0,0001	234	256,5	270	91%	87%	95%
0,001	266	279,5	295	95%	90%	95%
0,002	283	283,5	305	100%	93%	93%
0,003	292	292	309	100%	94%	94%
0,005	298,5	300	314	100%	95%	96%
0,01	303	302,5	322	100%	94%	94%
0,012	304	302,5	322	100%	94%	94%

Table 5.8: OFHC Cooper. Collected yield points obtained in compression test in strain rate $0.001s^{-1}$ for offset strain equals to 0.002.

The tension test has been performed with use of round 'dog-shaped' specimens, Fig. 3.4. The compression test in quasi-static and dynamic range has been performed with use of cylin-

drical specimen with diameter 10mm and height 12mm, Fig. 3.3.a. The geometry of double shear specimen is presented in Fig. 3.14. The samples have been cut at the same time, from the rod of the diameter 12mm. Results of quasi-static tension test are presented in Fig. 5.14.a and for quasi-static compression test performed in different strain rates, Fig. 5.14.b. Results of double shear tests are presented in Fig. 5.15.a. The method of correcting results of the biaxial compression test are presented in Section 3.4, Fig. 5.15.b.

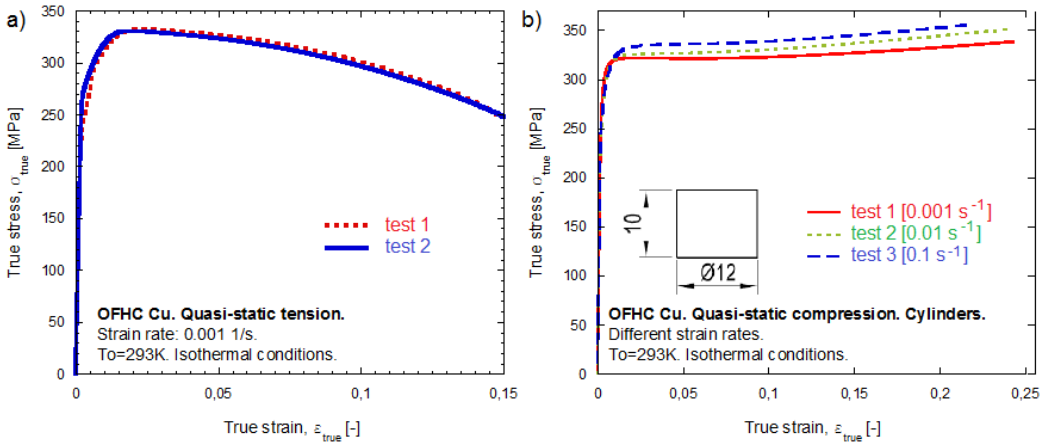

Figure 5.14: OFHC Cu. (a) Results of quasi-static tension test. (b) Results of quasi-static compression tests with use of cylindrical specimen.

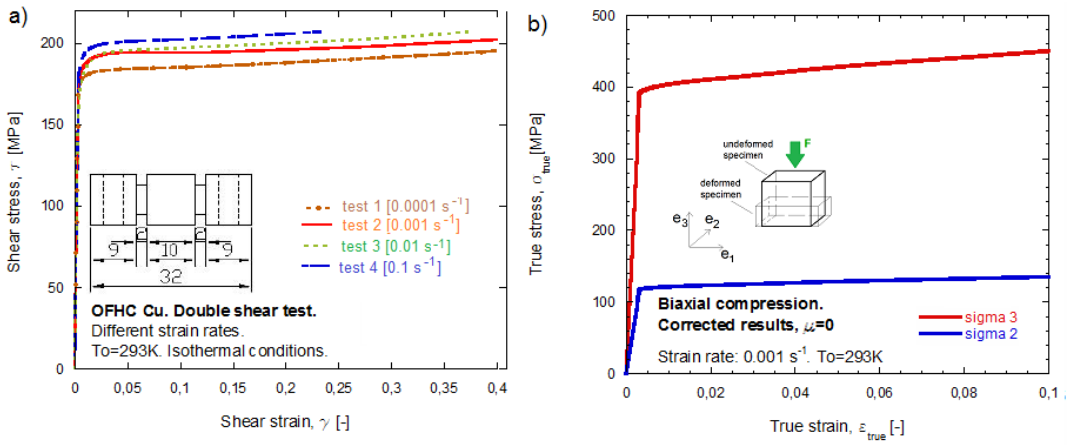

Figure 5.15: OFHC Cu. (a) Results of double-shear test. (b) Results biaxial compression test in strain rate equals to 0,001s^{-1}.

Compression - the SHPB test

The dynamic properties of the OFHC Cu have been examined with use if Split-Hopkinson Pressure Bar. Beneath there are presented results of dynamic tests - Fig. 5.16.a and their comparison with results of quasi-static compression test, Fig. 5.16.b). It can be noticed that for different strain rates the characteristics of material's deformation are similar.

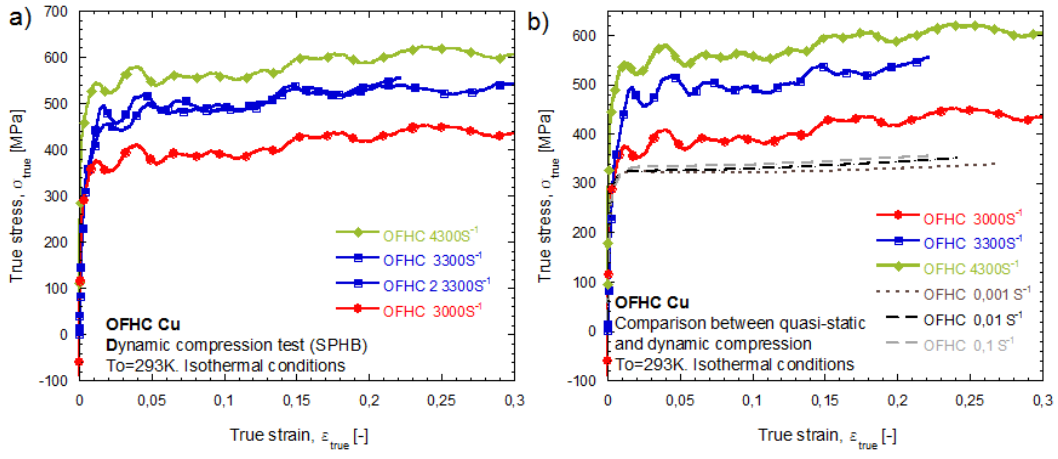

Figure 5.16: (a) Dynamic compression test results, (b) Comparison between results of quasi-static test and dynamic test.

For FCC structure type material, the influence of strain rate on yield limits can be represented by e.g. the Modified Rusinek-Klepaczko model, Eq. (6.3), or the Molinari-Ravichandran model, Eq.(6.18). For OFHC Cu the parameters of models Eq. (6.3) and Eq. (6.18) are presented in Tables 5.9 and 5.10.

Y [MPa]	T_o [K]	T_m [K]	$\dot{\varepsilon}_{max}$ [s^{-1}]	B_0 [MPa]	ν [-]	n_0 [-]	D_2 [-]	$\dot{\varepsilon}_{min}$ [s^{-1}]	D1 [-]	P [-]
40	300	1340	10^7	560.28	0,30447	0.492	0,0553	10^-5	0,0011932	0,0131

Table 5.9: OFHC Cu. Parameter for the Modified Rusinek-Klepaczko model, [Rodríguez-Martínez 2010].

The following set of constants describes the MR relation describing the material behaviour depending on strain, strain rate and temperature, constants for OFHC Cu found in [Molinari and Ravichandran 2005].

ρ (kg/m^3)	c (J/kg/K)	β	$\hat{\sigma}$ (MPa)	$\dot{\varepsilon}_0$ (s^{-1})	A (K)	δ_0 (μm)	δ_{r0}	a_r	ξ_r	ν_r	$\dot{\varepsilon}_{r0}$ (s^{-1})	δ_{s0} (μm)	a_s	ξ_s	ν_s	$\dot{\varepsilon}_{s0}$ (s^{-1})
8940	386	0.9	55	10^7	40×10^3	0.5	4.3	50	0.8	0	10^7	0.06	0.377	0.24	0.5	10^7

Table 5.10: OFHC Copper. Parameters for the Molinari-Ravichandran model, [Molinari and Ravichandran 2005].

The model MRK defines properly the changes in the rate sensitivity that the material exhibits due to variations in the plastic deformation at room temperature - Fig. 5.17.

The MRK constitutive relation is able to describe the material behaviour within the range of strain rates thanks to the dependence of the volume thermally activated (VTA) on plastic strain included into the model formulation, [Rodríguez-Martínez et al. 2009]. The MRK model is applied to describe the behaviour of as received OFHC copper. The OFHC Cu shows high dependence of plastic strain on the VTA, strain hardening strongly varies with strain rate and temperature, what is characteristic for FCC metals, [Nemat-Nasser et al. 1998a].

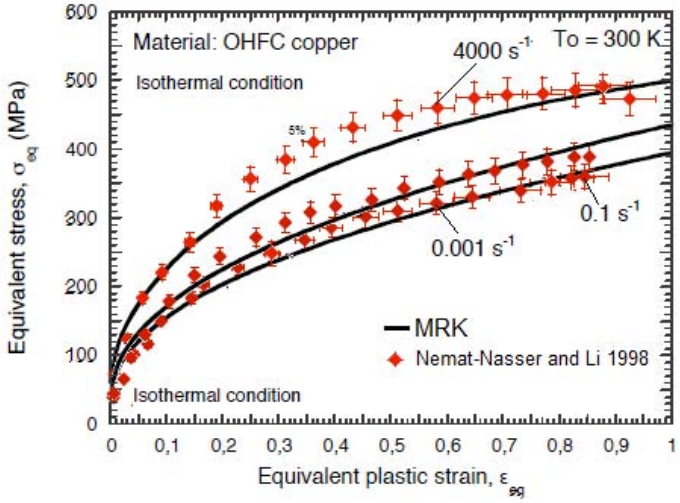

Figure 5.17: OFHC Copper. Description of the flow stress evolution as a function of the plastic strain by the MRK model and comparison with experiments at room temperature, [Rodríguez-Martínez 2010].

Strain rate sensitivity for OFHC Cu in Fig. 5.18. The MRK and MR models has been calibrated using the experimental data obtained in LaBPS. In addition to own experimental data, in the graph there are also presented literature data based on results of: [Follansbee 1986; Follansbee and Kocks 1988; Nemat-Nasser and Li 1998]. In case of OFHC Cu it can be claimed that material is strain rate sensitive.

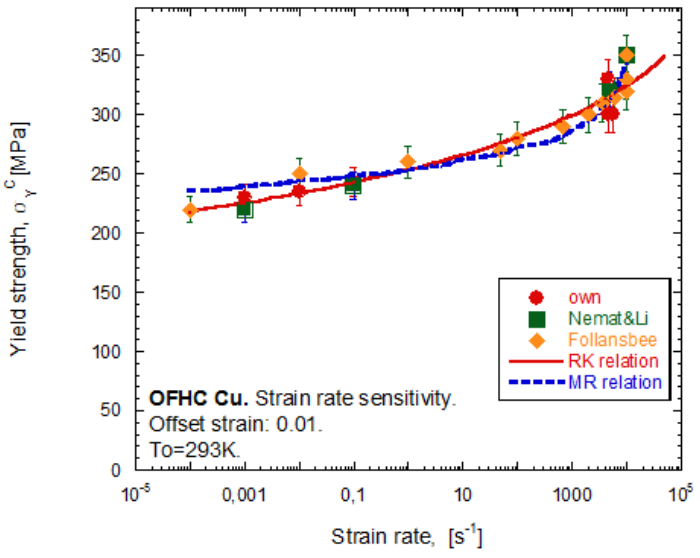

Figure 5.18: OFHC Copper. Strain rate sensitivity.

Concerning above, the OFHC Cu is strain rate sensitive. It can be concluded that the resulting tests confirm remarks found in mentioned above literature. Both the the MR model and the MRK model give a good approximation to the behaviour of the material with increasing strain rate.

5.3.2 Yield surface for OFHC Cu

The results of experimental tests presented in the previous sections can be used to obtain the surface of plasticity characterizing OFHC copper in different strain rates.

The results of stress tests for strain rate equals 0.001 s^{-1} allows to obtain the yield surface with use of the Burzyński criterion, (Eq. 4.34). The material is isotropic, the SD parameter slightly higher then 1. There is also presented comparison with the Huber-Mises criterion, Eq. (5.35). In Fig. 5.19 there are presented comparison between limit curves obtained due to the Burzyński criterion (solid line) and the Huber-Mises-Hencky criterion (dashed line), obtained respectively due to Eqs. (4.33) and (4.10) for the exemplary strain rate 0.001s^{-1} and offset strain equals to 0.002.

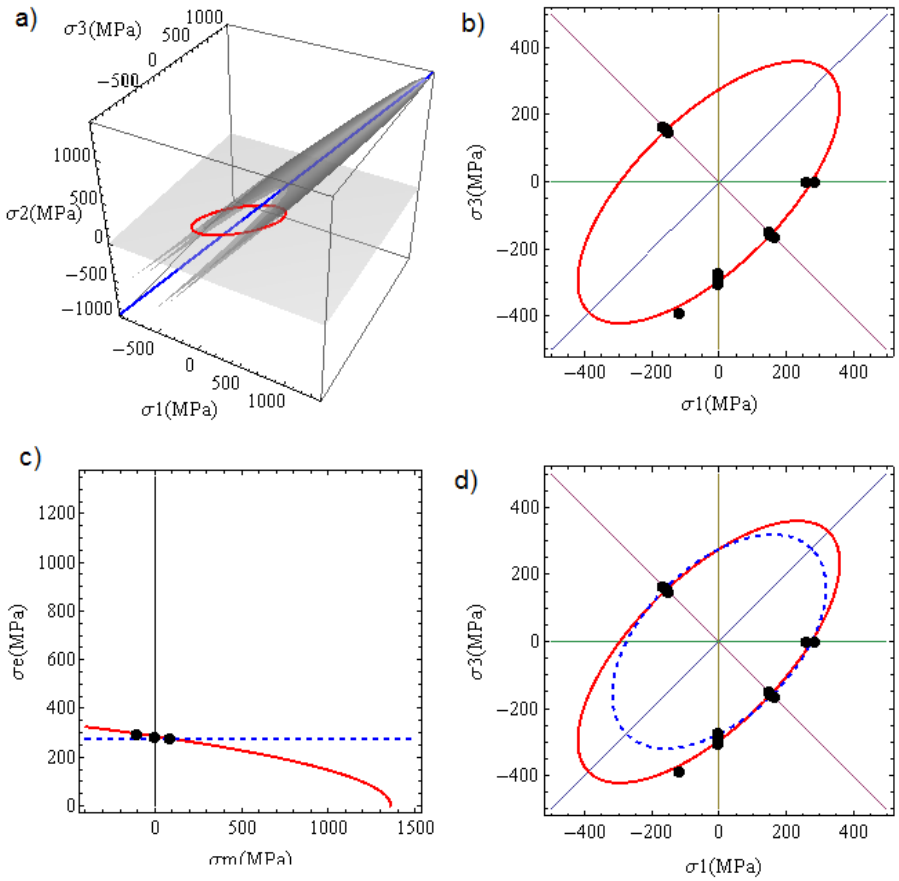

Figure 5.19: OFHC Cu. Presentation of the paraboloidal Burzyński condition in a) the space of principal stresses, b) the plane $\sigma_2 = 0$. Comparison with the HMH criterion presented in c) the meridional plane, d) the plane $\sigma_2 = 0$.

It can be noticed that for SD parameter almost equals 1, there is not much difference between the HMH yield curve and Burzynski yield curve. The obtained in the space of principal stresses surface is a paraboloid of revolution, but very elongated, this can be also notice on the meridional plane. In such a case the approximation of yield state given by the HMH is sufficient.

In Fig. 5.20 there is presented comparison between limit curves in plane $\sigma_2 = 0$ for data obtained in dynamic strain rates (solid lines) and quasi-static strain rate.

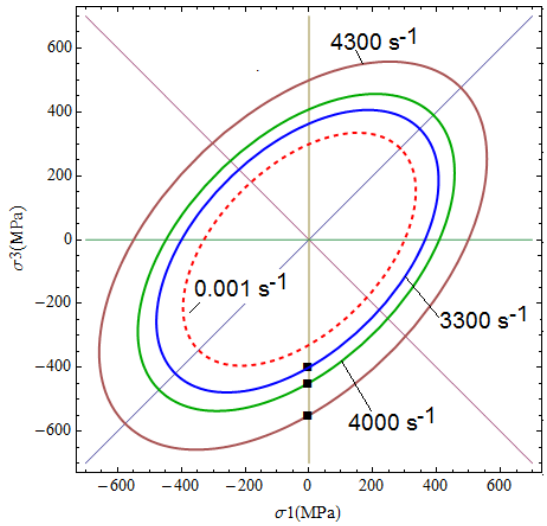

Figure 5.20: OFHC Copper. Comparison between limit curves in plane $\sigma_2 = 0$ for data obtained in dynamic strain rates (solid lines) and quasi-static strain rate.

It can be noticed that yield curve is increasing according to strain rate sensitivity. But the shape is different then for the yield curve obtained in quasi-static strain rate. This can be explained by the fact that for strain rate $0.001s^{-1}$ there have been performed a wide range of experiments - shear, tension and biaxial compression - due to which the additional point is obtained. Whereas, the only one data in dynamic range is - yield point in compression. Consequently, yield curve in dynamic range may be treated as rough approximation of the yield state.

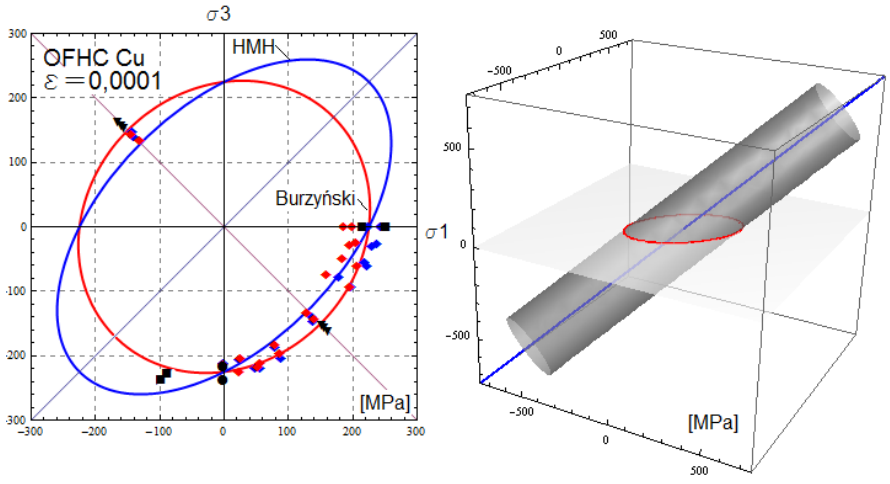

Figure 5.21: OFHC Copper - yield surface basing on the complex stress state: (a) the limit curves for offset strain 0.0001 in the plane $\sigma_2 = 0$, the Burzyński criterion - the red line, Huber-Mises criterion - blues line, (b) the plasticity surface.

In Fig. 5.21 there are presented limiting curves modelling the behaviour obtained for the complex state of stress test, carried out on the thin-walled tubes. The offset strain is equalled to 0.0001. Red line indicates the Burzyński criterion, the blue line - Huber-Mises criterion. Visualization of the yield surface in both cases is a cylinder.

In Table 5.11 there are collected yield points obtained in quasi-static tests of tension, compression and double shear, respectively: σ_Y^T, σ_Y^C, τ_Y and σ_Y^{CC}. Data are summarized for the three strain rates: 0.001s^{-1}, 0.01s^{-1}, 0.1s^{-1}. The yield limit values have been read for the six offset strains: 0.0001, 0.001, 0.002, 0.003, 0.005, 0.01. Method of measurement is presented in the Paragraph 3.1.2. Since, the quasi-static tension test has been performed for only one strain rate 0.001s^{-1}, Fig. 5.14 - for this one rate the strength differential parameter κ is calculated. It is close to 1 for each value of offset strain for strain rate 0.001s^{-1}.

a)

strain rate:	avarage values of yield limits: [MPa]					
0,001 [1/s]	σ_Y^C	σ_Y^T	κ	τ_Y	τ_{Yteor}	R_B
0,0001	237	237	1,00	146	136,83	**0,64**
0,001	275	261	1,05	154	154,68	**1,03**
0,002	294	272	1,08	156	163,27	**1,29**
0,003	305	283	1,08	158	169,62	**1,46**
0,005	310	303	1,02	163	176,95	**1,54**
0,01	313	318	0,98	167	182,15	**1,57**
0,012						

b)

strain rate:	avarage values of yield limits: [MPa]					
0,01 [1/s]	σ_Y^C	σ_Y^T	κ	τ_Y	τ_{Yteor}	R_B
0,0001	243	221	1,10	155	133,77	**0,23**
0,001	280	255	1,10	167	154,13	**0,56**
0,002	298	271	1,10	173	164,04	**0,70**
0,003	310	290	1,07	180	173,11	**0,77**
0,005	316	295	1,07	182	176,28	**0,81**
0,01	330	300	1,10	185	181,66	**0,89**

c)

strain rate:	avarage values of yield limits: [MPa]					
0,1 [1/s]	σ_Y^C	σ_Y^T	κ	τ_Y	τ_{Yteor}	R_B
0,0001	245	223	1,1	174	134,87	**0,20**
0,001	282	256	1,1	184	155,24	**0,14**
0,002	302	275	1,1	187	166,25	**0,37**
0,003	310	282	1,1	188	170,65	**0,47**
0,005	320	291	1,1	193	176,15	**0,50**
0,01	326	298	1,1	195	179,95	**0,55**

Table 5.11: OFHC Copper. Results of strength tests for various offset strains and strain rates. In last column there are summarized calculated due to relation (4.46) values of R_B correction coefficient.

Dependence between correction coefficient R_B on strain and strain rate calculated according to Eq. (4.46) is discussed in Section 4.5.6. Application of the relation depending on the strain and strain rate allows to obtain phenomenological description of material yielding. Function which approximates R_B coefficient allows also to estimate its values for strain rates which are not experimentally stutied. Due to relation Eq. (4.46) it is possible to calculate the R_B coefficient which bonds the macroscopic observation into one function. The values of coefficient are collected in last column of Table 5.11.

In Fig. 5.22 by solid lines there are marked functions describing tendency of behaviour of coefficient R_B for suitable strain rates. Function describing R_B coefficient increases together with increasing values of the offset strain, it has a constant, exponentially-increasing tendency. Whereas increasing of strain rate causes the decreasing of the level of function, as it is explained in Section 4.5.6. The values of R_B are symbolized with different points.

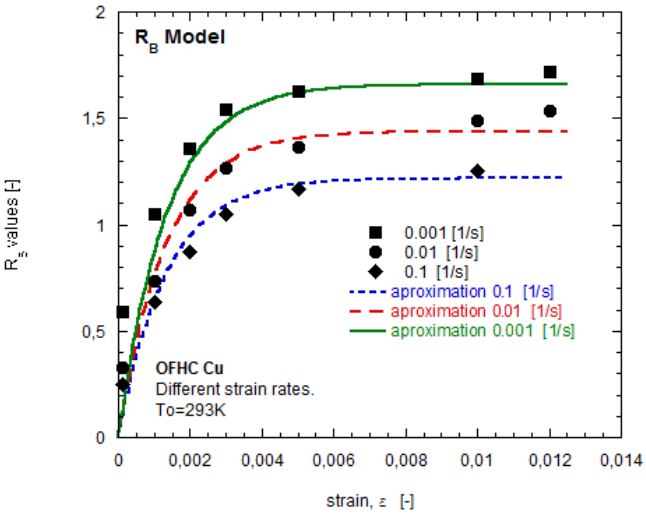

Figure 5.22: OFHC Copper. Dependence between values R_B and strain and strain rate.

The function which approximate the behaviour of R_B coefficient according to strain and strain rate is given by Eq. (4.48). The parameters of the function are identified and collected in Table 5.12.

OFHC Cu	A [-]	B [-]	C [-]	$\dot{\varepsilon_0}$ [s^{-1}]
	1.86	750	0.051	10^{-4}

Table 5.12: OFHC Copper. Values of parameters of function (4.48) approximating the tendency of R_B coefficient.

In Fig. 5.23 there is presented the comparison between yield curves obtained with use of Burzyński criterion for initially anisotropic materials and the Huber-Mises-Hencky criterion. Curves were find for strain rate 0.001 s^{-1}. It could be noticed there is discrepancy between both criteria. The value of it especially large for small offset strain definition (0.0001) and large values of it. The result of biaxial compression is crucial if it is supposed to chose which yield criterion is the most suitable. Due to the yield point in biaxial compression it can be stated that better approximation is assured by the Burzyński criterion.

The Fig. 5.24 presents the evolution of yield curve in plane $\sigma_2 = 0$ when strain rate is constant and equal to a) $0.001s^{-1}$, b)$0.01s^{-1}$, c) $0.1s^{-1}$ and when offset strain is constant and equal to d) 0.0001, e) 0.002, f) 0.1. It could be noticed that along with increasing strain rate the subsequent ellipses have bigger areas. The suitable experimental yield points also have larger values - what maybe it is not seen in the Figures but can be observed in Table 5.11. When strain rate is constant then the evolution of yield surface is presented along with increasing offset strain. The gradual elongation of limit curves is observed. It should be also noticed

that curves at strain rate equal to $0.001s^{-1}$ are narrower and more 'slender' than curves for strain rate equal to $0.01s^{-1}$, which also have the same tendency according to curves obtained at higher strain rate - $0.1s^{-1}$. In Figs. 5.24.d-e-f (with constant offset strain) - curves become more slender for lower strain rates. This is contributed to fact that values of R_B coefficient increase along with offset strain but their level decrease with the increase of strain rate - Table 5.11. For fixed offset strain - the lower strain rate, the higher level of R_B coefficient and it tends to its upper limit - 2.

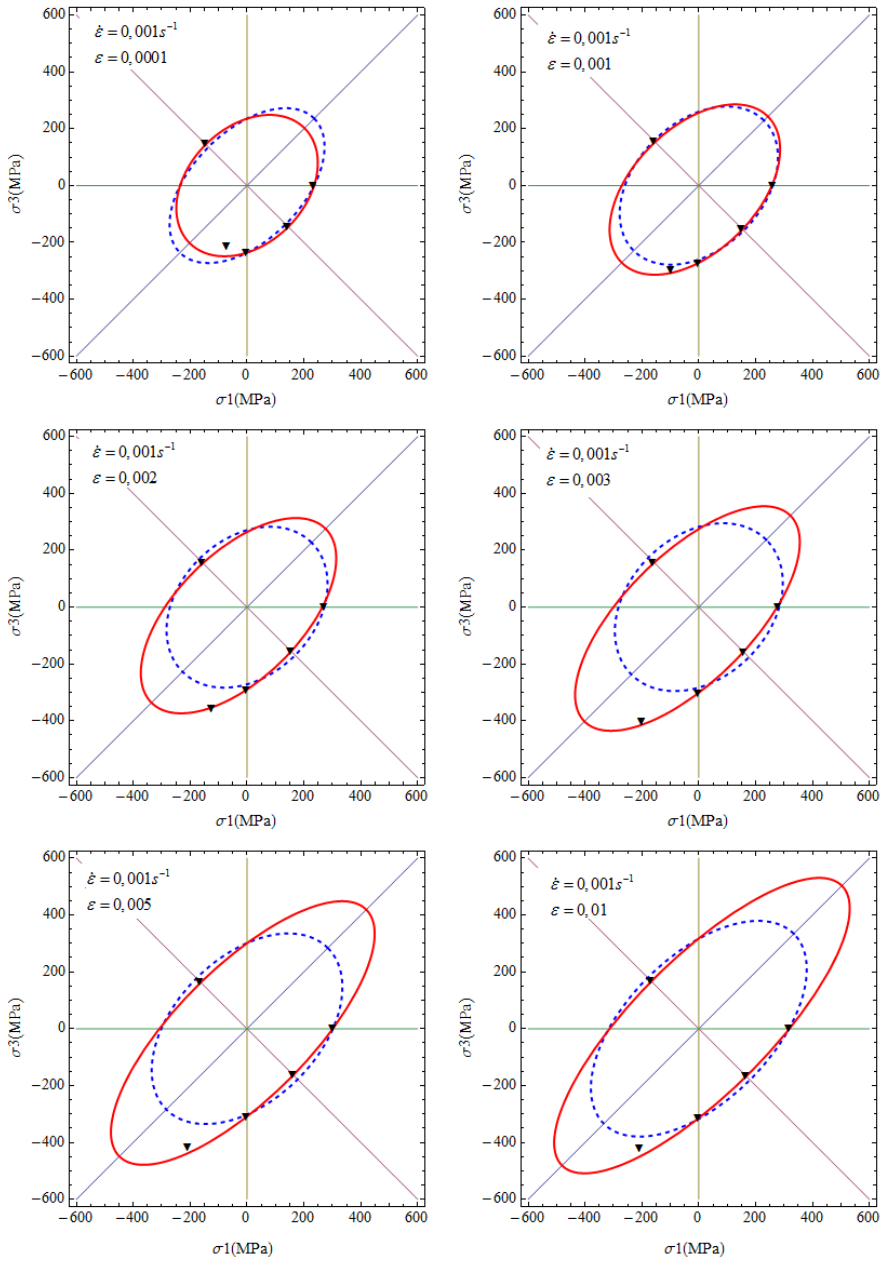

Figure 5.23: OFHC Copper. Presentation of the paraboloidal Burzyński condition in the plane $\sigma_2 = 0$.

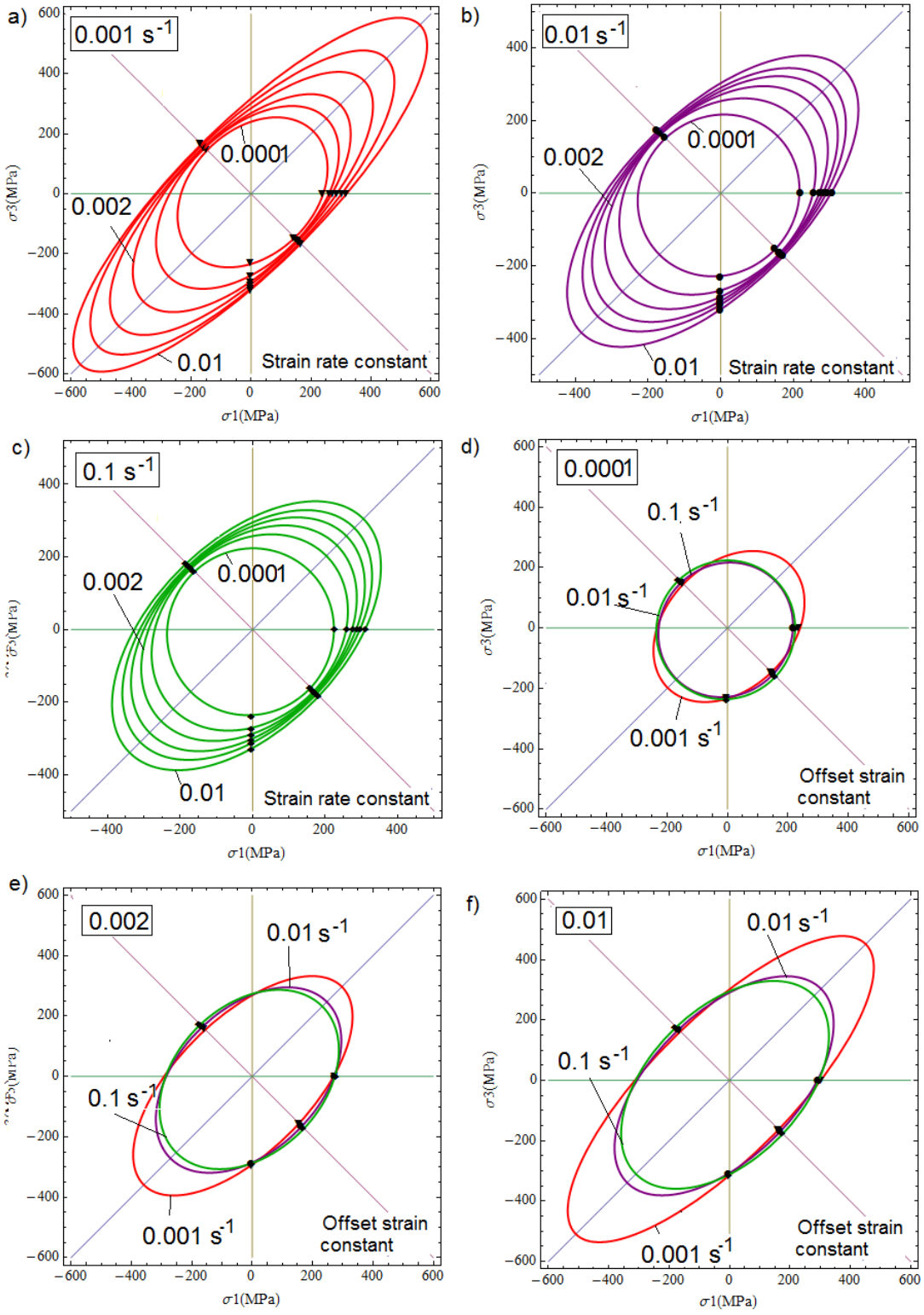

Figure 5.24: OFHC Copper. Summarizing of limit curves for (a, b, c) constant offset strains and (c, d, e) constant strain rates.

5.4 Applications for BCC materials - E335 steel

In this paragraph the results of strength tests are discussed for different metals. Firstly, the results collected by Theocaris [Theocaris 1995] are presented. Theocaris used experimental data collected by Taylor and Quinney [Taylor and Quinney 1931] and Lode [Lode 1926]. For data of steels and copper the yield surface and curves according to isotropic Burzyński criterion (4.34) are presented in Fig. 5.25. In this case the SD parameter equals to 1.3. The comparison with the HMH criterion allows to notice that Burzyński criterion gives better approximation of the onset of plasticity. Consequently, the assumption can be stated that there are metals that can be characterized by the asymmetry of elastic range.

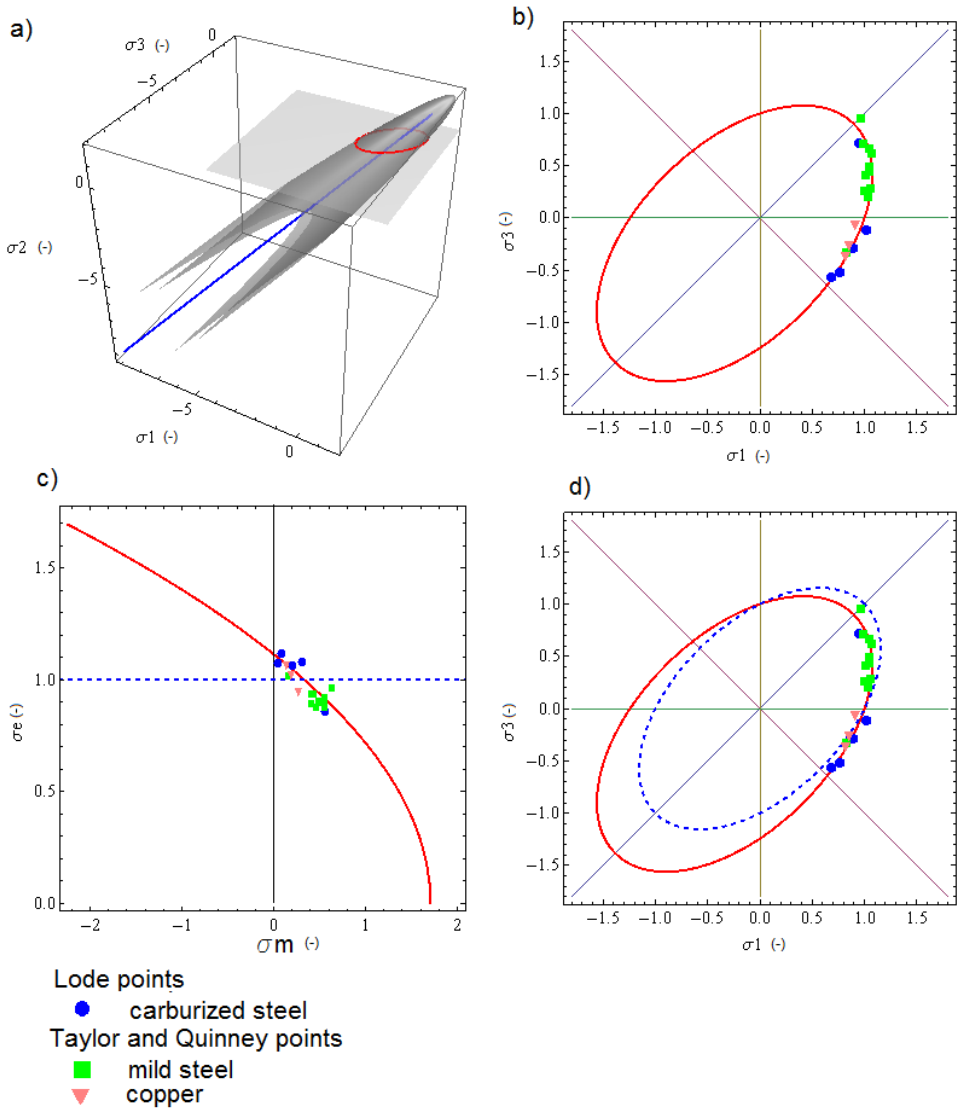

Figure 5.25: Presentation of the paraboloidal Burzyński condition in a) the space of principal stresses, b) the plane $\sigma_2 = 0$. Comparison with the HMH criterion presented in c) the meridional plane, d) the plane $\sigma_2 = 0$, applied for different kinds of metals, [Taylor and Quinney 1931; Lode 1926].

Yield state for several types of metal is presented - Fig. 5.25. Data are cited after [Taylor and Quinney 1931] for the mild steel, data concerning carburized steel have been cited after [Lode 1926] - all data have been found in the paper of [Theocaris 1995]. The experiments performed by authors of [Taylor and Quinney 1931] and also [Lode 1926] concerning yielding mode of ductile materials - copper and carburized steel are used to validate Burzyński criterion.

E335 is a steel used as structural component for different constructional industry. The data found in literature are presented in the Section 2.3 as well as information concerning the mechanical properties. Also analysis of microstructure and chemical composition are discussed in above mentioned Chapter. In this Section results of tests performed under different loading in different strain rates at room temperature are presented and discussed. Due to experimental data the yield strengths are defined and basing on them the yield state can be determined. Visualizing of yield state is possible due to yield surfaces plotted in the space of principal stresses and its cross-section. The discussion concerning the influence of strain and strain rate on the evolution of yield surface is also included.

5.4.1 Results of strength tests for E335

In this Section the results of experimental tests obtained for E335 steel are shown and discussed. For E335 there steel have been performed the strength tests at room temperature under isothermal conditions for different strain rates (the discussion on the experimental techniques is presented in Chapter 3):

- the quasi-static compression test,
- the quasi-static tension test,
- the double shear test,
- the complex test,
- the dynamic compression test with use of the Split-Hopkinson Pressure Bar.

Using E335 steel there has been also performed tensile test for round notched specimens, Fig. 4.25 - discussed in Section 4.6. In the notched zone of a round specimens the yielding is driven by the pressure influence. This conclusion is discussed in papers of e.g. [Wilson 2002; Bai and Wierzbicki 2008; Fernandez-Saez and Vadillo 2009]. The Huber-Mises-Hencky criterion, Eq. 4.10, does not describe accurately yielding of materials characterized by strength difference. The calculations with use of UMAT with implemented isotropic Burzyński criterion, Eq. 4.33, also proves above observations. The numerical simulation concerning analysis of tensile test performed with use of notched specimens made of E335 steel is reported in Section 4.6.

Tests in quasi-static strain range

In this part there are presented results of quasi-static tests.

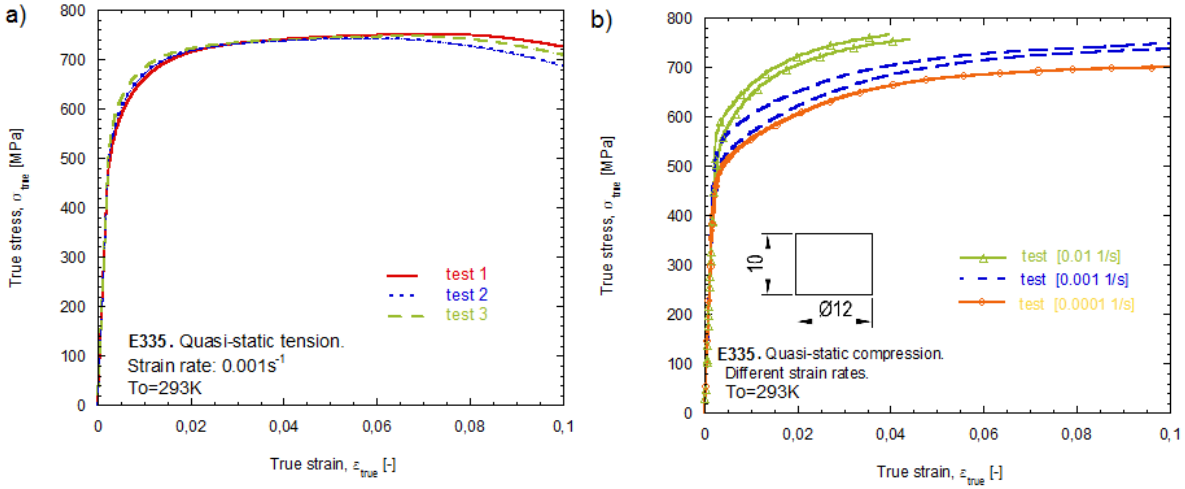

Figure 5.26: E335 steel. Results of quasi-static tests for different strain rates: a) tension and b) compression.

The tension test has been performed with use of round 'dog-shaped' specimens, Fig. 3.4. The compression test in quasi-static and dynamic range has been performed with use of cylindrical specimen with diameter 10mm and height 12mm, Fig. 3.3.a. The geometry of double shear specimen is presented in Fig. 3.14. Test results for quasi-static compression performed for different strain rates and with use of cylindrical specimens, and results of the quasi-static tensile test for strain rate 0.001 s^{-1} are presented in Fig. 5.26. In Fig. 5.27 there are presented results of the double shear test.

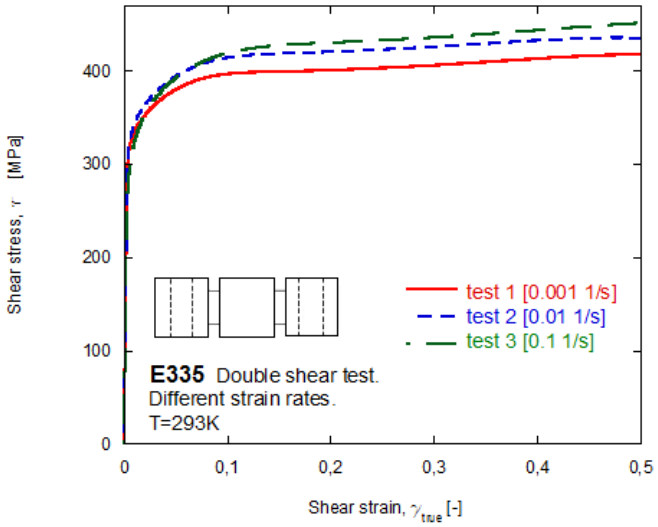

Figure 5.27: E335 steel. Results of double shear test for different strain rates.

In Figs. 5.26 and 5.27 it can be observed the increase of stress level along with increasing strain rate. The material has positive strain rate sensitivity what is compared with results of

dynamic tests - Fig. 5.33. For tensile test the maximum stress value is obtained in the strain equals to 0.075 and the average value of it is 720MPa.

The examined steel is an isotropic material with a yield limits in tension slightly different then yield limit in compression, Table 5.13. Consequently, the strength differential parametr is close to 1.07. That conclusion is confirmed also by results of numerical calculation with UMAT, Section 4.6. Young's modulus has been calculated due to results of the complex state stress test and it is assumed as 225GPa. Kirchoff's modulus is equals to 87GPa.

For strain rate equals 0.001 s^{-1} there are collected yield limits for the offset strain equals $\varepsilon_{offset} = 0.002$ and $\varepsilon_{offset} = 0.0001$, data are summarized in Table 5.13.a. For strain rate equals 0.01 s^{-1} the yield limits are summarized in Table 5.13.b and for the same offset strain values but strain rate equals 0.0001 s^{-1} the data are collected in Table 5.13.c. The tension test has been performed only for one strain rate: 0.001 s^{-1}, whereas the double shear test also for strain rates: 0.1 s^{-1} and 0.01 s^{-1}, the compression test: 0.0001 s^{-1} and 0.01 s^{-1}. Basing on results collected in Table 5.13 it can be concluded that E335 steel is a material which is characterized by the strength difference, $\kappa \neq 1$. In addition, yield limit in shear differs from value obtained with traditional approach, Eq. (4.30), the difference equals 10% and 20%.

Test	$\dot{\varepsilon} s^{-1}$	σ_Y [MPa] $\varepsilon_{offset} = 0.002$	**Avarage** [MPa] $\varepsilon_{offset} = 0.002$	σ_Y [MPa] $\varepsilon_{offset} = 0.0001$	**Average** [MPa] $\varepsilon_{offset} = 0.0001$
a)	$0.001 s^{-1}$				
Tension	0.001	540		405	
		560	540	420	423
		520		443	
Compression	0.001	550	558	420	450
		565		480	
Shear	0.001	317	323	295	305
		328		313	
κ Eq. (2.1)			1.05		1.07
τ_Y^H Eq. (4.30)			312		253
R_B Eq. (4.46)			0.85		0.07
b)	$0.01 s^{-1}$				
Compression	0.01	605	588	404	420
		570		435	
Shear	0.01	323	323	303	303
		323		303	
κ Eq. (2.1)			1.05		1.07
τ_Y^H Eq. (4.30)			348		248
R_B Eq. (4.46)			1.47		0.06

Table 5.13: E335 steel. Table of collected yield points from tests performed with the strain rate: a) $\dot{\varepsilon} = 0.001 s^{-1}$, b) $\dot{\varepsilon} = 0.01 s^{-1}$ defined for offset strain equals to $\varepsilon_{offset} = 0.002$ and for $\varepsilon_{offset} = 0.0001$.

Results of complex stress state test

The results of complex stress state test for thin-walled tubes are shown in Fig. 5.28. The points allowing for the approximation of an initial yield curve in the plane (σ, τ) have been found for the offset strain equals 0.0001. Summary of yield points obtained in the subsequent steps of the test is shown in Table 5.17. Details of the test technique are given in Section 3.5.

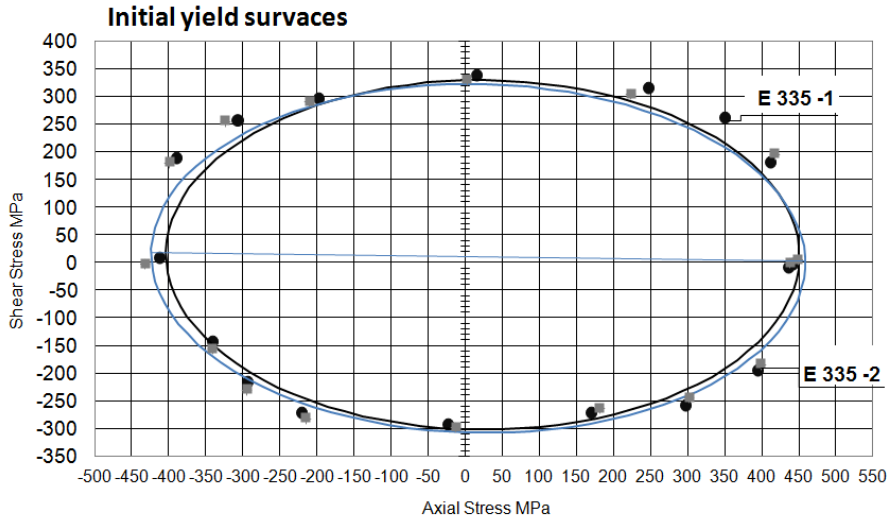

Figure 5.28: E335 steel. Results of the complex stress state test in plane the (σ, τ).

In the Fig. 5.29 there is presented the sequence of stresses which occurred in the material during the subsequent loadings. It could be noticed that yield points in compression are slightly lower then yield points in tension, this could be attributed to definition of the offset strain which equals to 0.0001.

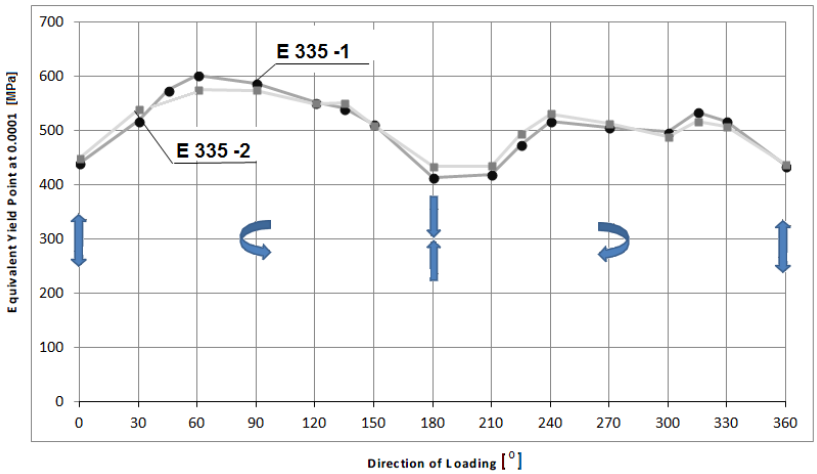

Figure 5.29: E335 steel. Relation between the yield points and the load directions.

As it is stated in Section 3.5 the initial curve determined in Fig. 5.28 has only mathematical character. Yield points in the plane (σ, τ) must be recalculated according to relation Eq. (3.18) to the coordinates given in the principal stresses. Then, basing on them it is possible to apply the Burzyński yield conception.

Results of dynamic compression test and constitutive models of material behaviour

In this part there are presented results of dynamic compression test. The obtained results are compared with quasi-static characteristic of material. Additionally, the analytical constitutive relation: the Johnson-Cook model and the Rusinek-Klepaczko model are applied.

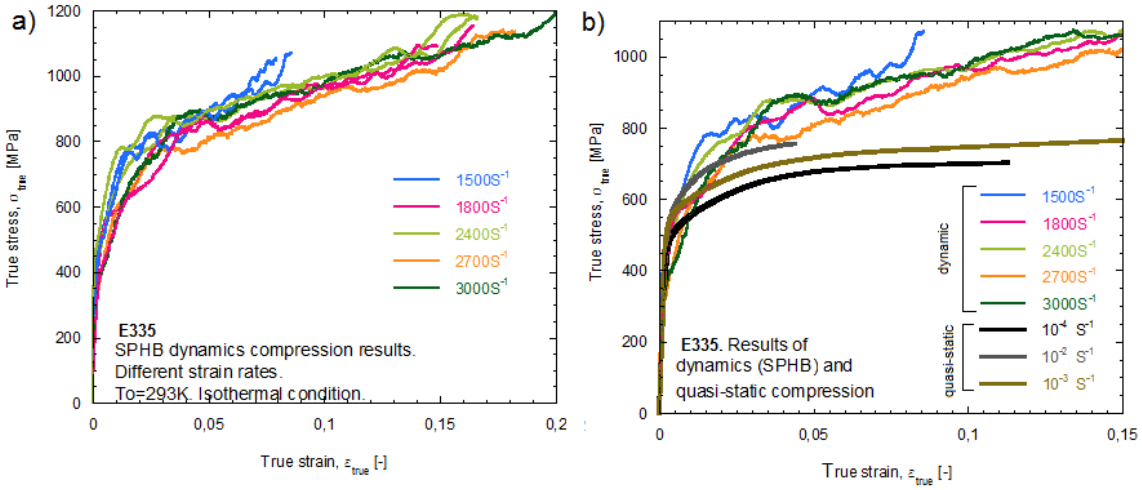

Figure 5.30: E335 steel. a) True stress-true strain curves for the dynamic compression test (SHPB), b) comparison between the results of dynamic and quasi-static compression.

Figure 5.30 shows the stress-strain curves for E335 steel for both quasi-static and dynamic compressive tests. The true stress - true strain curves obtained in the dynamic compression test with use of the Split-Hopkinson Pressure Bar, carried out at different strain rates are presented in Fig. 5.30.a. Their comparison with the results of quasi-static compression is also given in Fig. 5.30.b.

The parameters for the Johnson-Cook model, according to equation (6.1), for the E335 steel are collected in Table 5.14. Experimental curves for different strain rates compared with the modelling with use of the Johnson-Cook relation are presented in Fig. 5.31. The constitutive behaviour modelled with use of the Johnson-Cook model shows that flow of material is well defined. It is followed by strain softening and subsequent strain hardening. Rate sensitivity is manifested by increasing of yield and flow stress values along with increasing strain rate.

E335	A [MPa]	B [MPa]	n [-]	C [-]	$\dot{\varepsilon}_0$ [s^{-1}]
	450	487.16	0.26	0.01	10^{-4}

Table 5.14: E335 steel. Parameters of the Johnson-Cook model, Eq. (6.1).

The parameters of the Johnson–Cook model are estimated using experimental data of quasi-static compression. The obtained due to analytical modelling flow curves show good agreement with the results of experimental compression test in quasi-static strain rates. The discordancy between analytical prediction and experimental data is observed at the beginning of the true stress-true strain relation but the hardening of material seems to be well defined, Fig. 5.31.

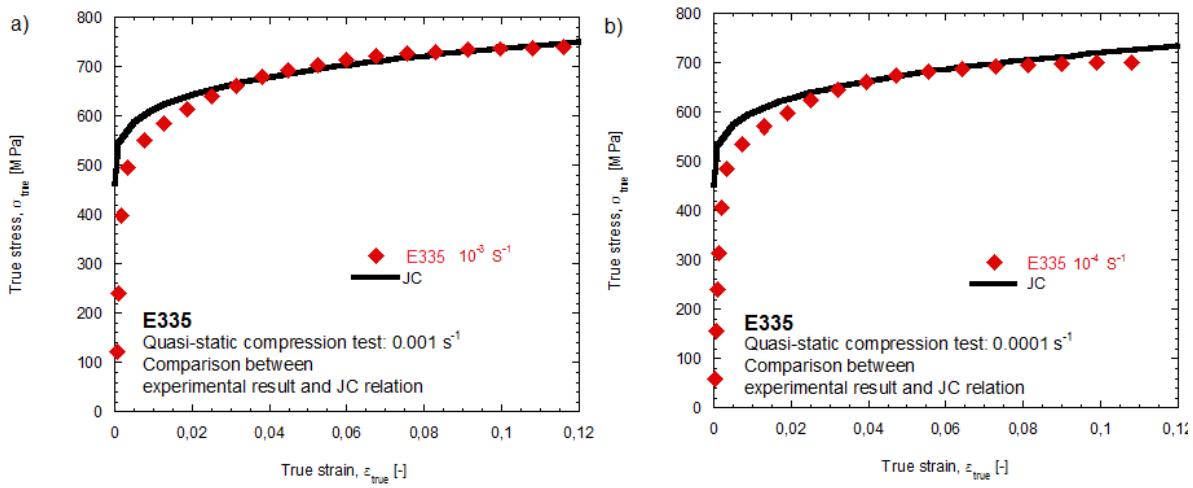

Figure 5.31: E335 steel. Model of the material behaviour obtained due to the Johnson-Cook model, Eq. (6.1), for quasi-static strain rates: a) $10^{-3}s^{-1}$ and b) $10^{-4}s^{-1}$.

The uniaxial compression tests have been conducted on E335 steel under quasi-static and dynamic conditions to determine the rate-dependent flow and post-yield behaviour of the material. Basing on the Rusinek-Klepaczko model, Eq. (6.9), [Klepaczko and Chiem 1986; Rusinek et al. 2005; 2007] the material behaviour in the dynamic strain rates is modelled - Fig. 5.32. It is noticed that the definition of the thermo-viscoplastic behaviour for the studied steel provided by the RK model is proper.

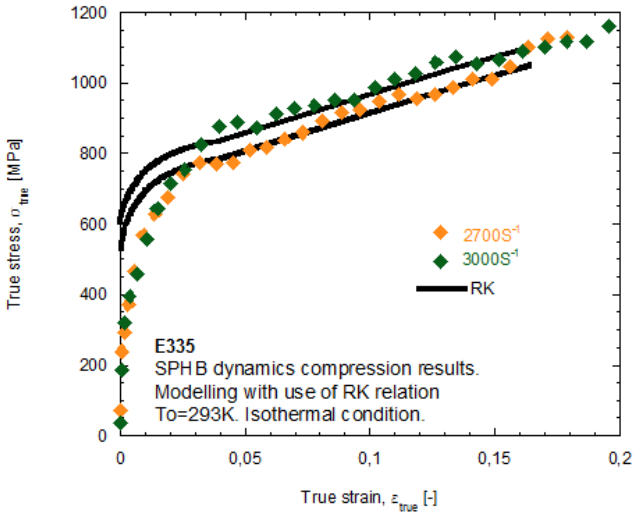

Figure 5.32: E335. Modelling of true stress-true strain curves for dynamic strain, comparison between the RK model and experimental results.

Parameters of the RK model are given in Table 5.15.

T_0 [K]	T_m [K]	ε_{max} $[s^{-1}]$	B_0 [MPa]	v [-]	n_0 [-]	D_2 [-]	$\dot{\varepsilon}_{min}$ $[s^{-1}]$	D_1 [-]	p [-]	σ^* [MPa]
300	1600	10^7	685.8	0.0174	0.014	0.061	10^{-5}	0.0187	0.019	440

Table 5.15: E335. Parameters of the Rusinek-Klepaczko model, Eq. (6.9), [Rusinek and Klepaczko 2001].

Parameters of the Molinari-Ravinchandran model, Eq. (6.18), described the E335 steel are collected in Table 5.16.

δ_{r0} $[\mu m]$	δ_{s0} $[\mu m]$	$a_r = a_s$	$\dot{\varepsilon}_{r0} = \dot{\varepsilon}_{s0}$ $[s^{-1}]$	$\dot{\varepsilon}_0$ $[s^{-1}]$	$\varepsilon_r = \varepsilon_s$	m	a	σ_{ref} [MPa]	b
4.3	0.06	0.7	10^4	10^4	0.8	0.45	13.651	1	0.0018

Table 5.16: E335 steel. Parameters of the Molinari-Ravichandran model, Eq. (6.17), [Molinari and Ravichandran 2005; Durrenberger et al. 2008].

Figure 5.33 shows the strain rate sensitivity of E335. Steel has a positive strain rate sensitivity. The material's behaviour is predicted with use of 2 models: the Molinari-Ravichandran model, Eq. (6.17) and the Rusinek-Klepaczko model, Eq. (6.9).

The sensitivity on the strain rate for E335 steel in accordance with the models (6.9) and (6.17) is presented in Fig. 5.33.

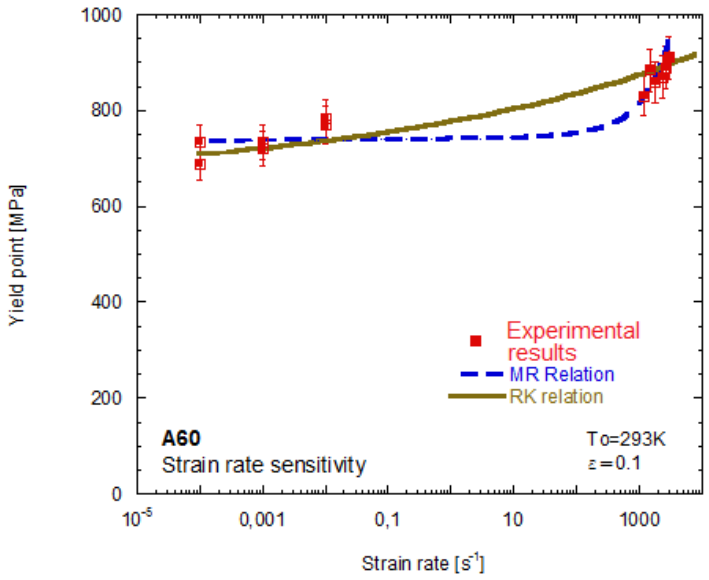

Figure 5.33: E335 steel. Sensitivity to strain rate.

As it is shown in Fig. 5.33 the RK and MR constitutive relation are capable of reproducing the non linear strain rate sensitivity of E335 steel. The MR model gives a better agreement between analytical prediction and experiment especially in high strain rate deformation.

5.4.2 Yield surface for E335

The yield curves obtained due to complex stress state is presented in Fig. 5.35. The yield points are determined for offset parameter equals to 0.0001. The summarized values read basing on Fig. 5.28 are collected in Table 5.17.

direction	test 1 σ_Y [MPa]	test 2 σ_Y [MPa]
0° tension	440	448
90° torsion	340	331
180° compression	413	433
270° torsion	292	296
360° tension	435	437

Table 5.17: E335 steel. Collected yield strengths for different direction of loadings in the complex stress state test.

Fig. 5.34.a shows the yield points obtained in the complex stress state test - presented previously in Fig. 5.28 where they are used to determine an initial yield surface obtained due to curve fitting.

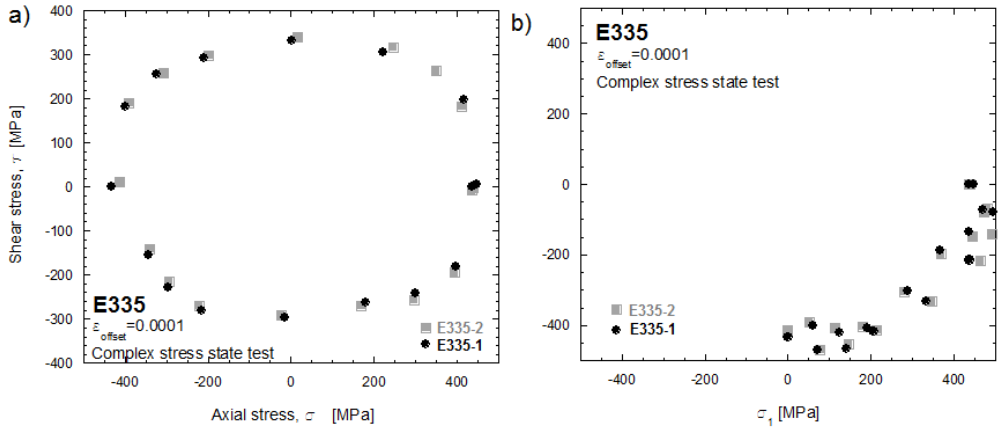

Figure 5.34: E335 steel. Yield points obtained in the complex test presented in the planes a) (σ, τ) and b) (σ_1, σ_3).

In Table 5.18 there are given data used to plot the yield curve basing on the results of the complex stress state test.

E335	quasi-static	$\varepsilon_{offset} = 0.0001$
σ_Y^C	460	$\kappa = 1$
σ_Y^T	460	$R_B = 0.15$
τ_Y	324	[MPa]
HMH:	σ^Y = 460	τ_Y^H=265

Table 5.18: E335 steel. Data used to obtain yield curve basing on the results of the complex stress state.

In Fig. 5.35 there are given yield curves defined for offset strain equals to 0.0001, data obtained at quasi-static strain rate.

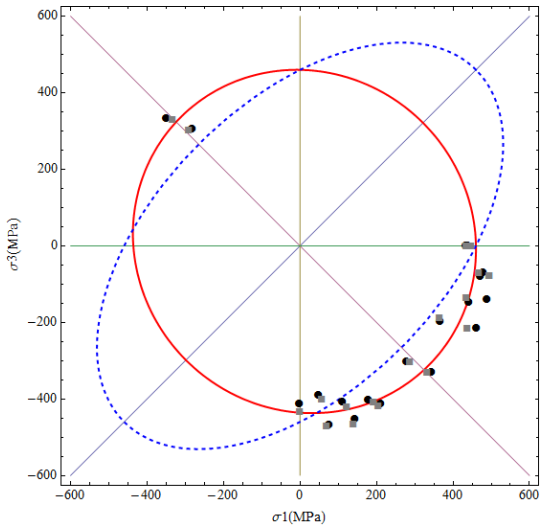

Figure 5.35: E335 steel. Comparison between yield curves obtained due to the Burzyński criterion (solid line) and the HMH criterion (dashed line) for offset strain equals to 0.0001.

In Fig. 5.35 it can be observed that there is a huge difference between limit curves obtained due to the HMH model, Eq. (4.10) and the Burzyński Model, Eq. (4.45). The reason is that there is a difference between yield point in shear obtained experimentally (325 MPa) and possible to obtained due to theoretical relation - Eq. 4.11. The difference is almost 20%, because the theoretical value is equals to 260MPa. In such a case the value of correction parameter R_B is equaled to 0.15.

In next part there are presented yield states prepared for data obtained in the quasi-static test which are reported in Figs. 5.26 and 5.27. The results of stress tests for strain rate equals 0.001 s^{-1} allows to obtain the yield surface with use of the Burzyński criterion, (Eq. 4.34). The material is isotropic, the SD parameter slightly higher then 1. There is also presented comparison with the Huber-Mises criterion, Eq. (5.35). The curves are plotted for the values of the yield strengths determined for an offset equals 0.002, data are collected in Table 5.13.

In Fig. 5.36 there are presented yield surface and its cross-sections for data obtained in tests at $\dot{\varepsilon} = 0.001s^{-1}$ and offset strain equals 0.002. It can be noticed that for SD parameter almost equals 1, there is not much difference between the HMH yield curve and Burzyński yield curve. The obtained in the space of principal stresses surface is a paraboloid of revolution, but very elongated, this can be also notice on the meridional plane. In such a case the approximation of yield state given by the HMH is sufficient.

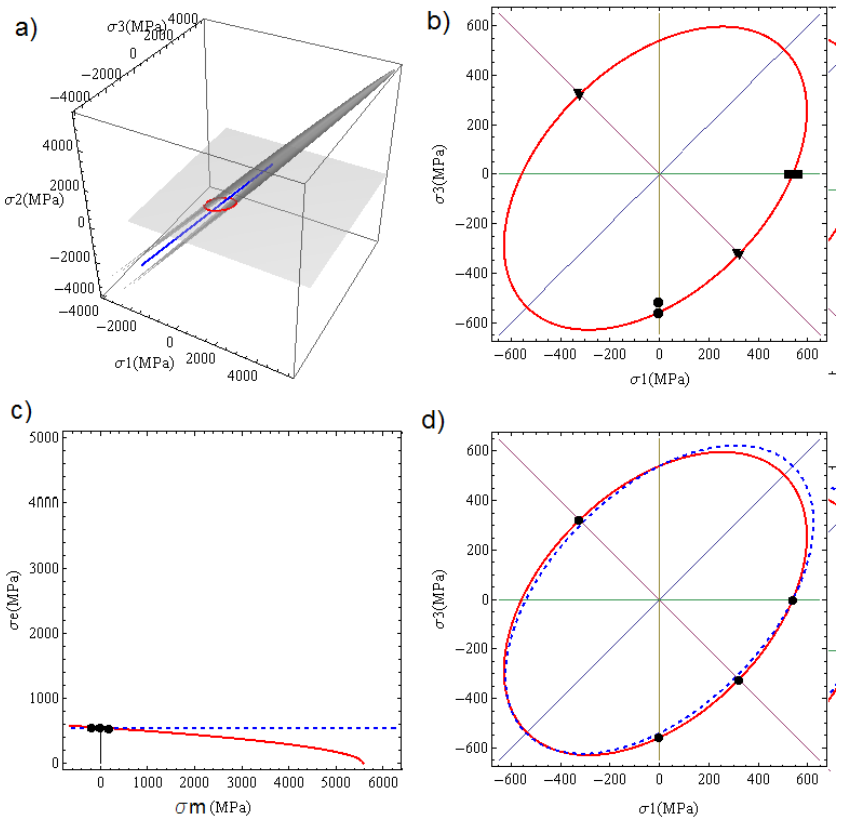

Figure 5.36: Presentation of the paraboloidal Burzyński condition in a) the space of principal stresses, b) the plane $\sigma_2 = 0$. Comparison with the HMH criterion presented in c) the meridional plane, d) the plane $\sigma_2 = 0$, applied for E335 steel.

Basing on the results of tests of compression, tension and shear performed in the quasi-static strain rates there have been determined yield points for different offset strains: 0.0001, 0.001, 0.002, 0.005, 0.01, 0.012. Discussion concerning offset strain is given in Section 3.1.2. Knowing yield points according to increasing offset strain allows to trace the evolution of yielding. Thus, there are defined yield strengths: $\sigma_Y^C, \sigma_Y^T, \tau_Y$ for seven offset definitions in four strain rates: 0.0001 s^{-1}, 0.001 s^{-1}, 0.01 s^{-1}, 0.1 s^{-1}. Because tensile test has been performed only for one strain rate (0.001 s^{-1}), only for this one strain rate it is possible to define SD parameter κ. For the the rest results it is assumed that SD parameter is equals to 1.07 as it was calculated - Table 5.13.

In Table 5.19 there are collected values of R_B coefficient obtained due to calculation with use of Eq. (4.46). Coefficient for each strain rate are marked according to suitable strain rate with different points in Fig. 5.37. In blue colour the values of R_B close to 1 are indicated. As it mentioned, when R_B parameter is equal to 1 the Burzyński criterion has a form of the Huber-Mises-Hencky criterion. Then there is not huge difference among these both criteria. It could be noticed that for each strain rate there is a value of offset strain for which material yielding can be approximated by the HMH approach. For most of offset definitions, the HMH criterion does not provide the proper approximation. In case of tests performed in $\dot{\varepsilon} = 0.001s^{-1}$ this offset definition is equals 0.2% (the most commonly used offset strain definition). It could be also noticed that the value of offset strain in which the HMH is the proper yield conditions increasing along with the strain rate increase.

offset strain [-]	strain rate [s^{-1}] 0.0001	0.001	0.01	0.1
0.0001	0.63971	0.42479	0.31439	0.14223
0.001	1.0246	0.85906	0.77088	0.63822
0.002	1.2098	1.1626	0.98915	0.87224
0.003	1.37	1.262	1.1573	0.93878
0.005	1.477	1.4131	1.2357	1.0516
0.01	1.5939	1.4503	1.2873	1.1245
0.012	1.6458	1.479	1.333	1.172

Table 5.19: E335 steel. Values of R_B correction parameters obtained due to calculation with use of Eq. (4.46).

Due to relation Eg. (4.46) it is possible to calculate the R_B coefficients - the values of parameter are presented in the Fig. 5.37, together with approximation of its behaviour resulted from relation (4.48). The function (4.48) describes the dependence of R_B coefficient on strain and strain rate. The parameters of the describing function are presented in Table 5.20.

E335	A [-]	B [-]	C [-]	$\dot{\varepsilon_0}$
	1.73	840	0.041	10^{-5}

Table 5.20: E335 steel. Paraments of function (4.48) describing the behaviour of R_B coefficient depending on strain and strain rate.

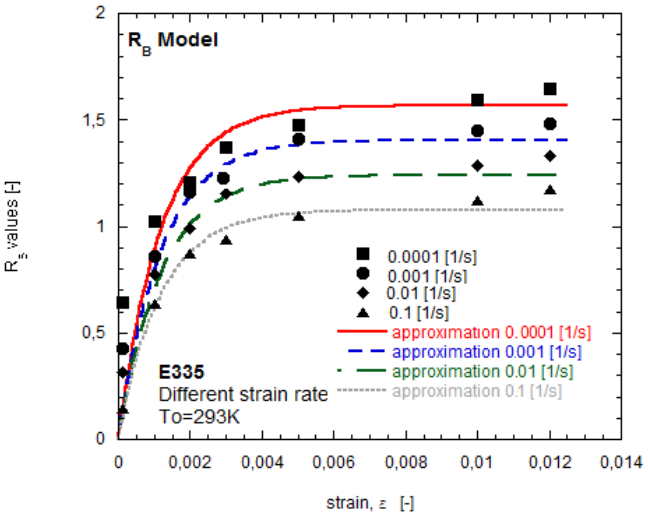

Figure 5.37: E335 steel. Approximation of R_B dependence on strain and strain rate obtained due to Eq. (4.48).

In Figs. 5.38 there are presented yield limits built basing on the experimental results, for which correction coefficient R_B is calculated, as it is shown in Paragraph 4.5.6. The values of R_B coefficient are collected in Table 5.19 and depicted in Fig. 5.37. The Fig. 5.38 presents the evolution of yield curve in plane $\sigma_2 = 0$ when strain rate is constant and equals a) $0.0001s^{-1}$, b) $0.001s^{-1}$, c)$0.01s^{-1}$, and when offset strain is constant and equal to d) 0.0001, e) 0.002, f) 0.01. It may be noticed that along with increasing strain rate the subsequent ellipses have

bigger areas. The suitably increasing experimental yield points also have larger values. It can be noticed that there is not much difference between the yield states obtained in strain rate equals 0.0001 s^{-1}. and 0.001 s^{-1} - Figs. 5.38.e-f. The material is more deformable along with increasing strain rate.

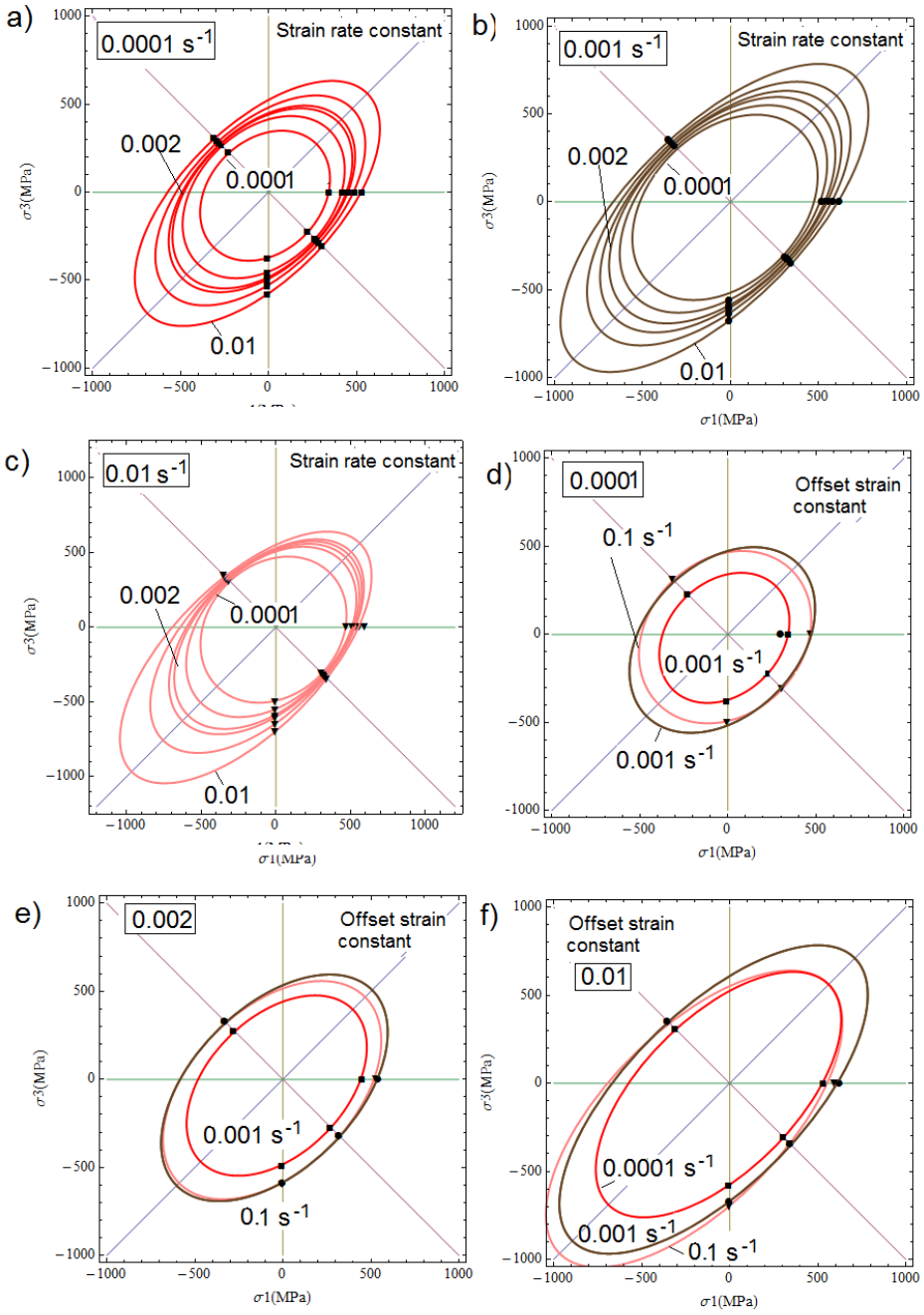

Figure 5.38: E335 steel. Presentation of the paraboloidal Burzyński condition in the plane $\sigma_2 = 0$ for different strain rates and offsets.

5.5 Applications for amorphous materials

Polymers are known to exhibit a strongly pronounced rate and temperature-dependent behavior, their response to tensile and compressive loading is asymmetric. Experimental results of polycarbonate at three different temperatures at quasi-static strain rates found in [Shaban et al. 2007] are use to investigate in the dependence of SD parameter on the temperature - Fig. 5.39. Beneath in Table 5.21 are collected yield points and calculated SD parameter κ, according to Eq. (2.1). It can be noticed that for test performed by Shaban in [Shaban et al. 2007] at the room temperature 23°C the yield points in tension and compression are larger then these ones obtained in the experiment performed in LaBSP, but the SD parameter is similar - $\kappa = 1.12$, whereas in the LaBPS $\kappa = 1.1$ - Table 5.21.

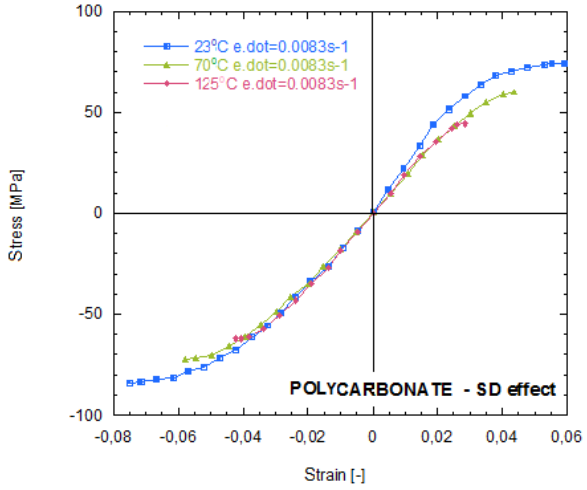

Figure 5.39: Experimental results of polycarbonate at different temperatures at quasi-static strain rates, [Shaban et al. 2007].

Beneath table with collected yield points and calculated SD parameter κ. The strength test

Temperature	$\dot{\varepsilon}s^{-1}$	ε_{offset}	σ_Y^C [MPa]	σ_Y^T [MPa]	κ [-]
23°C	0.0083	0.002	83	74	1.12
70°C	0.0083	0.001	70	60	1.16
125°C	0.0083	0.00025	62	53	1.17

Table 5.21: Polycarbonate - SD parameters at different temperatures, [Shaban et al. 2007].

performed in the LaBPS concerning the polycarbonate (PC) allows to prove above observations. The test for compression have been performed for a wide range of strain rates, [Colard and Rusinek 2012]. The dimensions of the specimens for compression have been 6 mm in height and 6 mm in diameter, geometry of shear samples are presented in Fig. 3.14. For compression tests, grease was used between the sample faces and the platens to minimize friction effect. Load data from the load cell and displacement data from the extensometer have been recorded using a data acquisition software.

Quasi-static, uniaxial compression, tension and double shear test at $\dot{\varepsilon} = 10^{-3}s^{-1}$ of polycarbonate have been conducted. The corresponding true stress–true strain curves and shear stress-shear strain curves were computed, the yielding strengths in tension, compression and shear resulted from test conducted at strain rate equals $0.001s^{-1}$ measured at offset strain equals 0.002 are collected in Table 5.22. The SD parameter obtained in the test at strain rate $0.001s^{-1}$ equals $\kappa = 1.1$.

5.5.1 SD effect in the polymers and its influence on the yield state

It has been established that the viscoplastic flow of glassy polymers starts when the stress exceeds the resistance to molecular segments rotation (Argon 1973). Softening may appear right after yielding. Upon further deformation, molecular alignment occurs. For semi-crystalline polymers, the viscoplastic flow is initiated in the amorphous phase before transitioning to the crystalline phase (Meyer and Pruitt 2001). Three deformation mechanisms of amorphous layers have been recognized: interlamellar shear which would lead to micro-cavities and then to lamellae separation at very large deformation and the rotation of stacks of lamellae. The viscoplastic deformation of crystalline phase is analogous to the viscoplastic deformation of crystallographic materials. Hence, at small strain, the dominant inelastic deformation mode is controlled by the amorphous phase. The properties of the amorphous phase in semi-crystalline polymers are different from those of the amorphous material alone, it can be expected that the viscoplastic flow of polymers at small deformation levels is governed by the molecular chain movement and entanglement. Consequently, polymers are pressure dependent materials, [Ghorbel 2008; Matadi Boumbimba et al. 2012].

Investigation of polymer properties under a hydrostatic loading assumes major significance, since pressure alters the character and mechanisms of the deformation processes, gives rise to transformations, and affects the melting point and other material characteristics. phase and polymorphic transformations, variation in porosity, etc. and the deformation mechanisms, which are associated with the effect of hydrostatic pressure.

The response of polymers to the mechanical loading is very complex, the deformation and the failure stress of polymers are effected by the hydrostatic pressure, as shows the difference observed between the stress-strain curves in uniaxial tension and uniaxial compression. This effect also leads to a pressure dependence of the yield and failure stresses. The effect of hydrostatic pressure on the yield behavior of polymers was demonstrated experimentally in e.g.: [Bridgman 1952; Raghava et al. 1973; Pae 1977; Ghorbel 2008].

A number of studies devoted to investigation of the laws governing the deformation and failure of polymers in tension, compression, and torsion under conditions of hydrostatic compression have appeared. Different plasticity and strength criteria - from the simplest modification of the Tresca criterion [Bowden and Raha 1970], along the rather general criterion proposed by Pae in [Pae 1977], to criteria incorporating three stress tensor invariants [Ghorbel 2008] - have been approved for description of the results. In this study the Burzyński hypothesis accounting for SD effect is used.

To describe pressure-depended behaviour of different polymers data concerning several polymeric materials have been used. The yield state of beneath listed polymers have been described with use of the yield theory of Burzyński given by Eq. (4.33).

- Polycarbonate (PC), results obtained in LaBPS, [Colard and Rusinek 2012] - Fig. 5.41,
- Different polymers, data collected by Theocaris, [Theocaris 1995] - Fig. 5.40,
- Polymethil methacrylate (PMMA) and epoxy compound, [Altenbach and Tushtev 2001] - Figs. 5.42 and 5.43,
- Polylactide (PLA), results obtained in LaBPS, [Bouchart et al. 2010; 2011].

Judging on obtained surfaces, SD parameter (2.1) for polymers corresponds to a rather broad range of values o, κ varies from 1.1 (PC) to 1.5 (Epoxy compound). For the majority of amorphous polymers SD ratio is 1.3 [Theocaris 1995] - Fig. 5.40. The Burzyński criterion for isotropic materials Eq. (4.34) includes strength differential effect, the onset of the plasticity seems to be better approximated with use of this approach.

Different polymers - literature-based data

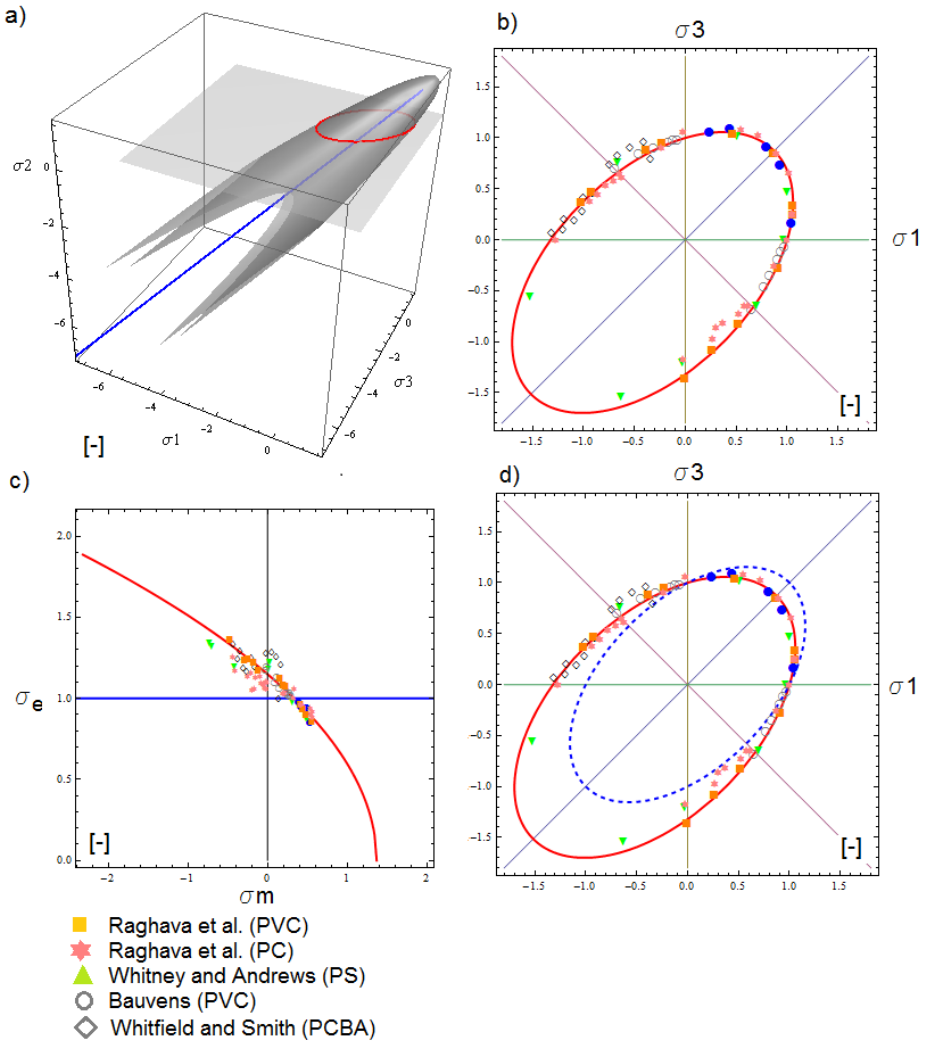

Figure 5.40: Presentation of paraboloidal Burzyński condition in a) the space of principal stresses, b) plane $\sigma_2 = 0$ in comparison with HMH criterion presented in c) the meridional plane, d) plane $\sigma_2 = 0$, applied for different kinds of polymers, data collected by Theocaris, [Theocaris 1995]

Polycarbonate (PC)

Due to data for PC collected in Table 5.22 it is possible to plot the yield surface using the Burzyński isotropic condition - Eq. (4.34). In Fig. 5.41 there are presented the visualizations of the yield surface and curves. The paraboloid of revolution built for values $\sigma_Y^C = 70MPa$, $\sigma_T^C = 64MPa$ and $\tau_Y = 39MPa$ has a peak remoted from the octahedral plane $byH = 249MPa$, whereas the radius of the circle traced in this plane is $R = 67MPa$. It can be noted that material is characterized by the SD parameter equals 1.1, consequently approximation of yielding state with use of the Huber-Mises-Hencky (HMH) criterion is not the very accurate.

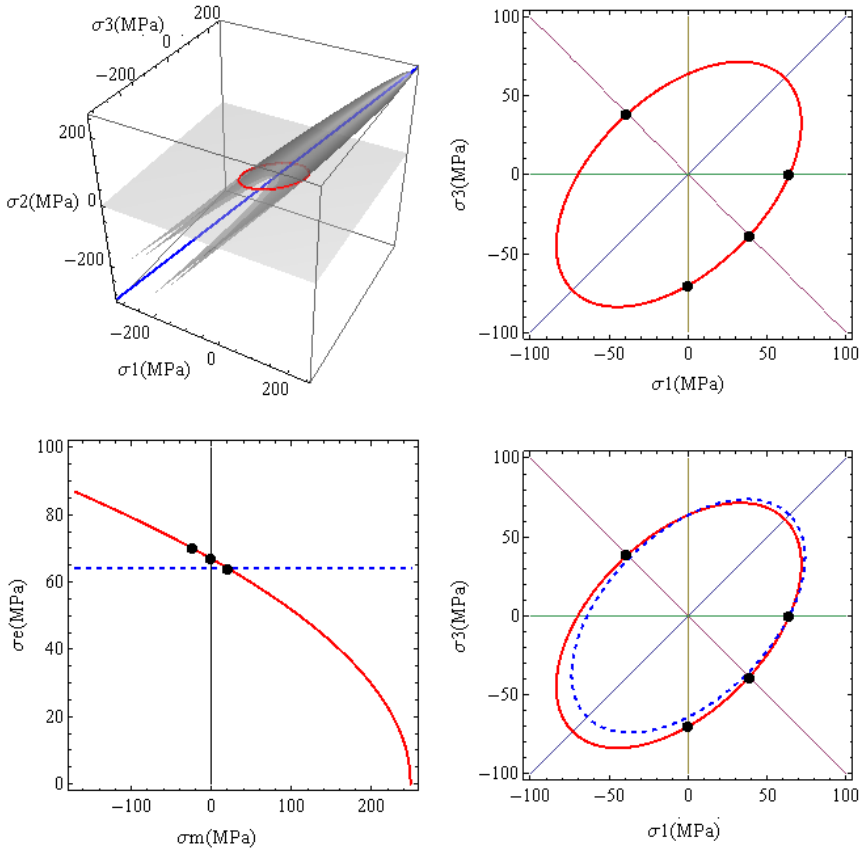

Figure 5.41: Presentation of the paraboloidal Burzyński condition Eq. (4.34) (red line) in a) the space of principal stresses, b) the plane $\sigma_2 = 0$, comprised with the HMH criterion Eq. (4.10) (blue dashed line) presented in c) the meridional plane, d) the plane $\sigma_2 = 0$, applied for the polycarbonate (black dots), [Colard and Rusinek 2012].

PC	quasi-static	$\varepsilon_{offset} = 0.002$
σ_Y^C	70	$\kappa = 1.1$
σ_Y^T	64	$R_B = 1$
τ_Y	39	[MPa]
HMH:	σ^Y = 64	τ_Y^H=36
	H=249	R=67

Table 5.22: Polycarbonate - material data, [Colard and Rusinek 2012].

Polymethil methacrylate (PMMA) - [Altenbach and Tushtev 2001]

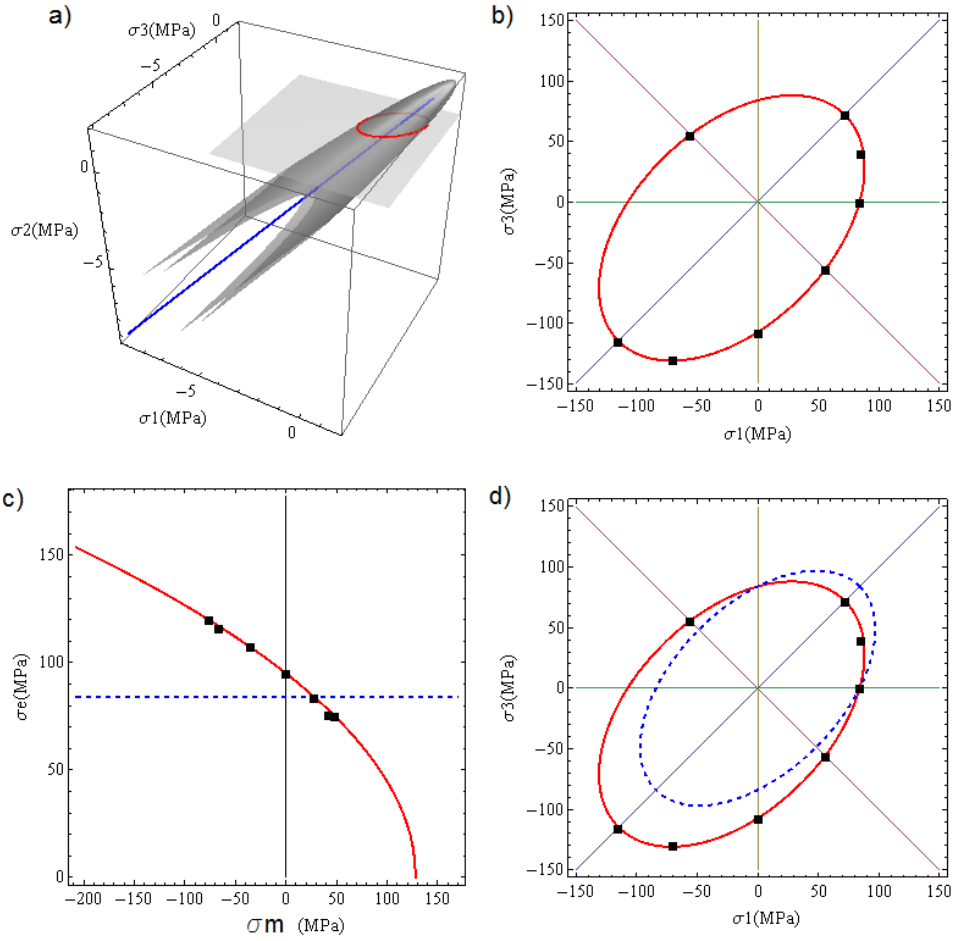

Figure 5.42: Presentation of the paraboloidal Burzyński condition in a) the space of principal stresses, b) the plane $\sigma_2 = 0$. Comparison with the HMH criterion presented in c) the meridional plane, d) the plane $\sigma_2 = 0$, applied for the polymethil methacrylate, experimental data collected by Altenbach & Tushtev, [Altenbach and Tushtev 2001].

Polymethil	quasi-static	$\varepsilon_{offset} = 0.002$
σ_Y^C	107	$\kappa = 1.28$
σ_Y^T	84	$R_B = 0.91$
τ_Y	55.7	[MPa]
HMH:	σ^Y= 84	τ_Y^H=54.8
	H=225	R=77

Table 5.23: Polymethil methacrylate - material data, [Altenbach and Tushtev 2001].

Epoxy compound - [Altenbach and Tushtev 2001]

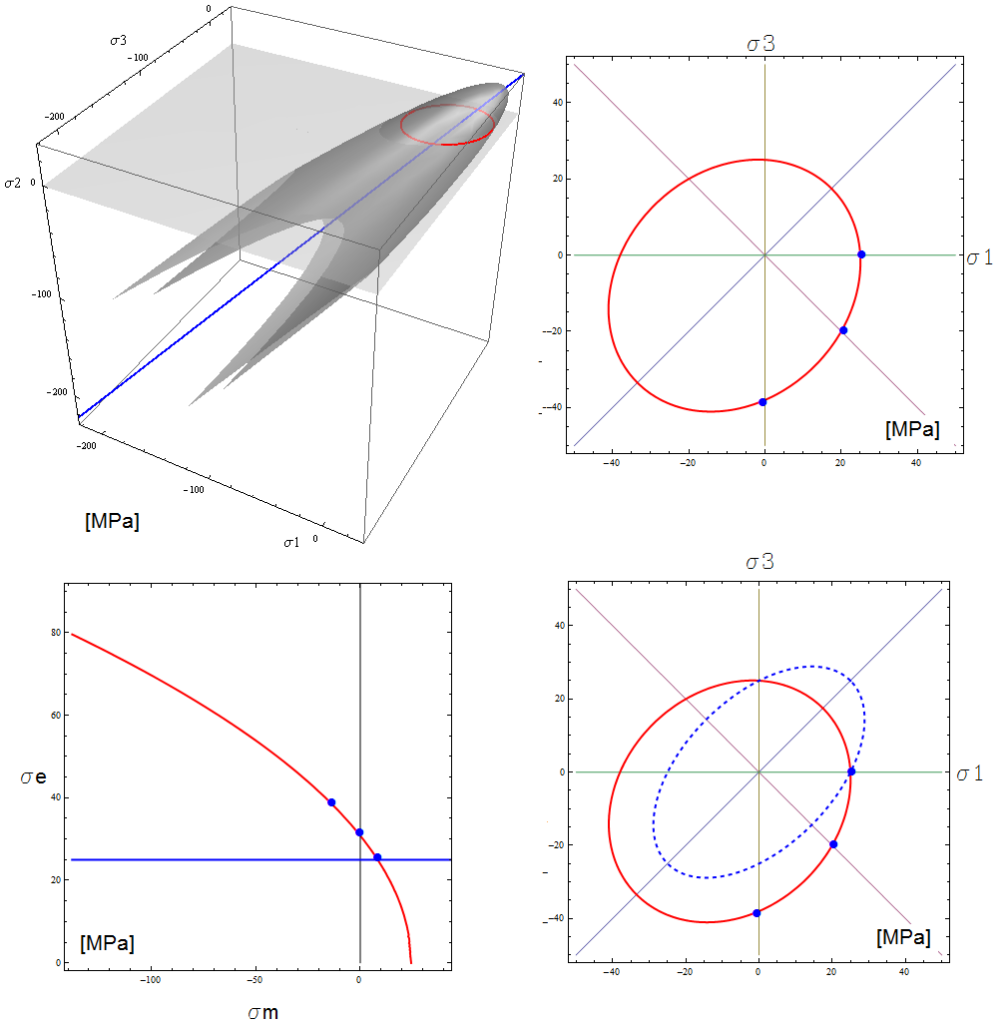

Figure 5.43: Presentation of the paraboloidal Burzyński condition in a) the space of principal stresses, b) the plane $\sigma_2 = 0$. Comparison with the HMH criterion presented in c) the meridional plane, d) the plane $\sigma_2 = 0$, applied for the epoxy compound, experimental data collected by Altenbach & Tushtev, [Altenbach and Tushtev 2001].

EPOXY COMPOUND	quasi-static	$\varepsilon_{offset} = 0.002$
σ_Y^C	38	$\kappa = 1.52$
σ_Y^T	25	$R_B = 0.375$
τ_Y	20	[MPa]
HMH:	σ^Y = 84	τ_Y^H=17.8
	H=61	R=26

Table 5.24: Epoxy compound - material data, [Altenbach and Tushtev 2001].

Polylactic acid (PLA)

In Fig. 5.44 there are presented results of the compression and tension test performed for PLA in one strain rate $\dot{\varepsilon} = 10^{-3}s^{-1}$. In the quasi-static tests there have been used specimens with a diameter and thickness of 6mm and 9mm. Whereas, in the tensile test the flat dog-bone specimens have been produced from the 5-mm-thick plates using a milling machine. A gage mark area has been of approximately 5mmx mm and a gage length of 10mm.

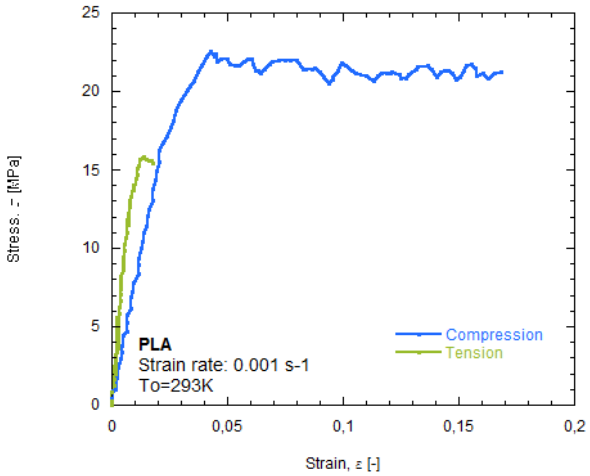

Figure 5.44: PLA - results of tensile and compressive test for a strain rate $\dot{\varepsilon} = 10^{-3}s^{-1}$, [Rusinek 2010].

In Fig. 5.45 there are presented results of double shear test - performed for a wide range of strain rates. The results are corrected to obtain the same Young's modulus.

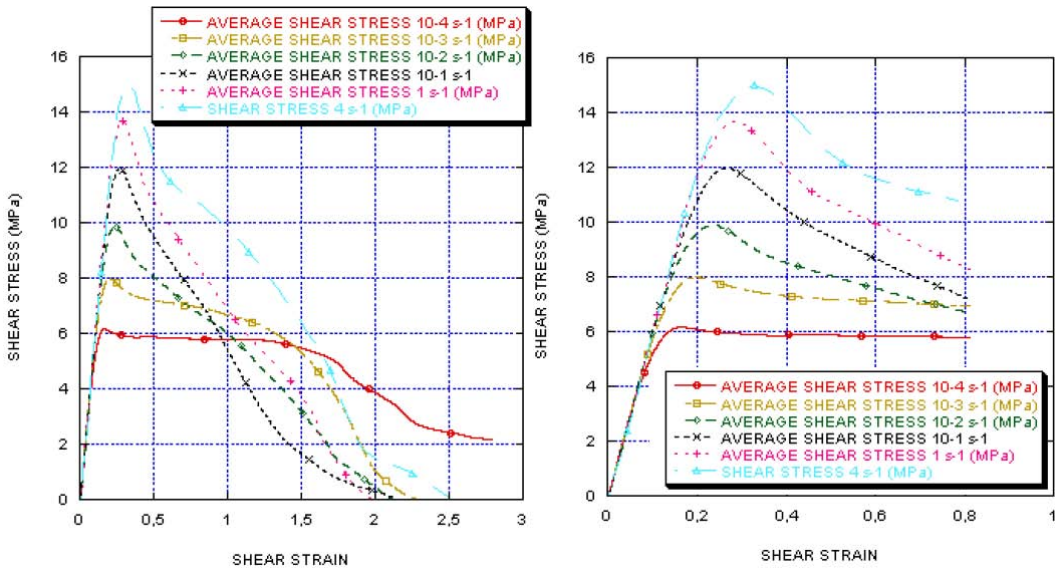

Figure 5.45: PLA - shear stress-shear strain ($\tau - \gamma$) curves for several strain rates, [Bouchart et al. 2010], [Bouchart et al. 2011].

Compressive test performed for a quasi-static strain rate allows to observe stable behaviour of a material without hardening. During the tensile test after tensile loading, the stress increased linearly with increasing strain - after showing the maximum stress, the stress decreased quickly. Cracks were observed and finally the specimens broke at the fracture point. The analyzed material is brittle.

The shear test results show a significant softening by a drop of shear stress-shear strain curves. The effect can be explained from a thermodynamic point of view by the transformation of a part of mechanical work into heat. According to this hypothesis, the heat spread through the material causing an increase in temperature which depends on the heat flux exchanged between the material and the surrounding. By considering that strain rate of the test is high enough not to allow the heat exchange to occur between the MDS specimen and the room environment (adiabatic) the increase in temperature causes a significant stress relaxation - especially for polymers, [Bouchart et al. 2010; 2011].

There is a large difference between levels of stresses for tension and compression - SD parameter is equals 1.4. Yield points are collected in the table.

It must be also noted that in Fig. 5.45 there are presented results of double shear test - Section 3.3, they are not accounted for the correction. The origin of correction are clarified in Section 3.3.2. Obtained curves must be multiplied by correction factors (3.10). If the value of yield strength in shear equals 8MPa, then after including correction factors it will be equals to 9.6MPa and this is value which is used to approximate the onset of the plasticity. Material data for polylactic acid - collected in Table 5.25.

There can be noticed the difference of SD parameter from 1, also, yield limit in shear is different then anticipated according to Eq. (4.11). Theses differences from the classical HMH approach allow to use Burzyński condition for anisotropic materials (4.45). Comparison between yield curves obtained with use of Eq. (4.45) and with HMH condition (4.10) allows to conclude that HMH is not a proper condition in case of PLA polymer. Data of tests performed for PLA polymer at strain rate $0.001s^{-1}$ are collected in the table. The origin of such differs could be contributed to brittle behaviour of the studied biopolymer. The amorphous structure is more sensitive on the fracture due to shear, what effects in the smaller value of a yield point in shear. The yield surface and yield curves for experimental data of PLA -Fig.5.46. The comparison between limit curves for PLA and PLA/PBAT polymers of different proportions - Fig. 5.51.

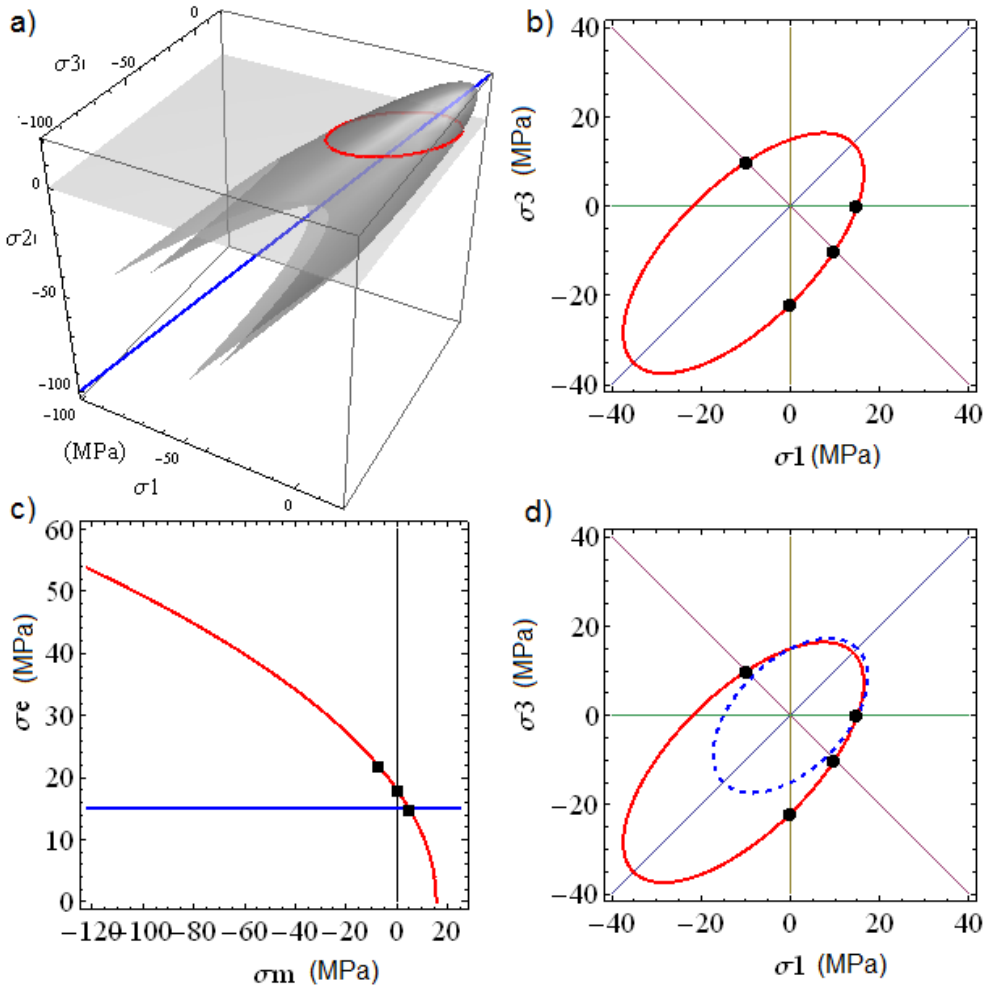

Figure 5.46: Presentation of the paraboloidal Burzyński condition Eq. (4.45) in a) the space of principal stresses, b) the plane $\sigma_2 = 0$. Comparison with the HMH criterion Eq. (4.10) presented in c) the meridional plane, d) plane $\sigma_2 = 0$, applied for the PLA.

PLA	$\dot{\varepsilon} = 10^{-3}$	max point
σ_Y^C	22	$\kappa = 1.46$
σ_Y^T	15	$R_B = 0.58$
τ_Y	9.6	[MPa]
HMH:	σ^Y= 15	τ_Y^H=10.48
	H=15.7	R=18.16

Table 5.25: Polylactic acid - material data, [Bouchart et al. 2010; 2011; Rusinek 2010].

5.5.2 Results for polycarbonate

Fig. 5.47 shows the PC yield strengths obtained in the compression test as a function of strain rate across wide range of strain rates, within the low to moderate rate regime. Experimental data collected by authors of [Shaban et al. 2007; Li and Lambros 2001; Siviour et al. 2005; Richeton et al. 2006; Mulliken and Boyce 2006; Rittel and Dorogoy 2008] and results obtained in the LaBPS - [Colard and Rusinek 2012].

In Fig. 5.47.b there are collected yield points from compressive tests in wide range of strain rates performed at the room temperature. Besides the results for PC obtained in the LaBPS, [Colard and Rusinek 2012], there are presented results found in the literature.

In [Richeton et al. 2006; Mulliken and Boyce 2006] there have been found the results for PC of compression test in the wide range of strain rate and temperature - Fig. 5.47. In [Shaban et al. 2007] there have been found data of behaviour of PC in tension and compression - Fig. 5.39. Due to the data collected by Shaban the SD parameter can be calculated. Knowing that SD parameter is independent from the strain rate, [Duckett et al. 1970], using values of yield strength in compression for different strain rates, [Richeton et al. 2006], and assuming that τ_Y fulfils relation (4.30) - it is possible to obtain yield surface for PC for different strain rates and temperatures.

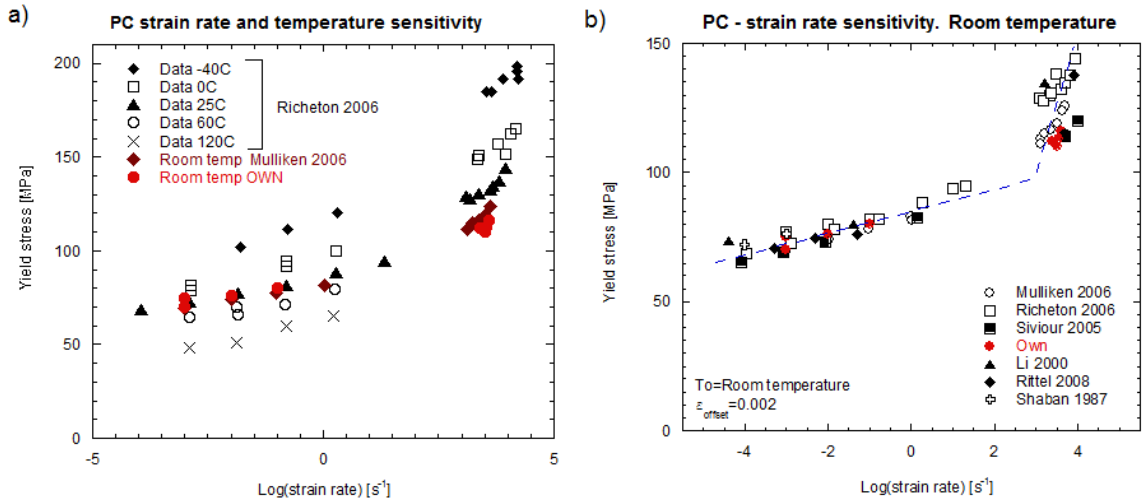

Figure 5.47: Polycarbonate. Strain rate and temperature sensitivity: a) for different strain rates and different temperatures, b) for different strain rates at the room temperature.

The yield stress is found to increase linearly with the logarithm of strain rate with a sharp increase in gradient at a strain rate of $10^3 s^{-1}$. It indicates that yield behavior can be explained and/or predicted in terms of a single activated process, [Mulliken and Boyce 2006]. PC shows a bilinear relationship, with increased strength at high strain rates and at low temperatures. This behaviour is attributed to the different molecular relaxations in the material. At high temperatures or low strain rates only the α relaxation (glass transition) plays a role in the polymer behaviour, whilst at low temperatures and high strain rates, the effect of the β relaxation is added to that of the α, [Bauwens-Crowet et al. 1972; Siviour et al. 2005]. The

authors of [Bauwens-Crowet et al. 1972] developed a model to explain such a behaviour of polymers. It is concluded that the increase in strength of PC at high strain rates is due to the β transition temperature being above room temperature at high rates. The yield behaviour is observed to transition to a regime of increasing strain rate sensitivity, beyond a threshold level particular to the polymers. Experiments indicated that this threshold level is determined both by temperature and strain rate, material transition could be induced by either decreasing the test temperature or increasing the test strain rate. The transition phenomenon was described in [Eyring 1936] (further followed by e.g. [Bauwens-Crowet et al. 1972]) who proposed the rate-activated processes acting to control the flow of a material. The theory assumes that processes are related to specific degrees of freedom of the polymer chains, thus, the transition observed in the yield behaviour is explained in terms of molecular-level motions. When a particular degree of freedom of the polymer chain suddenly becomes restricted at low temperatures and/or high strain rates, the overall material deformation resistance increases. At temperatures and strain rates below the transition threshold, only one restricted molecular motion - the α-process - contributes the material yield strength. Above the transition threshold the reported yield strength may be though of as a measure of the combined deformation resistance originating from two restricted motions - α and β.

The high-rate compressive behavior of polymers has been a topic of recent investigation, in contrast, the high-rate tensile behavior has not been thoroughly studied due to the complex nature of the experimental techniques. In [Sarva and Boyce 2007] there is given discussion on the tension test for PC in the low, moderate and high strain rates. In [Sarva and Boyce 2007] the effects of varying strain rate, overall imposed strain magnitude and specimen geometry on the mechanical response according tension test are examined. During the tensile test at high strain rates the large inhomogeneous elongation, single and double necking are observed.

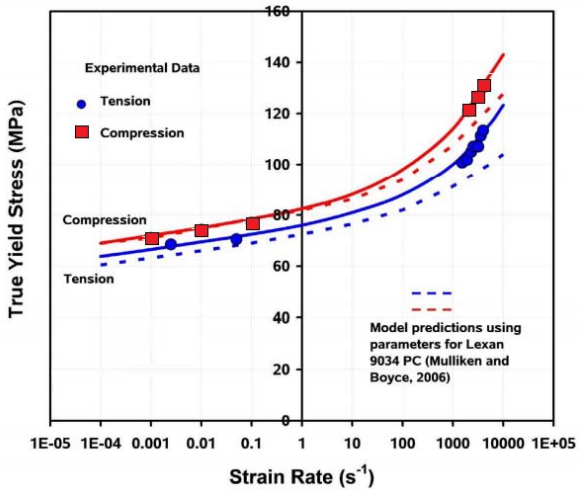

Figure 5.48: Polycarbonate. Comparison of the experimentally observed compressive and tensile yield stress values at various strain rates and the corresponding model predictions, [Sarva and Boyce 2007].

Fig. 5.48 shows a comparison of the experimentally observed true yield stress values in compression and tension for the investigated PC (and the corresponding model predictions discussed by authors). The yield stress values display an increased rate sensitivity at high rates

in both compression and tension. How it could be observed in the Fig. 5.48 the in tensile tests PC displays rate sensitivity. But at the same strain rates, the yield stress values are observed to be lower in tension than in compression, due to pressure sensitivity of yield. Compared to compression, the strain hardening in tension is more dramatic and occurs at lower strains, a result of the strain-induced alignment of polymer chains. In tension, the molecular chains align uniaxially along the axis of elongation, whereas, in compression, the chains align in a plane normal to axis of compression, giving the very different strain hardening behavior. The measurement of yield points values proved that SD parameter for PC is constant and equals 1.1.

In Fig. 5.49 there is presented the comparison between yield curves in the plane $\sigma_2 = 0$ and the meridional plane for yield points obtained in test performed in strain rates: $0.001s^{-1}$, $0.1s^{-1}$ and in dynamic strain rate: $1500s^{-1}$. Material data have been obtained in the LaBPS, [Colard and Rusinek 2012]. The SD parameter is assumed, as mentioned above, as equals to 1.1.

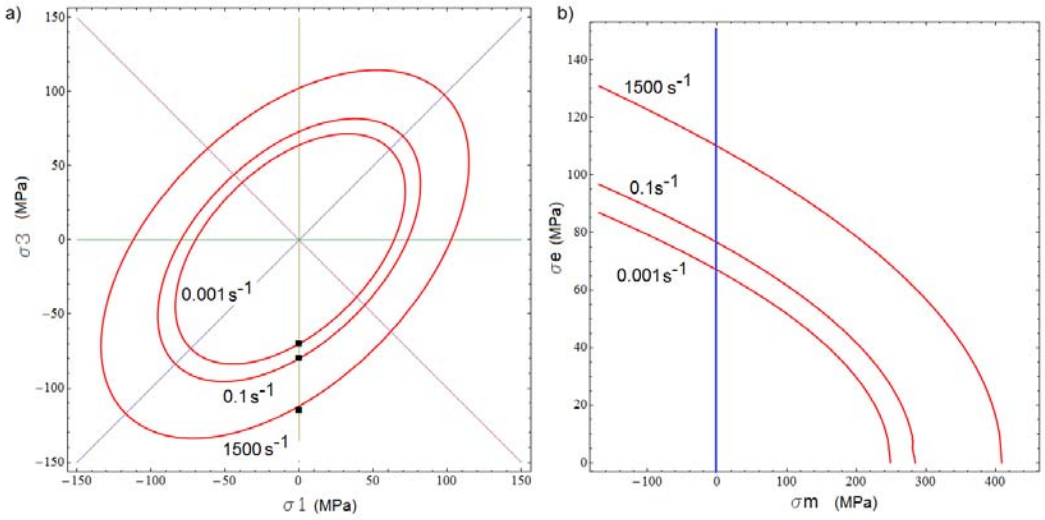

Figure 5.49: Comparison between yield curves in the plane $\sigma_2 = 0$ and the meridional plane for experimental results of PC for different strain rates: $0.001s^{-1}$, $0.1s^{-1}$, $1500s^{-1}$, [Colard and Rusinek 2012].

In Fig. 5.50 there are collected yield curves in the plane $\sigma_2 = 0$ built according to Burzyński criterion (4.34) for Polycarbonate, basing on data collected in Fig. 5.47. Judging on material data collected in Fig. 5.39 it can be concluded that SD parameter is different then 1 and in the further calculation it is close to 1.1. In Fig. 5.50 there are presented: 5.50.a) evolution of yield curve with increasing strain rate for test performed in the temp. 0°C, 5.50.b) 25°C and 5.50.c) 120°C. Then, in second column of the Fig. 5.50 there is given comparison between yield curves plot for one strain rate but obtained in different temperatures, so strain rates are equals in: Fig. 5.50.d) $\dot{\varepsilon} = 10^{-3}s^{-1}$, Fig. 5.50.e) $\dot{\varepsilon} = 10^{0}s^{-1}$, Fig. 5.50.f) $\dot{\varepsilon} = 10^{3}s^{-1}$.

It can be noticed that in the plane $\sigma_2 = 0$ the yield curves increase with the increasing strain rate in the constant temperature - Figs. 5.50.a-c. Whereas, in the constant strain rate rate the yield curves decrease with the increasing temperature - Figs. 5.50).d-f.

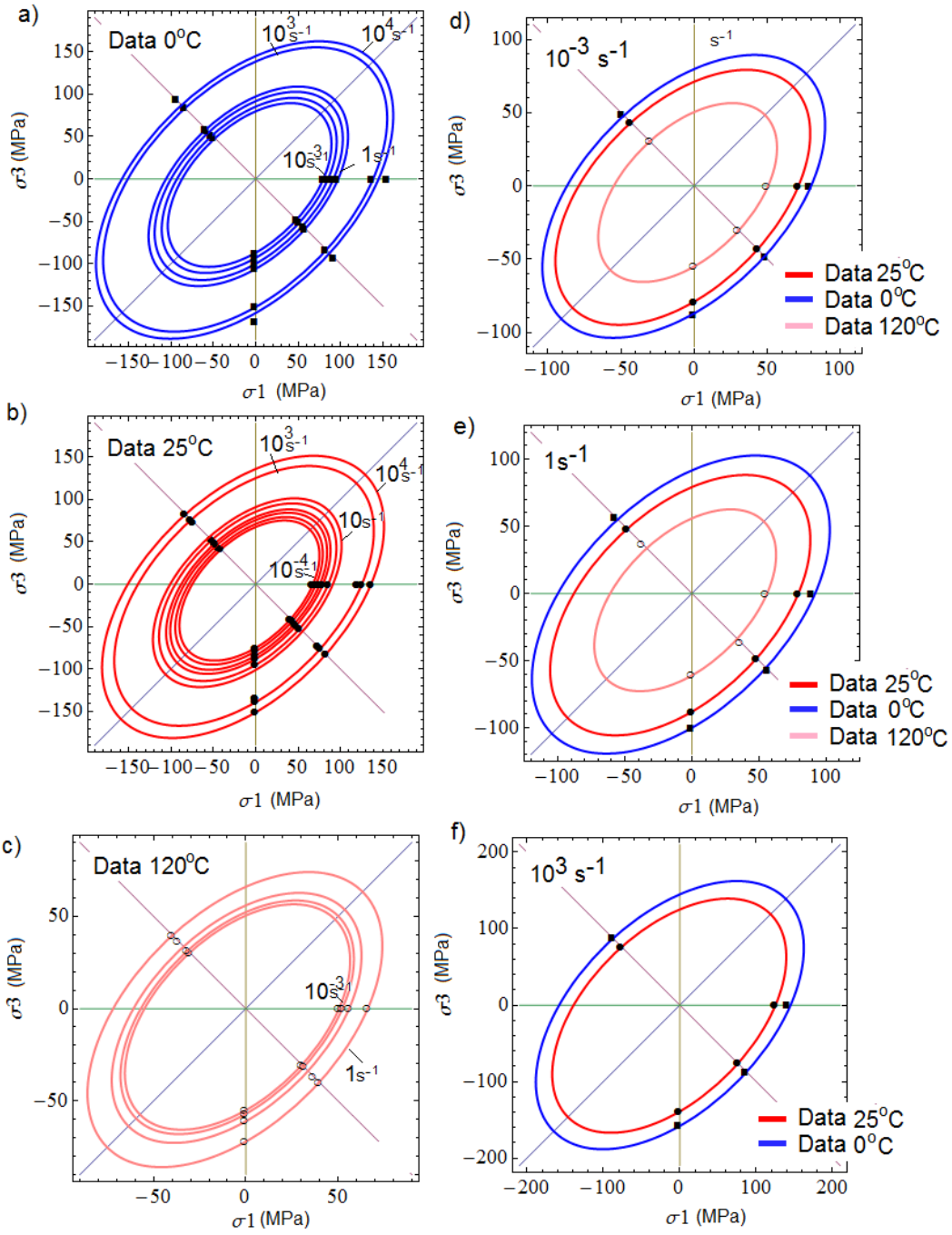

Figure 5.50: Evolution of the yield curves for PC in the plane $\sigma_2 = 0$, limit curves built with use of the Burzyński criterion (4.34). In the first column - constant temperatures: a) 25°C, b)60°C, c) 120°C; in the second column constant strain rates: d) $\dot{\varepsilon} = 10^{-3}s^{-1}$, e) $\dot{\varepsilon} = 10^{0}s^{-1}$, f) $\dot{\varepsilon} = 10^{3}s^{-1}$.

5.5.3 Results for PLA/PBAT

In [Nihida et al. 2011; Nishida et al. 2012] there are data concerning the stress-strain curves of PLA and PBAT polymer alloys measured at high strain rates ($600\check{}900s^{-1}$) using a split-Hopkinson pressure bar for tension test and a tensile split-Hopkinson bar. Also tests at low strain rates are performed, for compression loadings: $10^{-4}s^{-1} - 10^{1}s^{-1}$ and for tensile loading $10^{-4}s^{-1}$. The effects of the addition of dialkylperoxide (compatibilizing agent) and the mixing ratio of PLA and PBAT on the Young's modulus, the yield stress, the elongation at break, and fracture morphology are examined in the [Nishida et al. 2012]. The mixing ratios (weight fraction) of PLA and PBAT were 80:20, 70:30, and 60:40. In order to examine the effect of a compatibilizing agent, dialkyl peroxide was used at a weight ratio of one. Details of biopolymers structure, methodology of tests, results and conclusion are given in [Nihida et al. 2011; Nishida et al. 2012].

Plotting the yield curve - Fig. 5.51 - for material obtained only from PLA and comparing it with yield curves of composite polymers PLA/PBAT, it must be concluded that addition of Poly butylene adipate-co-terephthalate (PBAT) greatly improves the loading capacity of the resulted materials. The improvement of ductility must be also considerable.

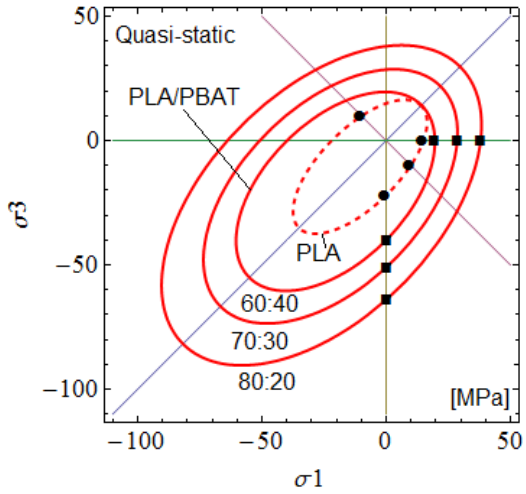

Figure 5.51: Comparison between yield curves for PLA/PBAT polymers with different proportion of compounds and pure PLA polymer (dashed curve).

In the present paragraph the influence of strain rate on the yield surface for PLA/PBAT polymers of different proportion of components is studied. Fig. 5.52 shows the effect of the strain rate on the yield stress, according to different proportion of the components - PLA/PBAT. For each polymer, the yield stress increased with the strain rate, what is commonly noticed in most polymers - e.g. [Richeton et al. 2006]. In case of PLA/PBAT it can be noticed the same tendency, both for tension and compression results, however - results in tension are less sensitive to strain rate - Fig. 5.52.b. Such behaviour could be explained by the strain-induced alignment of polymer chains. In tension, the molecular chains align uniaxially along the axis of elongation, whereas, in compression, the chains align in a plane normal to axis of compression, giving the very different strain hardening behavior, [Sarva and Boyce 2007].

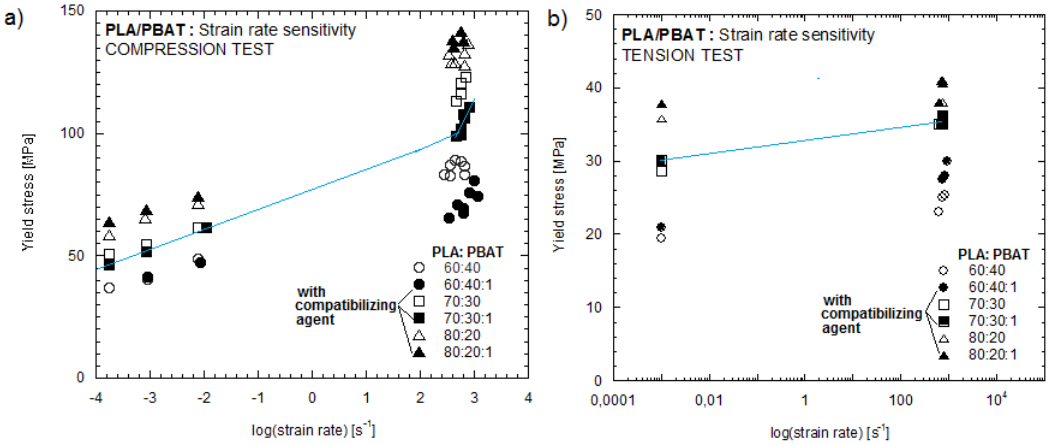

Figure 5.52: PLA/PBAT. Strain rate sensitivity in a) compression and b) tension test on maximum stress, basing on data found in [Nihida et al. 2011].

The histograms with comparison among results in quasi-static tensile test and dynamic tensile test are presented in Fig. 5.53. The bars shows that there is not much difference - around 5-7% - in the values of yield points in tension comparing between quasi-static and dynamic strain rate.

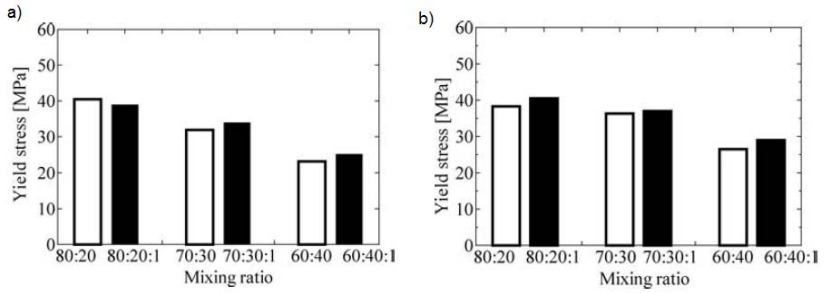

Figure 5.53: Effect of PBAT content on yield stress at a) low strain rate and b) high strain rate, [Nihida et al. 2011].

Components:	Quasi-static:			Dynamic:		
	κ	R	H	κ	R	H
60:40	2.04	28.81	12.8	3.4	46.1	11.84
60:40:1	1.9	29	14.73	2.6	43.78	14.52
70:30	1.78	38.45	22.4	3	60.62	17.5
70:30:1	1.79	40.31	22.66	3.27	65.17	17.26
80:20	1.68	49.31	31.2	3.52	71.35	17.68
80:20:1	1.86	49.11	25.93	3.34	74.94	19.51

Table 5.26: Comparison between SD parameter and characteristics of the yield surface - paraboloid of revolution due to Burzyński criterion Eq. (4.33).

Because in [Nihida et al. 2011; Nishida et al. 2012] there are no information about the results of shear test it is assumed that yield point in shear fulfils relation 4.30. To assess the yield state there is used the Burzyński criterion for isotropic materials (4.34) and the HMH

condition (4.10). In Fig. 5.54 the resulted yield curves for PLA/PBAT polymers of different proportions in dynamic and quasi-static strain rates are plotted. In the Table 5.26 there are collected parameters characterizing PLA/PBAT polymers in different proportions with or without addition of compatibilizing agent in dynamic and quasi-static strain rates. There are collected: - SD parameter κ, then as H - the distance from the octahedral plane to the peak of the paraboloid revolution, and as R - the radius of the circle which a paraboloid of revolution marks in the octahedral plane.

At the low strain rates the SD parameter decreases with the increasing content of PLA compound. Comparing SD for polymers with dialkylperoxide addition and without it: - the value of κ decreases 7% for 60:40:1 comparing to 60:40 proportion, it increases 10% for 80:20:1 and for 70:30:1 and 70:30 it is almost the same - 2% of difference. As for dynamic strain rates: generally, SD parameter increases with the increasing amount of PLA compound. But addition of dialkylperoxide makes the SD parameter smaller than its values for polymers without addition of compatibilizing agent. In Fig. 5.54 there is plotted the comparison between yield curves in the plane $\sigma_2 = 0$ and in the meridional plane in quasi-static and dynamic range of strain rate.

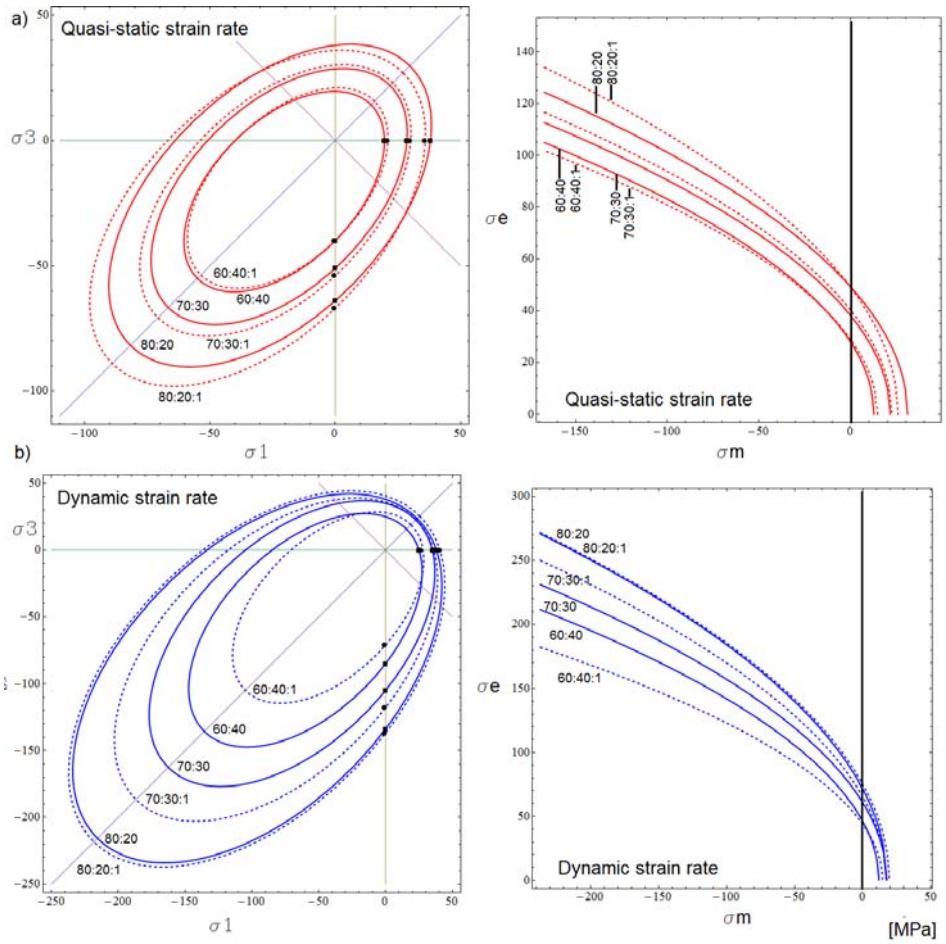

Figure 5.54: Yield curves in the plane $\sigma_2 = 0$ and the meridional plane for polymers with different proportions of PLA/PBAT for a) low strain rate and b) high strain rate. With dashed curves the polymers with addition of dialkylperoxide are indicated.

Chapter 6

Conclusions

The global overview and reflexion are made on the most important findings and achievements of the Thesis. An evaluation of the pre-defined objectives from the introductory Chapter is reported. In addition, the ideas and suggestions for future work are given.

The doctoral Thesis proposes physically consistent description of material's yielding, based on the results of experiments coupled with FEM simulations. The theoretical approach is based on the Burzyński yield hypothesis, Chapter 4.5. The material effort hypothesis is derived from the definition of variable limit energy of volume change and distortion, [Burzyński 2009]. In particular cases the yield criteria include asymmetry of elastic range Eq. (4.34) and, in extended form, it is applicable to initially anisotropic materials, Eq. (4.38).

The original Burzyński's proposal to describe yielding of the initially anisotropic materials is expressed by the multi-surface, therefore, in order to avoid corners a methodology of obtaining a smooth surface has been developed, Eqs. (4.40-4.44). The proposed extended formulation of the criterion, Eq. (4.45) allows to include phenomenological behaviour of materials as the function depending on the strain and strain rate, Eq. (4.48).

As a part of numerical modeling approach, the numerical analyses were performed in order to correct the inaccuracies of presented experimental results, Chapter 3. Additionally, the isotropic Burzyński condition Eq. (4.34) was implemented in finite element method via UMAT (user subroutine for ABAQUS). The exemplary results of calculations for notched specimen were presented in Section 4.6.1.

The versatility of the proposed yield description was shown by application to materials with amorphous structure and different cubic crystal systems: face-centered cubic crystal structure (FCC) and body-centered cubic crystal structure (BCC). As examples there were examined the following materials: - a FCC-structure type material - OFHC Cu, Oxygen Free High Conductivity Copper, a BCC-structure type material - E335, non alloy steel of high strength and example of the amorphous materials - polycarbonate (PC) and biopolymers (PLA/PBAT). For theses materials the throughout analyses were performed in order to obtain microstructural and mechanical properties via wide range of strength tests under various loading conditions, Chapters 2 and 5. There was also given an example application of criterion for

hexagonal close-packed (HCP) material - Mg Alloy AZ31, [Yoshikawa et al. 2008] for which due to the process of twinning the SD parameter is smaller than 1.

The experiments carried out for the analysed metallic materials and polymers, in quasi-static and dynamic strain rates allowed to obtain different values of yield points depending on the loading conditions. Besides, traditional quasi-static tension, compression tests and the tests of double shear, the complex stress state test and biaxial compression test were described and performed. The results allowed to obtain additional data providing possibility of more accurate description of the yield surface. The numerical analysis in FEM was prepared to correct inaccuracies and understand more deeply the occurring in material processes.

The number of exemplary data found in literature of materials sensitive to pressure and/or initially anisotropic were analysed is Section 5.5. For exemplary data of grey cast iron, metallic alloys, Ti-alloy and Mg-alloy the proposed in Chapter 4.5 yield criteria were validated and resulting yield surfaces and yield curves were visualized. Due to this, it was proved that proposed criteria give accurate approximation of yielding state in comparison to other commonly used yield conditions. The example of yield curves in plane $\sigma_2 = 0$ is given in Fig. 6.1. All examples were discussed in details in Chapter 5.

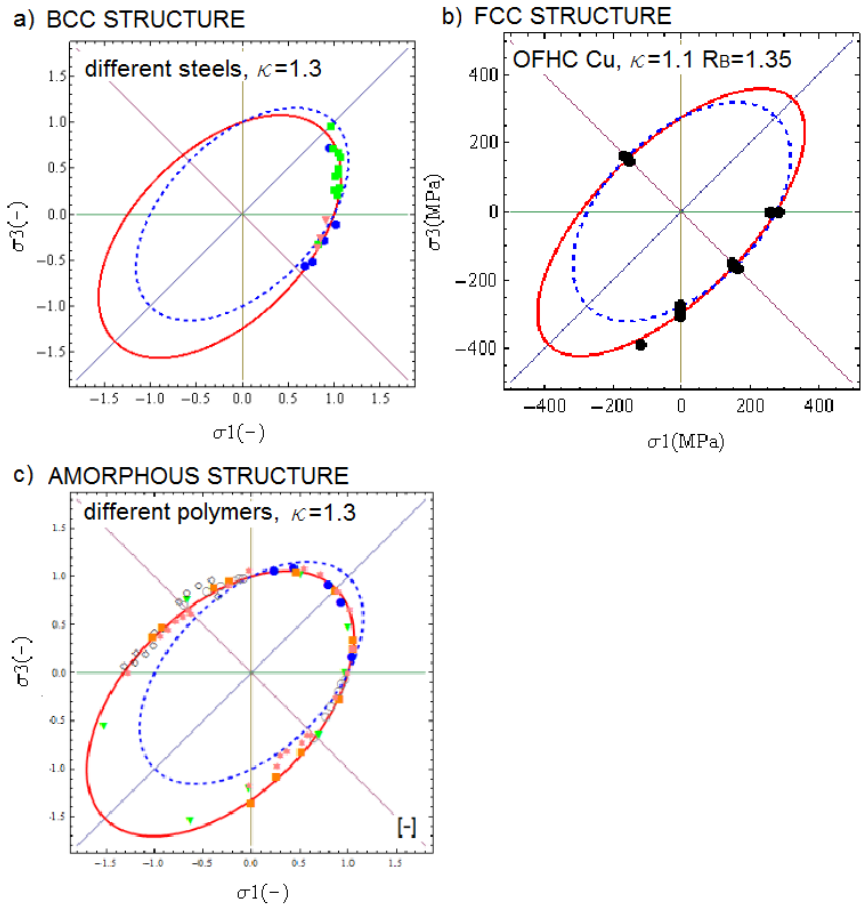

Figure 6.1: Application of Burzyński criteria to materials with different crystalline structure: a) BCC-structure type materials, b)FCC-structure type materials, c) amorphous materials.

Basing on discussion in Chapters 4.5 and 5, it can be summed up that due to Burzyński criteria the yield state of:
- BCC-structure type materials, Fig. 6.1.a, as example - different metals, [Theocaris 1995];
- FCC-structure type materials, Fig. 6.1.b, as example - OFHC Cu;
- amorphous materials, Fig. 6.1.c, as example - different polymers, [Theocaris 1995]
is properly described. Detailed formulations of proposed hypothesis include SD effect and texture influence. As it was presented in Chapter 5 on many examples, the resulting criteria seems to be an universal and widely applicable method to obtain description of the onset of plasticity.

The Thesis demonstrated the necessity of providing an integrated view over experiments and numerical simulation in order to obtain the description of onset of plasticity. To fulfill this aim, a specific methodology has been developed - the procedure which combines experimental techniques with numerical simulations supported by the accurate description of the material behaviour. Thus, investigation performed along with such approach allows to obtain assumed in the objectives of Thesis.

The original contributions of the Thesis can be outlined in the following points.

- Performing a wide experimental investigation in different loading conditions (compression, tension, shear, biaxial compression, complex stress state) in a wide range of strain rates allows to obtain the throughout mechanical characterization of the chosen materials (OFHC Cu, E335, PC and PLA/PBAT polymers).
- Designing, evaluation of the methodology and validation of the biaxial compression test; elaborating the model describing influence of friction during the biaxial compression process.
- The extension of the Burzyński criterion for initially anisotropic materials accounting for strain and strain rate.
- Elaborating the algorithms with use of the Wolfram Mathematica allowing to obtain and visualize the yield surface in the space of principal stresses, yield curves in the plane state of stress, the meridional plane and octahedral plane for the isotropic materials with SD effect and materials initially anisotropic.
- Preparation of the examples of yield surface and curves for a wide group of materials.
- Application of UMAT - user subroutine in Abqus/Standard implementing the isotropic Burzyński criterion.

The outlined conclusions could be relevant for different industrial applications, including implementation of elaborated Burzyński criteria in commercial FEM programs, what allow to broaden the range of application of the FEM programs. Also, an introduction of the new methodology of biaxial compression test in experimental procedures could help to verify the results of standard investigation. The implementation of algorithms visualizing yielding state can be an interesting method of graphical representation of yield state.

.

Below the publications related to this doctoral Thesis are listed:

- T. Frąś, Z. Nowak, P. Perzyna, R.B. Pęcherski: Identification of the model describing viscoplastic behaviour of high strength metals, Inverse Problems in Science and Engineering, 19, No 1, 17-30, 2011;
- T. Frąś, R.B. Pęcherski: Applications of Burzyński hypothesis of materials effort for isotropic solids, Mechanics and Control, 25, No 2, 45-50, 2010;
- T. Frąś, Z. Kowalewski, R.B. Pęcherski, A. Rusinek: Applications of Burzyński failure criterion. Part I. isotropic materials with asymmetry of elastic range, Engineering Transactions, 58, No 1-2, 3-13, 2010
- T. Frąś, A. Rusinek, R.B. Pęcherski, R. Bernier: Biaxial compression loading for initial anisotropy description of material, application to OFHC Copper- in preparation

Seminars and conferences:

- ECCOMAS International Symposium IPM 2009 Inverse Problems in Mechanics of Structures and Materials, 23-25.04.2009 r. Rzeszów - Łańcut, Poland; T. Frąś, Z. Nowak, P. Perzyna, R.B. Pęcherski: Identification of the model describing viscoplastic behaviour of high strength metals;

- 37th SOLID MECHANICS CONFERENCE, 6-10.09.2010 Warszawa, Poland; T. Frąś, A. Rusinek, R.B. Pęcherski: Experimental characterization and analytical modeling of the thermo-viscoplastic behaviour of metallic solids with use of static and dynamic tests coupled with in situ thermographic observations;

- Workshop: Constitutive modeling in applications for industrial processes, 1-3.09.2010 Kraków, Poland; T. Frąś, A. Rusinek, R.B. Pęcherski: Experimental validation of Burzyński paraboloid yield criterion;

- Zintegrowane Studia Podstaw Deformacji Plastycznej Metali PLASTMET 2010, 30.11-03.12.2010 Łańcut, Poland; T. Frąś, G. Vadillo, A. Rusinek, J. Fernández-Sáez, R.B. Pęcherski: Doświadczalna i numeryczna weryfikacja paraboloidalnego warunku plastyczności Burzyńskiego w procesie rozciągania okrągłych prętów z karbem ze stali konstrukcyjnej;

- Seminar, 17.11. 2010 ENIM Metz, France: Experimental and numerical verification of paraboloidal Burzyński yield condition in the process of tension of notched round bars of structural steel;

- Seminar, 15.03. 2011 AGH Kraków, Poland: Modelowanie powierzchni plastyczności metali z asymetrią zakresu sprężystego na podstawie badań doświadczalnych i numerycznej symulacji dla obciążeń quasi-statycznych i dynamicznych;

- International Conference High Speed Machining, 20-23.06.2011 Metz, France; T. Frąś, M. Nowak, Z. Nowak, R.B. Pęcherski, A. Rusinek: Analysis of strength diffrential effect and anisotropy in metal forming problems;

- Seminar, 25.11. 2011 ENIM Metz, France: Modeling of plastic yield surface of metals accounting for asymmetry of elastic range on the basis of experiments and numerical simulation in application for quasi-static and dynamic loading;

- Workshop: Dynamic Behavior of Materials and Safety of Structures, 2-4.05.2012, Poznan, Poland, T. Frąś, A. Rusinek, R.B. Pęcherski: Influence of moderate strains and strain rates on the yield surface of OFHC Copper;

- Seminar, 06.05.2012, IPPT PAN, Warszawa, Poland: Badania wytrzymałościowe miedzi beztlenowej wysokiej przewodności - OFHC Cu;

- Seminar,. 24.05. 2012, AGH, Kraków, Poland: Badania wytrzymałościowe miedzi beztlenowej wysokiej przewodności - OFHC Cu;

- 38th SOLID MECHANICS CONFERENCE, 27-31.08, 2012 Warszawa, Poland; T. Frąś, A. Rusinek, R.B. Pęcherski: Experimental investigation of the influence of moderate strains and strain rates on the yield surface of OFHC Copper;

- Seminar, 24.10.2012, Faculteit Ingenieurswetenschappen en Architectuur, Universitet Gent, Gent, Belgium: Biaxial compression test - experiment, simulation and modeling.

Appendixes

Appendix 1 - Constitutive models of strain rate sensitivity

Appendix 2 - Algorithm of Burzyński paraboloidal criterion

Appendix 3 - Project of biaxial compression set-up

.

Appendix 1 - Constitutive models of strain rate sensitivity

In this part are presented models which were used in the Thesis to describe material behaviour in wide strain rate ranges.

The Johnson-Cook model, [Johnson and Cook 1983]

A well-characterized equation of state model was developed by Johnson and Cook, [Johnson and Cook 1983]. The relation of state model is often used due to its simplicity and the availability of parameters for various materials of interest. The Johnson-Cook relation, [Johnson and Cook 1983]:

$$\sigma(\varepsilon_p, \dot{\varepsilon}_p, T) = \left[A + B\left(\varepsilon_p\right)^n\right]\left[1 + C\ln\left(\frac{\dot{\varepsilon}_p}{\dot{\varepsilon}_0}\right)\right]\left[1 - \left(\frac{T - T_0}{T_m - T_0}\right)^m\right] \tag{6.1}$$

where ε_p is the plastic strain, $\dot{\varepsilon}_p$ is strain rate, $\dot{\varepsilon}_0$ is the reference strain rate, A is the yield limit in compression, B, n are the material parameters, C is the sensitive parameter for strain rate, T is the current temperature, T_0 is the ambient temperature, T_m is the melting temperature, m is the material coefficient.

The Johnson–Cook equation, which is obtained from the phenomenological observations of experimental data at relatively low strain rates, cannot well describe the dynamic thermo-mechanical response of many materials at high strain rates, especially under the situations of high or low temperatures

The models applied for modelling materials behaviour in the dynamic strain rates

Macroscopic plasticity in metals is the result of dislocations moving through the crystal lattice. Thermal activation aids dislocation gliding, decreasing the intrinsic lattice friction in the case of most BBC metals and decreasing the strength of obstacles in the case of many FCC metals, [Rodríguez-Martínez 2010]. In both cases, thermal activation reduces the applied stress required to force the dislocation past obstacle, [Lennon and Ramesh 2004]. Consequently, the metals strain rate sensitivity is depended on its structure. There is needed to distinguish constitutive models for FCC and BCC metals.

In the Thesis dislocation-based constitutive relations founded on the concepts of thermal activation analysis and dislocation dynamics with application to FCC and BCC metallic alloys are used: the Rusinek-Klepaczko model (RK) or the Modified Rusinek-Klepaczko model (MRK), [Rodríguez-Martínez 2010], [Rusinek and Klepaczko 2001]. The RK model is suitable for describing the behaviour of metals with rate sensitivity independent of plastic strain. The MRK is suitable for defining the behaviour of metals showing dependence of strain on the volume thermally activated.

The Rusinek-Klepaczko model (RK) and Modified Rusinek-Klepaczko model (MRK), [Rusinek and Klepaczko 2001; Rodríguez-Martínez 2010]

Basing on the J_2 theory, the flow stress of a material $\sigma(\varepsilon_{pl}, \dot{\varepsilon}_{pl}, T)$ can be decomposed into equivalent athermal stress σ_μ and equivalent thermal stress σ^*, [Seeger 1957; Klepaczko 1975; Zerilli and Armstrong 1987], [Follansbee and Kocks 1988; Nemat-Nasser et al. 1998a], [Voyiadjis and Abed 2005; Voyiadjis and Almasri 2008]. The constitutive descriptions RK and MRK are based on the additive decomposition of the total stress, (6.2). Their advantage is a favourable macroscopic definition of the material behaviour under different types of solicitation and a formulation suitable for its implementation into FE codes. Models are noted for its versatility and easy calibration procedure, [Rodríguez-Martínez et al. 2009].

Additive stress distribution:

$$\sigma(\varepsilon_{pl}, \dot{\varepsilon}_{pl}, T) = \frac{E(T)}{E_0}\Big[\sigma_\mu(\varepsilon_{pl}) + \sigma^*(\varepsilon_{pl}, \dot{\varepsilon}_{pl}, T)\Big] \tag{6.2}$$

Effective stress, thermally activated, depending on the strain rate, σ^*:

- in the RK model:

$$\sigma^*(\dot{\varepsilon}_{pl}, T) = \sigma_0^*\Big[1 - D_1\Big(\frac{T}{T_m}\Big)\log\Big(\frac{\dot{\varepsilon}_{max}}{\dot{\varepsilon}_{pl}}\Big)\Big]^{\frac{1}{p}} \tag{6.3}$$

- or in the MRK model:

$$\sigma^*(\varepsilon_{pl}, \dot{\varepsilon}_{pl}, T) = B(\dot{\varepsilon}_{pl}, T)\cdot\varepsilon_{pl}^{n(\dot{\varepsilon}_{pl},T)}\cdot\Big[1 - D_1\Big(\frac{T}{T_m}\Big)\log\Big(\frac{\dot{\varepsilon}_{max}}{\dot{\varepsilon}_{pl}}\Big)\Big]^{\frac{1}{p}} \tag{6.4}$$

Internal stress, athermal, σ_μ :
- in the RK model:

$$\sigma_\mu(\varepsilon_{pl}, \dot{\varepsilon}_{pl}, T) = B(\dot{\varepsilon}_{pl}, T)\Big(\varepsilon_{off} + \varepsilon_{pl}\Big)^{n(\dot{\varepsilon}_{pl},T)} \tag{6.5}$$

- or in the MRK model:

$$\sigma_\mu = \sigma_Y \tag{6.6}$$

Young modulus:

$$E(T) = E_0\Big\{1 - \Big(\frac{T}{T_m}\Big)\exp\Big[\theta^*\Big(1 - \frac{T_m}{T}\Big)\Big]\Big\}$$

and:

$$B(\dot{\varepsilon}_{pl}, T) = B_0\Big[\Big(\frac{T}{T_m}\Big)\log\Big(\frac{\dot{\varepsilon}^{max}}{\dot{\varepsilon}_{pl}}\Big)\Big]^{-\nu} \tag{6.7}$$

Coefficient of plastic hardening:

$$n(\dot{\varepsilon}_{pl}, T) = n_0\Big[1 - D_2\Big(\frac{T}{T_m}\Big)\log\Big(\frac{\dot{\varepsilon}_{pl}}{\dot{\varepsilon}_{min}}\Big)\Big] \tag{6.8}$$

where:
- σ_0^* - effective stress at 0K,
- $D_1, D_2, p, n_0, B_0, \nu$ - material constant temperature-dependent,

- $\dot{\varepsilon}_{max}$ - maximum strain rate possible in the analysis,
- $\dot{\varepsilon}_{min}$ - minimum strain rate possible for the analysis,
- ε_{off} - offset strain
- E_0 - Young modulus in temperature 0K,
- θ^* - constant dependent on the thermal softening of the crystal lattice: for metal of type BCC $\theta^* = 0,6$ and type FCC $\theta^* = 0,9$.

Relation for the RK model for metals of BCC structure is given by (6.2), where the internal stress is given by (6.5) and the effective stress by (6.3) - Eq. (6.9).

$$\begin{aligned}\sigma(\bar{\varepsilon}^p, \dot{\bar{\varepsilon}}^p, T) &= B(\dot{\bar{\varepsilon}}^p, T)\Big(\varepsilon_0 + \bar{\varepsilon}^p\Big)^{n(\dot{\bar{\varepsilon}}^p, T)} \\ &\quad + B(\dot{\bar{\varepsilon}}^p, T) \cdot (\bar{\varepsilon}^p)^{n(\dot{\bar{\varepsilon}}^p, T)} \cdot \Big[1 - D_1\Big(\frac{T}{T_m}\log\frac{\dot{\varepsilon}^{max}}{\dot{\bar{\varepsilon}}^p}\Big)\Big]^{\frac{1}{p}}\end{aligned} \tag{6.9}$$

Relation for the MRK model for metals of FCC structure is given by the equation (6.2) with the internal stress given by the relation (6.6) and the effective stress by (6.4) - Eq. (6.10).

$$\sigma(\bar{\varepsilon}^p, \dot{\bar{\varepsilon}}^p, T) = Y + B(\dot{\bar{\varepsilon}}^p, T) \cdot (\bar{\varepsilon}^p)^{n(\dot{\bar{\varepsilon}}^p, T)} \cdot \Big[1 - D_1\Big(\frac{T}{T_m}\log\frac{\dot{\varepsilon}^{max}}{\dot{\bar{\varepsilon}}^p}\Big)\Big]^{\frac{1}{p}} \tag{6.10}$$

where $B(\dot{\bar{\varepsilon}}^p, T)$ and $(\dot{\bar{\varepsilon}}^p, T)$ are given by (6.7) i (6.8).

The Molinari-Ravichandran model (MR), [Molinari and Ravichandran 2005], [Durrenberger et al. 2008]

The proposed phenomenological constitutive model is based on the physically observed phenomena that any characteristic length associated to the microstructure of a metal (for instance the cell size) undergoes a reduction with increasing strain for temperatures which are not too high in relation to its melting point, [Durrenberger et al. 2008].

In the MR model, for the BCC metals, the basic assumption is is additive property of stress tensor (6.2), with the the assumption that $E(T) = E_0 = E$. Then:

$$\sigma_\mu = \sigma_0(d)\Big(\frac{1}{\delta}\Big) \tag{6.11}$$

$\sigma_0(d)$ - characteristic for the initial value of the resistance stress, dependent on average grain diamter d. Effective length ratio δ depends on the deformation, according to the relation:

$$\frac{d\delta}{d\varepsilon} = -\frac{\delta_r}{\delta_s}\Big[\delta^2 - \delta_s\delta\Big] \tag{6.12}$$

where δ_r is dimensionless characteristic length scale refinement rate parameter, and δ_s is the saturation size of the characteristic length scale at relatively large strains. Both parameters are

dependent on the strain rate and temperature:

$$\delta = \frac{\delta_s}{1-(1-\delta_s)\exp(-\delta_r \varepsilon)} \tag{6.13}$$

$$\delta_r = \delta_{r0}\Big(1 + a_r\Big(\frac{\dot{\varepsilon}}{\dot{\varepsilon}_{r0}}\Big)^{\xi r}\Big(\frac{T}{T_0}\Big)^{-vr}\Big) \tag{6.14}$$

$$\delta_s = \delta_{s0}\Big(1 - a_s\Big(\frac{\dot{\varepsilon}}{\dot{\varepsilon}_{s0}}\Big)^{\xi s}\Big(\frac{T}{T_0}\Big)^{-vs}\Big) \tag{6.15}$$

To identify the model the 10 parameters must be found.

Effective stress σ^* is expressed by the relation:

$$\sigma^* = \sigma_{ref}\Big\langle a - bT\ln\Big(\frac{\dot{\varepsilon}_0}{\dot{\varepsilon}}\Big)\Big\rangle^{\frac{1}{m}} \tag{6.16}$$

σ_{ref} - the reference stress, typically $\sigma_{ref} = 1$, $\dot{\varepsilon}_0$ - reference strain rate, a, b - material constants, m - instantaneous rate sensitivity, usually m is close to 0.5.

Thus, for the BCC type metals, the MR model is as follows:

$$\sigma(\varepsilon_{pl}, \dot{\varepsilon}_{pl}, T) = \sigma_0(d)\Big(\frac{1}{\delta}\Big) + \sigma_{ref}\Big\langle a - bT\ln\Big(\frac{\dot{\varepsilon}_0}{\dot{\varepsilon}}\Big)\Big\rangle^{\frac{1}{m}} \tag{6.17}$$

For the FCC metals:

$$\sigma(\varepsilon_{pl}, \dot{\varepsilon}_{pl}, T) = \hat{\sigma}(d)\Big(\frac{\delta_0}{\delta}\Big)\Big(\frac{\dot{\varepsilon}}{\dot{\varepsilon}_0}\Big)^{\frac{1}{m}} \tag{6.18}$$

Appendix 2 - Algorithm of Burzyński paraboloidal criterion

Burzyński criterion for isotropic materials with asymmetry of elastic range $\sigma_Y^C \neq \sigma_Y^T$

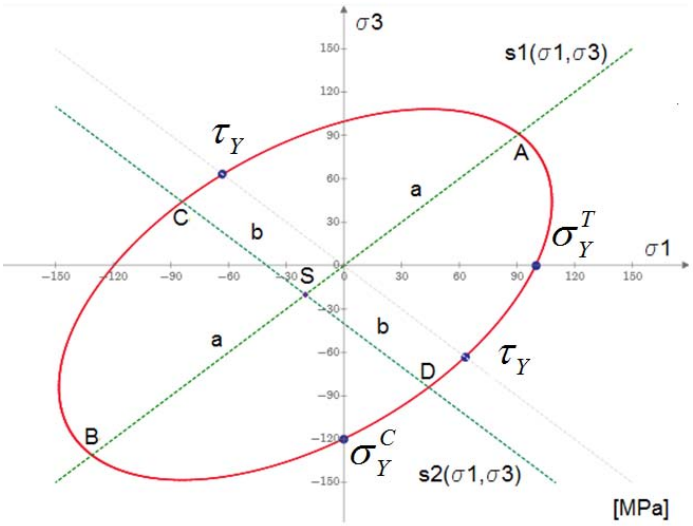

1. Formulation of the yield curve in the 3-d space of principal stresses $(\sigma_1, \sigma_2, \sigma_3)$ where σ_1 is the maximum principal stress, σ_2 is the medium principal stress, σ_3 is the minimum principal stress

$$f(\sigma_1,\sigma_2,\sigma_3) = \sigma_1^{\,2} + \sigma_2^{\,2} + \sigma_3^{\,2} - \left(\sigma_2\sigma_3 + \sigma_1\sigma_2 + \sigma_1\sigma_3\right) + \left(\sigma_Y^C - \sigma_Y^T\right)\left(\sigma_1 + \sigma_2 + \sigma_3\right) - \sigma_Y^C\sigma_Y^T$$

where σ_Y^C is the yield strength in the compression, σ_Y^T is the yield strength in tension, τ_Y yield strength in shear fulfilling relation $\tau_Y = \sqrt{\dfrac{\sigma_Y^C\sigma_Y^T}{3}}$

In the plane $\sigma_2 = 0$ the criterion has a form:

$$f(\sigma_1,\sigma_3) = \sigma_1^{\,2} + \sigma_3^{\,2} - \sigma_1\sigma_3 - \left(\sigma_Y^C - \sigma_Y^T\right)\left(\sigma_1 + \sigma_3\right) - \sigma_Y^C\sigma_Y^T$$

2. Calculating the centre of symmetry, S:

$$\begin{cases} \dfrac{d}{d\sigma_1} f(\sigma_1,\sigma_3) = 0 \\ \dfrac{d}{d\sigma_3} f(\sigma_1,\sigma_3) = 0 \end{cases} \rightarrow \; S = \left(S_x, S_y\right) \quad \text{and} \; S_x = S_y$$

3. Calculating the intersection of the ellipse with the axis of symmetry.

The axis of symmetry are given:

$$s_1(\sigma_1,\sigma_3)=\frac{d}{d\sigma_1}f(\sigma_1,\sigma_3)+\frac{d}{d\sigma_3}f(\sigma_1,\sigma_3)=0$$

$$s_2(\sigma_1,\sigma_3)=\frac{d}{d\sigma_1}f(\sigma_1,\sigma_3)-\frac{d}{d\sigma_3}f(\sigma_1,\sigma_3)=0$$

and:

$$s_1(\sigma_1,\sigma_3)=\sigma_1-\sigma_3$$

$$s_2(\sigma_1,\sigma_3)=\sigma_1+\sigma_3+2(\sigma_Y^C-\sigma_Y^T)$$

The intersections of the axis of symmetry must give the centre of symmetry.

4. Solving the equations

$$\begin{cases} f(\sigma_1,\sigma_3)=0 \\ s_1(\sigma_1,\sigma_3)=0 \end{cases} \text{ and } \begin{cases} f(\sigma_1,\sigma_3)=0 \\ s_2(\sigma_1,\sigma_3)=0 \end{cases}$$

gives four points of the intersections of the ellipses with the axis (A,B,C,D):

$$A=(A_0,A_1),\qquad B=(B_0,B_1)$$

$$C=(C_0,C_1),\qquad D=(D_0,D_1)$$

The semi-major and semi-minor axis of the ellipse (a,b):

$$a=\sqrt{(A_0-S)^2+(A_1-S)^2}=\sqrt{(B_0-S)^2+(B_1-S)^2}$$

$$b=\sqrt{(C_0-S)^2+(C_1-S)^2}=\sqrt{(D_0-S)^2+(D_1-S)^2}$$

5. The final formulation of the ellipse:

$$\begin{bmatrix} y_b(t) \\ x_b(t) \end{bmatrix}=\overbrace{\begin{bmatrix} \sin(45°) & \cos(45°) \\ \sin(45°) & -\sin(45°) \end{bmatrix}}^{\text{rotation matrix}}\begin{bmatrix} a\cos(t) \\ b\sin(t) \end{bmatrix}+S$$

$$\begin{bmatrix} y_b(t) \\ x_b(t) \end{bmatrix}=\begin{bmatrix} \frac{\sqrt{2}}{2}a\cos(t)+\frac{\sqrt{2}}{2}b\sin(t)+S_y \\ \frac{\sqrt{2}}{2}a\cos(t)-\frac{\sqrt{2}}{2}b\sin(t)+S_x \end{bmatrix}$$

These parametric equations are plotted in the plane $\sigma_2=0$.

Burzyński criterion for isotropic materials is presented by paraboloid of revolution with axes of symmetry given by relation: $\sigma_1 = \sigma_2 = \sigma_3$

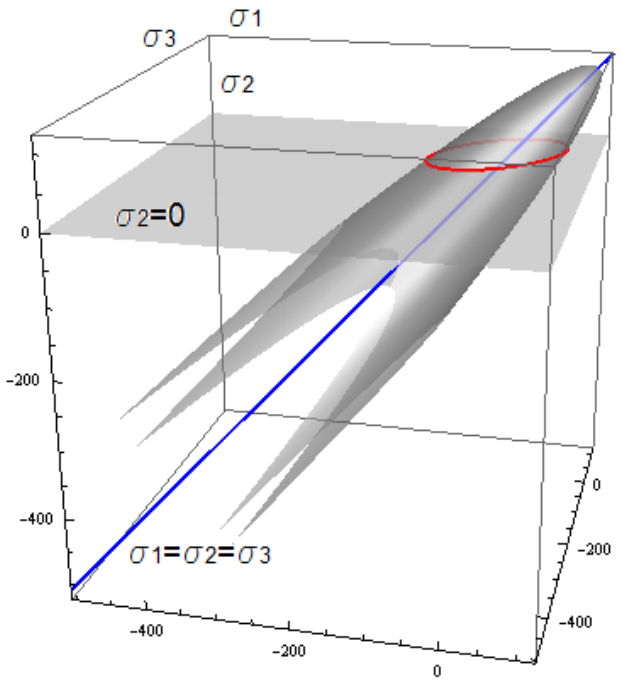

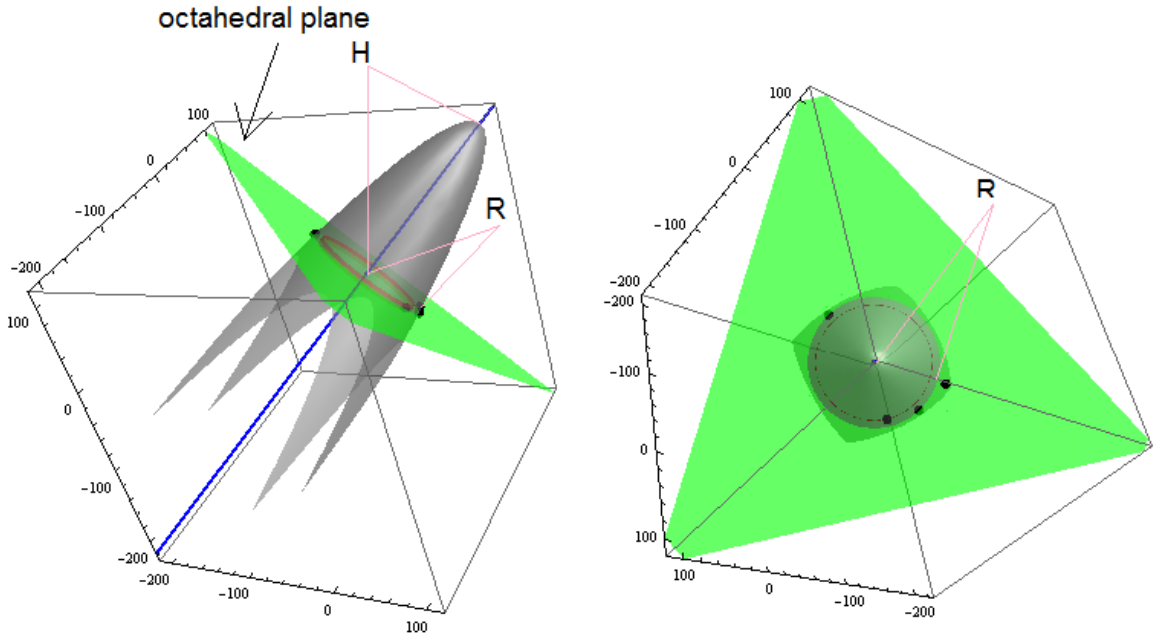

$$f(\sigma_1,\sigma_2,\sigma_3) = \sigma_1^{\,2} + \sigma_2^{\,2} + \sigma_3^{\,2} - \left(\sigma_2\sigma_3 + \sigma_1\sigma_2 + \sigma_1\sigma_3\right) + \left(\sigma_Y^C - \sigma_Y^T\right)\left(\sigma_1 + \sigma_2 + \sigma_3\right) - \sigma_Y^C\sigma_Y^T$$

1. Determining the peak of the paraboloid of revolution:

$$\begin{cases} f(\sigma_1,\sigma_2,\sigma_3)=0 \\ \sigma_1=\sigma_2=\sigma_3 \end{cases} \quad \rightarrow S_p=(s_x,s_y,s_z)$$

2. Determining the length from the peak to the octahedral plane: $H=\sqrt{3s^2}$
3. The crossection of the paraboloid in the octahedral plane is given by a circle. The radius of the circle R:

$$\begin{cases} f(\sigma_1,\sigma_2,\sigma_3)=0 \\ \frac{\sigma_1}{\sqrt{3}}+\frac{\sigma_1}{\sqrt{3}}+\frac{\sigma_1}{\sqrt{3}}=0 \end{cases} \quad \rightarrow r$$

The length of a radius is $R=\sqrt{2r}$

4. The rotation matrix:

$$\alpha=\begin{bmatrix} 0.211 & -0.789 & -0.577 \\ -0.789 & 0.211 & -0.577 \\ 0.577 & 0.577 & -0.577 \end{bmatrix}$$

These are direction cosines of the axis of symmetry $\sigma_1=\sigma_2=\sigma_3$.

5. The final formulation of the paraboloid of revolution is given:

$$P(\xi,\eta)=\alpha\begin{bmatrix} \xi \\ \eta \\ \frac{H}{R^2}\left(\xi^2+\eta^2\right)-H \end{bmatrix}$$

Appendix 3
Project of biaxial compression set-up

Coupe A-A

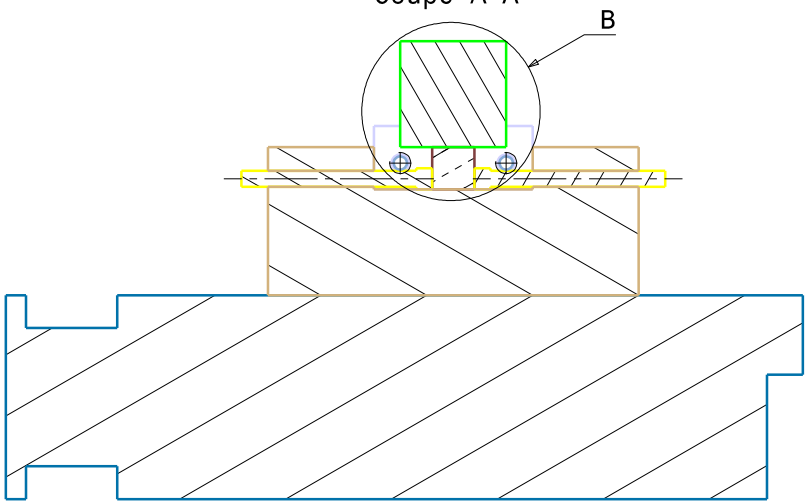

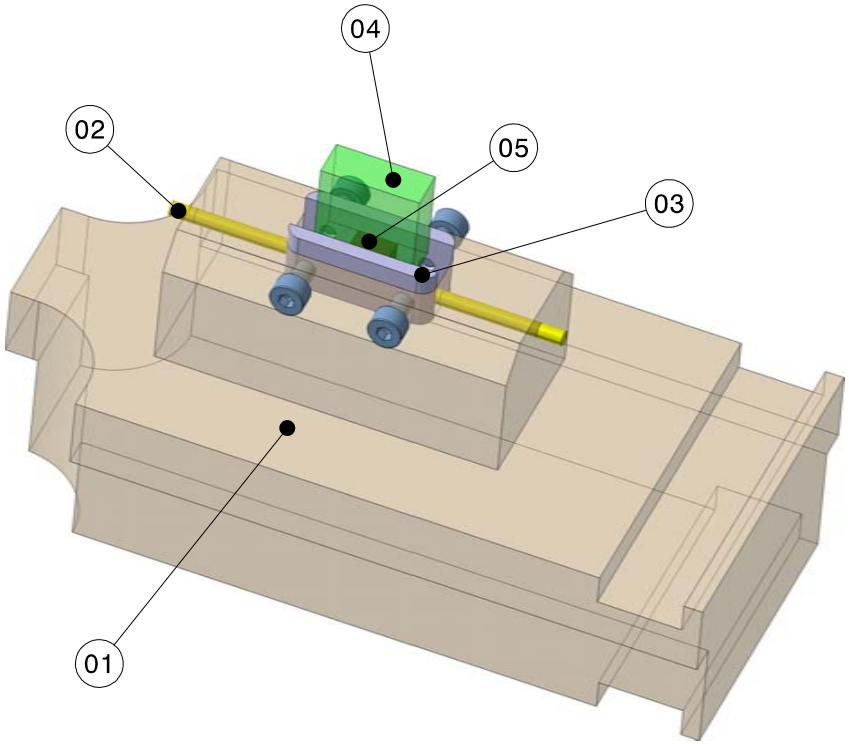

Détail B

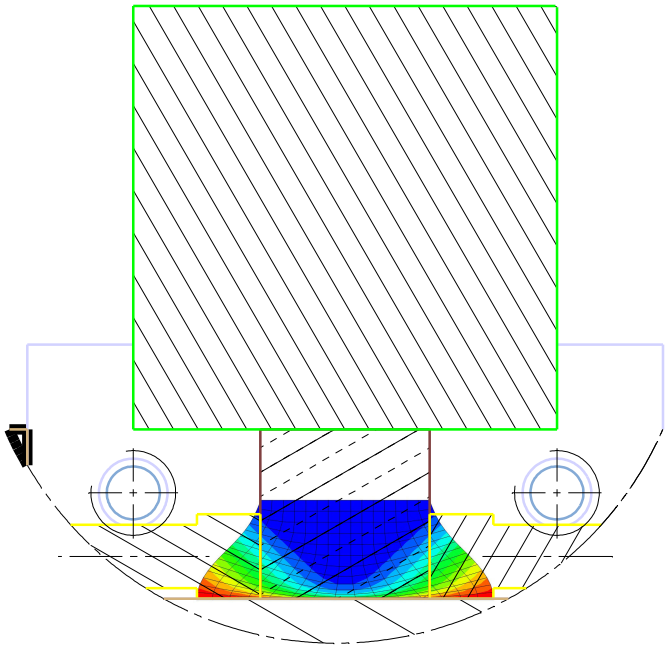

Nomenclature de biaxecomp

N°	Nom	Matière	Nombre
01	01_Pièce adaptatrice biaxe comp	42CD4	1
02	02_Guide	42CD4	2
03	03_Cale	42CD4	2
04	04_Poincon	42CD4	1
05	Eprouvette	Cuivre	20
06	ISO 4762 SCREW M4x8 STEEL HEXAGON SOCKET HEAD CAP	Acier	4

DESSINATEUR : T.FRAS; R.BERNIER	Créé le : 11/10/2011 Modifié le : 11/10/2011	BIAXE COMP	enim
Matière :	TAILLE A3	Montage biaxe compression	AGH
Nombre : 1	ECHELLE 1:1	LaBPS ECOLE NATIONALE D'INGENIEURS DE METZ	

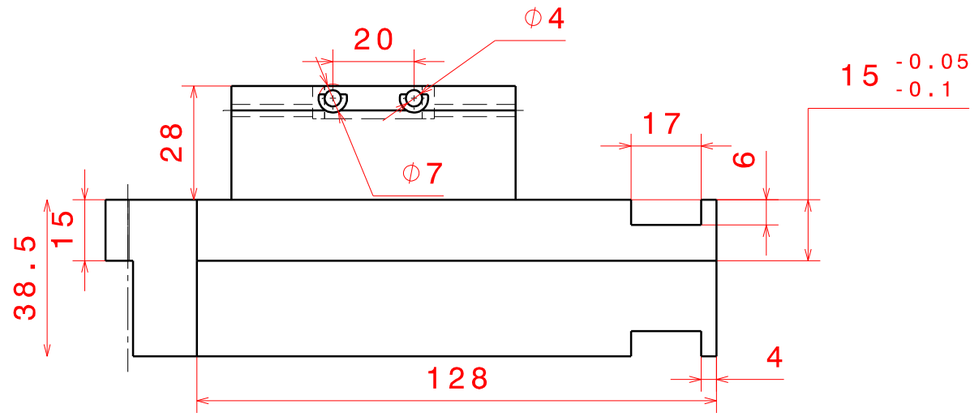

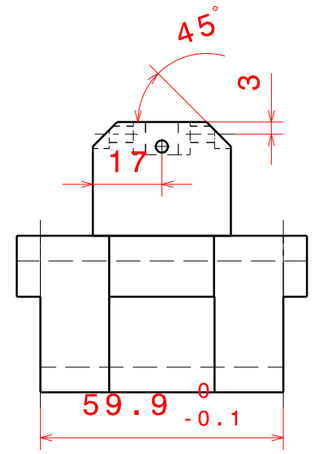

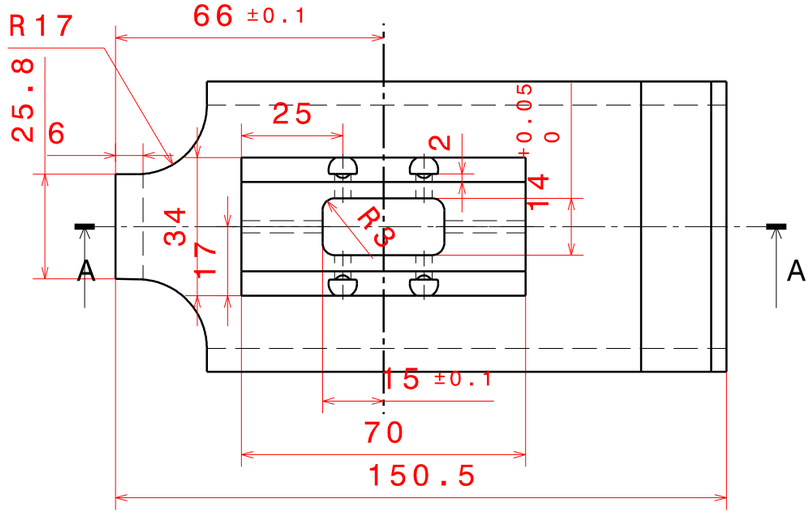

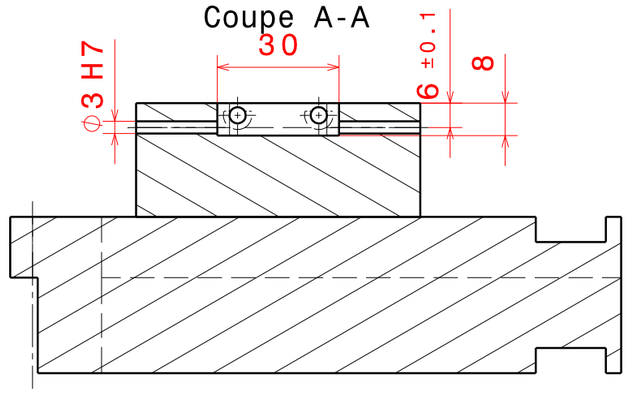

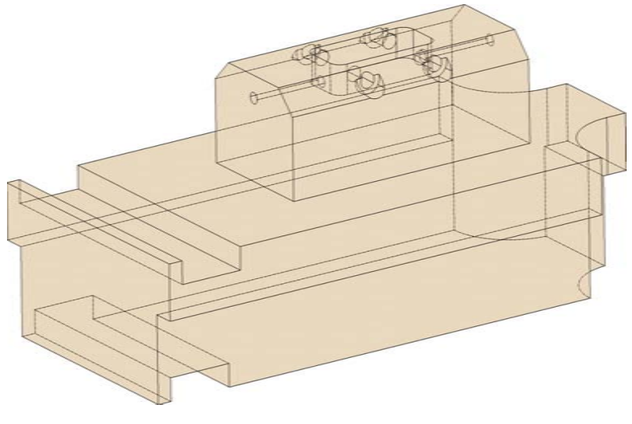

DESSINATEUR : T.FRAS ; R.BERNIER		01_Pièce adaptatrice
Créé le : 11/10/2011 Modifié le : 11/10/2011		AGH
TAILLE A3		BIAXE COMPRESSION
ECHELLE 2:3	LaBPS LABORATOIRE DE MÉCANIQUE BIOMÉCANIQUE • POLYMÈRE • STRUCTURES	ECOLE NATIONALE D'INGENIEURS DE METZ enim École nationale d'ingénieurs de Metz

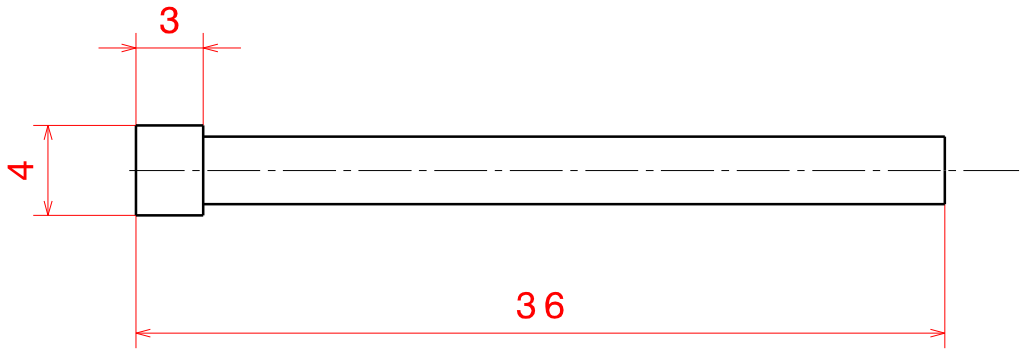

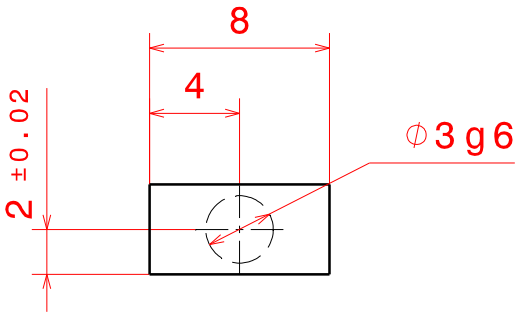

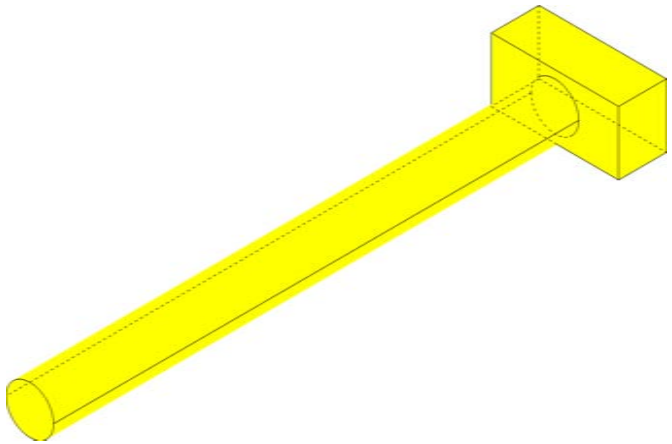

Tolérance générale : +/-0.2

Matière : 42CD4		LaBPS LABORATOIRE DE MÉCANIQUE BIOMÉCANIQUE • POLYMÈRE • STRUCTURES — 02 Guide	
Nbre : 2		BIAXIALE COMPRESSION	AGH
Taille : A4	Echelle: 3:1	DESSINATEUR : T. FRAS, R.BERNIER Dessiné le : 11/10/2011 Modifié le : 11/10/2011	enim École nationale d'ingénieurs de Metz

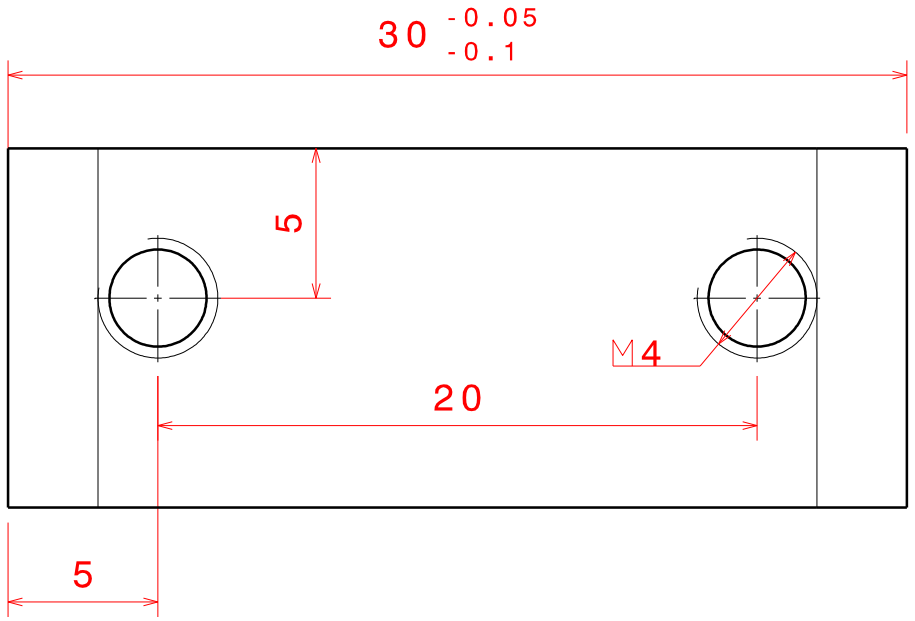

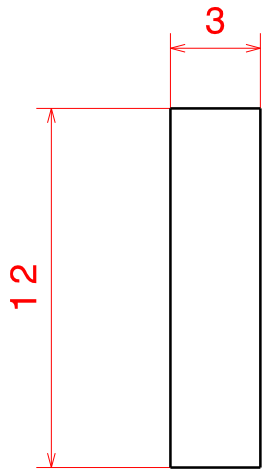

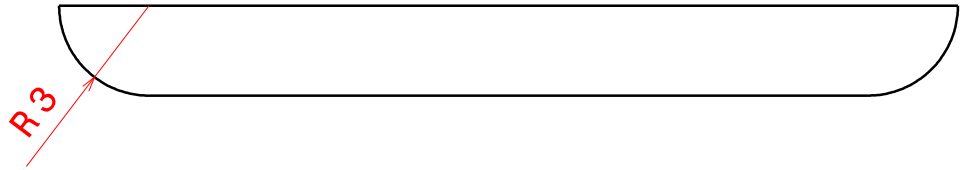

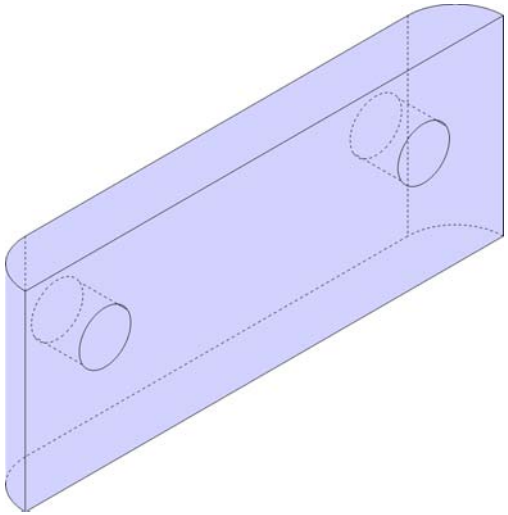

Tolérance générale : +/-0.2

Matière : 42CD4		LaBPS	03 Cale
Nbre : 2			BIAXIALE COMPRESSION
Taille : A4	Echelle: 3:1	DESSINATEUR : T. FRAS, R.BERNIER Dessiné le : 11/10/2011 Modifié le : 11/10/2011	enim École nationale d'ingénieurs de Metz AGH

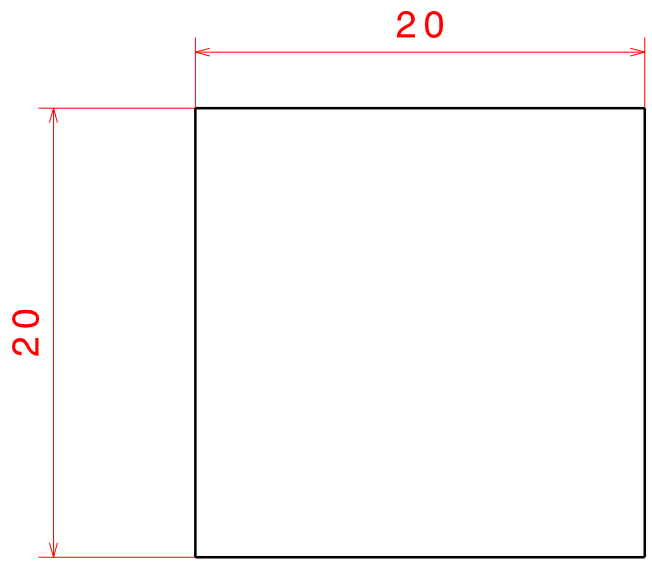

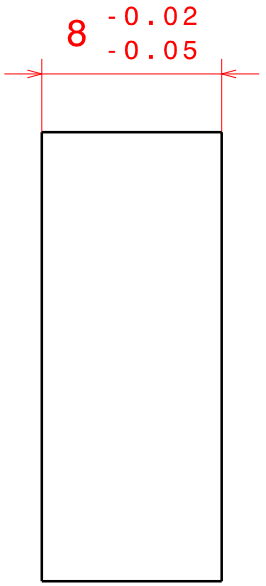

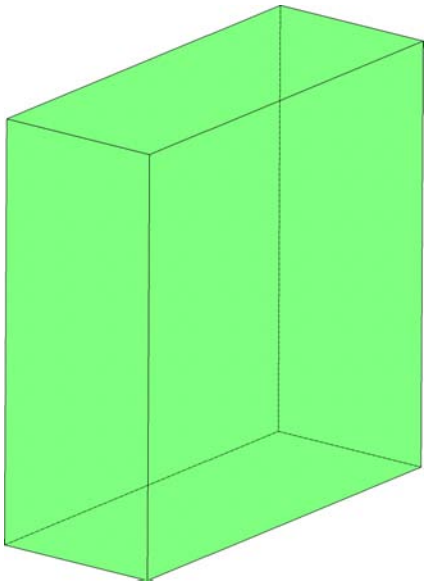

Tolérance générale : +/-0.2

Matière : 42CD4		LaBPS	04 Poinçon
Nbre : 1			BIAXIALE COMPRESSION
Taille : A4	Echelle: 3:1	DESSINATEUR : T. FRAS, R.BERNIER Dessiné le : 11/10/2011 Modifié le : 11/10/2011	enim École nationale d'ingénieurs de Metz AGH

References

ASTM E9 - 09 Standard test methods of compression testing of metallic materials at room temperature. *ASTM International, West Conshohocken*, DOI: $10.1520/E0009 - 09$, 2009.

ASTM E8 / E8M - 11 Standard test methods for tension testing of metallic materials. *ASTM International, West Conshohocken*, DOI: $10.1520/E0008 - E0008M - 11$, 2011.

M. Akiyama, T. Kuboki, K. Oikawa, K. Matsui, and K. Terada. Influence of carbon content and carbide morphology of carbon steels on stress-strain curve in vicinity of yield point. *Materials Science and Technology*, 18(11):1272 – 1278, 2002.

H. Altenbach and K. Tushtev. A new static failure criterion for istropic polymers. *Mech. Comp. Mater.*, 37(5-6):475–482, 2001.

H. Altenbach and A. Zolochevsky. *Erweiterte* D*eformationsmodelle und* V*ersagenskriterien der* W*erkstoffmechanik*. Stuttgart, Deutscher Verlag für Grundstoffindustrie, 1995.

H. Altenbach and A. Zolochevsky. A generalied failure criterion for three-dimensional behaviour of isotropic materials. *Engng Fract. Mech.*, 54(1):75–90, 1996.

H. Altenbach, G. B. Stoychev, and K. N. Tushtev. On elastoplastic deformation of grey cast-iron. *International Journal of Plasticity*, 17(5):719–736, 2001.

L. Alvarez, C. J. Luis, and I. Puertas. Analysis of the influence of chemical composition on the mechanical and metallurgical properties of engine cylinder blocks in grey cast iron. *Jnl Mater. Proc. Techn.*, 153-154(1):1039–1044, 2004.

E. Arruda, M. Boyce, and H. Quintus-Bosz. Effects of initial anisotropy on the finite strain deformation behavior of glassy polymers. *International Journal of Plasticity*, 9(7):783–811, 1993.

N. Bahlouli, D. Pessey, C. Raveyre, J. Guillet, S. Ahzi, A. Dahoun, and J. M. Hiver. Recycling effects on the rheological and thermomechanical properties of polypropylene-based composites. *Materials & Design*, 33(1):451–458, 2012.

Y. Bai and T. Wierzbicki. A new model of metal plasticity and fracture with pressure and Lode dependence. *International Journal of Plasticity*, 24(6):1071–1096, 2008.

E. Ball and P. Prangnell. Tensile-compressive yield asymmetries in high strength wrought magnesium alloys. *Scr. Metall. Mater.*, 31(2):111–116, 1994.

F. Barlat, J. C. Brem, J. W. Yoon, K. Chung, K. Dick, R. E. Lege, D. J. Pourboghrat, F. Choi, and E. Chu. Plane stress yield function for aluminium alloy sheets, Part i: Formulation. *International Journal of Plasticity*, 19(9):1297–1319, 2002.

C. Bauwens-Crowet, J. C. Bauwens, and G. Homes. Tensile yield-stress behavior of glassy polymers. *Jnl Polymer. Sci.*, 7(4):176–183, 1969.

C. Bauwens-Crowet, J. C. Bauwens, and G. Homes. The temperature dependence of yield of polycarbonate in uniaxial compression and tensile tests. *Jnl Mater. Sci.*, 7(2):176–183, 1972.

A. J. Becker. *The strength and siffness of steel under biaxial loading*, volume 1. Univ. of Illinois Bull., 1916.

S. Belhabib, H. Haddadi, M. Gaspérini, and P. Vacher. Heterogeneous tensile test on elasto-plastic metallic sheets: Comparison between fem simulations and full-field strain measurements. *International Journal of Mechanical Sciences*, 50(1):14–21, 2008.

J. F. Bell. *The Experimental Foundations of Solid Mechanics*. Springer Berlin, 1973.

A. Bhattacharyya, D. Rittel, and G. Ravichandran. Effect of strain rate on deformation texture in OFHC Copper. *Scripta Materialia*, 52(7):657–661, 2005.

W. Bier and S. Hartmann. A finite strain constitutive model for metal powder compaction using a unique and convex single surface yield function. *Eur. Jnl Mech. A/Sol.*, 25(6): 1009–1030, 2006.

D. Bigoni and A. Piccolroaz. Yield criteria for quasibrittle and frictional materials. *International Journal of Solids and Structures*, 41(11):2855–2878, 2004.

J. F. W. Bishop and R. Hill. A theoretical derivation of the plastic properties of a polycrystalline face-centered metal. *Philosophical Magazine*, 42(1):1298–307, 1951a.

J. F. W. Bishop and R. Hill. A theory of the plastic distortion of a polycrystalline aggregate under combined stresses. *Philosophical Magazine*, 42(327):414–427, 1951b.

F. Bonnavand, A.N. Bramley, and D. J. Mynors. A fast new numerical tool for designing pre-stressed dies for backward extrusion. Part 2: numerical analysis. *Jnl Engng Manufacture*, 215(2):181–193, 2001.

V. Bouchart, M. Coulibaly, and A. Rusinek. Polylactic acid behaviour under shear loading for a wide range of strain rates. *ENIM Internal Report*, pages 1–12, 2010.

V. Bouchart, M. Coulibaly, and A. Rusinek. Corn pole resin CPR-M2 under shear loading for a wide range of strain rates. *ENIM Internal Report*, pages 1–7, 2011.

P. B. Bowden and S. Raha. The formation of microshear bands in polystyrene and polymethylmethacrylate. *Philosophical Magazine*, 22(177):463–482, 1970.

J. D. Bressan and R. K. Unfer. Construction and validation tests of a torsion test machine. *Jnl Mater. Proc. Techn.*, 179(1):23–29, 2006.

P. W. Bridgman. The compressibillity of hydrogen to high pressures. *Recueil des Travaux Chimiques des Pays-Bas*, 42(7):568–571, 1923.

P. W. Bridgman. The effect of hydrostatic pressure on the fracture of brittle substances. *Jnl Appl. Phys.*, 18(1):246, 1947.

P. W. Bridgman. *Studies in Large Plastic Flow and Fracture With Special Emphasis on the Effects of Hydrostatic Pressure*. McGraw-Hill, New York, 1952.

M. Brunig. Numerical simulation of the large elastic–plastic deformation behavior of hydrostatic stress-sensitive solids. *International Journal of Plasticity*, 15(11):1237–1264, 1999.

M. Brunig, S. Berger, and H. Obrecht. Numerical simulation of the localization behavior of hydrostatic-stress-sensitive metals. 42(11):2147–2166, 1999.

W. T. Burzyński. Teoretyczne podstawy hipotez wytężenia, Czasopismo Techniczne 47 (1929) 1-4; English translation: Theoretical foundations of the hypotheses of material effort. *Engng Trans.*, 56(1):269–305, 2008.

W. T. Burzyński. Studjum nad hipotezami wytężenia. Akademja Nauk Technicznych, Lwów 1928; also Dzieła Wybrane, Polska Akademia Nauk, PWN Warszawa 1982; also Selected passages from Włodzimierz Burzyński's doctoral dissertation: Study on material effort hypotheses,. *Engng Trans.*, 57(1):185–215, 2009.

Beradaý C., M. Berveiller, and P. Lipinski. Plasticity of metallic polycrystals under complex loading path. *International Journal of Plasticity*, 3(2):143–62, 1987.

J. R. Cahoon, W. H. Broughton, and A. R. Kutzak. The determination of yield strength from hardness measurements. *Met. Trans.*, 2(7):1979–1983, 1971.

W. D. Callister and D. G. Rethwisch. *Fundamentals of Materials Science and Engineering. An Integrated Approach*. John Wiley & Sons, 3rd edition, 2005.

J. D. Campbell and W. G. Ferguson. Temperature and strain-rate dependence of the shear strength or mild steel. *Philosophical Magazine*, 21(169):63–75, 1970.

F. Carrasco, P. Pages, J. Gamez-Perez, O. Santana, and M. Maspoch. Processing of poly (lactic acid): Characterization of chemical structure, thermal stability and mechanical properties. *Polymer Degradation Stability*, 95(2):116–125, 2010.

J. Casey and H. Jahedmotlagh. The strength-differential effect in plasticity. *International Journal of Solids and Structures*, 20(4):377–393, 1984.

J. Casey and T. D Sullivan. Pressure dependency, strength-differential effect and plastic volume expansion in metals. *International Journal of Plasticity*, 1(1):39–62, 1985.

O. Cazacu and F. Barlat. Application of representation theory to describe yielding of anisotropic aluminum alloys. *Int. Jnl Eng. Sc.*, 41(12):1367–1385, 2003.

O. Cazacu and F. Barlat. A criterion for description of anisotropy and yield differential effects in pressure-insensitive metals. *International Journal of Plasticity*, 20(11):2027–2045, 2004.

O. Cazacu, B. Plunkett, and B. Barlat. Orthotropic yield criterion for hexagonal close packed metals. *International Journal of Plasticity*, 22(7):1171–1194, 1997.

J. L. Chaboche. Thermodynamic formulation of constitutive equations and application to the viscoplasticity and viscoelasticity of metals and polymers. *International Journal of Solids and Structures*, 18(18):2239–2254, 1997.

J. L. Chaboche. The strain-rate, temperature and pressure dependence of yield of isotropic poly(methylmethacrylate) and poly(ethylene terphtalate). *International Journal of Plasticity*, 24(10):1642–1693, 2008.

R. Chait. Factors influencing the strength differential of high strength steels. *Met. Trans.*, 3 (2):369–375, 1972.

J. Chakrabarty. *Applied Plasticity*. Springer, 2000.

W. Chen and B. Song. *Split Hopkinson (Kolsky) Bar: Design, Testing and Applications Weinong*. Springer, 2010.

W. F. Chen. On the Coulomb yield surface and rate of dissipation of energy. *Soil Mechanics and Theories of Plasticity*, 1(1):1–18, 1968.

T. Cheng-wen, X. Shan-na, W. Lu, C. Zhi-yong, W. Fu-chi, and C. Hong-nian. Effect of temperature on mechanical behavior of AZ31 magnesium alloy. *Trans. Nonferrous Met. Soc. China*, 17(1):41–45, 2007.

G. Y. Chin, E. A. Nesbitt, and A. J. Williams. Anisotropy of strength in single crystals under plane strain compression. *Acta Metallurgica*, 14(4):467–476, 1966.

R. M. Christensen. Yield functions/failure criteria for isotropic materials. *Proc. Roy. Soc. London*, 453(1):1473–1491, 1997a.

R. M. Christensen. Yield functions, damage states, and intrinsic strength. *Mat. Mech. Solids*, 5(3):285–300, 1997b.

R. M. Christensen. A two-property yield, failure (fracture) criterion for homogeneous, isotropic materials. *Jnl Engng. Mat. Tech.*, 126(1):45–52, 2004.

R. M. Christensen. Exploration of ductile, brittle failure characteristics through a two parameter yield/failure criterion. *Materials Science and Engineering A*, 394(1):417–424, 2005.

R. M. Christensen. A comprehensive theory of yielding and failure for isotropic materials. *Jnl Engng. Mat. Tech.*, 129(2):1–37, 2006a.

R. M. Christensen. Yield functions and plastic potentials for bcc metals and possibly other materials. *Jnl. Mech. of Mats. and Structs.*, 1(1):195–212, 2006b.

L. F. Coffin. The flow and fracture of brittle materials. *Journal of Applied Mechanics. Transactions of the ASME*, 17(3):223–248, 1950.

L. Colard and A. Rusinek. Experimental behavior characterization and modeling of pmma and pc for a wide range of strain rates and temperatures. *subbmited*, 2012.

C. A. Coulomb. Essai sur une application des regles des maximis et minimis a quelquels problemesde statique relatifs a la architecture. *Mem. Acad. Roy. Div. Sav.*, 7:343–387, 1773.

S. Das, A. Ghosh, and S. Chatterjee. The effect of cooling rate on structure and properties of a HSLA forging. *Scripta Materialia*, 48(1):51–57, 2003.

R. S. DeFries. The estimation of yield strength from hardness measurements. *Report Watervliet Arsenal*, 1975.

L. Dietrich and G. Socha. Analysis of a thermally induced phase transformation strain state for the TiNi shape memory alloy under a complex stress state. *Jnl Strain Analysis*, 37(1): 151–161, 2002.

L. Dietrich and G. Socha. Accumulation of damage in A336 GR5 structural steel subject to complex stress loading. STRAIN, 48(1):279–285, 2012.

L. Dietrich, P. Grzywna, A. Chojnacki, J. Kraskowski, and D. Petniak. Report on complex stress state tests performed on specimens made of AlSi8Cu3 and AlSi7MgCu0.5 alloys. *IPPT PAN*, 2010.

R. D. Doherty, D. A. Hughes, F. J. Humphreys, J. J. Jonas, D. Juul-Jensen, M. E. Kassnerf, W. E. King, T. R. McNelley, H. J. McQueen, and A. D. Rollettj. Current issues in recrystallization: a review. *Materials Science and Engineering A*, 238(2):219–274, 1997.

D. Drucker. Plasticity theory, strength-differential (SD) phenomenon, and volume expansion in metals and plastics. *Met. Trans.*, 4(3):667–673, 1973.

D.C. Drucker and W. Prager. Soil mechanics and plastic analysis or limit design. *Q. Appl. Math.*, 10(2):157–165, 1952.

R. A. Duckett, S. Rabinowitz, and I. M. Ward. The strain-rate, temperature and pressure dependence of yield of isotropic poly(methylmethacrylate) and poly(ethylene terphtalate). *Jnl Mater. Sci.*, 5(10):909–915, 1970.

J. Duffy, J. D. Campbell, and R. H. Hawley. On the use of a torsional split hopkinson bar to study rate effects in 1100-0 aluminum. *Journal of Applied Mechanics. Transactions of the ASME*, 38(1):83–91, 1971.

L. Durrenberger, A. Molinari, and A. Rusinek. Internal variable modeling of the high strain-rate behavior of metals with applications to multiphase steels. *Materials Science and Engineering A*, 468(1-2):297–304, 2008.

H. Eyring. Viscosity, plasticity and diffusion as examples of absolute reaction rates. *Jnl Chemical Phys.*, 4(1):283–291, 1936.

J. Fernandez-Saez and G. Vadillo. An analysis of Gurson model with parameters dependent on triaxiality based on unitary cells. *Eur. Jnl Mech. A/Sol.*, 28(3):417–427, 2009.

F. B. Fletcher and J. P. Hirth M. Cohen. Temperature dependence of the strength-differential effect in hardened steels. *Met. Trans.*, 5(4):905–908, 1974.

P. S. Follansbee. High-strain-rate deformation of FCC metals and alloys. *Report. Los Alamos National Lab., NM (USA)*, 1(1), 1985.

P. S. Follansbee. High-strain-rate deformation of FCC metals and alloys. *Metallurgical Applications of Shock-Wave and High-Strain-Rate Phenomena*, 1(1):451–479, 1986.

P. S. Follansbee and U. F. Kocks. A constitutive description of the deformation of copper based on the use of the mechanical threshold stress as an internal state variable. *Acta Metallurgica*, 1(1):81–93, 1988.

H. Fromm. In: Handbuch der physikalischen und technishchen mechanik. *Proc. Am. Soc. Civ. Eng*, 4, 1931.

K. J. Frutschy and R. J. Clifton. High temperature pressure shear plate impact experiments on OFHC Copper. *Journal of the Mechanics and Physics of Solids*, 46(10):1723–1743, 1998.

J. Galán, L. Samek, P. Verleysen, K. Verbeken, and Y. Houbaert. Advanced high strength steels for automotive industry. *Revista de metalurgia*, 48(2):118–131, 2012.

C. Y. Gao and L. C. Zhang. A constitutive model for dynamic plasticity of FCC metals. *Materials Science and Engineering A*, 527(13):3138–3143, 2010.

X. Gao, T. Zhang, M. Hayden, and Ch. Roe. Effects of the stress state on plasticity and ductile failure of an aluminum 5083 alloy. *International Journal of Plasticity*, 25(12):2366–2382, 2009.

X. Gao, T. Zhang, J. Zhou, S. M. Graham, M. Hayden, and Ch. Roe. On stress-state dependent plasticity modeling: Significance of the hydrostatic stress, the third invariant of stress deviator and the non-associated flow rule. *International Journal of Plasticity*, 27(2):217–231, 2011.

X. Gao, T. Zhang, J. Zhou, S. M. Graham, M. Hayden, and Ch. Roe. Modeling the ductile fracture behavior of an aluminum alloy 5083-H116 including the residual stress effect. *Engng Fract. Mech.*, 85(1):103–116, 2012.

C. Y. Gaoa, W. R. Lua, L. C. Zhang, and H. X. Yan. A constitutive description of the thermo-viscoplastic behavior of body-centered cubic metals. *Materials and Design*, 36(1):671–678, 2012.

G. Gary and W. K. Nowacki. Essai de cisaillement plan applique a des toles minces. *Journal de Physique*, IV(4):65–70, 1994.

E. Ghorbel. A viscoplastic constitutive model for polymeric materials. *International Journal of Plasticity*, 24(11):2032–2058, 2008.

A. Gilat. Torsional Kolsky bar testing. *ASM Handbook*, 8:505–515, 2000.

A. Glema, T. Łodygowski, and W. Sumelka. Nowacki's double shear test in the framework of the anisotropic thermo-elasto-viscoplastic material model. *Jnl Theor. Appl. Mech.*, 48(4): 973–1001, 2010.

A. Graf and W.F. Hosford. Calculations of forming limit diagrams for changing strain paths. *Met. Trans.*, A(24):2497–2503, 1993.

R. Grassi and I. Cornet. Fracture of grey cast-iron tubes under biaxial stresses. *Journal of Applied Mechanics. Transactions of the ASME*, 16(1):178–182, 1949.

J. J. Guest. On the strength of ductile materials under combined stress. *Philos. Mag.*, (50): 69–133, 1900.

Y. Guo and Y. Li. A novel approach to testing the dynamic shear response of Ti-6Al-4V. *Acta Mechanica Solida Sinica*, 25(3):299–311, 2012.

A. L. Gurson. Continuum theory of ductile rupture by void nucleation and growth. Part i – Yield criteria and flow rules for porous ductile media. *Jnl Engng. Mat. Tech.*, 99(1):2–15, 1977.

B. T. Haigh. The strain energy function and the elastic limit. *Engineering*, (109):158–160, 1920.

K. S. Havner. Channel die compression revisited: application of a set of basic crystal hardening inequalities to (1 1 0) loading. *Mech. Mater.*, 39(6):610–622, 2007a.

K. S. Havner. Corrigendum to channel die compression revisited: application of a set of basic crystal hardening inequalities to (1 1 0) loading. *Mech. Mater.*, 39(9):893–895, 2007b.

K. S. Havner. Comparative evaluation of a viscoplastic power-law and rate-independent crystal plasticity in channel die compression. *Mech. Mater.*, in press, 2012.

K. S. Havner and P. L. Sue. Theoretical analysis of the channel die compression test - II. first- and second-order analysis of orientation (1 1 0) (0 0 1) (1 1 0) in FCC crystals. *Journal of the Mechanics and Physics of Solids*, 33(3):285–313, 2007.

S. S. Hecker. Yield surfaces in prestrained aluminum and copper. *Met. Trans.*, 2(8):1971–2077, 1970.

S. S. Hecker. Experimental investigation of corners in the yield surface. *Acta Mech.*, 13(1-2): 69–86, 1972a.

S. S. Hecker. Influence of deformation history on the yield locus and stress-strain behavior of aluminum and copper. *Met. Trans.*, 4(4):1973–1985, 1972b.

H. Hencky. Über einige statisch bestimmte Falle des Gleichgewichts in plastischen Korpern. *Z. Angew. Math. Mech.*, 1923.

H. Hencky. Zur Theorie plastischer Deformationen. *Z. Angew. Math. Mech.*, 1924.

H. D. Hibbitt, B. I. Karlsson, and P. Sorensen. Abaqus 6.10. user manual. 2010.

J. P. Hirth and M. Cohen. On the strength-differential phenomenon in hardened steel. *Met. Trans.*, 1(1):3–8, 1970.

H. E. Hjelm. Yield surface for grey cast iron under biaxial stress. *Jnl Engng. Mat. Tech.*, 116 (2):148–154, 1994.

B. Hopkinson. A method of measuring the pressure produced in the detonation of high explosives or by the impact of bullets. *Philos. Trans. R. Soc.*, A 213:437–456, 1914.

L. W. Hu and K. D. Pae. Inclusion of the hydrostatic stress component in formulation of the yield condition. 275(6):491–502, 1963.

W. Hu. A novel quadratic yield model to describe the feature of multi-yield-surface of rolled sheet metals. *International Journal of Plasticity*, 23(12):2004–2028, 2007.

W. Hu and Z. R Wang. Multiple-factor dependence of the yielding behavior to isotropic ductile materials. *Computational Materials Science*, 32(1):31–46, 2005.

M. T. Huber. *O podstawach teorji wytrzymałości*, volume XV. Prace Mat.-Fiz. Warszawa, 1904.

M. T. Huber. Właściwa praca odkształcenia jako miara wytężenia materiału Czasopismo Techniczne Lwów 1904 also English translation: Specific work of strain as a measure of material effort. *Archives of Mechanics*, 56:173–190, 2004.

N. J. Huffington. Reexamination of the plastic flow criterion for copper. *Technical Report BRL-TR-3368*, page 1–25, 1992.

E. Ibraim, A. Diambra, A.R. Russell, and D. Muir Wood. Assessment of laboratory sample preparation for fibre reinforced sands. *Geotextiles and Geomembranes*, 34(1):69–79, 2012.

S. Ivorra, R. Irles, L. Estevan, J. M. Adam, F. J. Pallares, and B. Ferrer. Drucker-Prager yield criterion application to study the behavior of CFRP confined concrete under compression. *World Congress on Housing*, 1, 2010.

D. J.Alexander and I. J. Beyerlein. Anisotropy in mechanical properties of high-purity copper processed by equal channel angular extrusion. *Materials Science and Engineering A*, 410 (1):480–484, 2005.

T. Jankowiak, A. Rusinek, and T.Łodygowski. Validation of the Klepaczko–Malinowski model for friction correction and recommendations on Split Hopkinson Pressure Bar. *Finite Elem. Anal. Des.*, 10(47):1191–1208, 2011.

J. Jiang, Y. Wu, and X. Zhao. Application of Drucker-Prager plasticity model for stress-strain modeling of FRP confined concrete columns. *Procedia. Eng.*, 14(1), 2011.

G. R. Johnson and W. H. Cook. A constitutive model and data for metals subjected to large strains, high strain rate and high temperatures. *Proceedings of the 7th International Symposium on Ballistics.* H*ague,* N*ethedlands*, 21, 1983.

B.L. Juneja. *Fundamentals of Metal Forming Processes*. Indian Institute of Technology, delhi, india edition, 2010.

A. S. Khan and P. Cheng. Study of three elastic-plastic constitutive models by non-proportional finite deformations of OFHC Copper. *International Journal of Plasticity*, 12 (6):737–759, 1996.

A. S. Khan and P. Cheng. An anisotropic elastic-plastic constitutive model for single and poly-crystalline metals. II–experiments and predictions concerning thin-walled tubular OFHC Copper. *International Journal of Plasticity*, 14(1-3):209–226, 1998.

A. S. Khan and B. Farrokh. A strain rate dependent yield criterion for isotropic polymers: low to high rates of loading. *Eur. Jnl Mech. A/Sol.*, 29(2):274–282, 2010.

A. S. Khan, B. Farrokh, and R. Kazmi. Multiaxial and non-proportional loading responses, anisotropy and modeling of Ti–6Al–4V titanium alloy over wide ranges of strain rates and temperatures. *International Journal of Plasticity*, 23(6):931–950, 2007.

J. R. Klepaczko. Thermally activated flow and strain rate history effects for some polycrystalline FCC metals. *Materials Science and Engineering A*, 18(1):121–135, 1975.

J. R. Klepaczko. A practical stress-strain-strain rate-temperature constitutive relation of the power form. *Jnl Mech. Working Technol.*, 15(2):143–165, 1987.

J. R. Klepaczko. An experimental technique for shear testing at high and very high strain rates. The case of mild steel. *Int. Jnl Impact Eng.*, 15(1):25–39, 1994.

J. R. Klepaczko and C. Y. Chiem. On rate sensitivity of FCC metals, instantaneous rate sensitivity and rate sensitivity of strain-hardening. 34(1):29–54, 1986.

J. R. Klepaczko and J. Z. Malinowski. *Dynamic frictional effects as measured from the split* H*opkinson pressure bar in high velocity deformation of solids*. IUTAM Symposium Tokyo Japan, Springer-Verlag Berlin, 1977.

H. Kolsky. An investigation of the mechanical properties of materials at very high rates of loading. *Proc. Phys. Soc.*, pages 676–682, 1949.

H. Kolsky. *Stress Waves in Solids*. Dover Publications Inc., New York, 1952.

J. Koplik and A. Needleman. Void growth and coalescence in porous plastic solids. 24(8): 835–853, 1988.

A. G. Kostryzhev. Bauschinger effect in Nb and V microalloyed line pipe steels. *PhD Thesis*, Birmingham University, 2009.

H. Kuhn and D. Medlin. ASM H*andbook:* M*echanical* T*esting and* E*valuation*. Materials Park, ASM International, 2000.

M. Kuroda. A phenomenological plasticity model accounting for hydrostatic stress-sensitivity and vertex-type of effect. *Mech. Mater.*, 36(3):285–297, 2004.

M. Kuroda and V. Tvergaard. A phenomenological plasticity model with non-normality effects representing observations in crystal plasticity. *Journal of the Mechanics and Physics of Solids*, 49(6):1239–1263, 2001.

O. Kwon and A. J. DeArdo. On the recovery and recrystallization which attend static softening in hot-deformed copper and aluminum. *Acta Metallurgica*, 38(1):41–54, 1990.

L. Landau and E. Lifshitz. *Theory of Elasticity*, volume 7. Boston, MS: Butterworth Heinemann, 3 edition, 1986.

A. M. Lennon and K. T. Ramesh. The influence of crystal structure on the dynamic behavior of materials at high temperatures. *International Journal of Plasticity*, 20(2):269–290, 2004.

Z. Li and J. Lambros. Strain rate effect on the thermomechanical behaviour of polymers. *International Journal of Solids and Structures*, 38(20):3549–562, 2001.

R. Liang and A. S. Khan. A critical review of experimental results and constitutive models for BCC and FCC metals over a wide range of strain rates and temperatures. *International Journal of Plasticity*, 15(9):963–980, 1999.

P. Lipinski and M. Berveiller. Elasto-plasticity of micro-inhomogeneous metals at large strains. *International Journal of Plasticity*, 5(2):149–72, 1989.

W. Lode. Versuche äber den einfluss der mittleren hauptspannung auf das fliessen der metalle. *Z. der Physic*, 36:913–919, 1926.

X. Y. Lou, M. Li, R. K. Boger, S. R. Agnew, and R. H. Wagoner. Hardening evolution of AZ31b Mg sheet. *International Journal of Plasticity*, 23(1):44–86, 2007.

Y. Lou, H. Huh, and J. W. Yoon. Consideration of strength differential effect in sheet metals with symmetric yield functions. *Int. Jnl Mech. Sc.*, 66(1):214–223, 2013.

J. Lu and G. Ravichandran. Pressure dependent flow behavior of Zr41.2Ti13.8Cu12.5Ni10Be22.5 bulk metallic glass. *Jnl Mater. Res.*, 18(9):2039–2048, 2003.

J. Lubliner. *Plasticity Theory*, volume 1. Dover Publications, Inc., Mineola, New York edition, 2008.

A. C. Lund and C. A. Schuh. Yield surface of a simulated metallic glass. *Acta Materialia*, 51 (18):5399–5411, 2003.

R. Mahnken. Strength difference in compression and tension and pressure dependence of yielding in elasto-plasticity. 190(39):5057–5080, 2001.

L. E. Malvern. *Introduction to the mechanics of a continous medium*. Prentice-Hall, Inc., 1969.

A. Mandrea, S. Rebegea, and A. Rusinek. WASP User's Manual. *Available from: rusinek@enim.fr*, pages 1–10, 2010.

A. M. Maniatty, J. S. Yu, and T. Keane. Anisotropic yield criterion for polycrystalline metals using texture and crystal symmetries. *International Journal of Solids and Structures*, 36 (35), 1999.

G. Mann, J. R. Griffitths, and C. H. Caceres. Hall-Petch parameters in tension and compression in cast MG-2Zn alloys. *Jnl Alloys Compounds*, 378(1/2):188–191, 2004.

Y. Mao-hong. Advances in strength theories for materials under complex stress state in the 20th century. *Applied Mechanics Reviews*, 55(3):169–218, 2002.

J. Marin. Failure theories of materials subjected to combined stresses. *Proc. Am. Soc. Civ. Eng.*, (61):851–867, 1935.

R. Matadi Boumbimba, K. Wang, N. Bahlouli, S. Ahzi, Y. Rémond, and F. Addiego. Experimental investigation and micromechanical modeling of high strain rate compressive yield stress of a melt mixing polypropylene organoclay nanocomposites. *Mech. Mater.*, 52(1): 58–68, 2012.

H. J. McQueen and J. J. Jonas. *Treatise on Materials Science and Technology, Plastic Deformation of Materials*. Academic Press, New York edition, 1975.

H. W. Meyer and D. S. Kleponis. An analysis of parameters for the Johnson-Cook strength model for 2-in-thick rolled homogeneous armor. ARL-TR-*2528*, 1:1–27, 2001.

L. W. Meyer and T. Halle. Shear strength and shear failure, overview of testing and behavior of ductile metals. *Mech. Time-Depend. Mater.*, 15(4):327–340, 2011.

S. L. Meyer. *Data Analysis for Scientists and Engineers*. J. Willey New York, 1975.

M. J. Michno and W. N. Findley. An historical perspective of yield surface investigations for metals. *Int. Jnl Non-Lin. Mech.*, 11(1):59–82, 1976.

O. Mohr. Welche umstande bedingen die elastizitatsgrenze und den bruch eines materials. *Zeitschrift des Vereins Deutscher Ingenieure Band*, (44):1524–1530, 1900.

O. Mohr. Abhaldungen aus dem Gebiete der Technischen Mechanik. *Ernst Berlin*, (2):1–20, 1914.

A. Molinari and G. Ravichandran. Constitutive modeling of high-strain-rate deformation in metals based on the evolution of an effective microstructural length. *Mech. Mater.*, 37(7): 737–752, 2005.

T.W. Montemarano. High strength low alloy steels in naval construction. *Jnl Ship Prod.*, 2 (3):145–162, 1986.

A. D. Mulliken and M. C. Boyce. Mechanics of the rate-dependent elastic–plastic deformation of glassy polymers from low to high strain rates. *International Journal of Solids and Structures*, 43(5):1331–1356, 2006.

A. Nadai. *Theory of flow and fracture of solids*, volume I. McGraw-Hill Book Company, 2nd edition, 1950.

A. L. Nadai. Plastic behavior of metals in the strain-hardening range. *Jnl Appl. Phys.*, 8(3): 205–213, 1937.

A. Needleman and V. Tvergaard. An analysis of ductile rupture in notched bars. *Journal of the Mechanics and Physics of Solids*, 32(6):461–490, 1984.

S. Nemat-Nasser. A micromechanically-based constitutive model for frictional deformation of granular materials. *Journal of the Mechanics and Physics of Solids*, 48(6):1541–1563, 2000.

S. Nemat-Nasser and Y. Li. Flow stress of FCC polycrystals with application to OFHC Copper. *Acta Materialia*, 46(2):565–577, 1998.

S. Nemat-Nasser, J. B. Isaacs, and M. Q. Liu. Microstructure of high-strain, high strain- rate deformed tantalum. *Acta Materialia*, 46(4):1307–1325, 1998a.

S. Nemat-Nasser, L.Ni, and T.Okinaka. A constitutive model for FCC crystals with application to polycrystalline OFHC Copper. *Mech. Mater.*, 30(4):325–341, 1998b.

S. Nemat-Nasser, W. G. Guo, and D. P. Kihl. Thermomechanical response of AL-6XN stainless steel over a widerange of strain rates and temperatures. *Journal of the Mechanics and Physics of Solids*, 49(8):1823–46, 2001.

M. Nihida, H. Ichihara, and N. Fukada. Evaluation of dynamic compressive properties of PLA/PBAT polymer alloys using split Hopkinson pressure bar method. *Engng Trans.*, 59 (1):21–30, 2011.

M. Nishida, H. Ichihara, H. Watanabe, N. Fukuda, and H. Ito. Effect of Dialkyl Peroxide blending on tensile properties of PLA/PBAT polymer alloys. *Engng Trans.*, 60(2): 171–184, 2012.

M. Nowak. Internal report PPS IPPT PAN - new formulation of Burzyński criterion. 2012.

M. Nowak and Z. Nowak. Internal report PPS IPPT PAN - the isotropic Burzyński criterion implemented in User Soubroutine for Abaqus Standard. 2012.

Z. Nowak, P. Perzyna, and R. B. Pęcherski. Description of viscoplastic flow accounting for shear banding. *Arch. Metall. Mat.*, 52(2):217–222, 2002.

K. Osakada. History of plasticity and metal forming analysis. *Jnl Mater. Proc. Techn.*, 210 (11):1436–1454, 2010.

K. D. Pae. The macroscopic yielding behavior of polymers in multiaxial stress field. *Jnl Mater. Sci.*, 12(6):1209–1214, 1977.

B. Paul. *Macroscopic Criteria for Plastic Flow and Brittle Fracture*, volume II. Academic Press New York, 1968.

R.B. Pęcherski. Constitutive modelling of plastic flow accounting for micro—shear banding. *Advances in Engineering Plasticity and its Applications (AEPA'1996)*, 123(1):123–128, 1996.

R.B. Pęcherski. Macroscopic effects micro-shear banding in plasticity of metals. *Acta Mech.*, 131(3-4):203–224, 1998.

J. Peirs. Experimental characterisation and modelling of the dynamic behaviour of the Titanium Alloy Ti6Al4V.

J. Peirs, P. Verleysen, J. Degrieck, and F. Coghe. The use of hat-shaped specimens to study the high strain rate shear behaviour of Ti6Al4V. *Int. Jnl Impact Eng.*, 37(6):703–714, 2010.

J. Peirs, P. Verleysen, and J. Degrieck. Experimental study of the influence of strain rate on fracture of Ti6Al4V. *Procedia Engineering*, 10:2336–2341, 2011a.

J. Peirs, P. Verleysen, W. Tirry, L. Rabet, D. Schryvers, and J. Degrieck. Dynamic shear localization in Ti6Al4V. *Procedia Engineering*, 10(1):2342–2347, 2011b.

J. Peirs, W. Tirry, B. Amin-Ahmadi, F. Coghe, P. Verleysen, L. Rabet, and J. Degrieck. Microstructure of adiabatic shear bands in Ti6Al4V. *Materials Characterization*, 75(1):79–92, 2013.

P. Perzyna. Thermodynamic theory of viscoplasticity. *Advances in Applied Mechanics*, 11(1): 313–354, 1971.

P. Perzyna. *Section 9.5 - Thermo-Elasto-Viscoplasticity and Damage.* H*andbook of Materials Behavior Models*, volume III. Elsevier, by Jean Lemaitre edition, 2001.

P. Perzyna. The thermodynamical theory of elasto-viscoplasticity accounting for microshear banding and induced anisotropy effects. *MECHANICS*, 27(1):25–42, 2008.

D. Pessey, N. Bahlouli, S. Pattofatto, and S. Ahzi. Polymer composites for the automotive industry: characterisation of the recycling effect on the strain rate sensitivity. *International Journal of Crashworthiness*, 13(4):411–424, 2008.

W. Prager. On the use of singular yield conditions and associated flow rules. *Journal of Applied Mechanics. Transactions of the ASME*, 1(20):317–320, 1953.

Copper Development Association Publications. High conductivity coppers for electrical engineering. *Copper Development Association Publication*, 122(1):1–80, 1998.

R. S. Raghava, R. M. Caddell, and G. Yeh. The macroscopic yield behavior of polymers. *Jnl Mater. Sci.*, 8(2):225–232, 1973.

R. S. Raghava, R. M. Caddell, and A. G. Atkins. Pressure dependent yield criteria for polymers. *Materials Science and Engineering A*, 13(2):113–120, 1974.

B. Raniecki and Z. Mróz. Yield or martensitic phase transformation conditions and dissipation functions for isotropic, pressure-insensitive alloys exhibiting SD effect. *Acta Mech.*, 195 (1-4):1–22, 2008.

E. F Rauch. Plastic anisotropy of sheet metals determined by simple shear tests. *Materials Science and Engineering A*, 241(1):179–183, 1998.

D. Rees. Yield functions that account for the effects of initial and subsequent plastic anisotropy. *Acta Mech.*, 43(3-4):223–24, 1982.

J. Richeton, S. Ahzi, K. S. Vecchio, F. C. Jiang, and R. R. Adharapurapu. Influence of temperature and strain rate on the mechanical behavior of three amorphous polymers: Characterization and modeling of the compressive yield stress. *International Journal of Solids and Structures*, 43(7):2318–2335, 2006.

O. Richmond and W. A. Spitzig. Pressure dependence and dilatancy of plastic flow. In: Theoretical and Applied Mechanics, Proceedings of the 15th International Congress of Theoretical and Applied Mechanics. 24(1):377–386, 1980.

D. Rittel and A. Dorogoy. A methodology to assess the rate and pressure sensitivity of polymers over a wide range of strain rates. *Journal of the Mechanics and Physics of Solids*, 56 (11):3191–3205, 2008.

D. Rittel, S. Lee, and G. Ravichandran. A shear-compression specimen for large strain testing. *Exp. Mech.*, 42(1):58–64, 2002a.

D. Rittel, G. Ravichandran, and S. Lee. Large strain constitutive behavior of OFHC Copper over a wide range of strain rates using the shear compression specimen. *Mech. Mater.*, 34 (10):627–642, 2002b.

J. A. Rodríguez-Martínez. Advanced constitutive relations for modeling thermo-viscoplastic behaviour of metallic alloys subjected to impact loading. *PhD Thesis*, Madrid University, 2010.

J. Rodríguez-Martínez, A. Rusinek, and A. Arias. Relation between strain hardening of steel and critical impact velocity in tension. *Jnl Theor. Appl. Mech.*, 47(3):645–665, 2009.

M. Ros and A. Eichinger. In: Die Bruchgefahrfester Korper Bericht. *ENPA. Zurich*, 4(172), 1949.

Z. Rosenberg, Y. Ashuach, Y. Yeshurun, and E. Dekel. On the main mechanisms for defeating AP projectiles, long rods and shaped charge jets. *Int. Jnl Impact Eng.*, 36(4):588–596, 2009.

A. Rusinek. Mechanical behaviour of AZ31 magnesium alloy. *LaBPS Report*, 2011.

A. Rusinek and J. R. Klepaczko. Shear testing of a sheet steel at wide range of strain rates and a constitutive relation with strain-rate and temperature dependence of the flow stress. *International Journal of Plasticity*, 17(1):87–115, 2001.

A. Rusinek, R. Zaera, J. R. Klepaczko, and R. Cheriguene. Analysis of inertia and scale effects on dynamic neck formation during tension of sheet steel. *Acta Materialia*, 53(20): 5387–5400, 2005.

A. Rusinek, R. Zaera, and J. R. Klepaczko. Constitutive relations in 3-d for a wide range of strain rates and temperatures – application to mild steels. *International Journal of Solids and Structures*, 44(17):5611–5634, 2007.

A. Rusinek, J. A. Rodríguez-Martínez, J. R. Klepaczko, and R. B. Pęcherski. Analysis of thermo-visco-plastic behaviour of six high strength steels. *Materials and Design*, 30(5): 1748–1761, 2009.

A. Rusinek, J. A. Rodríguez-Martínez, and A. Arias. A thermo-viscoplastic constitutive model for FCC metals with application to OFHC Copper. *Int. Jnl Mech. Sc.*, 52(2):120–135, 2010.

I. Nihida & A. Rusinek. Internal report LaBPS ENIM - PLA SD effect. 2010.

S. S. Sarva and M. C. Boyce. Mechanics of polycarbonate during high-rate tension. 2(10): 1854–1850, 2007.

F. Schleicher. Die energiegrenze der elastizität. *Z. Angew. Math. Mech.*, 6(199), 1926.

C. A. Schuh and A. C. Lund. Atomistic basis for the plastic yield criterion of metallic glass. *Nature Materials*, 2(7):449–452, 2003.

A. Seeger. *The mechanism of glide and work-hardening in face centered cubic and hexagonal close-packed metal.* I*n:* D*islocations and* M*echanical* P*roperties of* C*rystals*. J. Willey, New York, 1957.

A. Shaban, R. Mahnken, L. Wilke, H. Potente, and H. Ridder. Simulation of rate dependent plasticity for polymers with asymmetric effects. *International Journal of Solids and Structures*, 44(18):6148–6162, 2007.

(Ed.) W. Sharper. *Experimental Solid Mechanics*. Springer-Verlag, 2008.

W. Q. Shen, J. F. Shao, D. Kondo, and B. Gatmiri. A micro–macro model for clayey rocks with a plastic compressible porous matrix. *International Journal of Plasticity*, 36(1):64–85, 2012.

A. A. Silano, S. K. Bhateja, and K. D. Pae. Effect of hydrostatic pressure on the mechanical behavior of polymers: polyurethane, polyoxymethylene, and branched polyethylene. *Int. Jnl Polym. Mater.*, 3(2):117–131, 2007.

J. C. Simo. A j_2 flow theory exhibiting a corner-like effect and suitable for large-scale computation. *Meth. Appl. Mech. Engng.*, 62(2):169–194, 1987.

C. R. Siviour, S. M. Walley, W. G. Proud, and J. E. Field. The high strain rate compressive behaviour of polycarbonate and polyvinylidene difluoride. *Polymer*, 46(26):12546–12555, 2005.

J. J. Skrzypek and R. B Hetnarski. *Plasticity and creep:* T*heory, examples, and problems*. Begell house, 1993.

M. C. Smith. *Principals of physical metallurgy*. Harper and Brothers Publishers, New York edition, 1956.

W. A. Spitzig and O. Richmond. Effect of hydrostatic pressure on the deformation behavior of polyethylene and polycarbonate in tension and in compression. 19(16):1129–1139, 1979.

W. A. Spitzig and O. Richmond. The effect of pressure on the flow stress of metals. *Acta Metallurgica*, 3(32):457–463, 1984.

W. A. Spitzig, R. J. Sober, and O. Richmond. Pressure dependence of yielding and associated volume expansion in tempered martensite. 23(7):885–893, 1979.

G. Stokes. *On the discontinuity of arbitrary constants which appear in divergent developments*, volume 10. Transactions of the Cambridge Philosophical Society, i edition, 1867.

D. Tabor. *The Hardness of Metals*. C*larandon* P*ress* O*xford*, 1951.

H. A. Taiebat and J. P. Carter. Flow rule effects in the Tresca model. *Comput. Geotechnics*, 35(3):500–503, 2008.

A. B. Tanner. Modeling temperature and strain rate history effects in ofhc cu. *PhD Thesis*, G*eorgia* I*nstitute of* T*echnology*. Georgia University, 1998.

A. B. Tanner and D. L. McDowell. Deformation, temperature and strain rates sequence experiments on OFHC Cu. *International Journal of Plasticity*, 15(4):375–399, 1999.

G. Taylor and H. Quinney. The plastic distortion of metals. *Phil. Trans. Roy. Soc.*, A230: 323–362, 1931.

M. Teaca, I. Charpentier, M. Martiny, and G. Ferron. Identification of sheet metal plastic anisotropy using heterogeneous biaxial tensile tests. *International Journal of Mechanical Sciences*, 52(4):572–580, 2010.

P. Tewari, S. S. Bhatnagar, and B. R. Nijhawan. Theoretical considerations for substitutions in alloy steels. pages 360–367, 1966.

P. S. Theocaris. Failure criteria for isotropic bodies revisited. *Engng Fract. Mech.*, 51(2): 239–264, 1995.

P. S. Theocaris and T. P. Philippidis. The paraboloidal failure surface of initially anisotropic elastic solids. *Jnl Reinf. Plast. and Comp.*, 6(4):378–395, 1987.

S. P. Timoshenko. *History of Strength of Materials*. McGraw-Hill, New York, 1953.

H. Tresca. Mémoire sur l'écoulement des corps solides soumis a de fortes pressions. *C.R. Acad. Sci. Paris*, (24):754, 1864.

S. W. Tsai and E. M. Wu. General theory of strength for anisotropic materials. *Jnl Comp. Mat.*, 5(1):58–80, 1971.

G. Vadillo and J. Fernandes-Saez. An analysis of Gurson model with paramters dependent on triaxiality based on unitary cells. *Eur. Jnl Mech. A/Sol.*, 28(3):417–427, 2009.

G. Vadillo, J. Fernández-Sáez, and R. B. Pęcherski. Some applications of Burzyński yield condition in metal plasticity. *Materials and Designs*, 32(2):628–635, 2011.

N. Vandresse, Ch. Destyaud, S. Girard-Insadri, and M. Darrieulat. Channel-die compression at high temperature. *Materials Science and Engineering A*, 4(476):322–332, 2008.

P. Verleysen, J. Peirs, J. Van Slycken, K. Faes, and L. Duchene. Effect of strain rate on the forming behaviour of sheet metals. *Journal of Materials Processing Technology*, 211(8): 1457–1464, 2011.

R. von Mises. *Mechanik der festen Körper im plastisch-deformablen Zustand*, volume 1. Göttin. Nachr. Math. Phys., 1913.

G. Z. Voyiadjis and F. H. Abed. Microstructural based models for BCC and FCC metals with temperature and strain rate dependency. *Mech. Mater.*, 37(2):355–378, 2005.

G. Z. Voyiadjis and A. H. Almasri. A physically based constitutive model for FCC metals with applications to dynamic hardness. *Mech. Mater.*, 40(6):549–563, 2008.

M. Vural, A. Molinari, and N. Bhattacharya. Analysis of slot orientation in shear-compression specimen (scs). *Exp. Mech.*, (57):1–192, 2010.

W. M. Wang, L. J. Sluys, and R. de Borst. Viscoplasticity for instabilities due to strain softening and strain-rate softening. *International Journal for Numerical Methods in Engineering*, 40(20):3839–3864, 1997.

H. M. Westergaard. On the resistance of ductile materials to combined stresses. *Jnl Franklin Inst.*, (189):627–640, 1882.

F. Wever and W. E. Schmid. Texturen kaltverformter. *Metalle. Z. Metallk.*, 22:133–140, 1930.

C. D. Wilson. A critical reexamination of classical metal plasticity. *Journal of Applied Mechanics. Transactions of the ASME*, 69(1):63–68, 2002.

L. Wu, S. Agnew, D. Brown, G. Stoica, B. Clausen, A. Jain, D. Fielden, and P. Liaw. Internal stress relaxation and load redistribution during the twinning–detwinning-dominated cyclic deformation of a wrought magnesium alloy, ZK60A. *Acta Materialia*, 56(14):3699–3707, 2008.

T. Yamura, M. Omiya, T. Sakai, and P. Viot. Evaluation of compressive properties of PLA/PBAT polymer blends. *Asian Pacific Conference for Materials and Mechanics*, 2009.

T. Yoshikawa, M. Tokuda, T. Inaba, H. Iwasaki, K. Machino, and N. Deguchi. Plastic deformation of AZ31 magnesium alloy under various temperature conditions. *Jnl Soc. Mat. Sci. Japan*, 57(7):688–695, 2008.

P. Zattarin, P. Lipinski, and A. Rosochowski. Numerical study of the influence of microstructure on subsequent yield surfaces of polycrystalline materials. 46(9):1377–1398, 2004.

F. J. Zerilli and R. W. Armstrong. Dislocation-mechanics-based constitutive relations for material dynamics calculations. *Jnl Appl. Phys.*, 61(5):1816–1825, 1987.

B. Zhang and V. P. W. Shim. Determination of inelastic heat fraction of OFHC Copper through dynamic compression. *Int. Jnl Impact Eng.*, 37(1-3):50–68, 2010.

M. Życzkowski. Combined loadings in the theory of plasticity. *Int. Jnl Non-Lin. Mech.*, 2 (11):173–205, 1967.

M. Życzkowski. Discontinuous bifurcations in the case of the Burzyński–Torre yield condition. *Acta Mech.*, 132(1-4), 2001.